UNIVERSITAT DE BARCELONA

# Synthesis and Study of Functionalized Porphyrins as Organophotoredox Catalysts

Pol Torres Yeste

# SYNTHESIS AND STUDY OF FUNCTIONALIZED PORPHYRINS AS ORGANOPHOTOREDOX CATALYSTS

Pol Torres Yeste


UNIVERSITAT DE BARCELONA

Secció de Química Orgànica

Facultat de Química

Universitat de Barcelona

# SYNTHESIS AND STUDY OF FUNCTIONALIZED PORPHYRINS AS ORGANOPHOTOREDOX CATALYSTS

Pol Torres Yeste

Director de la Tesi Doctoral:

**Dr. Albert Moyano Baldoire**

Departament de Química Inorgànica i Orgànica

Secció de Química Orgànica

Universitat de Barcelona

Programa de Doctorat en Química Orgànica

Facultat de Química

UNIVERSITAT DE BARCELONA

Barcelona, Setembre 2022

**Synthesis and study of functionalized porphyrins as organophotoredox catalysts**

Thesis submitted in partial fulfillment for the award of degree of Doctor in Chemistry by the University of Barcelona

**Pol Torres Yeste**

Under the guidance of:

**Dr. Albert Moyano Baldoire**

Este armazón de huesos y pellejo
de pasear una cabeza loca
se halla cansado al fin, y no lo extraño,
pues aunque es la verdad que no soy viejo,
de la parte de vida que me toca
en la vida del mundo, por mi daño
he hecho un uso tal, que juraría
que he condensado un siglo en cada día.

Así, aunque ahora muriera,
No podría decir que no he vivido;
que el sayo, al parecer nuevo por fuera,
conozco que por dentro ha envejecido.

Ha envejecido, sí; ¡pese a mi estrella!
Harto lo dice ya mi afán doliente;
que hay dolor que al pasar su horrible huella
graba en el corazón, si no en la fuente

**Gustavo Adolfo Bécquer**

Quisiera empezar agradeciendo a mi tutor, el Dr. Albert Moyano, por todo el conocimiento transmitido a lo largo de toda la Tesis Doctoral, así como por todos los momentos vividos. Ha sido un placer trabajar bajo tu tutela. Agradecer también al Dr. Xavier Companyó por toda la ayuda en estos dos últimos años, sin él no hubiéramos llegado a desarrollar el proyecto hasta el objetivo marcado. También acordarme del Dr. Joaquim Crusats por todo el tiempo dedicado a que este trabajo pudiera realizarse correctamente y la enseñanza sobre las porfirinas. Gracias a vosotros he podido realizar este trabajo y desarrollarme como químico.

Acordarme de toda la gente que ha pasado por el laboratorio estos últimos cuatro años. Al Dr. Aitor Arlegui, eskerrik asko irakatsi zenidan denbora guztiagatik eta bizitako uneengatik. A Marc por empezar juntos este proyecto. A Marian y Lucas porque, pese a las circunstancias que nos tocó vivir, me gustó mucho trabajar y aprender de vosotros. A Ana y Laura por todos los momentos, dramas, frustraciones y risas compartidos tanto fuera como dentro del laboratorio, me llevo a dos grandes personas. A Mario y Jordi por compartir conmigo la última (y más difícil) etapa de la Tesis, gracias por hacerme más ameno el proceso. A Diego por todo lo aportado al desarrollo del proyecto. Todo esto también es parte vuestra.

Agradecer a los compañeros del Departamento. A Fernanda por mantenerme siempre al día de los cotilleos (lo que te gusta a ti marujear). A Araceli (no solo por ser la mejor química inorgánica de toda España y aguantarme una semana en Granada), Clara, Edu, Elías, Gabriela y por amenizar la hora de comer, las conversaciones random y los diversos momentos vividos fuera de la Facultad, ojalá os hubiera conocido antes. A Oliver, un gran químico, muchas gracias por todo el tiempo que invertiste en ayudarme a solucionar algunos de los problemas que fueron surgiendo durante el transcurso de esta Tesis, sin ti, nada de esto hubiera sido posible.

Arnav, darling, it was a great pleasure to have met you. To my two favorite Croatian girls, Lucija and Megie, I celebrate the great friendship created, jebeno dobar izlet! To Stephany for all gossip times while working.

Acordarme, por supuesto, de Josep, por ayudarme tantísimo en los múltiples dramas que he tenido con el HPLC, y de Toñi, por aportar su alegría cada vez que entraba al laboratorio. No por último tiene que ser menos importante, tengo que darle las gracias a Suchi por el diseño de la portada.

Acordarme de mis amigos, en especial a Sibil y a Zafra por aguantarnos desde primero de carrera, por muchísimos años más con vosotros, a Jeanette por ser única y a miniña por la suerte que tuve de conocerte y por continuar esto más allá de febrero. Finalmente, acordarme de la familia, porque sin ellos nada de esto hubiera sido posible. No te preocupes padre que ya me voy de casa.

The present work has been carried out at the Chirality Emergence, Amplification and Transfer Research Group (CHEAT, 2022 SGR 02), and has been funded by FEDER, Ministerio de Ciencia, Innovación y Universidades, through the research projects CTQ2017-87864-C2-1-P and PID2020-116846GB-C21.


## CHAPTER INDEX

## SUMMARY

**Keywords:** *Aldehydes, Asymmetric Catalysis, Diazoacetates, Diels-Alder, Organocatalysis, Photoredox Catalysis, Porphyrins, $\alpha$-alkylation*

Visible-light photocatalysis is currently one of the hottest research areas in organic chemistry, due to the possibility that offers to form C-C and C-Het bonds in a green, non-toxic and efficient way. Although visible-light photocatalysis has been the object of unabated interest in the last few years, the development of catalytic enantioselective light-driven processes is still an extremely challenging task. That is why a large number of research groups have dedicated their efforts to trying to make photocatalysis coexist with asymmetric catalysis. In this sense, asymmetric photocatalytic transformations have been successfully achieved by using two different methodologies; the so-called dual catalysis, where photocatalysts are combined with chiral co-catalysts that work in a tandem fashion for a single chemical reaction, and the so-called, bifunctional catalysis, where a single catalyst perform both photo- and organo-catalysis, being the latter the less explored methodology due to the complexity of finding and synthesizing a suitable bifunctional catalyst.

In the last years, porphyrins, such as *meso*-tetraphenylporphyrin (TPP), have showed up as a suitable organic photocatalyst for the development of new methodologies for the construction of new C-C and C-Het bonds, thus avoiding the use of metal-based photocatalysts. In this field, some recent works show their capacity for acting as photoredox catalysts in the racemic organophotocatalytic $\alpha$-alkylation reaction of aldehydes with diazoacetates, being unexplored their asymmetric version.

In the light of our interest of new catalytic applications of porphyrins, we were particularly attracted by these reports. This present work is focused on the study of the asymmetric Diels-Alder cycloaddition in both thermal and photochemical conditions and development of a practical enantioselective version of the organophotocatalytic $\alpha$-alkylation of aldehydes with diazoacetates. Moreover, we present different porphyrin-based bifunctional photoaminocatalysts based on the combination of both an organocatalyst (chiral secondary amines) and a photocatalyst (porphyrin).

# RESUMEN

**Palabras clave:** *Aldehídos, Catálisis Asimétrica, Catálisis fotoredox, Diazoacetatos, Diels-Alder, Organocatálisis, Porfirinas, $\alpha$-alquilación*

La fotocatálisis con luz visible es actualmente una de las áreas de investigación más candentes en química orgánica, debido a la posibilidad que ofrece de formar enlaces C-C y C-Het de una manera no tóxica y eficiente. Aunque la fotocatálisis con luz visible ha sido objeto de un gran interés en los últimos años, el desarrollo de procesos catalíticos enantioselectivos mediados por luz sigue siendo extremadamente difícil. Por ello, un gran número de grupos de investigación han dedicado sus esfuerzos a intentar que la fotocatálisis coexista con la catálisis asimétrica. En este sentido, las transformaciones fotocatalíticas asimétricas se han logrado con éxito utilizando dos diferentes metodologías; la llamada catálisis dual, donde un fotocatalizador se combina con un co-catalizador quiral que trabajan en tándem para una única reacción química, y la llamada catálisis bifuncional, donde un único catalizador realiza tanto las funciones de foto- y organo-catalizador, siendo esta última la metodología menos explorada debido a la complejidad de encontrar y sintetizar un catalizador bifuncional adecuado.

En los últimos años, las porfirinas, como la *meso*-tetrafenilporfirina (TPP), han aparecido como un fotocatalizador orgánico adecuado para el desarrollo de nuevas metodologías para la construcción de nuevos enlaces C-C y C-Het, evitando de esta manera el uso de fotocatalizadores basados en metales. En este campo de investigación, algunos trabajos recientes muestran la capacidad de estas de actuar como catalizadores fotoredox en la reacción organofotocatalítica racémica de $\alpha$-alquilación de aldehídos con diazoacetatos, estando su versión asimétrica inexplorada.

Debido a nuestro interés por las nuevas aplicaciones catalíticas de las porfirinas, nos sentimos especialmente atraídos por estos trabajos. El presente trabajo se centra en el estudio de la cicloadición asimétrica de Diels-Alder bajo tanto condiciones térmicas como fotoquímicas y en el desarrollo de una versión enantioselectiva para la $\alpha$-alquilación de aldehídos con diazoacetatos. Además, presentamos diferentes fotoaminocatalizadores bifuncionales basados en porfirinas mediante la combinación de un organocatalizador (aminas secundarias quirales) y un fotocatalizador (porfirina).

The following criteria have been followed in this report for the use of acronyms and abbreviations. Below is shown a list of abbreviations and acronyms that have been used.

**ACDC:** Asymmetric Counteranion-Directed Catalysis
**ACN:** Acetonitrile
**AcOEt:** Ethyl Acetate
**AcOH:** Acetic Acid
**aq.:** Aqueous
**ATP:** Adenosine Triphosphate
**BNAH:** 1-Benzyl-1,4-dihydronicotinamide
**Boc:** *tert*-Butyloxycarbonyl
**$Boc_2O$:** Di-*tert*-butyl dicarbonate
**cat.:** Catalyst
**Cbz:** Carbobenzyloxy
**COF:** Covalent-Organic Framework
**COSY:** Correlation Spectroscopy
**DABCO:** 1,4-Diazabicyclo[2.2.2]octane
**DCM:** Dichloromethane
**DIPEA:** *N,N*-Diisopropilethylamine
**DMF:** *N,N*-Dimethylformamide
**DMSO:** Dimethyl Sulfoxide
**DNA:** Deoxyribonucleic Acid
**DNP:** 2,4-Dinitrophenol
**Dr:** Diastereomeric Ratio
**EDA:** Ethyl Diazoacetate
**ee:** Enantiomeric Excess
**equiv.:** Equivalents
**ESI:** Electrospray Ionization
**ET:** Energy Transfer
**FG:** Functional Group
**HPLC:** High-Performance Liquid Chromatography
**HRMS:** High Resolution Mass Spectroscopy
**HSQC:** Heteronuclear Single Quantum Coherence
**$H_2TPPS_4$:** 5,10,15,20-(Tetra-*p*-sulfonatophenyl)porphyrin

**HOMO:** Highest Occupied Molecular Orbital

**IEDDA:** Inverse Electronic Demand Diels-Alder

**IR:** Infrared

**IPA:** Isopropyl Alcohol

**ISC:** Intersystem Crossing

**IUPAC:** International Union of Pure and Applied Chemistry

**KHDMS:** Potassium bis(trimethylsilyl)amide

**Lm:** Lumen

**LUMO:** Lowest Unoccupied Molecular Orbital

**MOF:** Metal-Organic Framework

**MMFF:** Molecular Mechanics Force Field

**MS:** Mass Spectroscopy

**$Na_4TPPS_4$:** Sodium 4,4',4'',4'''-(Porphyrin-5,10,15,20-tetrayl)tetrabenzenesulfonate

**NaOAc:** Sodium Acetate

**NHC:** N-Heterocyclic Carbene

**NMR:** Nuclear Magnetic Resonance

**NOESY:** Nuclear Overhauser Effect Spectroscopy

**PCC:** Pyridinium Chlorochromate

**PET:** Photo-induced Electron Transfer

**PMP:** *p*-Methoxyphenyl

**PTC:** Phase-Transfer Catalysis

***p*-TsOH:** *para*-Toluenesulfonic Acid

**RC:** Rauhut-Currier

**ROESY:** Rotational Overhauser Effect Spectroscopy

**Rh(TSPP):** Rhodium(III) 5,10,15,20-tetrakis(*p*-sulfonylphenyl)porphyrin

**RPE:** Retinal Pigment Epithelium

**SCE:** Saturated Calomel Electrode

**$S_EAr$:** Aromatic Electrophilic Substitution

**SET:** Single Electron Transfer

**SOMO:** Singly-Occupied Molecular Orbital

**$S_N2$:** Bimolecular Nucleophilic Substitution

**TEMPO:** 2,2,6,6-Tetramethyl-1-piperidinyloxyl

**THF:** Tetrahydrofuran

**TLC:** Thin Layer Chromatography

**TMS:** Trimethylsilyl (or Tetramethylsilane)

**TPFPP:** 5,10,15,20-Tetrakis(pentafluorophenyl)porphyrin

**TPP:** 5,10,15,20-Tetraphenylporphyrin

**UV-Vis:** Ultraviolet-Visible

# CHAPTER 1. INTRODUCTION

## 1.1. ASYMMETRIC ORGANOCATALYSIS

The use of small chiral organic molecules as catalysts for the enantioselective construction of chiral compounds is known as asymmetric organocatalysis. Although several enantioselective chemical transformations that used exclusively organic chiral molecules as promoters had already been reported, it was not until 2000 than the foundations of this new domain were laid with the publication of two important articles in the field by MacMillan and collaborators[1] and by List, Barbas III and Lerner.[2]

Due to the multitude of advantages that offers this new area, (for instance, those of using cheap and affordable catalysts, and the possibility of running most reactions in open-air conditions with simple laboratory equipment) in the past two decades it has been stablished as an alternative to enzymatic or to metal-promoted catalysis, especially for the obtention of products with applications in medicinal chemistry.[3,4] In this context, two key points must be emphasized:

- Green chemistry → Organocatalytic chemistry is focusing its efforts on trying to recreate well-established procedures for the formation of building blocks, such as those based on Michael or aldol reactions, that can take place in aqueous media. The avoidance of volatile and harmful organic solvents, as well as toxic and expensive transition metals, opens a whole range of possibilities in green chemistry.[5,6]

- Modes of activation → Several modes of activation are operative in asymmetric organocatalytic reactions. From a mechanistic perspective, organocatalytic modes of activation can be classified according to (a) the covalent or non-covalent character of the substrate-catalyst interactions and (b) the chemical nature of the organocatalyst (Brønsted acid/base, Lewis acid/base…). The different modes of activation involved in asymmetric organocatalysis are summarized in Figure 1.[7]

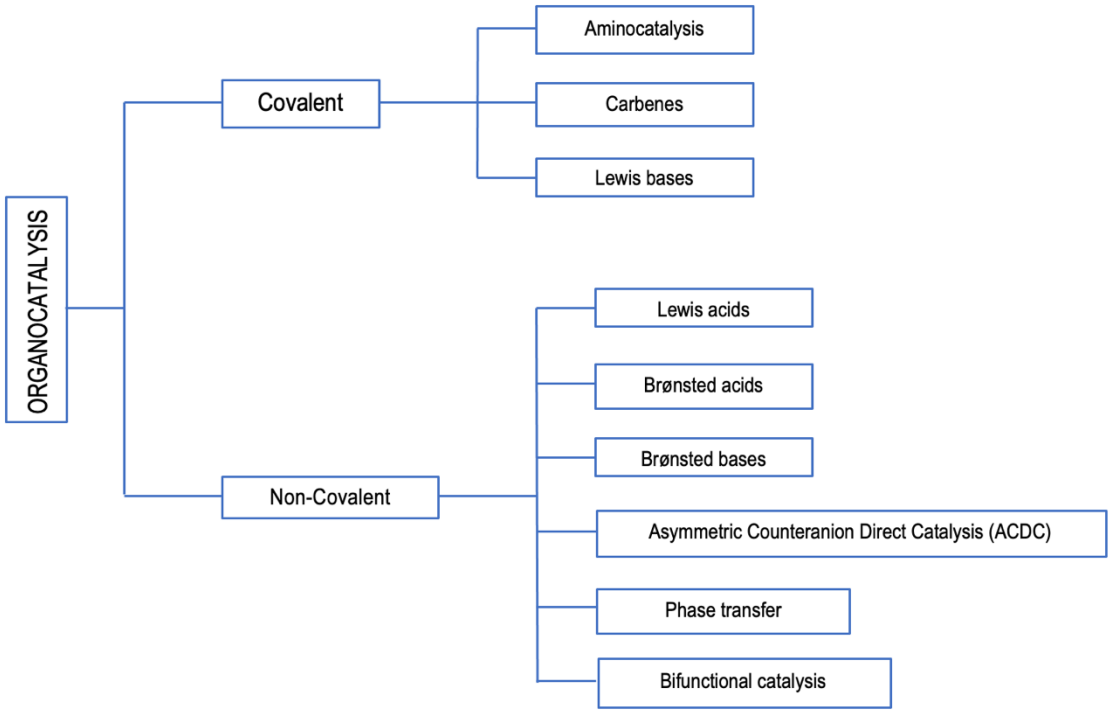


Figure 1. Modes of activation in asymmetric organocatalysis.

This work is based on the use of amines as catalysts that lead to the formation of nitrogenated reactive intermediates (aminocatalysis). According to the chemical nature of those intermediates, aminocatalytic processes can be classified into enamine- and iminium ion-promoted catalysis.

### 1.1.1. L-PROLINE AS AN ASYMMETRIC ORGANOCATALYST

Organic chemists observed that some small chiral organic molecules such as α-aminoacids could catalyze aldol and Michael reactions. In this context L-Proline plays a domineering role.

L-Proline is the only one of the 21 proteinogenic aminoacids containing a pyrrolidine moiety in its structure. This singularity gives a great advantage over the other aminoacids in the formation of an enamine intermediate. That is why in the beginnings of the 1970s, Hajos *et. al.* and Wiechert *et. al.* independently reported the first enantioselective *intramolecular* direct aldol reaction catalyzed by L-Proline, known as the Hajos-Parrish-Eder-Wiechert-Sauer reaction (Figure 2).[8,9]

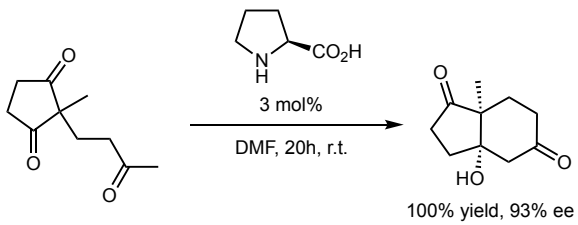


Figure 2. First enantioselective aldol reaction catalyzed by L-Proline.

Although this reaction was extensively used, especially in the field of stereoselective steroid synthesis, it was not until three decades later, when the first L-Proline catalyzed enantioselective *intermolecular* direct aldol reaction was reported by List, Barbas III and Lerner in organic media (Figure 3).[2]

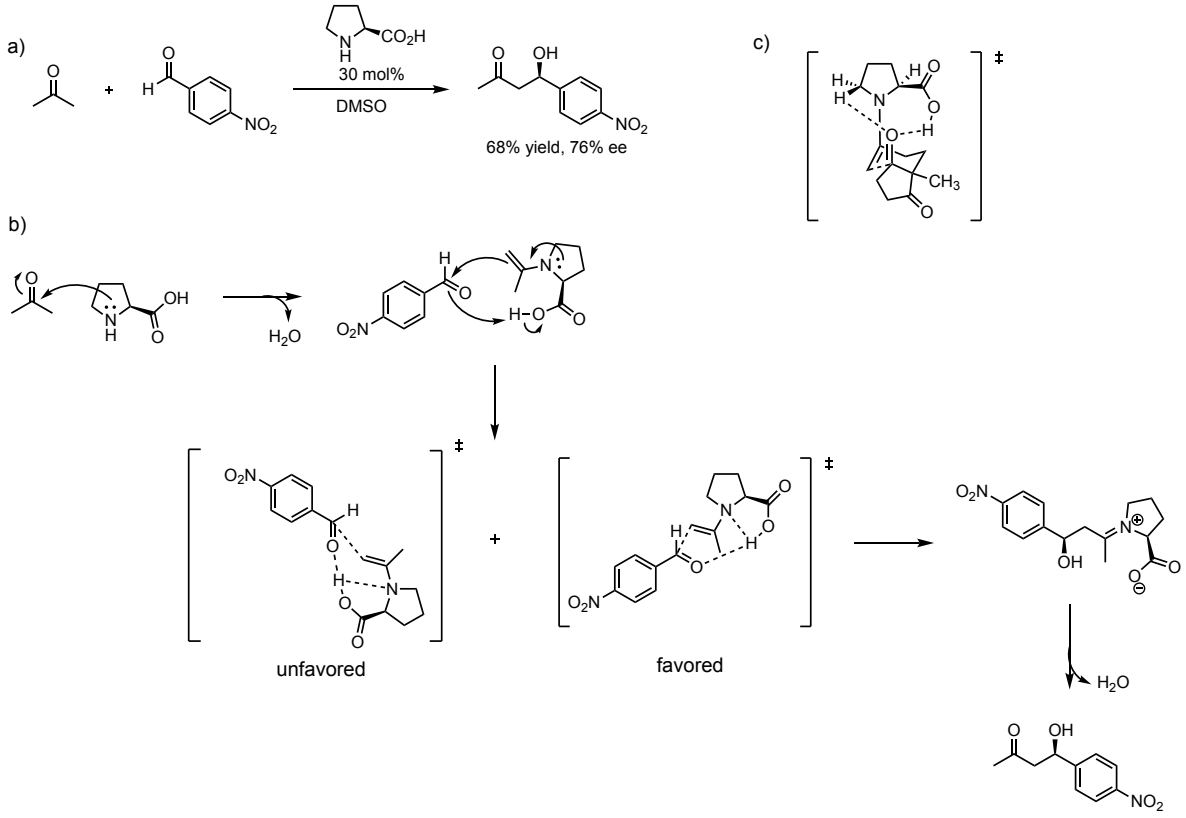


Figure 3. (a) Barbas-List L-Proline catalyzed intermolecular aldol reaction, (b) Proposed mechanism for the intermolecular aldol reaction and (c) Proposed transition state for the Hajos-Parrish-Eder-Wiechert-Sauer reaction.

As shown in Figure 3b, L-Proline is capable of reacting with acetone leading to the formation of an enamine. We could define this first stage as one of the key points of the reaction due to the fact that this enamine gives up electrons more easily than the starting carbonyl. It is important to note that is the acid group of L-Proline the one that regulates the enantioselectivity of the reaction, directing the approach of the aldehyde. This is defined as the other key point of the reaction, since

this direct approach gives rise to two cyclic transition states of six atoms, where one of them (the so-called List-Houk transition state) is much more favored due to a minimization of the repulsive energetic interactions between both reagents. Finally, the nucleophilic attack takes place, generating an intermediate iminium ion that, via hydrolysis, leads to the final product.

Likewise, another reason why the List-Houk mechanism is of great importance is the fact that it allowed to understand the enantioselectivity observed in the Hajos-Parrish-Eder-Wiechert-Sauer reaction, by means of the proposed intermediate shown in Figure 3c.

One of the main problems of using L-Proline as catalyst is the low solubility that it has in non-protic solvents, and that is why both Hajos, Wiechert and List used very polar organic solvents, such as DMF or DMSO. Later on, Pihko *et. al.* observed that L-Proline catalyzed reactions were accelerated by the addition of 1 to 10 equivalents of water into the organic media and demonstrated that an appropriate volume of water can remarkably enhance the rate as well as the enantioselectivity.[10,11]

Another source of problems is the carboxylic acid group of L-Proline, that in spite of being essential for the catalysis, can lead to secondary reactions, such as the acid group decarboxylation. Due to this fact, organic chemists have developed several L-Proline derivatives lacking the carboxylic acid, in order to achieve good yields and stereoselectivities. Some examples are shown in Figure 4 and are discussed below.

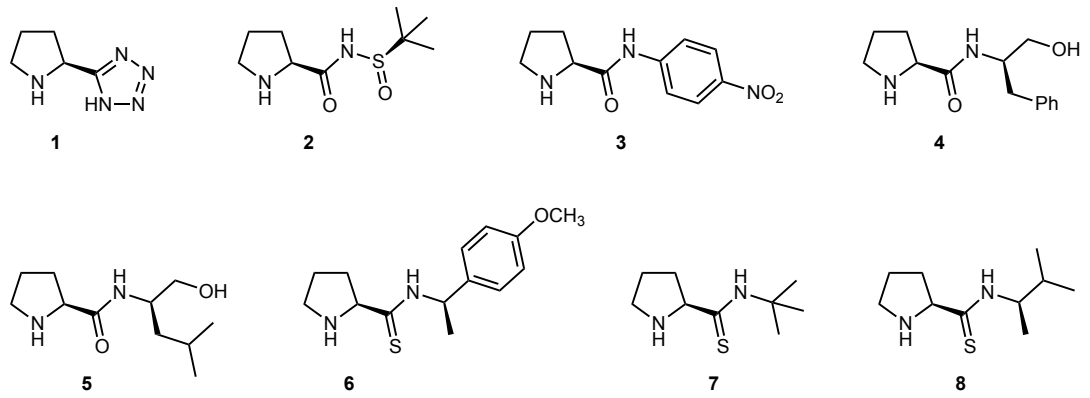


Figure 4. Alternative derivates of L-Proline used as catalysts.

In 2004, Ley *et. al.* reported the synthesis of tetrazole **1** and its use in different asymmetric Mannich-type reactions. In the article the authors reported high enantioselectivities (95-99%) by reacting different cyclic and acyclic carbonyl-containing compounds with *N*-PMP-protected $\alpha$-imino

ethyl glyoxylate.[12] In the same year, Yamamoto *et. al.* reported the use of the tetrazole **1** as a catalyst for different aldol reactions, reporting highly enantioselectivities (82-97%).[13]

In 2011, Robak *et. al.* demonstrated the utility of *N*-sulfinyl amide **2** for the enantioselective aldol reaction between *p*-nitrobenzaldehyde and acetone. Highly enantioselectivities (89-96% ee) were obtained.[14]

In 2009, Chimni *et. al.* reported highly diastereo- (96/4) and enantioselective (88-96% ee) direct asymmetric aldol reactions between *p*-nitrobenzaldehyde and cyclohexanone when the (*L*)-prolinamide derivate **3** was used as organocatalyst and the reaction was performed in a pH range of 4-5.[15]

In 2003, Wu and co-workers reported high enantiomeric excesses (33-93%) while using L-prolineamide derivatives, as compounds **4** and **5**, in the direct asymmetric aldol reaction between 4-nitrobenzaldehyde and acetone.[16]

In 2006, Gryko *et. al.* reported highly enantioselective (37-99%) in direct asymmetric aldol reactions between *p*-cyanobenzaldehyde and acetone when a 20 mol% of L-prolinethioamide derivatives, as compounds **6**-**8**, were used as the catalyst.[17] In the article it was demonstrated that the higher acidity of the thioamide NH group compared with amido NH group increased both the reactivity and the enantioselectivities of the aldol reactions, which implies that the thioamide group is able to form stronger hydrogen bonds with the aldehyde, following the Houk-List mechanism shown in Figure 3b.

### 1.1.2. ASYMMETRIC AMINOCATALYSIS

Asymmetric aminocatalysis involves reactions catalyzed by both primary and secondary chiral amines. The catalysis takes place via enamine and/or iminium ion intermediates.

While the Barbas-List proline-catalyzed enantioselective intermolecular aldol reaction stands out as the first clearly formulated example of the potential of chiral enamine intermediates in asymmetric catalysis, the enantioselective, chiral imidazolidinone-catalyzed Diels–Alder reaction described by MacMillan and co-workers in the same year revealed the general applicability of chiral iminium intermediates for this purpose (Figure 5).

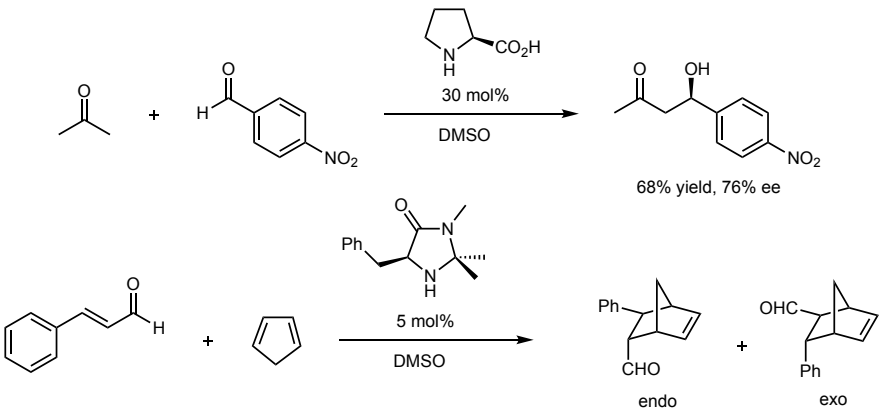


Figure 5. MacMillan's Diels-Alder reaction and List and Barbas III Aldol reaction.

### 1.1.2.1. Asymmetric aminocatalysis via chiral enamines

Asymmetric aminocatalysis taking place through chiral enamines has become one of the most used modes of activation in asymmetric organocatalysis, especially in the study of the enantioselective α-functionalization of enolizable aldehydes and ketones with a wide variety of electrophiles.[18] The general mechanism for the chiral amine-catalyzed α-functionalization of an aldehyde is depicted in Scheme 1.

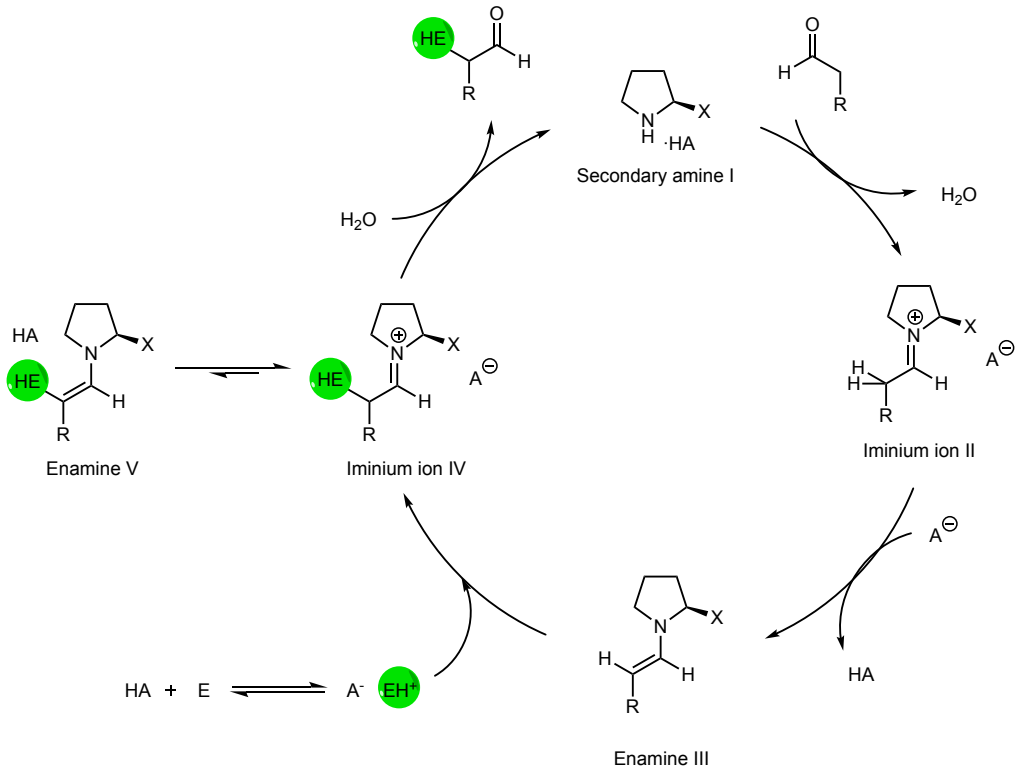


Scheme 1. General mechanism for the α-functionalization of an aldehyde through chiral enamine catalysis.

A chiral 2-substitued pyrrolidine I, acting together with an external Brønsted acid co-catalyst HA, has been chosen as the most representative catalytic system. The catalytic cycle starts with the acid-promoted (HA) condensation between the secondary amine I and the aldehyde to be functionalized, leading to the formation of an iminium ion II. Then, the conjugated base of the acid ($A^-$), by deprotonation of one of the $\alpha$-acidic protons of iminium ion II, produces the key nucleophilic enamine intermediate III. Next, this enamine undergoes a nucleophilic attack to the electrophile, forming iminium ion IV, where a new bond formation can be observed. Notice that iminium ion IV can be in equilibrium with enamine V, but the cycle continues with its hydrolysis, leading to the regeneration of the secondary amine I, the acid co-catalyst (so that the cycle re-starts again) and the desired $\alpha$-functionalized aldehyde.

Obviously, the co-catalyst, a Brønsted acid, can also be introduced as the solvent, or as a functional group of the secondary amine, as it happens in L-Proline and in its derivatives shown in Figure 4.

The catalytic cycle efficiency relies on three factors: (a) the quick and quantitative formation of iminium ion II, (b) the easy conversion of iminium ion II to key enamine III, (c) the nucleophilic activity of key enamine III and (d) the slow direct reaction between aminocatalyst I and the electrophile, which would lead to the deactivation of the secondary amine.

Enamine III is the key intermediate for the determination of the configuration of the reaction product, since the stereochemical curse of the reaction depends on its nature (Scheme 2).

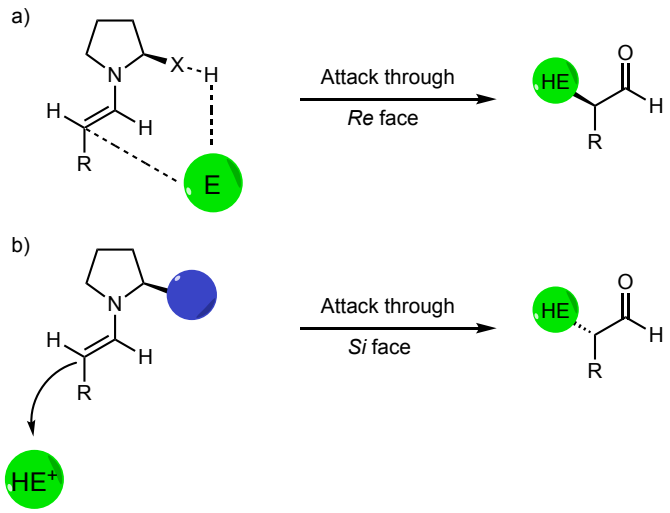


Scheme 2. Stereochemistry model for the $\alpha$-functionalization of carbonyl compounds through enamine catalysis.

If the X substituent contains an acidic hydrogen that can form a hydrogen bond with the incoming electrophile, for instance a carboxylic acid, a tetrazole, an amide or an ammonium ion, the attack will be intramolecular and will take place by the same face in which the chiral substituent is located, following the Houk-List model[19] (Scheme 2a). However, if there is no possibility to form any hydrogen bond, the attack will be directed by steric effects and will take place by the face to that occupied by the substituent (Scheme 2b).[7b]

### 1.1.2.2. Asymmetric aminocatalysis via chiral iminium ions

The other important mode of activation in asymmetric aminocatalysis is iminium catalysis. The general concept of chiral iminium catalysis was introduced by MacMillan in the context of the imidazolidinone catalysis of enantioselective Diels–Alder reactions,[1] and was soon extended to the asymmetric β-functionalization of α,β-insaturated aldehydes, via Michael reaction.[20,21]

The MacMillan mechanism for the catalysis of the Diels-Alder reaction between cinnamaldehyde and cyclopentadiene by a chiral imidazolidinone is shown in Scheme 3.

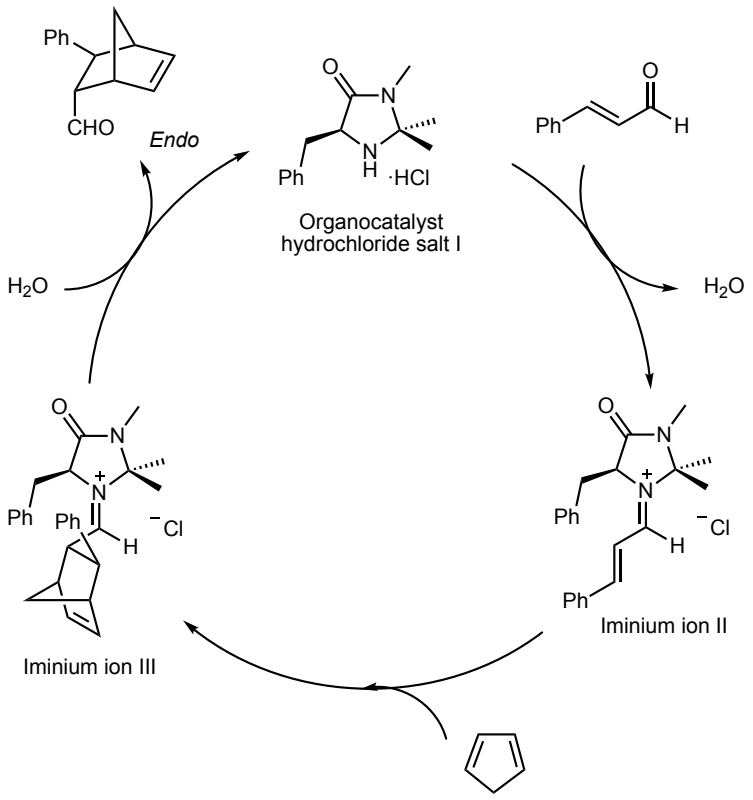


Scheme 3. Mechanism for the chiral imidazolidinone-mediated Diels-Alder reaction between cinnamaldehyde and cyclopentadiene via chiral iminium ion catalysis.

The catalytic cycle starts with the acid-promoted condensation between the organocatalyst hydrochloride salt I and the α,β-unsaturated aldehyde (cinnamaldehyde), leading to the formation of key iminium ion II, that is much more electrophilic than the aldehyde and readily undergoes the Diels-Alder reaction with the dienophile (cyclopentadiene), forming intermediate III. This iminium intermediate, by hydrolysis, leads to the regeneration of the hydrochloride salt of the aminocatalyst I (so that the cycle starts again) and the desired cycloaddition product.

The catalytic cycle efficiency was attributed to (a) the LUMO-lowering activation in the condensation step between organocatalyst I and cinnamaldehyde and (b) the kinetic lability of iminium ion II.[1]

Iminium ion II is the "key intermediate" of the reaction since the stereochemistry curse of the reaction depends on its structure (Scheme 4).

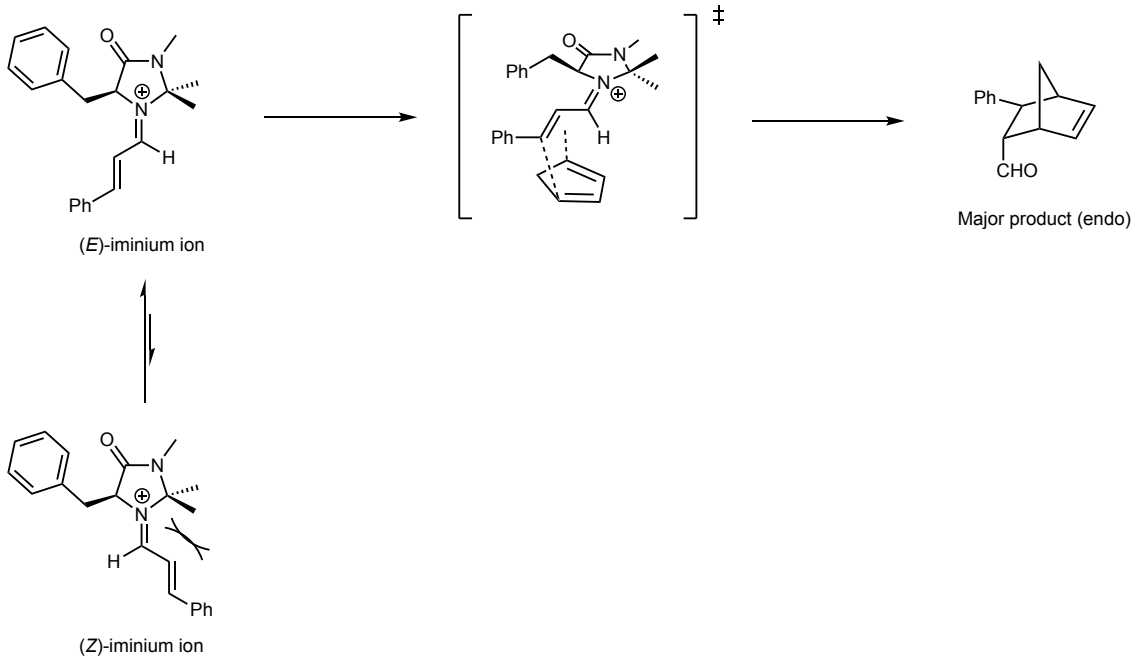


Scheme 4. Stereochemistry control proposed by MacMillan and co-workers for the Diels-Alder reaction catalyzed by chiral iminium ion.

To understand we have to take a look in two important points (a) the formation of (*E*)-iminium ion, where its selectivity reasons to avoid the non-bonding interactions with the two geminal methyl and (b) the benzyl group, that is blocking *Re* face (by π stacking interactions) and exposing *Si* face for the cycloaddition reaction.

## 1.2. PORPHYRINS[22]

### 1.2.1. GENERAL INTRODUCTION

Porphyrins are a group of heterocyclic macrocycle organic compounds constituted by four pyrrole subunits cyclically interconnected by methine bridges through their Cα. The most simple structure is porphine (Figure 6a), a chemical compound of exclusively theoretical interest. Porphyrins, then, are substituted porphines.[23]

Porphyrin's stability is linked to the tetrapyrrolic macrocycle, due to the presence of a planar, continuous cycle of 18 π electron system, conferring aromaticity to the molecule (Figure 6b). With a total of 26 π electrons, porphyrins typically absorb strongly in the visible region of the electromagnetic spectrum, *i.e.*, they are deeply colored.

The porphyrin nucleus can be found in synthetic molecules, such as phthalocyanines. Porphyrins have been also the target of many studies in biological chemistry [24-26] since their role in the metabolism of living organisms was discovered.[27] The basic porphyrin structure is present in many important biomolecules, such as hemoglobin (involved in blood oxygen-transport) or vitamin $B_{12}$, necessary for the correct function of the brain[28] (Figure 6c).

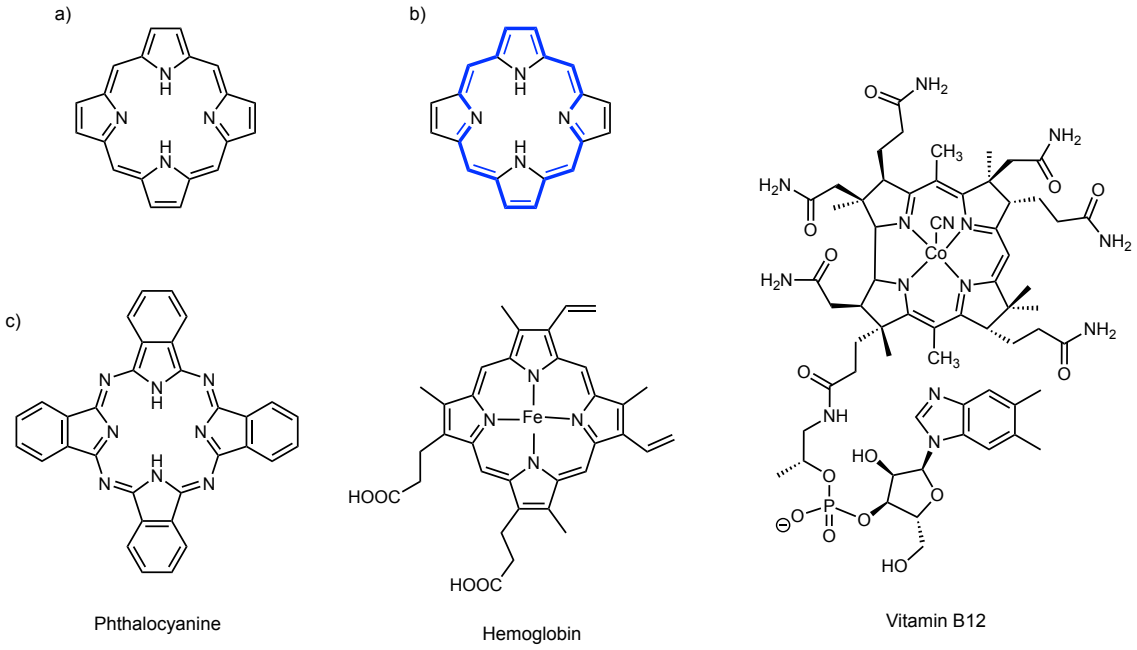


Figure 6. a) Porphine structure, b) cyclic 18 π electron system for porphine and c) some examples of important porphyrin-based structures.

In 1963, Gouterman and co-workers[29] proposed the so-called "four orbital" model, that explained qualitatively the UV-Vis spectra of porphyrins. According to this model, the absorption bands of porphyrins arise from the four possible electronic transitions between the two degenerated highest occupied π orbitals, $a_{1u}$ and $a_{2u}$, and the two degenerated lowest unoccupied π* orbitals, $e_{gx}$ and $e_{gy}$ (Figure 7a, b). Although in principle these four transitions should take place at the same wavelength, the interaction between the four possible singlet excited states gives rise to the two main groups of transitions observed in the UV-Vis spectra of the porphyrins (Figure 7c). The first one, appearing between 400-475 nm, is called the Soret band and corresponds to the transition between the ground state ($S_0$) and the higher energetic excited states ($S_2$). The second group, observed between 550-700 nm and that is responsible of the porphyrin color, corresponds to transitions (Q bands) between the ground state ($S_0$) and the lower energetic excited states ($S_1$).

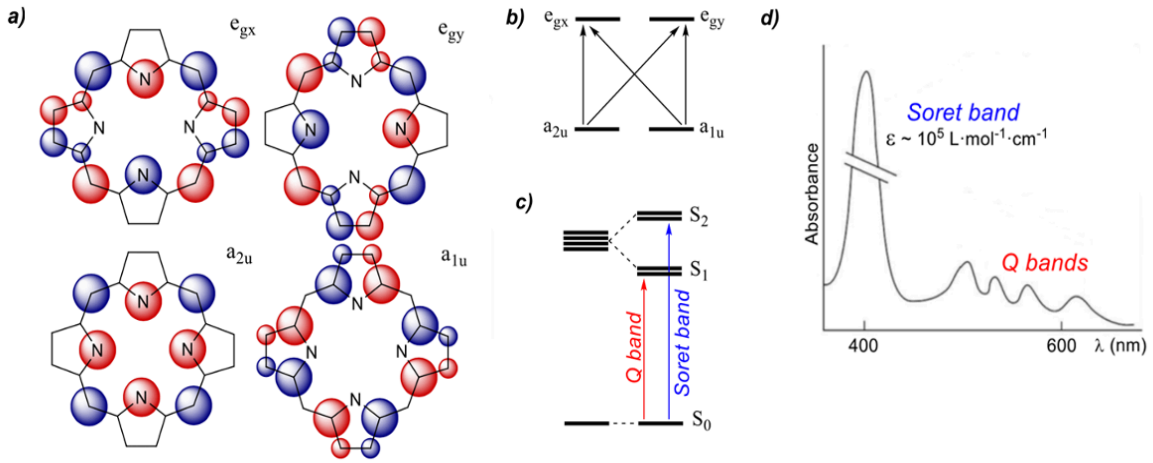


Figure 7. a) Representation of the four Gouterman's orbitals for porphyrins. b) Electronic transitions between doubly degenerate HOMO and LUMO. c) Energy levels and electronic transitions between electronic levels. d) Typical UV-Vis spectra of a porphyrin[30]

### 1.2.2. ACIDITY OF PORPHYRINS

The species found in a porphyrin solution depend fundamentally on the pH of the medium (Scheme 5). In neutral medium, porphyrins are found in its free-base form ($H_2P$), with two protons inside the macrocycle center, presenting a bright purple color. In a strongly basic medium, the pyrrolic nitrogens can be deprotonated, forming the deprotonated monomer ($P^{-2}$). On the other hand, in acidic medium (pH < 4.5), all pyrrole units of the porphyrins core are *N*-protonated ($H_4P^{+2}$), dyeing the solution a dark green color.

$$P^{-2} \underset{-2H^+}{\overset{+2H^+}{\rightleftharpoons}} H_2P \underset{-2H^+}{\overset{+2H^+}{\rightleftharpoons}} H_4P^{+2}$$

Scheme 5. General scheme of porphyrins acid-basic equilibriums.

All these acid-base equilibriums in which the porphyrins are involved, causes that the UV-Vis spectra of porphyrins is dependent on the protonation degree of the porphyrin core (Figure 8). There are two main differences between the UV-Vis spectra of the free-base form ($H_2P$) and the *N*-protonated form ($H_4P^{+2}$) of a porphyrin (a) the shift of the Soret band, with the *N*-protonated porphyrin ($H_4P^{+2}$) showing a greater shift towards the visible region of the spectrum (430-435 nm) than its free-base form ($H_2P$, 410-415 nm), and (b) the wide difference in the Q bands, while in the *N*-protonated form ($H_4P^{+2}$) these appear between 600-680 nm, in the free-base form ($H_2P$) they are observed between 500-550 nm. It is also important to note that the four Q bands in the free-base form of the porphyrin ($H_2P$) are reduced to two in the *N*-protonated form ($H_4P^{+2}$) due to the increase in symmetry when the tetrapyrrolic core of the porphyrin is protonated.

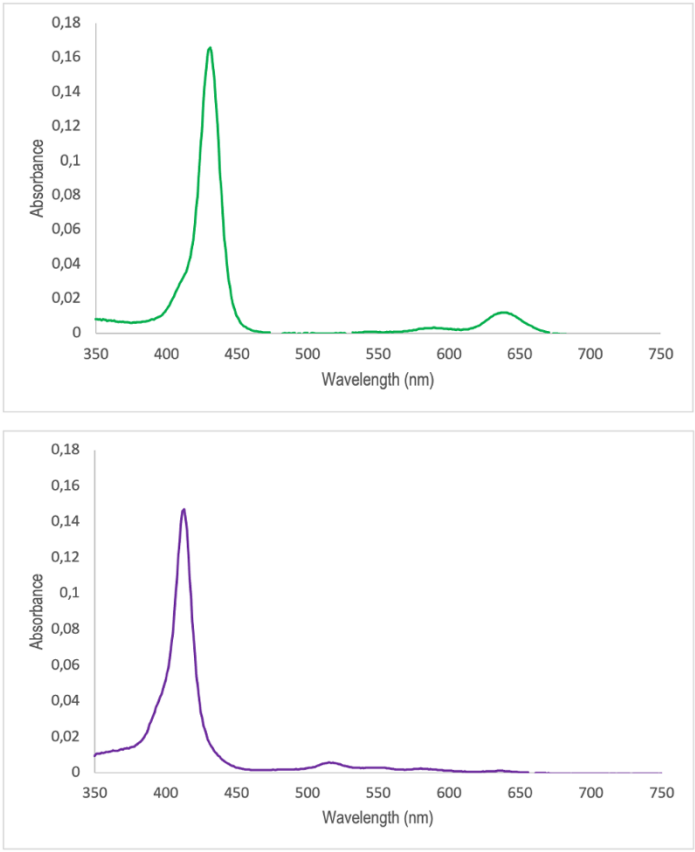


Figure 8. UV-Vis spectra of the diprotonated $H_4P^{+2}$ (pH = 2.78, top) and the neutral $H_2P$ (pH = 5.00, bottom) forms of (*S*)-4,4',4''-(20-(pyrrolidin-2-ylmethyl)porphyrin-5,10,15-triyl)tribenzenesulphonate. Solvent: MilliQ water. Concentration: C = $3.69 \times 10^{-6}$ M. Optical path length: l = 1 dm.

### 1.2.3. SYNTHESIS OF PORPHYRINS

Beyond the area of natural products, there is a wide range of possibilities for the design of synthetic porphyrins for specific applications (Figure 9), (a) metalloporphyrins, where almost every di- and trivalent metal can be coordinated to the porphyrin core, conveying new electronic properties and of interest in electrochemistry, (b) β-pyrrole substituted porphyrins, that, as shown in Figure 6, play an important role in biological chemistry, and (c) *meso*-substituted porphyrins, that are the easiest to synthesize and offer the greatest synthetic variety, with applications in photocatalysis and in supramolecular chemistry.

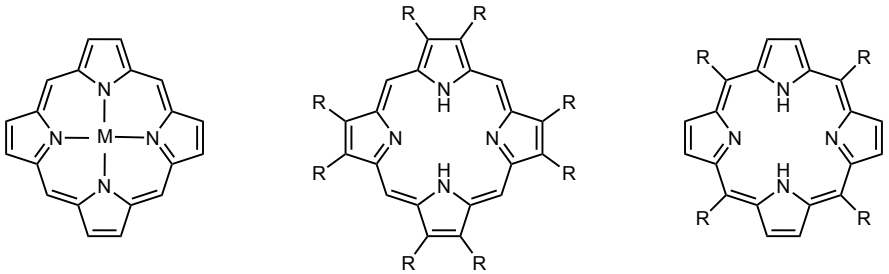


Figure 9. Different structures of substituted porphyrins.

#### 1.2.3.1. Metalloporphyrins

Any porphyrin derivative in which at least one of the central nitrogen atoms forms a bond to a metal atom (M) is called a metalloporphyrin.[31] They are present, for instance, in chlorophyll (M = Mg), hemoglobin (M = Fe) or vitamins (M = Co in vitamin $B_{12}$).

The majority of the metallic elements in the periodic table form equatorial bonds while coordinating with the porphyrins, leading to a square planar geometry, but it was observed that some metals, especially the transition metals, are capable of adding extra axial bonds to the structure, with the possibility of adding one (square pyramidal geometry) or two (tetragonally distorted or octahedral geometry) axial bonds (Figure 10).

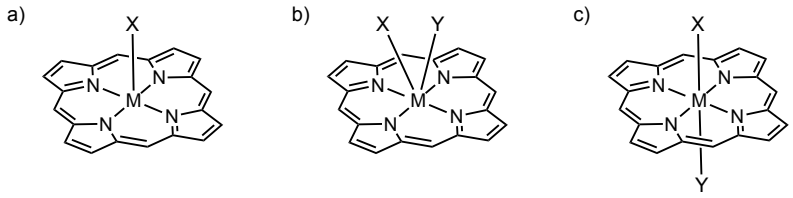


Figure 10. Different substituents spatial layout for metalloporphyrins.

In fact, the geometry of the metalloporphyrin depends on the nature of the hexacoordinated transition metal, since early and lower transition metals are too big to fit in the porphyrin core, coordinating above the plane of the porphyrin core and leading to two axial *cis* ligands (Figure 10b), while middle transition metals lead to two axial *trans* ligands (Figure 10c), due to their smaller size.[32]

The demetallation of porphyrins takes place in an acid medium, substituting the coordinated metal by two protons. In the same way that depending on the metal that coordinates to the porphyrin we have different types of geometry, the same happens with the demetallation, not all metalloporphyrins are demetallized in the same acidic conditions. Empirical demetallation stabilities were defined,[32] using the metal size, the degree of covalent metal-porphyrin bonding and the oxidation state as parameters, leading to the following classification (a) class I, fully resistant to $H_2SO_4$ 98%, (b) class II, demetallized with $H_2SO_4$ 98%, (c) class III, demetallized with HCl 37%, (d) class IV, demetallized with glacial acetic acid, and (e) class V, demetallized in neutral $H_2O$.

The first synthesis of a metalloporphyrin was described in 1920s by Fischer.[33] But, during years, various methods have been developed, being the ones explained next the more used:

- Acetate method[34] → this method is based on the transfer of the relatively acidic NH porphyrin protons to the acetate ion. The porphyrin is heated to reflux with the acetate salt of a divalent metal, and the metalloporphyrin is obtained by crystallization and filtration of the reaction crude. The method is applied to all divalent metal ions, except those that are unstable in acetic acid

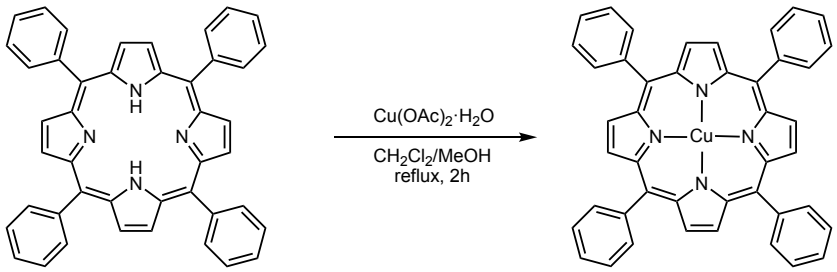


Figure 11. Metalation of 5,10,15,20-tetraphenylporphyrin with copper(II) acetate.

- Taking advantage of Fischer's previous work, Sarkar and co-workers, in 2007, reported an optimized method using chloride salts of divalent metals instead of acetate salts (Figure 12).[35]

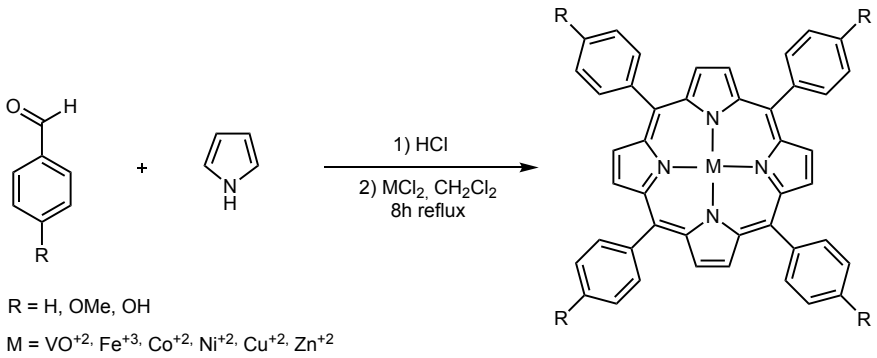


Figure 12. General procedure for the metalation of a porphyrin using a divalent metal chloride.

Metalloporphyrins have been studied due to their many applications in chemistry, such as, molecular recognition,[36] building blocks for tailored materials[37] or molecular electronic devices[38] in material chemistry, electrochemistry[39] or catalytic oxidations and oxidative DNA cleavage[23] and photodynamic therapy agents[40] in photocatalysis.

### 1.2.3.2. β-Pyrrole substituted porphyrins

Porphyrins substituted at the β-pyrrolic positions are specially interesting due to their important role in the metabolism of living organisms, since as it is shown in Figure 6, the vast majority of natural porphyrins have β-pyrrolic substituents. Notice that in all of natural porphyrin-based structures there is a metal coordinated to the N atoms of the tetrapyrrolic macrocycles, favoring electronic transference due to new porphyrin-porphyrin interactions, having importance due to the fact that they participate in a large number of natural of both energy and electronic transfer processes.[41]

The synthesis of β-pyrrole substituted porphyrins is relatively straightforward, since a β-substituted pyrrole can be reacted with an aldehyde in the ring formation process or, once the basic tetrapyrrolic cycle is formed from pyrrole, β-substituents can be added by a $S_EAr$-type reaction to the metallated porphyrin.[42] The need of the metal coordination is because the dianionic character of the porphyrin core in a metallated porphyrin increases the electron density in the pyrrole moieties, facilitating the electrophilic attack, and the potentially nucleophilic N atoms are protected by the N-metal bond. In a subsequent demetallation step, the desired β-pyrrole substituted porphyrin is obtained.

Most applications of β-pyrrole substituted porphyrins are in the field of electrochemistry, for instance, electron transfer processes or the formation of dimers.[43-45]

### 1.2.3.3. *Meso*-substituted porphyrins

Although *meso*-substituted porphyrins do not possess the substitution pattern of natural β-pyrrole substituted porphyrins, they have reached a huge interest in organic chemistry due to their simple synthesis, which allows to access to a wide range of porphyrins that can be applied in many different research fields. In Scheme 6 is shown the mechanistic scheme for the formation of a *meso*-substituted porphyrin by condensation between an aldehyde and pyrrole.

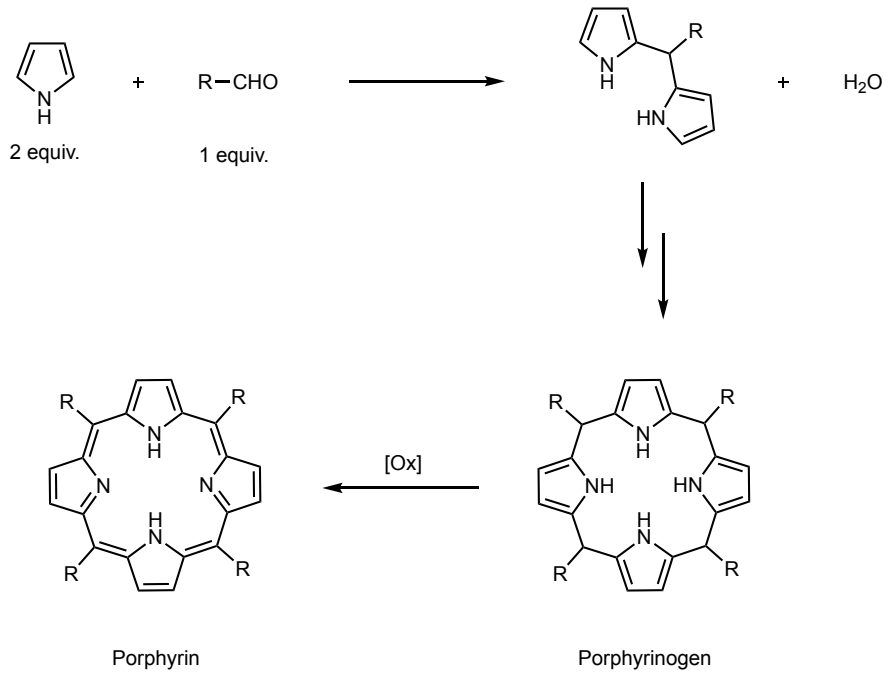


Scheme 6. General mechanistic scheme for the formation of a *meso*-substituted porphyrin.

The first attempts to synthesize a *meso*-substituted porphyrin were due to Rothermund,[46,47] who in 1935 and in 1936 reported the synthesis of *meso*-tetramethylporphyrin and porphine, respectively, by combining pyrrole and the corresponding aldehydes (acetaldehyde and formaldehyde) in high concentrations. Later on, in 1941, Rothermund reported the synthesis of *meso*-tetraphenylporphyrin (TPP) by the condensation of pyrrole and benzaldehyde.[48] Both procedures are based on the same principles, high concentration of both pyrrole and the aldehyde, high temperature and long reaction times. The obtained yields were quite low (7.5-9%).

A more efficient synthetic method for *meso*-substituted porphyrins was developed and reported by Adler and Longo[49] in 1967. The procedure consists in the open-air condensation of pyrrole with an aldehyde in refluxing acetic acid or propionic acid. The porphyrin then, is obtained by crystallization (Figure 13).

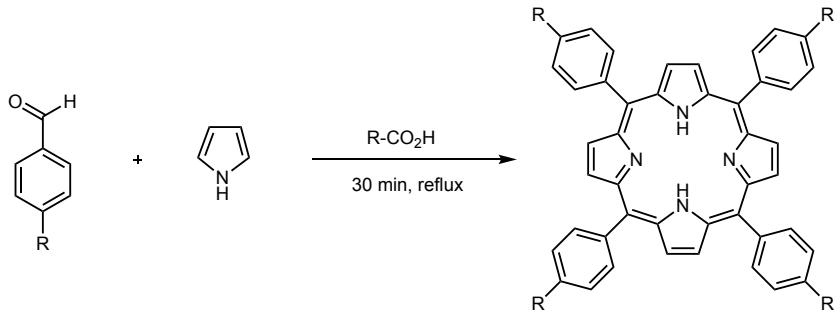


Figure 13. Adler and Longo proposed synthesis of *meso*-substituted porphyrins.

The best yields (25-30%) were obtained when propionic acid was used as solvent. This method allows the synthesis of different and more complex porphyrins by combining pyrrole with different kinds of aldehydes and solved some drawbacks that appeared in Rothermund synthesis, for instance, the use of high concentrations of reagents and the long reaction times, but presents an inconvenient, since Adler and Longo's method is only suitable for aromatic aldehydes.

This problem was solvent by Lindsey,[50] proposing a softer method in two steps (Figure 14) (a) the pyrrole and the aldehyde condensation, which is performed in dichloromethane at room temperature for 3 h in presence of a catalytic amount of a Lewis acid, forming the porphyrinogen, and (b) the porphyrinogen oxidation, by adding *p*-chloranil to the mixture and heating up to reflux for 1 h.

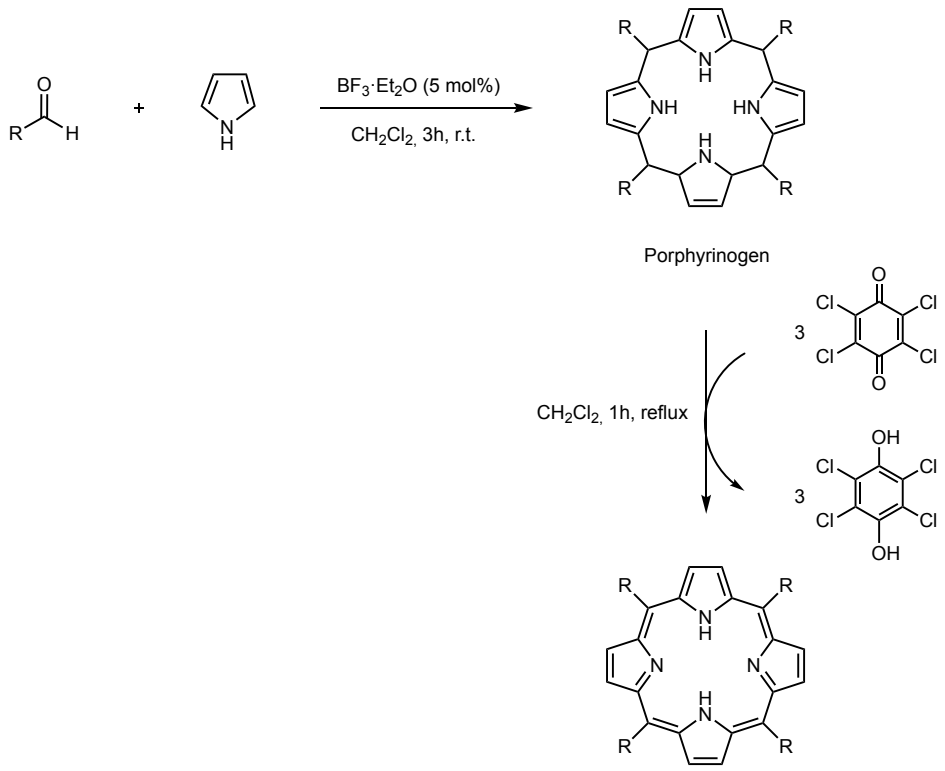


Figure 14. Synthesis of *meso*-substituted porphyrins using Lindsey method.

In order to obtain porphyrins with two different substituents A and B at the *meso* positions, pyrrole has to be condensed with two different aldehydes A-CHO and B-CHO, but this can give rise to a complex mixture of porphyrins (Figure 15). Nevertheless, some unsymmetrical porphyrins can be synthesized with good yields by mixed condensation.[51,52]

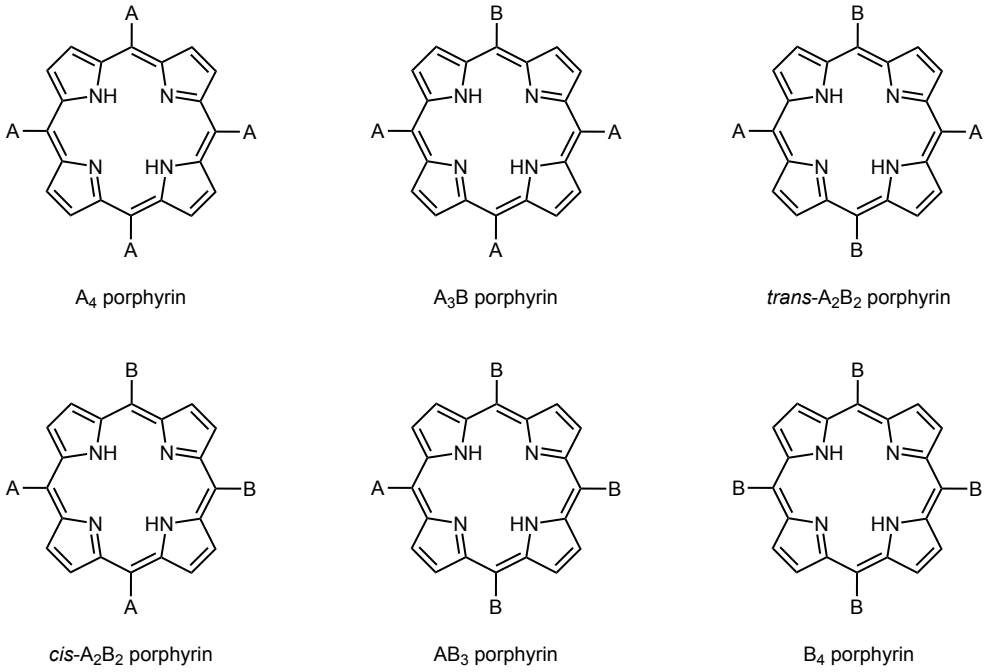


Figure 15. Mixture of porphyrins obtained when pyrrole is reacted with a mixture of aldehydes.

Supposing that the two aldehydes A-CHO and B-CHO have the same reactivity, it can be easily shown (*i.e.*, by finding the maximum value of the function $4 \cdot x^3 \cdot (1-x)$, that represents the statistical yield of the $A_3B$ porphyrin, which is common to want to obtain, with x = molar fraction of aldehyde A-CHO, see Figure below) that the ideal stoichiometry is 3 equivalents of A-CHO per 1 equivalent of B-CHO (x = 0.75). Applying Newton's binomial theorem, the following probabilities are obtained (Figure 16).

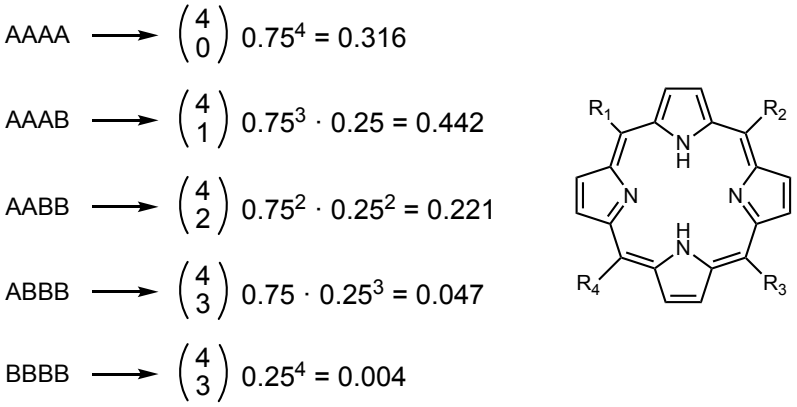


Figure 16. Calculation of the probabilities of obtaining each of the six possible products, using a ratio 3:1 of the aldehydes A–CHO : B–CHO, using Newton's binomial theorem, obtaining both isomers for AABB porphyrins, showing the combined percentage of both of them.

Therefore, assuming an overall 30% yield of porphyrins, yields in the range of 10-15% are expected for the $A_3B$ porphyrin with the Lindsey or the Adler and Longo synthesis, provided that the differently substituted porphyrins can be separated by chromatography. If aldehyde A-CHO is much less polar than B-CHO, the $A_4$ porphyrin will be eluted on the first place and can be easily separated from the remaining components of the mixture; usually, by means of a second, more accurate chromatographic purification, the $A_3B$ porphyrin can be isolated.

Another option for the synthesis of unsymmetrical *meso*-substituted porphyrins relies on the selective functionalization of the $A_4$ porphyrin. In the case of the *meso*-tetraphenylporphyrin, we can perform a $S_EAr$-type reaction, for instance sulfonation or nitration. Since these reactions take place in strongly acidic media, the porphyrin core will be protonated (*Cf*. $TPPH_4^{+2}$). In this way, the β-pyrrolic positions are deactivated towards the electrophilic attack, that will take preferentially place on the phenyl rings, mostly in the *para* positions due to the interplay between electronic and steric effects. Although this procedure will generally lead to mixtures of differently substituted porphyrins, strong differences in polarity will enable the chromatographic purification of the desired

product. As an example, see the preparation of 5-(*p*-nitrophenyl)-10,15,20-tetraphenylporphyrin in Scheme 7.[53]

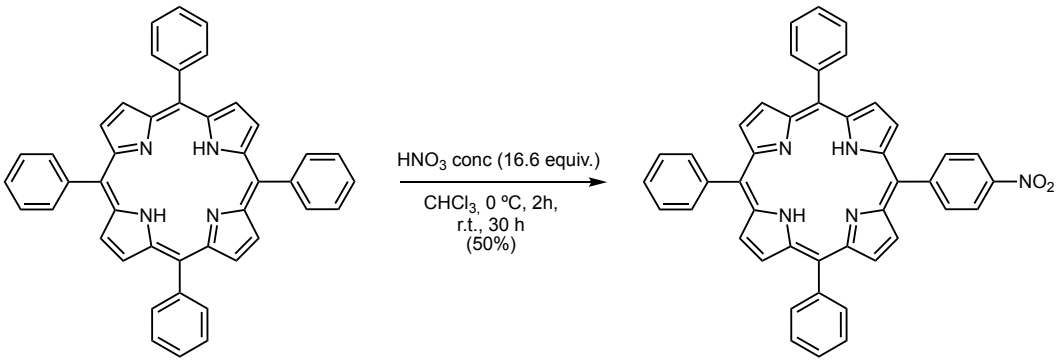


Scheme 7. $S_EAr$ nitration of *meso*-tetraphenylporphyrin. Chromatographic purification: silica gel column, using as eluent a mixture of hexane/$CH_2Cl_2$ (1/1).

### 1.2.4. SELF ASSEMBLY OF PORPHYRINS

Some molecules can form supramolecular aggregates by self-assembly, leading to supramolecular complex structures with different properties than those of their monomers. This phenomenon is called homoassociation and takes place in solution when the solute-solute interactions are more energetically favorable than the solute-solvent ones.[54]

Due to the planarity and the big size of the tetrapyrrolic macrocycle, the aggregation of porphyrins is favored. There are different types of intermolecular interactions that lead to the homoassociation of porphyrins, for instance, $\pi$-$\pi$ weak interactions in free porphyrins or $\pi$-$\pi$ strong interactions in metalloporphyrins.[55]

In solution, there are several factors that influence the aggregation of porphyrins, for example, the nature of the porphyrin, concentration, solvent, pH, ionic forces, temperature or electronic and stereochemical effects. These factors are accentuated in the case of sulfonated porphyrins, especially electronic effects.[56] These aggregates can be classified in two groups, (a) *J*-aggregates (edge-to-edge interaction of the chromophores) and *H*-aggregates (face-to-face interaction of the chromophores).

In aqueous environment, sulfonated porphyrins form *J*-aggregates in acidic medium (pH between 1 and 4), since the tetrapyrrolic macrocycle is protonated and the sulfonate groups are ionized. By switching on of ion-pair contacts between the cationic porphyrin centers and the anionic

sulfonate groups of the periphery, *J*-aggregates are formed (see Figure 17 for a schematic representation of these aggregates of the acidic form of tetra-*meso*-(*p*-sulfonatophenyl)porphyrin, $H_4TPPS_4^{+2}$).

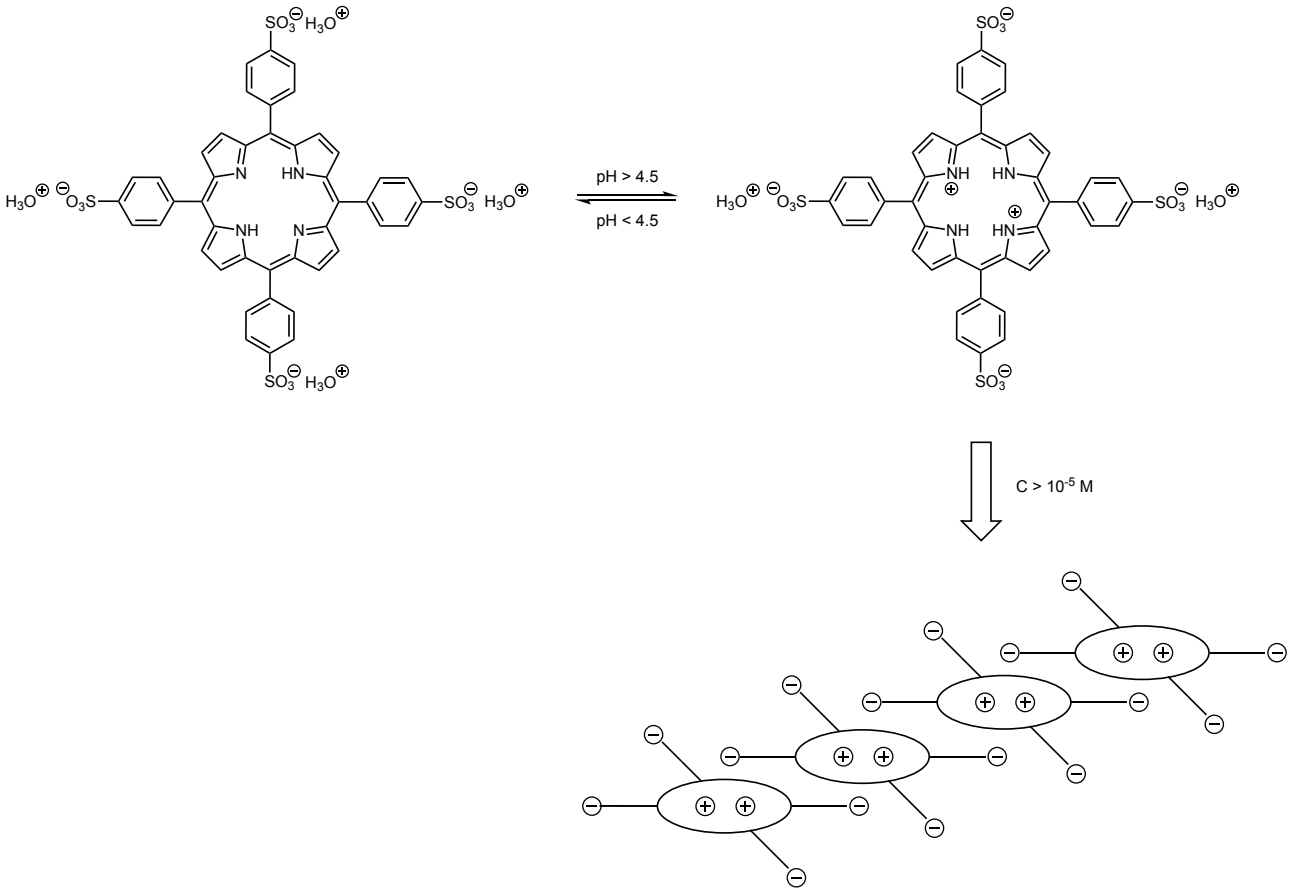


Figure 17. Monodimensional J-aggregate structure of *meso*-(tetra-*p*-sulfonatophenyl)porphyrin.

The self-assembly of porphyrins can be studied by UV-Vis spectroscopy since important changes in the spectra are observed, especially in the Soret Band. In the monomeric deprotonated porphyrin, this band appears at approximately 430 nm, while when the porphyrin is forming *J*-aggregates, it appears at approximately 489 nm as a consequence of a bathochromic shift. In a similar way, the Q bands undergo both a displacement to higher wavelengths and an increase in intensity upon aggregation. At concentrations of $10^{-5}$ M or lower, the deprotonated porphyrin $H_2TPPS_4$ in solution is found in the monomeric form (Figure 18 right). When the concentration reaches de $10^{-4}$ M range, the *J*-aggregate is clearly observed (Figure 18 left).

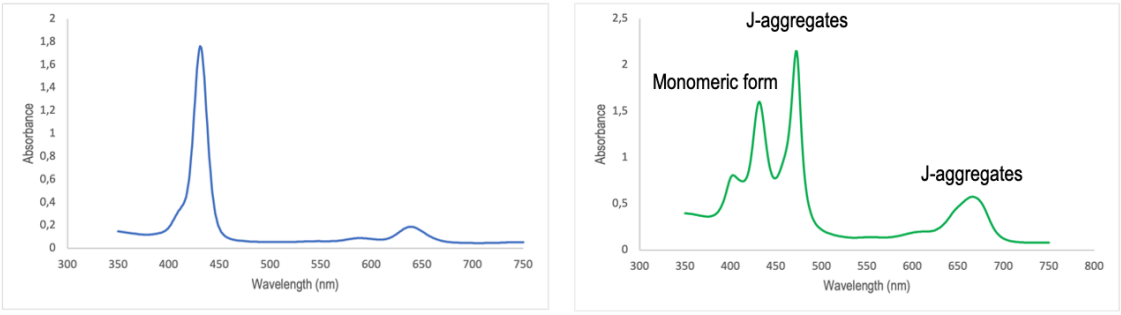


Figure 18. UV-Vis spectra of a porphyrin core protonated porphyrin at different concentration. Right, $3.779 \times 10^{-5}$ M, where the monomers are the major species and left, $1.107 \times 10^{-4}$ M, where the J-aggregates are the major species. Solvent: Aqueous solution of pH 1. Optical path length: l = 1 dm.

## 1.2.5. AMINO-FUNCTIONALIZED PORPHYRINS AS ORGANOCATALYSTS

The modulation of the catalytic activity by the formation of self-assembled supramolecular catalysts has been studied by several groups in the past two decades, but the use of aggregation/dissociation processes for the reversible switching of catalytic activity has remained relatively unexplored. Amphiphilic *meso*-(4-sulfonatophenyl)porphyrins constitute one of the simplest systems whose aggregation state can be controlled by means of an external stimulus, such as stated before, the pH of the medium or the porphyrin concentration.[57]

A few years ago, our group considered applying the self-aggregation of porphyrins for the control of the organocatalytic activity. Several sulfonated porphyrins monosubstituted in a *meso*-position with cyclic (achiral or chiral) secondary amines were synthesized (Figure 19), to promote reactions taking place via enamine or iminium ion in water, with the expectation that they would show pH- and concentration-dependent catalytic activities.[53,57,58]

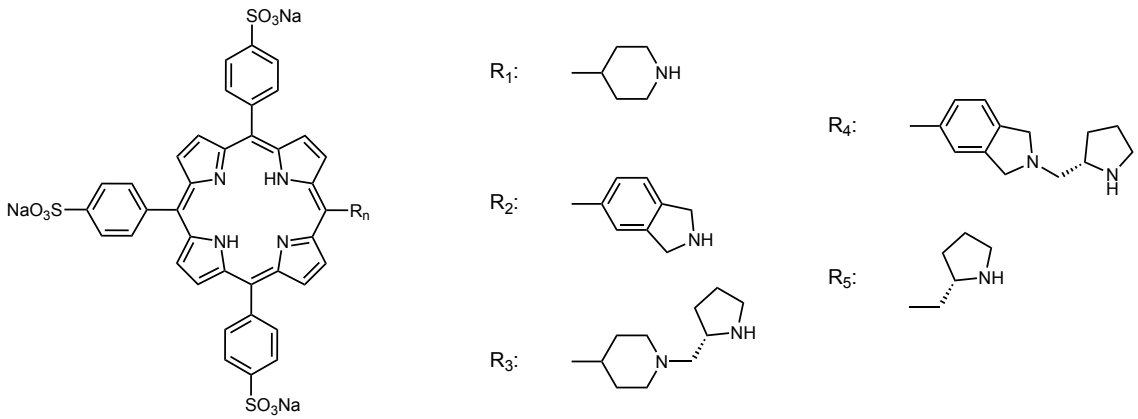


Figure 19. Different porphyrins synthesized and tested as organocatalysts in the group since 2014.

These porphyrins showed remarkable catalytic activity in aldol-type reactions (Scheme 8, see the aldolic reaction between cyclohexanone and *p*-nitrobenzaldehyde in presence of $R_1$-porphyrin as organocatalyst). When chirality was attempted to be introduced by acidification of the medium (pH < 4), to favor the *J*-aggregates formation, we saw null catalytic activity due to the formation of totally insoluble *J*-aggregates. On the other hand, the insolubility shown by the aforementioned *J*-aggregates allowed us to easily recycle the catalyst.

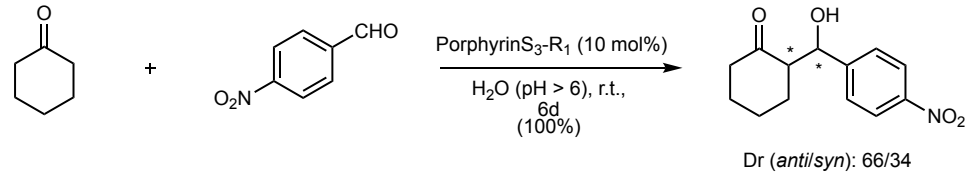


Scheme 8. Aldolic reaction catalyzed by an amphiphilic porphyrin.

The synthetic strategy we developed (formation of the *N*-Boc $A_3B$ porphyrin followed by a sulfonation plus deprotection step) allowed us to synthesize and evaluate the catalytic activity of a wide range of sulfonated amino-functionalized porphyrins, as well as the chirality induction via the formation of chiral supramolecular *J*-aggregates.

We decided to study next the catalytic activity of the non-sulfonated amino-functionalized porphyrins, that should be easily obtained from the *N*-Boc $A_3B$ porphyrin intermediates.

## 1.3. VISIBLE-LIGHT PHOTOCATALYSIS

### 1.3.1. GENERAL INTRODUCTION

Photochemistry, or the promotion of chemical reactions by light, was first recognized as a powerful and innovative tool in organic chemistry in the 19th century by the Italian chemist Giacomo Ciamician. Initially, the lack of equipment for the construction of appropriate artificial irradiation systems, lead to the use of sunlight as energy source.[59] Despite all the difficulties, Giacomo and co-workers described a wide range of photochemical sunlight-promoted reactions, being the most historically relevant one the intramolecular photo-induced [2+2] cycloaddition of carvone (Figure 20).[60]

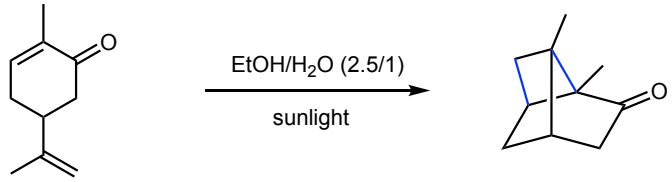


Figure 20. Intramolecular photo-induced [2+2] cycloaddition of carvone described by Giacomo Ciamician.

A few years later, Ciamician characterized photochemistry as an environmentally friendly strategy in organic chemistry, based on the use of a green source as light for the promotion of reactions.[61]

Over the last century, the efficient, non-toxic and non-traditional construction of carbon-carbon and carbon-heteroatom bonds has become one of the most pursued challenges in organic chemistry. Since the vast majority of organic compounds do not absorb in the visible region of the electromagnetic spectrum, photochemical reactions were traditionally performed under UV-light irradiation. Due to the high energy and reactivity of the open-shell radical intermediates involved in these processes, undesired transformations were often observed, and efficient enantioselective photocatalytic reactions were practically unknown.[62]

For these reasons, photochemistry remained relatively in the background until the appearance of suitable visible-light photosensitizers and photocatalysts, that has led to widely used, new and unique photochemical activation modes (Figure 21).[63-69]

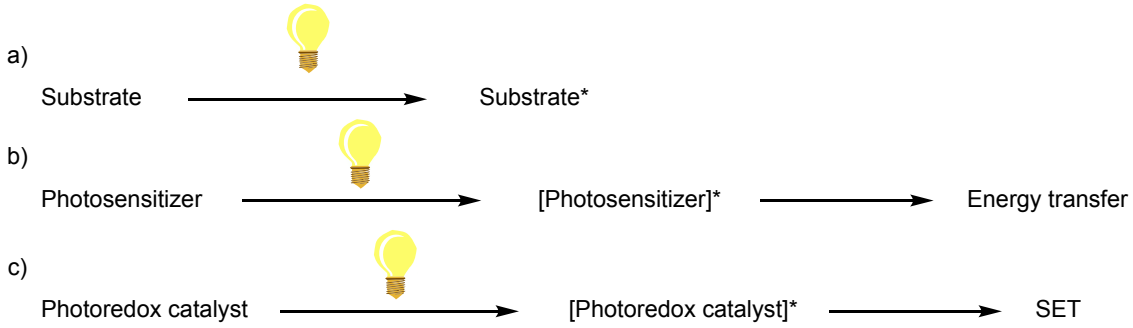


Figure 21. Different strategies in photochemistry and photocatalysis.

In Figure 21 are shown the most common activation modes for photochemical reactions, (a) direct excitation of the compound with the appropriate light source, (b) indirect excitation of the target compound by an energy transfer process using a suitable photosensitizer and (c) the photocatalyst in its excited state gets engaged into a Single Electron Transfer (SET) process, in which the reagent can be either oxidized or reduced.

### 1.3.2. PHOTOSENSITIZATION PROCESS

The so-called *First Law of Photochemistry* states that light (photons) must be absorbed to have an effect. In some cases, the molecule that absorbs a photon is thermically deexcited or transformed into a different ground-state species before having the opportunity to interact with other molecules in the system. But if the half-life of the photoexcited species is long enough, it can transfer its energy to another molecule in the system before falling back to the ground state. In this situation, the molecule absorbing the photon is called a photosensitizer, that can transfer energy to a substrate.[70]

The IUPAC defines photosensitization as "the process by which a photochemical or photophysical alteration occurs in one molecular entity as a result of initial absorption of radiation by another molecular entity called photosensitizer. In mechanistic photochemistry the term is limited to cases in which the photosensitizer is no consumed in the reaction"[71] (A typical example is that of Figure 22, in which the complex $[Ru(bpy)_3Cl_2]$ acts as a photosensitizer).

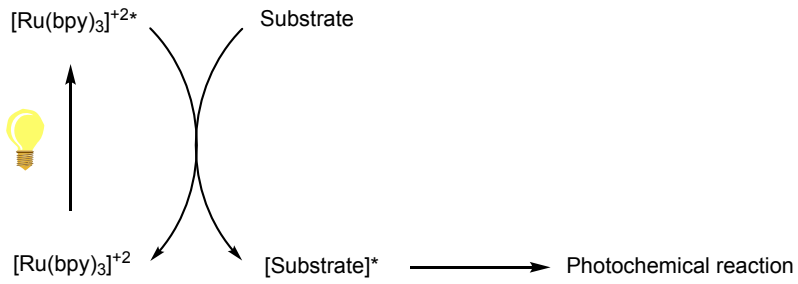


Figure 22. Photosensitization process for $[Ru(bpy)_3]^{2+}$ photocatalyst.

In some cases, the excited singlet photosensitizer is able to directly transfer its energy to a ground state molecule, leading to its excitation. On the other hand, the most common approach for a sensitization process is the one in which the energy is transferred to the substrate from a long-lived triplet excited state (obtained by fast intersystem crossing (ISC) from the initially formed singlet excited state), carrying on the reaction by the intermediacy of birradicals.[72]

Photosensitizers are not usually consumed during the photosensitization process, and they just simply return to their ground state once the photosensitization process is complete. But, in some cases, photosensitizers are photobleached through a competitive process in which, upon light-absorption, photosensitizer molecules switch to a different molecular form unable to absorb light at the initial wavelength. Photosensitizers are principally studied for their contribution to fields such as energy harvesting, photocatalysis and cancer therapy.[73-74]

There are two main pathways for photoreactions taking place via a photosensitization process, (a) type I, where the photosensitizer is excited to its triplet state by light irradiation followed by intersystem crossing, and subsequently interacts with substrate (different from molecular oxygen) to regenerate the photosensitizer in its ground state and promoting the photoreaction, via excitation of the substrate, to lead to the desired product, and (b) type II, where the photosensitizer is also excited to its triplet state and, first, reacts with a ground state triplet oxygen molecule, promoting its excitation to singlet state reactive oxygen species, that reacts subsequently with the substrate, promoting the photoreaction than then leads to the desired product (Figure 23).[75]

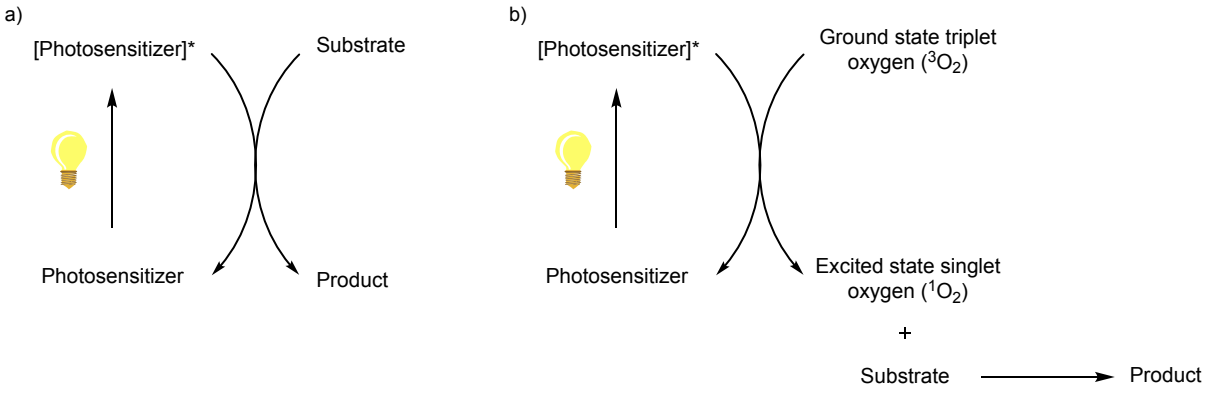


Figure 23. Illustration of the two types of photosensitizers, (a) type I, where the photosensitizer is quenched by a different chemical substrate than oxygen, and (b) type II, where the photosensitizer is quenched by a ground state oxygen molecule.

Photosensitizers, in organic chemistry, can be classified in basically two types, (organo)metallic and purely organic photosensitizers.[76-78]

Metallic photosensitizers are metal atom-based compounds, where the metal atom is bound to, at least, one organic ligand which favors the electronic metal-ligand interactions. Metal atoms used are usually Ir, Rh or Ru, that have filled high energy d-orbitals, promoting metal-ligand charge transfer, due to the low energetic gap between HOMO and LUMO orbitals. Although the vast majority of them are synthetic, we can also find some natural organometallic photosensitizers.

Organic photosensitizers are carbon-based molecules that absorb light in presence of oxygen to produce reactive oxygen species. They are normally highly conjugated systems with a strong electron delocalization, leading to a smaller energetic gap between HOMO and LUMO orbitals, making them enter to the triplet state more efficiently (Figure 24).

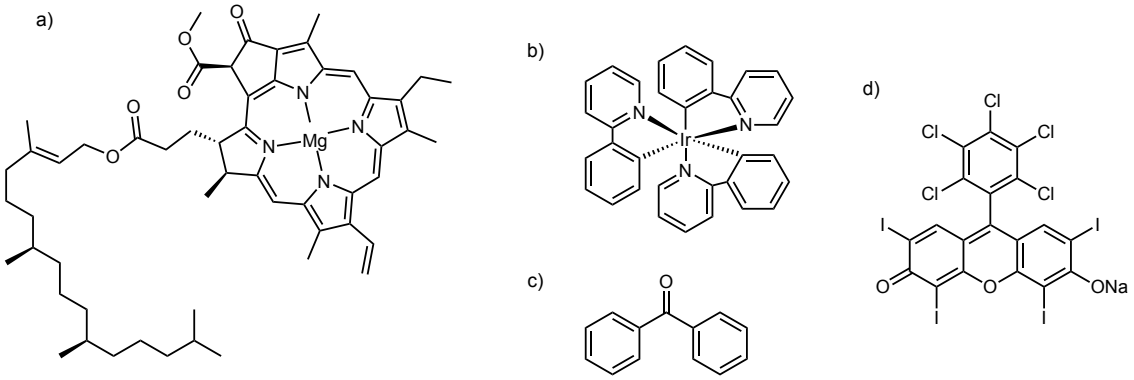


Figure 24. Some examples of organometallic photosensitizers, (a) chlorophyll A and (b) tris-(2-phenylpyridine)iridium (III), and organic photosensitizers, (c) benzophenone and (d) rose Bengal.

### 1.3.3. PHOTOREDOX CATALYSIS

In organic chemistry, several different redox reactions have been developed and widely used in the synthesis, for instance, of pharmaceuticals. Initially, redox reactions relied in the stoichiometric use of oxidating or reducing agents, and were classified as a non-green chemical reactions, due to the generation of chemical waste, the lot of energy required, the use of toxic reagents (metals) or high temperatures to perform the reaction. More recently, new chemical routes have been reported to perform redox reactions in a greener way, such as electrocatalysis or photoredox catalysis.[79]

Historically, photoredox catalysis was first recognized and extensively studied for its application in inorganic[80] and in materials chemistry,[81] but it was not until the present century that the potential of photoredox catalysis for sustainable organic synthesis has been fully exploited, especially for the use of renewable sources such as visible light, the fact that photoredox reactions can be carried on in mild conditions (they can be conducted at room temperature), and/or the small amount of subproducts formed.[82]

Photoredox catalysis is currently one of the hottest research areas in organic chemistry, and in the last years, the number of publications has increased by a factor of 10, culminating in more that 500 articles in 2016, for example.[83] To understand this recent explosion in this field, we will take a look at some previous key examples that paved the way to current researchers in the field.

The first visible-light promoted photoredox catalysis organic reaction, reported by Chyongjing Pac and co-workers[84] in 1981, was the photo-reductive hydrogenation of electron-poor olefins with dihydropyridines, using $(Ru(bpy)_3Cl_2$ as a photocatalyst (Figure 25).

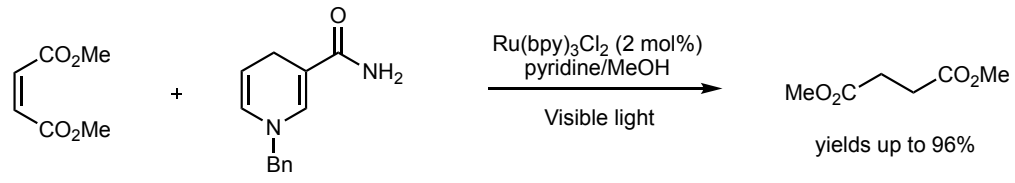


Figure 25. Photoreduction of alkenes reported by Pac and co-workers.

The second one was reported in 1990 by Fukuzimi and co-workers[85] with the photocatalytic reduction of phenyl halides, again using $Ru(bpy)_3Cl_2$ as photocatalyst (Figure 26).

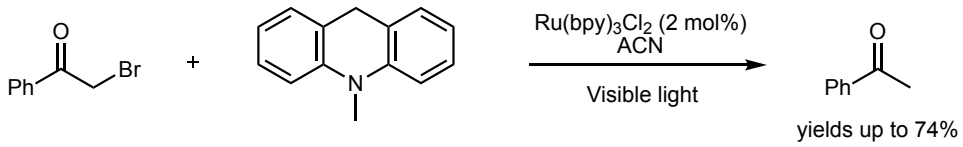


Figure 26. Reductive dehalogenation of α-bromoacyl compounds reported by Fukuzimi and co-workers.

Between these two articles, in 1984, the first photocatalytic oxidation was reported by Cano-Yelo and co-workers[86] with the photo-oxidation of carbinols employing a Ru(II) complex as a photocatalyst (Figure 27).

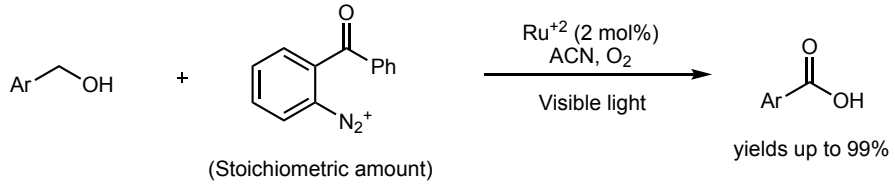


Figure 27. Photocatalytic oxidation of carbinols reported by Cano-Yelo and co-workers.

While the examples published during the 1980s and 1990s provide some early precedent for the concept of visible light-mediated photoredox catalysis, the dramatic increase of interest in this field is attributed to three important papers published between 2008 and 2009.

The first to go on scene was a paper published by Yoon and co-workers[87] reporting the visible-light photoredox catalysis of intramolecular [2+2] enone cycloadditions (Figure 28).

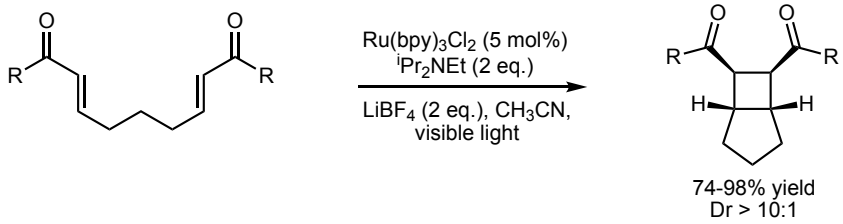


Figure 28. Intramolecular [2+2] photoredox cycloaddition reported by Yoon and co-workers.

In the same year, MacMillan and Nicewicz[88] published a paper where they combined photoredox catalysis with enantioselective organocatalysis, by means of a dual catalytic system employing imidazolidinones as organocatalysts and $Ru(bpy)_3Cl_2$ as photocatalyst, for the direct

asymmetric alkylation of aldehydes with alkyl bromides, a reaction that could not be achieved by asymmetric organocatalysis alone (Figure 29).

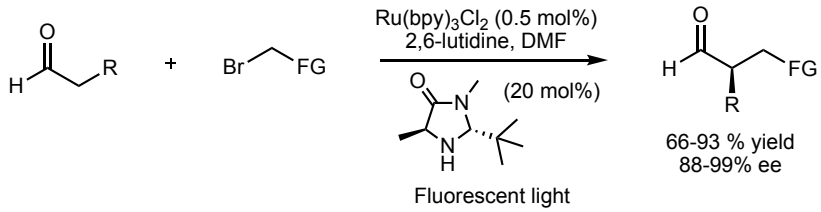


Figure 29. Pioneering asymmetric α-alkylation of aldehydes, using a dual photocatalytic system, reported by MacMillan and co-workers.

Finally, in 2009, Stephenson and co-workers[89] proposed a green procedure for the electron-transfer reductive photoredox catalysis dehalogenation reaction. By using $Ru(bpy)_3Cl_2$ as photocatalyst, they were able to develop a tin-free procedure for these type of reactions, demonstrating the green character of photoredox catalysis (Figure 30).

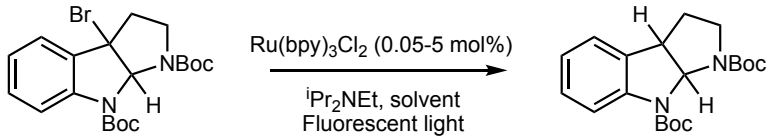


Figure 30. Green photoredox reductive dehalogenation reaction proposed by Stephenson and co-workers.

Photoredox is based on photo-induced electron transfer processes (PET), usually Single Electron Transfer (SET), between an inactivated substrate, or an intermediate, and the excited photoredox catalyst, irradiated at a specific wavelength, inducing the substrate to enter new reaction paths that could not be possible under thermal conditions.[90-92]

Photocatalysts that undergo SET processes are usually metal-complexes or organic dyes, that through light-visible irradiation reach a triplet excited state that promotes the photochemical reaction. The key point in these processes is the relatively high lifetime of this excited state, due to the fact that the direct transition to the singlet ground state is a spin-forbidden transition, allowing the electron transfer.[62]

Once the photocatalyst is subjected to visible-light irradiation, it is excited from its ground singlet state to the lowest singlet excited state. Then, via ISC process, the excited photocatalyst is converted into its triplet excited state (Figure 31). It is worth to say that some organophotocatalysts

can react from their singlet excited state, but usually it is the triplet excited state the one that promotes SET processes.[78]

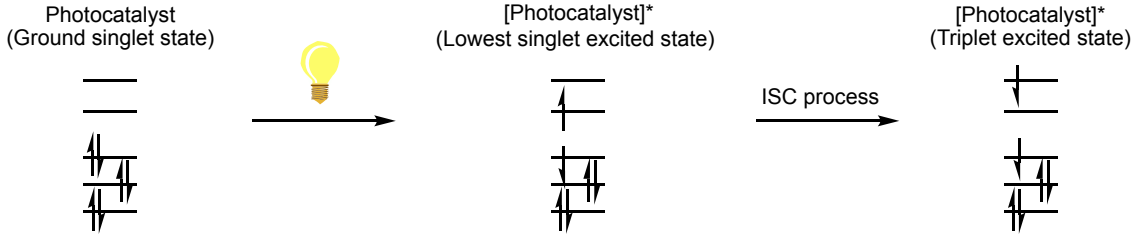


Figure 31. Simplified molecular orbital representation for the singlet and triplet excited states of a general photoredox catalyst involved in a SET process.

Another key point is that photoredox catalysts, in their ground state, are relatively poor oxidants and reductants. But the visible-light irradiation of these compounds can evolve by SET processes due to the unique ability of these compounds of acting both as strong oxidants and as reductants while being in their triplet excited state, contrasting to their behavior in the ground state.[93] Due to the excitation, the photocatalyst presents a hole in the single-occupied orbitals (the lowest energy SOMO) which makes it capable of accepting one electron in a SET process from an electron-donor substrate, acting as an oxidant. But at the same time, the photocatalyst presents an electron in a high-energy orbital (the highest energy SOMO) that can easily be transferred in a SET process to an electron-acceptor substrate[94] (Figure 32).

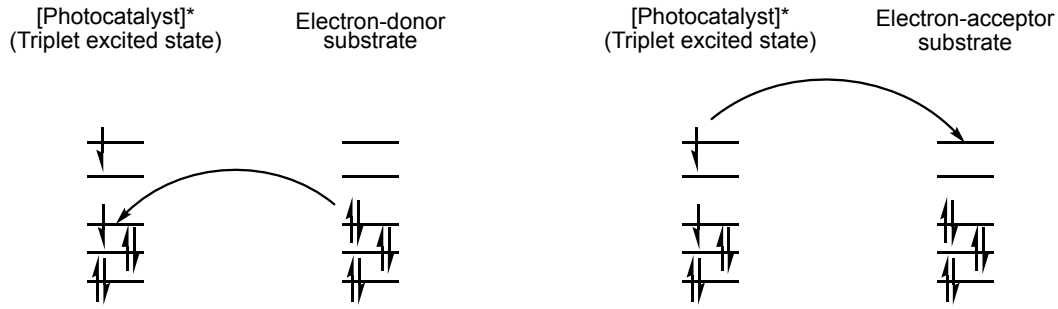


Figure 32. Photocatalyst behavior in SET processes acting as an oxidant (left) and as a reductant (right).

In this way, and as is shown in Scheme 9, an excited photocatalyst can go back to the singlet ground state through two different catalytic cycles. If the photoexcited catalyst acts as an oxidant, it is converted to an anion radical, that can transfer the extra electron to an electron-accepting intermediate or substrate (reductive quenching). On the other hand, if it acts as a reductant, it is converted to a cation radical, that can oxidize an electron-donating species (oxidative quenching). The actual catalytic cycle will be determined by the equilibrium constant values of each SET step,

that can be evaluated from the redox potentials of each individual species ([Photocatalyst]*, [Photocatalyst]+·, [Photocatalyst]-·, A, D).

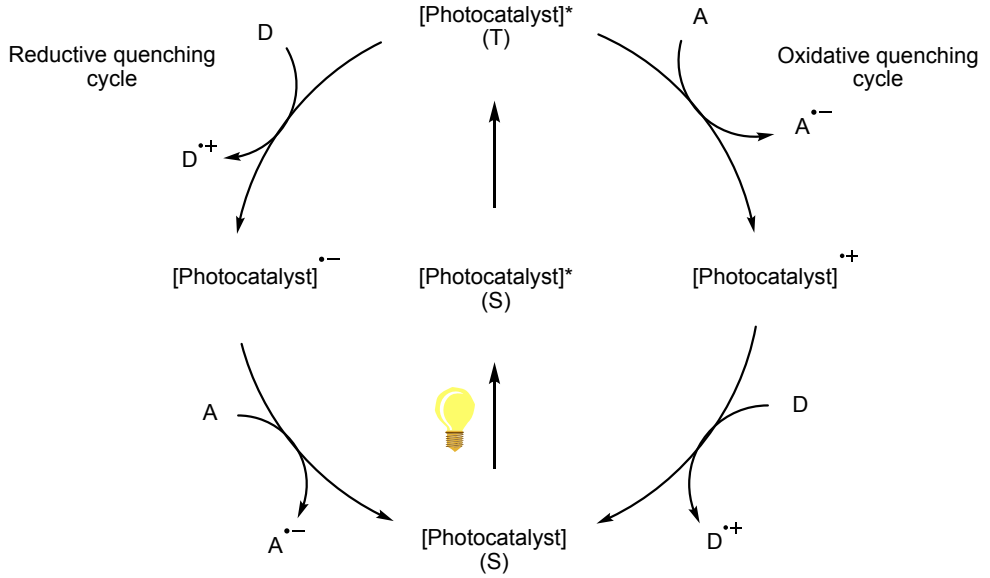


Scheme 9. Reductive (left) and oxidative (right) quenching cycles for a general photocatalyst. A = electron-acceptor substrate, D = electron-donor substrate, S = singlet state and T = triplet state.

Photoredox catalytic reactions are divided into three classes, depending on the overall redox transformation of the substrate, (a) net reductive, (b) net oxidative and (c) redox neutral. For the two first, a stoichiometric amount of a reducing or an oxidative agent, respectively, is needed to close the cycle.

### 1.3.3.1. Net reductive reactions

Net reductive reactions are those in which the substrate is reduced using a photoredox catalyst in presence of a stoichiometric amount of a reducing agent. In this type-reactions, the excited photocatalyst is oxidized, acting as the reductant, and the reducing agent is needed to restore the oxidated photocatalyst to the ground state. 1-Benzyl-1,4-dihydronicotinamide (BNAH) and *N*,*N*-diisopropilamine (DIPEA) are the most commonly reducing agents used.

This kind of reactions have been studied for their applications in, for example, the reduction of electron-poor alkenes,[84] tandem epoxide-opening/allylation of ketoepoxides[95] or the reductive dehalogenation for the construction of new carbon-carbon and carbon-heteroatom bonds.[96,97] In Scheme 10 is shown the mechanism for the net reduction of electron-poor alkenes showed in Figure 25, using BNAH as the stoichiometric reducing agent.[84]

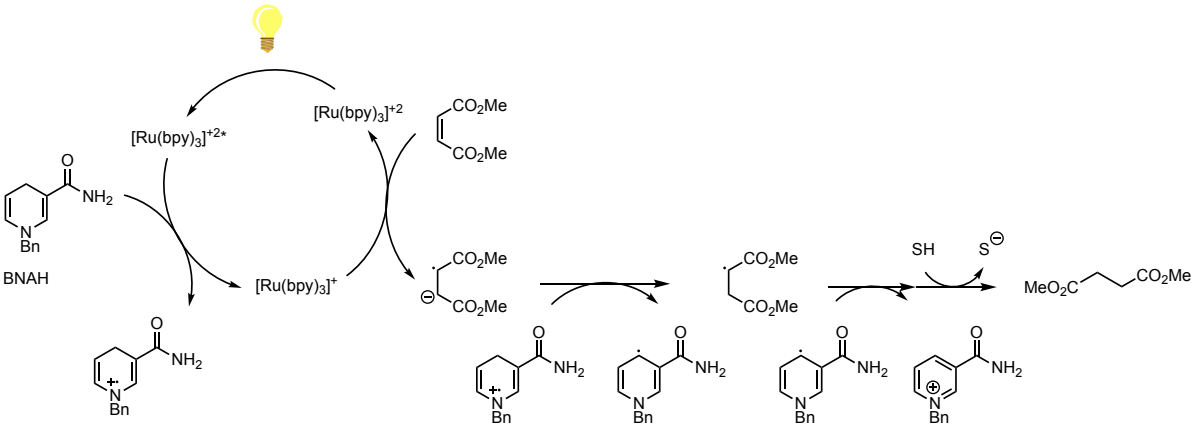


Scheme 10. Proposed mechanism for the reductive photoredox catalysis reaction of poor-alkenes.

As shown in the mechanism, the function of BNAH is to reduce the excited photocatalyst [([Ru]$^{2+}$)*] through a reductive SET process, leading to a reduced photocatalyst ([Ru]$^{+}$), capable of reducing the substrate via an oxidative SET process, in order to recover the ground state photocatalyst [([Ru]$^{2+}$)]. Then, the oxidized BNAH transfers a proton to the substrate radical anion, forming a radical that accepts an electron from the BNAH radical leading to the reduced alkene after protonation from the solvent.

### 1.3.3.2. Net oxidative reactions

Net oxidative reactions are those in which the substrate is oxidized using a photoredox catalyst in presence of a stoichiometric amount of an oxidant agent. In this type of reactions, the excited photocatalyst is reduced, acting as the oxidant, and the oxidating agent is needed to restore the ground-state photocatalyst, being oxygen gas ($O_2$) the most commonly used oxidant agent.

This kind of reactions has been studied for its applications in, for example, oxidative cyclizations[98,99] or in the formation of iminium ions, that can be trapped by a variety of nucleophiles giving rise to aza-Henry,[100,101] Strecker, Sakurai, Mannich or Friedel-Crafts type-reactions.[102] In Scheme 11 is shown the proposed mechanism for the net-oxidative aza-Henry reaction, using oxygen gas as the stoichiometric oxidant agent.[100]

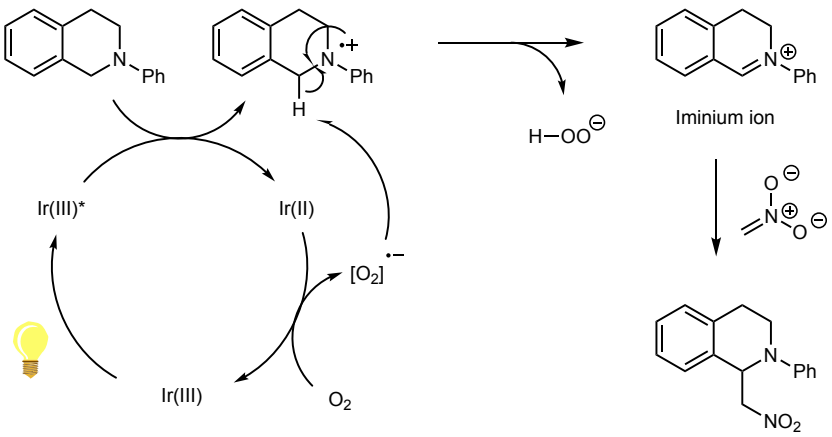


Scheme 11. Proposed mechanism for a net-oxidative photoredox system of a catalytic aza-Henry C-H functionalization.

As shown in the mechanism, molecular oxygen oxidizes the reduced photocatalyst, in order to restore it, via oxidative SET process. The formed peroxide anion interacts with the oxidized radical cation substrate, formed via reductive SET process with the excited photocatalyst, leading to the formation of the iminium ion via hydrogen transfer. This iminium ion can be reacted with many nucleophiles, in this case, since an aza-Henry reaction is shown, methyleneazinate (the conjugate base of nitromethane) is chosen as the nucleophile, leading to the new carbon-carbon bond formation.

### 1.3.3.3. Redox-neutral reactions

Redox-neutral reactions are those in which the substrates are both reduced and oxidized, participating in both SET processes of the catalytic cycle, with no net change on the oxidation state between the starting material and the final product. In this type of reactions, the photocatalyst is brought back to its original state by the reagents, that is why no external reducing or oxidant stoichiometric agent is required.

Synthetic applications of photocatalytic redox neutral reactions include [2+2] cycloadditions,[103,104] [4+2] cycloadditions,[105] C-H arylation of amines[106] and decarboxylative couplings.[107-109] The proposed mechanism for the photoredox decarboxylative coupling between an aromatic compound and an aminoacid is shown in Scheme 12.[107]

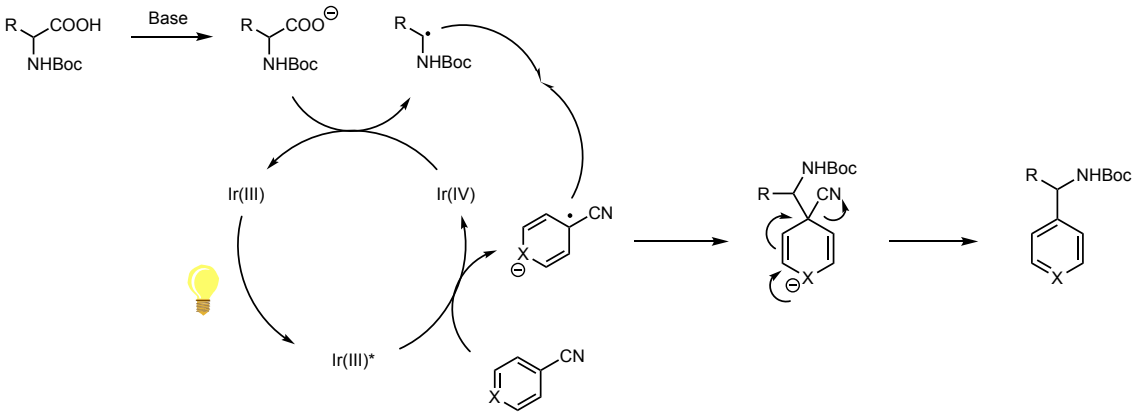


Scheme 12. Proposed mechanism for the redox-neutral decarboxylative coupling between a cyano-substituted aromatic compound and an aminoacid.

As is shown in the mechanism, the iridium photocatalyst is both oxidized and reduced via SET processes by the starting materials. First, the excited photocatalyst is oxidized by the ciano-substituted aromatic compound, generating an anion radical compound, that reacts with the radical generated by the decarboxylation of the aminoacid concomitantly with the reduction of the previously oxidized photocatalyst via SET process, forming the new C-C bond. Finally, the cyanide anion group acts as the leaving group, leading to the final product.

### 1.3.4. ASYMMETRIC SYNTHESIS IN VISIBLE-LIGHT PHOTOCATALYSIS

An important aspect of visible-light photocatalysis is the fact that the photocatalytic cycle can be coupled to other types of catalysis, giving rise to endless possibilities in the field of asymmetric synthesis, especially considering the fact that many traditional reactions have been reported, via photocatalysis, under milder conditions than those already reported under thermal conditions.

Although photocatalysis and asymmetric catalysis have been widely studied in the last decades, the combination of the two remained in the background for two main reasons, (a) in conventional thermal processes, the reaction is due to the lower activation energy, guiding the reaction down the selective catalytic path, which is so fast than even secondary racemic reactions may not occur, and (b) in photochemical reactions, the photocatalyst performs its function in a higher energy state than in thermal chiral catalysis. This means that the excited photocatalyst has enough energy to promote both stereocontrolled and racemic processes.[62]

However, the recent strong impact that photocatalysis has had in organic synthesis has led a large number of research groups to dedicate their efforts to trying to make photocatalysis coexist with asymmetric catalysis, resulting in a wide range of new modes of activation (Figure 33).

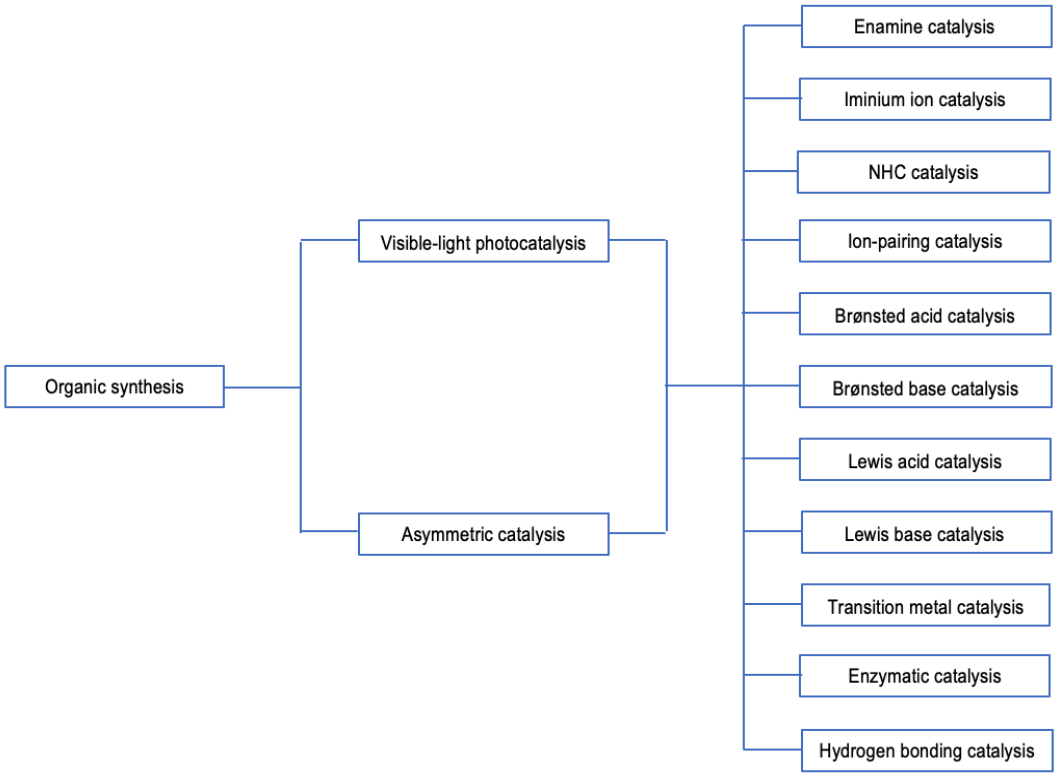


Figure 33. Modes of activation in asymmetric visible-light photocatalysis

The first enantioselective photocatalytic reaction was reported by Hammond and co-workers in 1965[110] with the *cis*/*trans* isomerization of racemic *trans*-1,2-diphenylcyclopropane, using chiral naphthalene derivatives as photosensitizers (Figure 34).

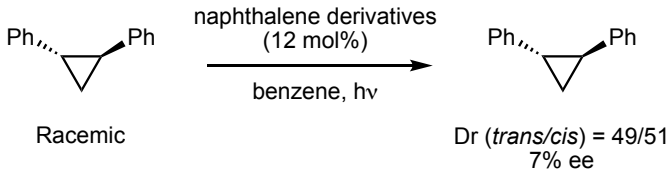


Figure 34. Enantioselective photo-isomerization of racemic 1,2-diphenylcyclopropane reported by Hammond and co-workers

As it can be seen, although this reaction is cataloged as enantioselective, both the diastereomeric and the enantiomeric excesses obtained were quite low, causing the field to be relegated until, 25 years later, Schuster and co-workers,[111] in 1990, reported the enantioselective photocatalysis of the Diels-Alder reaction, using (-)-BDCN as photosensitizer (Figure 35).

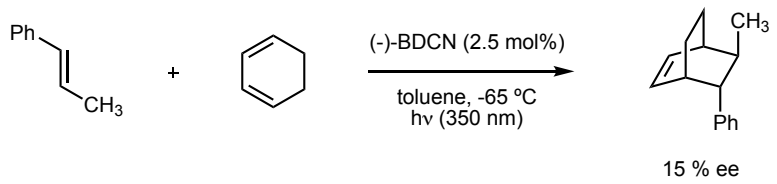


Figure 35. Enantioselective Diels-Alder reaction reported by Schuster and co-workers (the absolute stereochemistry of the product was not reported).

Notice that, as it happened in Hammond's photoisomerization, the enantiomeric excesses were still low, although they were better than those reported by its predecessor. One had to wait until 1999 to see the first photocatalytic reaction with relatively high enantiomeric excesses, when Inoue and co-workers[112] reported the exciplex-mediated photo-isomerization of (*Z*)-cycloheptene (Figure 36). As it is shown, although both the diastereomer ratio and the enantiomeric excess were good enough, the obtained yield was very poor.

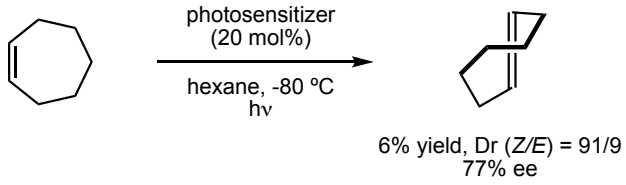


Figure 36. Exciplex-mediated photo-isomerization reported by Inoue and co-workers.

### 1.3.4.1. Enantioselective enamine catalysis and photocatalysis

In recent years, asymmetric aminocatalysis via chiral enamines has been extended to enantioselective photochemistry, due to two important features of enamines, (a) the presence of a high-energy HOMO that can easily interact with the LUMO or the SOMO of an electrophile, and (b) their easy oxidation to a cation radical, making them reactive with a wide range of substrates. Enantioselective enamine photocatalysis has been studied in two main fields, the $\alpha$-alkylation and the $\alpha$-oxygenation of aldehydes.[113]

In Figure 37 are shown some examples of chiral secondary amines used as organocatalysts in some enantioselective photochemical reactions.

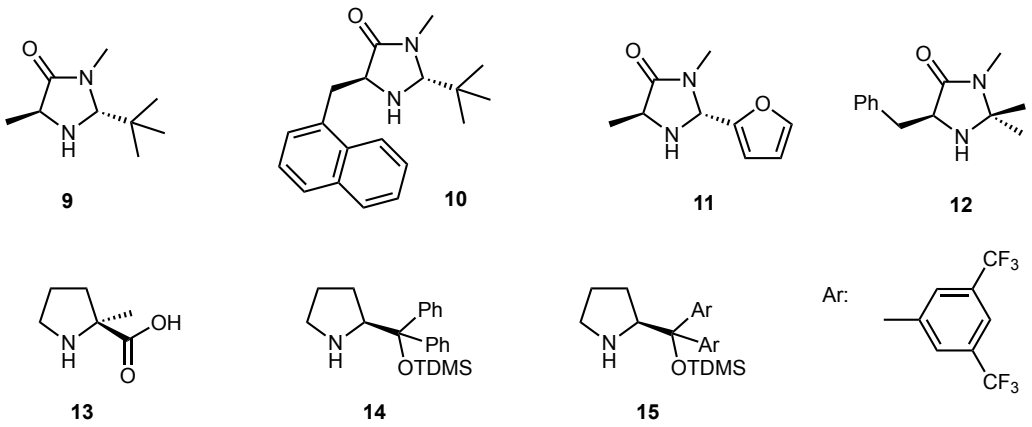


Figure 37. Structures of representative chiral amines for enamine catalysis in enantioselective photochemical reactions.

As stated before, in 2008, MacMillan and co-workers[88] reported the first enantioselective α-alkylation of aldehydes combining photocatalysis with organocatalysis, by reacting a wide number of aldehydes with electron-deficient α-bromocarbonyls, using a 20 mol% of imidazolidinone **9** as the organocatalyst, and taking place with good yields and enantiomeric excesses (Figure 38).

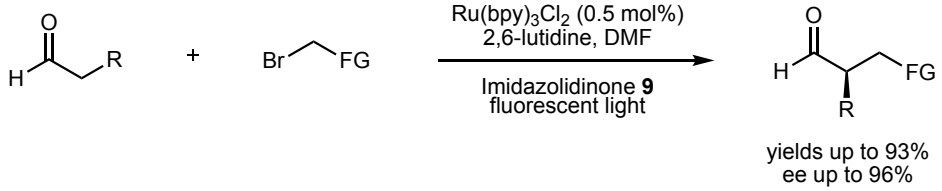


Figure 38. Enantioselective α-alkylation of aldehydes reported by MacMillan and co-workers employing chiral imidazolidinone **9**.

The mechanism initially proposed by MacMillan and Nicewicz involves the interplay between a neutral photoredox catalytic cycle and an enamine-mediated organocatalytic cycle. They based their hypothesis into two important concepts, (a) the introduction of the SOMO catalysis, based in the formation of a 3π-radical cation, via one-electron enamine oxidation, with a SOMO that can activate new enantioselective transformations (Figure 39),[114] and (b) the energetically preferred low-barrier open-shell towards two-electron pathways.

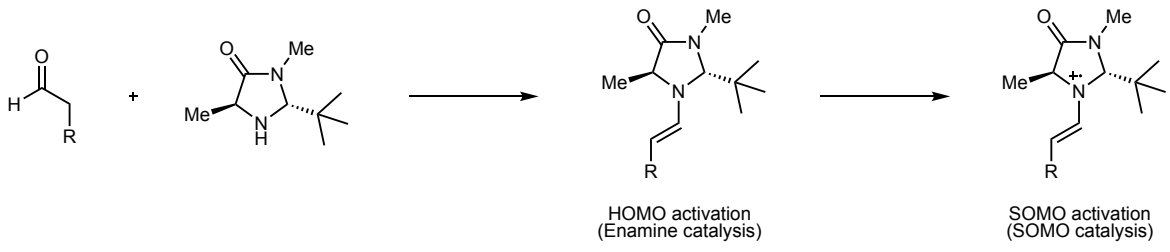


Figure 39. Chemical steps on the formation of the SOMO-activated intermediate.

The general mechanism proposed is based in the interplay of two catalytic cycles that take place simultaneously; the organocatalytic cycle, that leads to the formation of an electron-rich enamine, and the photoredox catalytic cycle to generate the electron-deficient radical (Scheme 13).

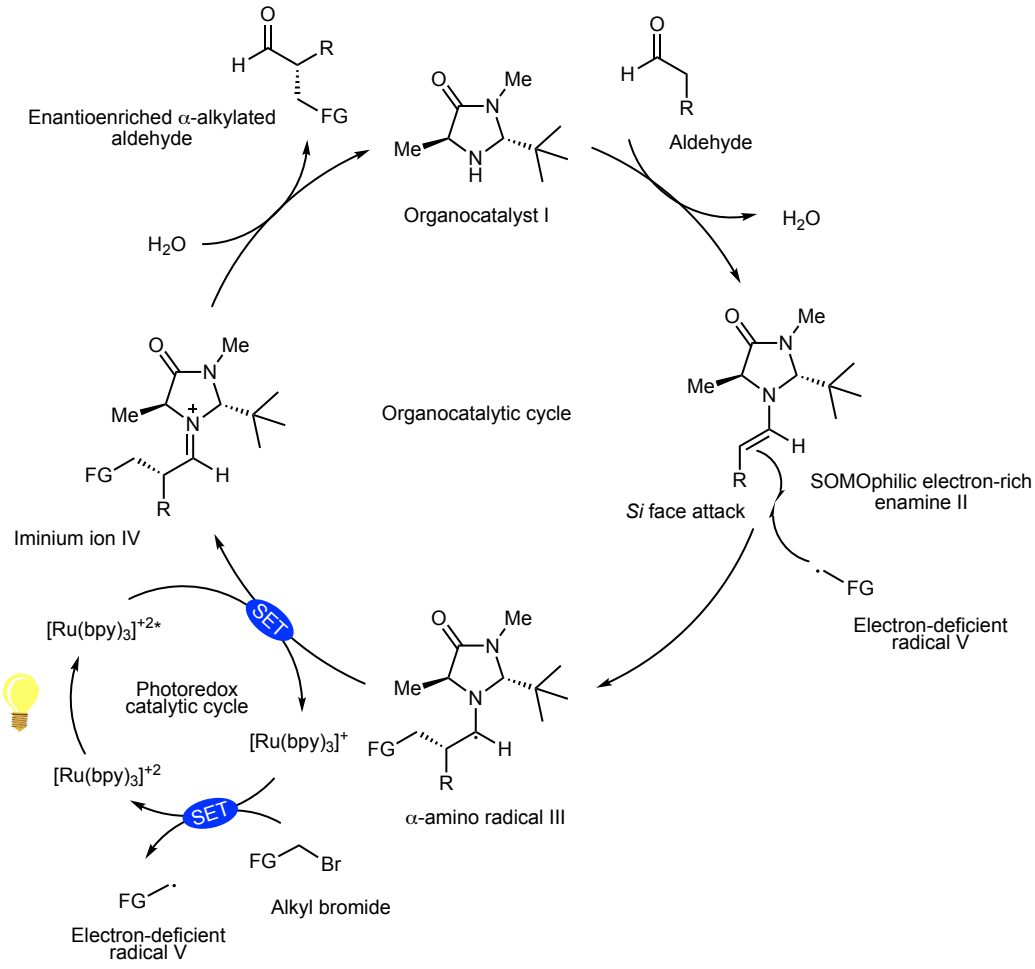


Scheme 13. General mechanism for the enantioselective α-alkylation of aldehydes.

By irradiating the photocatalyst ($Ru(bpy)_3^{+2}$), this is capable of taking a photon from the light irradiation to reach its excited state ($[Ru(bpy)_3^{+2}]^*$), where is capable of acting as both oxidant and reductant. Then, since the organocatalytic cycle is not yet able to advance to the formation of the α-aminoradical III, the authors argue that the reduction of the photocatalyst takes place by taking an electron from a sacrificial quantity of enamine II. Once $Ru(bpy)_3^{+}$ is formed, it is oxidized via SET process with the alkyl bromide, regenerating the photocatalyst and leading to the formation of electron-deficient radical V.

Simultaneously, the organocatalytic cycle starts with the formation of the SOMOphilic electron-rich enamine II by the condensation of the aldehyde and organocatalyst I. At this point, the cycles

merge in the alkylation step, when the newly formed electron-rich enamine II reacts with electron-deficient radical V, furnishing α-amino radical III, that, since it is a highly oxidable specie, a new convergence of both cycle in a SET process gives rise to the formation of iminium ion IV. Finally, the α-alkylated aldehyde is obtained by hydrolysis.

In terms of enantioselectivity, the mechanism presents two key points, (a) the choice of the organocatalyst since it must ensure a fixed conformation for enamine II. This way, organocatalyst I projects the 2π electron system away from the bulky *tert*-butyl groups, while the (*E*)-enamine is formed to minimize the non-bonding interactions with the imidazolidinone ring (Scheme 14a), and (b) in electron-rich enamine II, the methyl group blocks the *Re* face, leaving the *Si* face free for the addition of electron-deficient radical V (Scheme 14b).

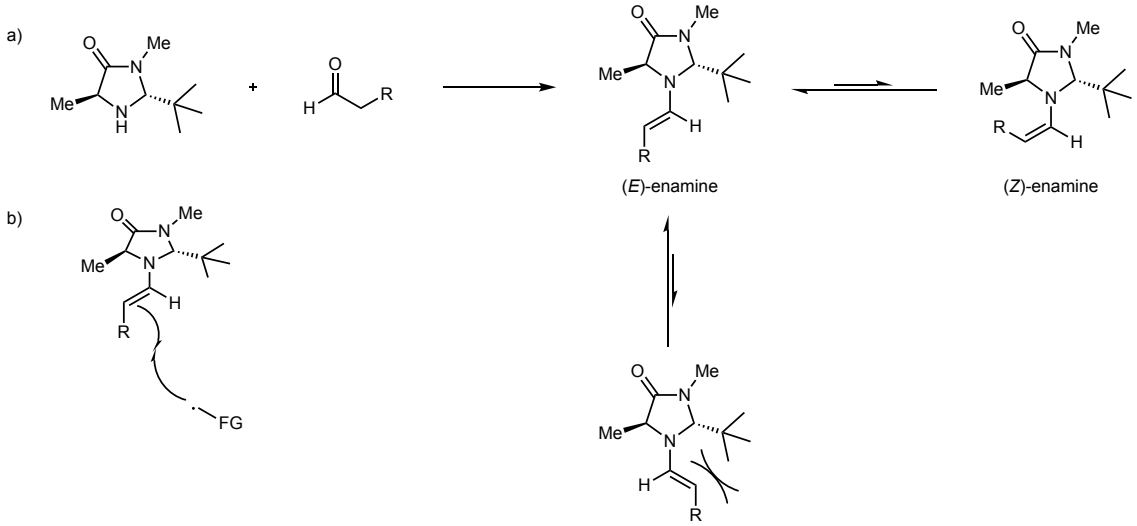


Scheme 14. a) Enamine equilibrium conformation and b) Control of the enantioselectivity of the reaction by steric hindrance of the *tert*-butyl group.

One year later, in 2009, MacMillan and co-workers[115] expanded this dual photocatalytic system to the preparation of α-trifluoromethylated aldehydes. They reported the coupling of aldehydes with trifluoromethyliodides by employing a 20 mol% of imidazolidinone **9** as organocatalyst and an iridium (III) complex as photocatalyst, obtaining similar results as in their previous work (Figure 40).

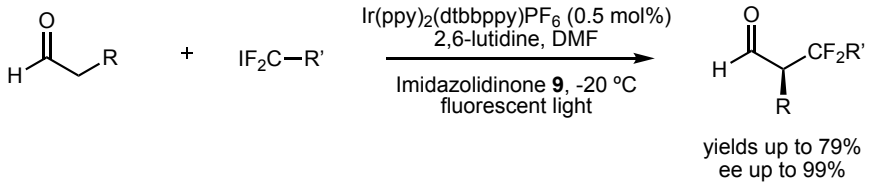


Figure 40. Enantioselective α-trifluoromethylation of aldehydes reported by MacMillan and co-workers.

It should be noticed that these results were only obtained at -20 ºC, and that the reaction did not work at room temperature. In the following years, MacMillan's group expanded their α-alkylation reaction to other kinds of coupling partners, such as α-bromoacetonitriles[116] or simple olefins.[117]

Two years later, in 2011, Zeitler and co-workers[118] reported the use of an organic dye for the α-alkylation of aldehydes by using Eosin Y as photocatalyst. The fact of using an organic dye as photocatalyst instead of the ones normally used for this kind of reactions, offers a green alternative in photochemistry. The work is based in MacMillan's reaction, for instance the alkylation of *n*-octanal with electron-deficient α-bromocarbonyls, using a 20 mol% of imidazolidinone **9** (Figure 41). The same reaction was later reported by Ferroud and co-workers[119] using rose Bengal as photocatalyst, achieving both procedures similar results to the ones reported by MacMillan.

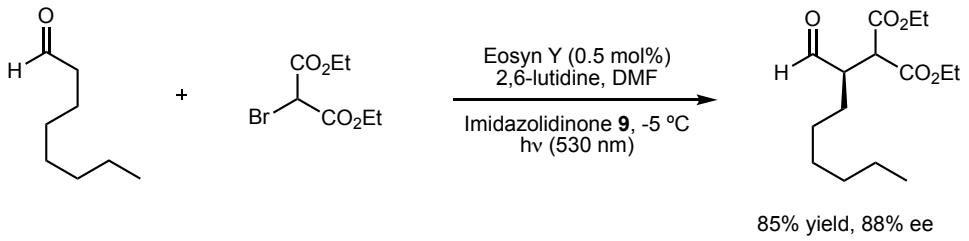


Figure 41. Enantioselective α-alkylation of aldehydes, using an organic dye as photocatalyst, reported by Zeitler and co-workers.

In recent years, many groups are trying to develop single-catalyst strategies, where both photocatalytic and organocatalytic activities are present in the same molecule. Thus, the first research group to report a bifunctional catalysis strategy for the enantioselective α-alkylation of aldehydes was Melchiorre's group. Between 2013 and 2017, they published several articles[120] in which they disclosed two important facts, (a) that it is possible to perform highly enantioselective reactions via enamine organocatalysis without the use of an external photocatalyst (Figure 42a), and (b) that this is due to the photoactivity of some chiral enamines; upon visible-light irradiation, their electronic excited state is capable of acting as a strong reducing agent, through the formation of a charge-transfer complex, leading to the formation of a radical when reacted with bromomalonate derivatives (Figure 42b).

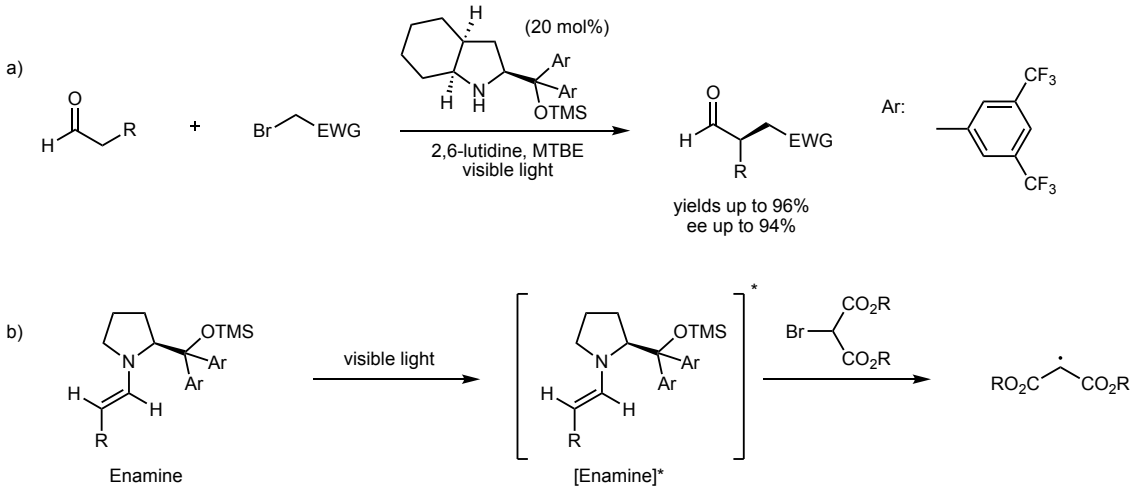


Figure 42. (a) Bifunctional enantioselective α-alkylation of aldehydes reported by Melchiorre and co-workers

In 2018, Alemán and co-workers[121] reported a bifunctional system for the α-alkylation of aldehydes by combining the highly enantioselective organocatalytic activity of imidazolidinones with photoactive thioxanthones (Figure 43).

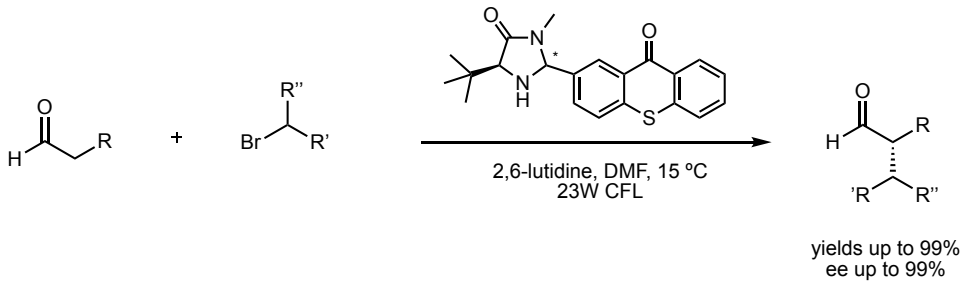


Figure 43. Bifunctional enantioselective α-alkylation of aldehydes reported by Alemán and co-workers.

In the field of α-oxygenation of aldehydes, the first example of an enantioselective reaction was reported in 2004 by Córdova and co-workers,[122] by using a dual catalytic system based in the photosensitization of molecular oxygen to its reactive singlet excited state, using 5,10,15,20-tetraphenylporphyrin (TPP) as a photosensitizer (Figure 44).

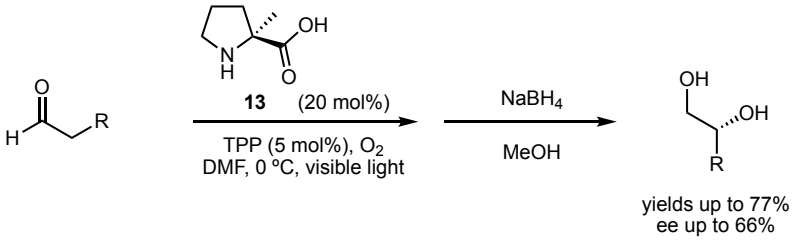


Figure 44. α-photooxygenation of aldehydes reported by Córdova and co-workers.

Some years later, in 2015, Gryko and co-workers[123] tried to reproduce Córdova's work and expand it to different aminoacids and L-Proline derivatives, obtaining results that were different from those reported by Córdova (Figure 45).

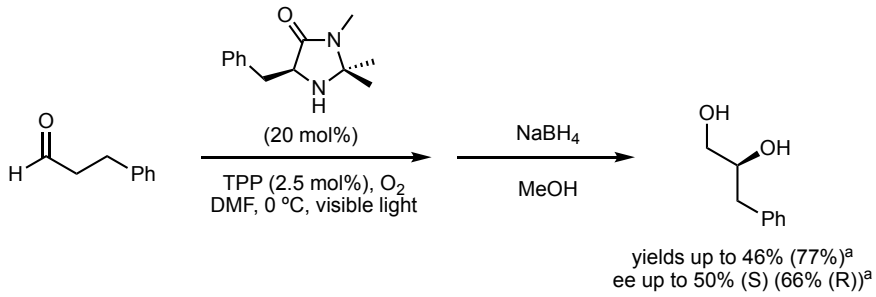


Figure 45. Gryko's obtained results in the attempt of reproducing Córdova's α-photooxygenation of aldehydes. [a]Results reported by Córdova and co-workers.

More recently, in 2019, Gryko and co-workers[124] reported the α-photooxygenation of chiral aldehydes. Gryko suggested that, based in preliminary studies, a stereocenter at the β-position should have a strong impact in the control of the reaction stereoselectivity. So, different chiral β-substituted aldehydes were used, obtaining the following results (Figure 46).

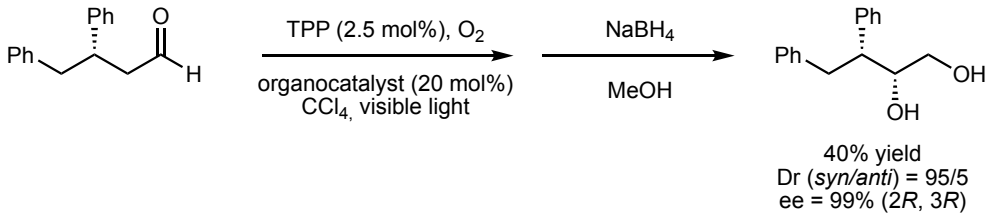


Figure 46. α-photooxygenation of chiral β-substituted aldehydes reported by Gryko and co-workers.

### 1.3.4.2. Iminium ion catalysis and photocatalysis

Historically, amines have been used as catalyst in the Michael addition of several nucleophiles to α,β-insaturated aldehydes and ketones, by the reversible formation of iminium ion intermediates. Due to the lower energy of the LUMO of iminium ions compared to that of the parent unsaturated carbonyls, which results in an enhancement of electrophilicity, that greatly facilitates their interaction with nucleophiles. In recent years, asymmetric aminocatalysis via chiral iminium ion intermediates has been extended to enantioselective photocatalysis. Several chiral secondary amines, such as the ones showed in Figure 37, have been developed with this finality, especially the ones that derive from L-Proline. Enantioselective iminium ion photocatalysis has been studied

in two main fields, photocycloadditions and β-alkylation of α,β-insaturated aldehydes and ketones.[113]

The first studies about photocycloadditions were reported by Mariano's group[125,126] in the 2000s with the intramolecular [2+2] photocycloaddition (Figure 47). Two interesting aspects to comment in Mariano's system are that (a) the iminium ion salt is already formed before the photoreaction was performed, instead of been generated *in situ* and (b) the substituents in the C2 and C5 positions of pyrrolidine were crucial, since depending on the functional group, the quenching of the iminium ion may occur via SET process in its singlet excited state.

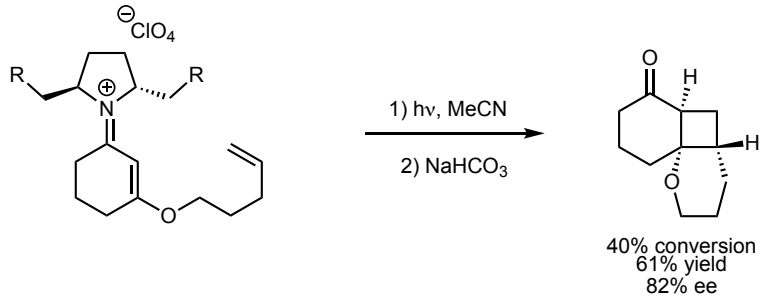


Figure 47. Intramolecular [2+2] photocycloaddition reaction reported by Mariano's group, where the reaction stereoselectivity decreases at higher conversations.

In 2020, Alemán and co-workers[127] reported a bifunctional photocatalytic system for the intermolecular [2+2] photocycloaddition via iminium ion intermediate (Figure 48). They reported that, during the reaction mechanism, the formation of an intramolecular charge transfer complex allows the preferential excitation of a transient generated chiral iminium ion, that controls the reaction stereoselectivity.

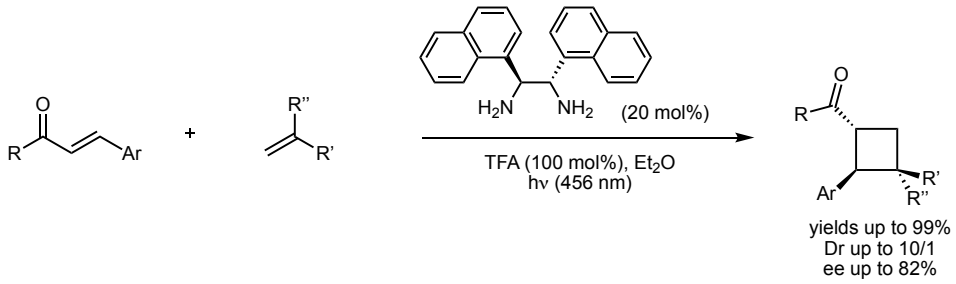


Figure 48. Bifunctional enantioselective aminocatalytic [2+2] photocycloaddition reported by Alemán and co-workers.

The first asymmetric β-alkylation of enones was reported by Melchiorre and co-workers[128] with the highly enantioselective β-addition to cyclic α,β-insaturated ketones by employing benzodioxole or aniline derivatives as alkylation agents (Figure 49).

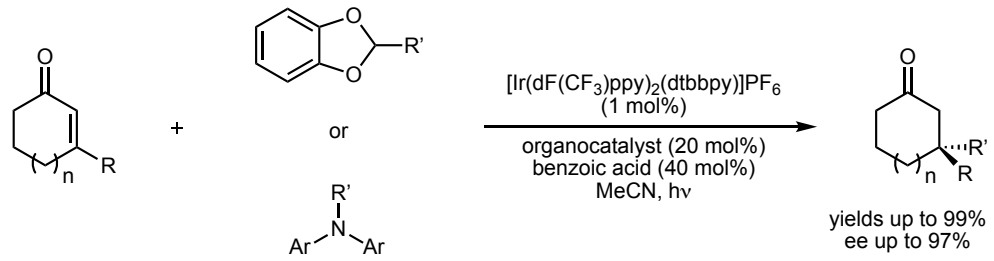


Figure 49. Enantioselective β-addition to cyclic α,β-insaturated ketones reported by Melchiorre and co-workers.

Between 2017 and 2020, Melchiorre's group published several papers[129] in which the first bifunctional system for the β-addition to α,β-insaturated aldehydes, by using a chiral photoactive organocatalyst and taking advantage of the unique excited state reduction potential of iminium ion (Figure 50).

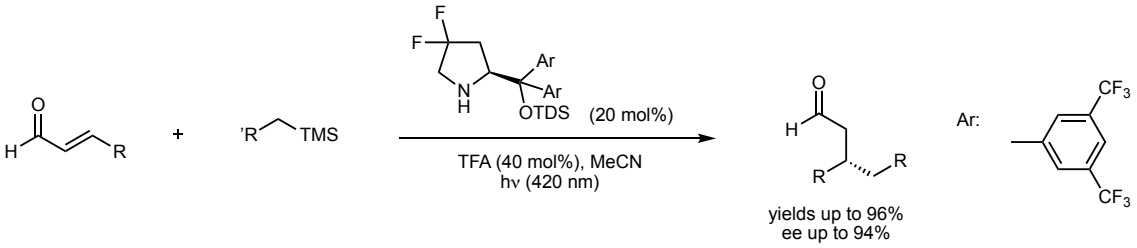


Figure 50. Bifunctional enantioselective β-functionalization of enals reported by Melchiorre and co-workers.

### 1.3.5. PORPHYRINS AS PHOTOCATALYSTS

Due to the 18 π electron aromatic system, that confers, among other characteristics, unique electronic properties which can be easily tuned by adding different substituents to the core (β-pyrrolic positions) or in the peripheries (*meso*-positions), porphyrins are considered adequate compounds to act as photocatalysts.[130]

Porphyrins have the appropriate electronic levels for both acting as photosensitizer and being engaged in SET processes for many photoprocesses.[131] That is because of their long lifetime of their triplet excited state ($10^{-6}$ s), generated via ISC, rather than their singlet excited state ($10^{-9}$ s).

Therefore, as happens with many other photocatalysts, porphyrins in their excited state, can act both as oxidants ($E_{1/2}(TPP/TPP^{-\cdot}) = -1.03$ V // $E_{1/2}(TPP^*/TPP^{-\cdot}) = +0.42$ V) and as reductants ($E_{1/2}(TPP^{+\cdot}/TPP) = +1.03$ V // $E_{1/2}(TPP^{+\cdot}/TPP^*) = -0.42$ V).[132] The ground-state and the excited-state redox potentials are referenced against the saturated calomel electrode (SCE). For comparison, the corresponding values for the commonly used $Ru(bpy)_3Cl_2$ photocatalyst are:

$E_{1/2}(Ru^{2+}/Ru^{+}) = -1.33$ V // $E_{1/2}([Ru^{2+}]^*/Ru^{+}) = +0.77$ V
$E_{1/2}(Ru^{3+}/Ru^{2+}) = +1.29$ V // $E_{1/2}(Ru^{3+}/[Ru^{2+}]^*) = -0.81$ V

As can be seen, photoexcited TPP is both less oxidant and less reductant than $Ru(bpy)_3Cl_2$.

### 1.3.5.1. Porphyrins as photosensitizers

Porphyrins have been extensively used as photosensitizers for singlet oxygen generation. As previously state, a photosensitization process consists in the excitation via light irradiation of the photosensitizer that is capable of promoting singlet oxygen molecule formation by transferring its excess of energy to the ground-state triplet oxygen, while returning to its ground state. The generated singlet oxygen molecule promotes the photochemical reaction. Since singlet oxygen is a very reactive electrophile, the use of a porphyrin compound as an oxygen photosensitizer has been studied, principally, in cycloadditions and in heteroatom oxidation reactions.[133,134]

The most studied pericyclic reactions using a porphyrin derivative for singlet oxygen formation are [2+2] and [4+2] cycloadditions. In this context, the first reaction was reported in 1944 by Schenck and Ziegler[135] with the gram scale preparation of ascaridole, taking advantage of a natural porphyrin-based photosensitizer, such as chlorophyll A (Figure 51).

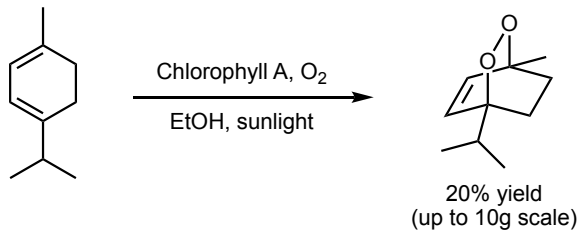


Figure 51. Ascaridole preparation reported by Schenck and Ziegler.

However, it was not until 2004 that TPP appeared in the literature as a photosensitizer when Meunier and co-workers[136] described the photooxygenation of $\alpha$-terpinene to synthesize

ascaridole, as reported by Schenck and Ziegler. The difference lies in that ascaridole was used as a synthetic intermediate for the preparation of new antimalarial drugs (Figure 52).

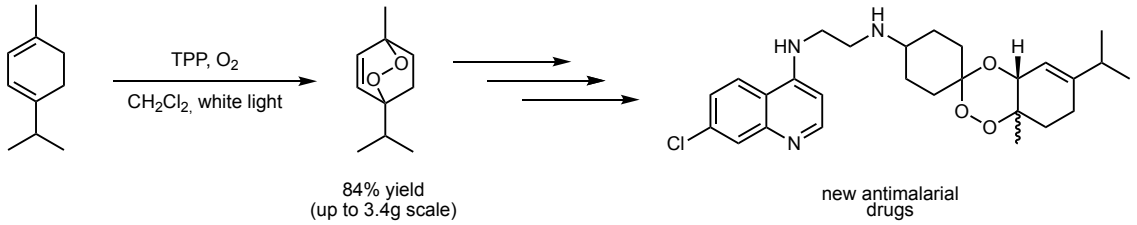


Figure 52. Antimalarial drug synthesis using a porphyrin (TPP) as photosensitizer.

Other differences are the use of white light instead of sunlight, as well as the reaction yield, that improved considerably while lowering the scale. Another important aspect to take in consideration is that porphyrins have been used as photosensitizer in many protocols for the synthesis of novel drugs, such as in the synthesis of the antimalarial API artemisin,[137] some industrial processes for pharmaceutical companies[138,139] and the synthesis of carbasugars,[140] interesting for their medicinal applications, such as the preparation of quercitol derivatives[141] (Figure 53).

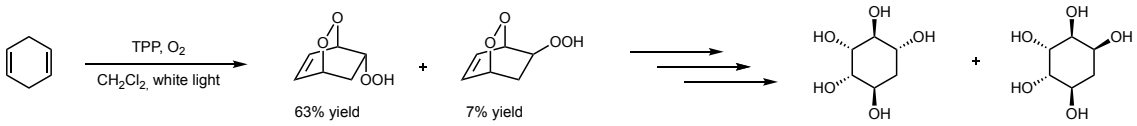


Figure 53. Preparation of quercitol derivates reported by Balci and co-workers.

Between 2018 and 2020, some new applications of porphyrins as photosensitizers have been reported for the synthesis of, for instance, (-)-oxycodone,[142] rhodonoid derivatives[143] or other products, such as furans or tropone.[144]

In 2012, Meng and co-workers[145] reported an alternative strategy for the enantioselective oxidation reaction by using a chiral phase-transfer catalyst (PTC) to induce the enantioselectivity in the reaction for the synthesis of $\alpha$-hydroxy-$\beta$-keto esters (Figure 54), reporting good yields and moderate enantiomeric excesses.

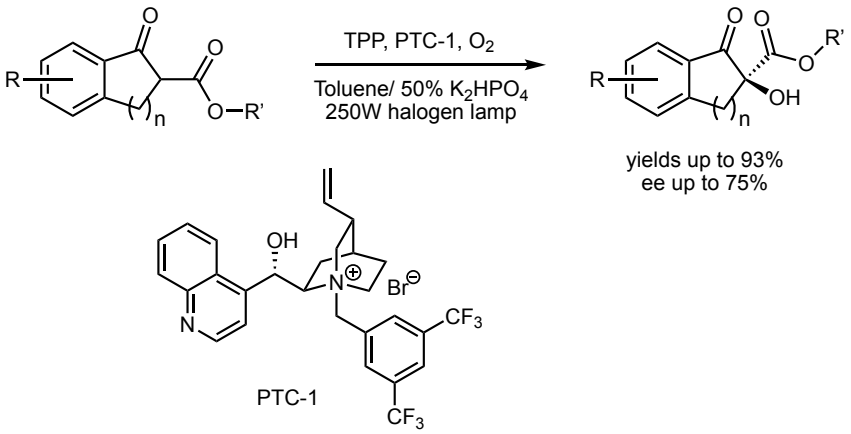


Figure 54. Synthesis of α-hydroxy-β-keto esters reported by Meng and co-workers.

Some years later, Meng's group improved their procedure by developing a new PTC.[146] Finally, in 2018, Meng and co-workers[147] developed a bifunctional photo-organocatalyst for the oxidation of both β-keto esters and β-keto amides (Figure 55).

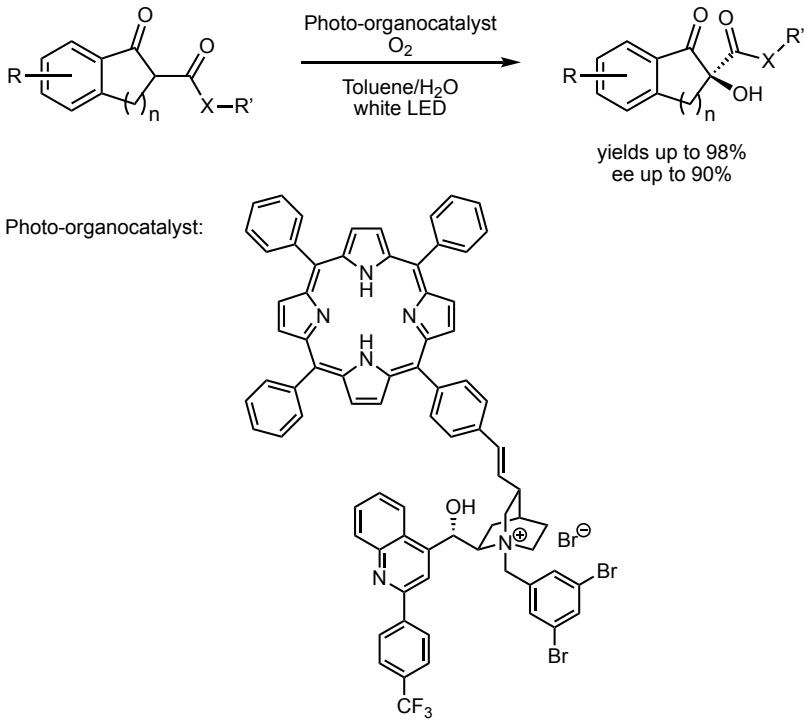


Figure 55. Bifunctional system reported by Meng and co-workers.

Porphyrins have also been used as photosensitizers in heteroatom oxidations, specially of sulfur and nitrogen. In this context, the oxidation of sulfides to sulfoxides has several applications in medicine and pharmacology.[148] In the same article, the authors reported the sulfur oxidation by using protonated TPP ($H_4TPP^{+2}$) with different counterions, showing pretty good results (Figure

56). The good results were attributed to the protonation of the porphyrin since, under light irradiation, showed an increase of its photocatalytic activity leading to a better formation of singlet oxygen.

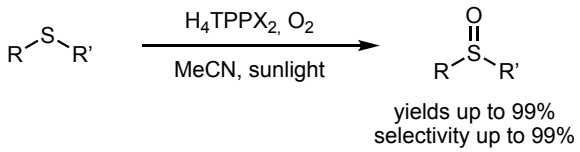


Figure 56. Oxidation of sulfides using protonated TPP reported by Mojarrad and Zakavi.

In the same year, heterogeneous catalysis was reported employing a porous aromatic framework porphyrin-based photocatalyst[149] and a covalent organic framework,[150] showing equal photocatalytic activity than porphyrin monomers with an important advantage, their easily recovery and reuse, observing in some cases no decrease in the photocatalytic activity even after four times.

The nitrogen oxidation has been principally studied in the oxidation of amines to imines, with important applications in, for instance, the formation of $\alpha$-aminoacids.[151] The first to report an amine oxidation were Chen and co-workers[152] with the oxidation of secondary amines, observing that the oxidized site was the less substituted (Figure 57).

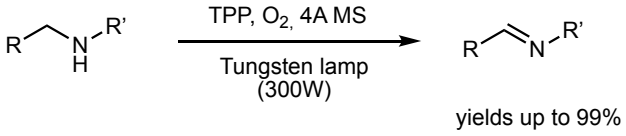


Figure 57. Secondary amines oxidation reported by Che and co-workers.

Since 2015, heterogeneous catalysis has been reported employing some MOF porphyrins[153] and 2D porphyrins-COFs,[154] obtaining similar results as their monomers.

### 1.3.5.2. Porphyrins as photoredox catalysts

Porphyrins as photoredox catalysts has been less explored than as photosensitizers, despite the fact that porphyrins can be applied in both oxidative and reductive processes, just as some important photoredox catalysts, such as $[Ru(bpy)_3]^{+2}$, $Ir(ppy)_3$ and Eosin Y.[155] However, recently some new methodologies for the construction of new carbon-carbon and carbon-heteroatom bonds using porphyrin and metalloporphyrin derivatives have been developed.

In 2017, Gryko and co-workers[156] reported a green procedure for the photoarylation of aromatic five-membered heterocycles, by using *meso*-arylated porphyrin derivatives as photoredox catalysts, being tetrakis(pentafluorophenyl)porphyrin (TPFPP) the more efficient catalyst (Figure 58). The authors saw that electron-poor porphyrins had a better catalyst behavior than electron-rich or even neutral porphyrins, but they couldn't find the cause.

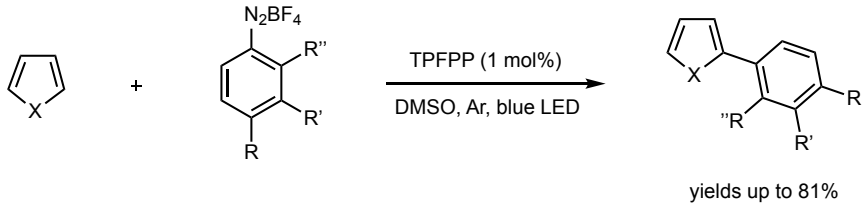


Figure 58. Photoarylation of aromatic five member heterocycles reported by Gryko and co-workers.

On the other hand, porphyrin and chlorin derivatives have been studied for their photomedical applications.[157,158] Recent studies[131] demonstrate the efficiency of TPFPP as photoredox catalyst in the arylation of enol acetates (Figure 59). The mentioned efficiency was attributed to both the thermodynamically able photooxidation process once TPFPP is excited and the rapid $TPFPP^{+}$ to TPFPP reduction process.

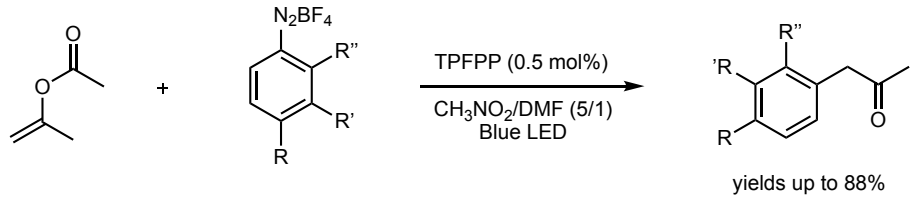


Figure 59. Arylation of enol acetates reported by de Oliveira and co-workers.

Metalloporphyrins have been mostly studied for industrial processes, such as the oxidation of cyclohexane to cyclohexanone, chalcogenylation reaction or selenylation and thiolation reactions of anilines.[159,160] For instance, Ni-TPP was used as photoredox catalyst for some coupling reactions between N-phenyltetrahydroisoquinoline and dimethyl malonate, nitromethane and indoles, giving equal or even better yields than with the originally used photocatalysts.[161,162]

In 2014, MacMillan and co-workers[163] demonstrated the use of Ni in a dual platform by combining Ni metallo-catalysis with photocatalysis for the formation of new $sp^3$-$sp^3$ and $sp^3$-$sp^2$ bonds. Although MacMillan and co-workers didn't use any porphyrin derivative for their coupling reactions, this paper became the precursor of many subsequently reported studies of

metalloporphyrins in dual photoredox catalysis.[164] For example, in 2015, Fu and co-workers[164c] reported the application of several rhodium (III) porphyrin derivatives in the hydration of terminal alkynes to ketones (Figure 60a) and in the highly regioselective defluorination of perfluoarenes (Figure 60b).

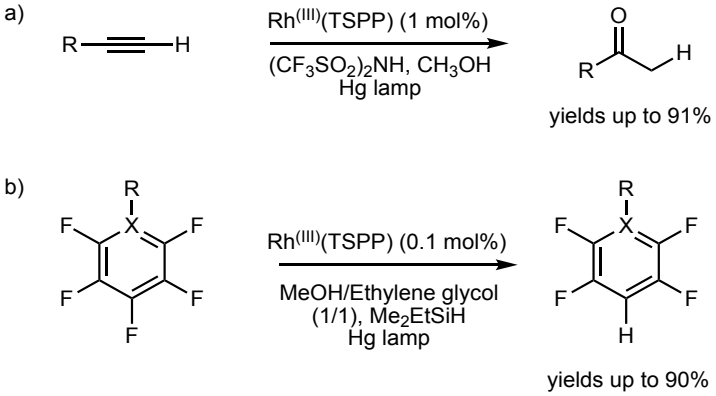


Figure 60. a) Hydration of terminal alkynes. b) Regioselective defluorination of perfluoroarenes. $Rh^{(III)}$(TSPP) = Rhodium (III) tetrakis(*p*-sulfonylphenyl)porphyrin.

Heterogeneous photocatalytic systems have been developed in the last years for photoredox catalysis. Among them, Zr-based MOF frameworks,[165] porphyrins supported in CN materials[166] or multifunctional Fe-based MOF frameworks[167] have been used, showing in all cases good yields and recovery cycles, since after five times of reuse, no decrease in their photocatalytical activity was observed.

Porphyrins containing other heteroatoms have shown interesting catalytic photoredox activity due to their different electronical properties from those of regular $N_4$-porphyrins, what makes them absorb and emit light at lower energies. A very representative example was reported in 2016 by Derksen and co-workers[168] with the dehalogenation of $\alpha$-functionalized carbonyl-containing compounds under red light irradiation (Figure 61).

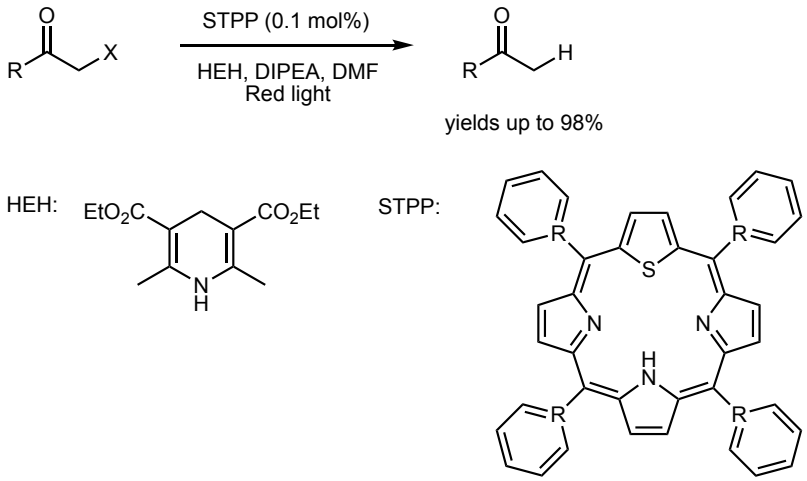


Figure 61. Dehalogenation of α-functionalized carbonyl-containing compounds reported by Derken and co-workers, using a non-N4-porphyrin as photoredox catalyst. X = Br, Cl.

In 2016, Gryko and co-workers[169] reported the α-alkylation of aldehydes using TPP and Zn-TPP as photocatalysts. They argued that the porphyrin is involved in both energy transfer and SET processes in two connected cycles, demonstrating the fact that porphyrins can act both as photosensitizers and as photoredox catalyst (Figure 62). The mechanism of this reaction will be discussed in Chapter 5.


Figure 62. α-Alkylation of aldehydes reported by Gryko and co-workers, using diazo compounds as alkylating agents.

# CHAPTER 2. OBJECTIVES

The objectives set in the context of this PhD Thesis, following the topics developed in the previous Chapter, are the following:

[1] The development of a dual catalysis system for photochemical Diels-Alder cycloadditions through the merging of photoredox catalysis with asymmetric aminocatalysis via iminium ion. The use of porphyrins as photocatalysts and of imidazolidinones, of general structure **16** (Figure 63), as organocatalysts was proposed.

**16-I** **16-II**

Figure 63. Imidazolidinones to be used as organocatalysts in the photochemical Diels-Alder reactions.

[2]. The synthesis of porphyrin derived imidazolidinones, of general structure **17** (Figure 64), and their subsequent use as bifunctional photocatalysts for the photochemical cycloadditions studied in the previous objective.

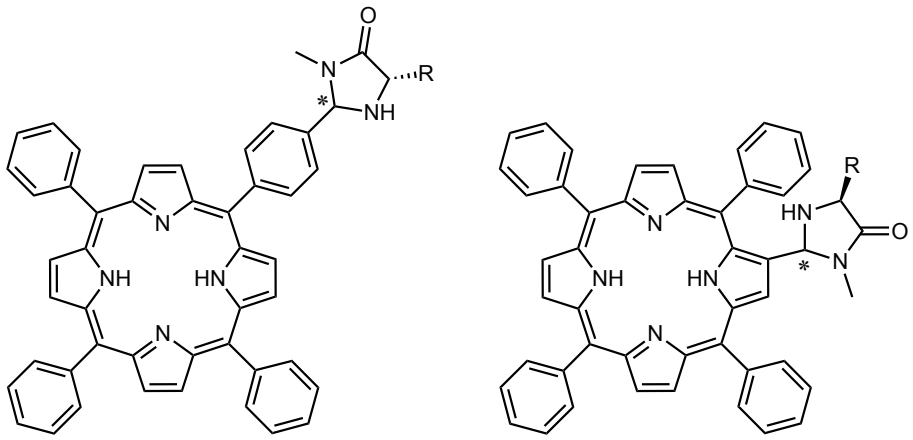

**17-I** **17-II**

Figure 64. Imidazolidinones-based amino-functionalized porphyrins synthesized in this present work.

[3]. The study of the enantioselectivity of the photochemical $\alpha$-alkylation reaction of aldehydes, using a porphyrin as photocatalyst, through the coupling of photoredox catalysis and asymmetric aminocatalysis via enamine, by using chiral pyrrolidines based on L-Proline as organocatalysts.

[4]. The synthesis of L-Proline-derived amino-functionalized porphyrins, of general structure **18** (Figure 65), and their subsequent use as bifunctional photocatalysts for the photochemical α-alkylation reactions of aldehydes studied in the previous objective.

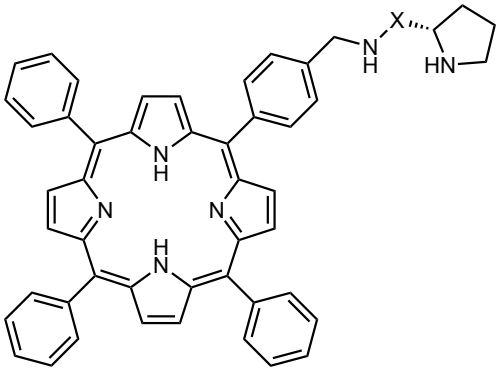


**18**

Figure 65. L-Proline-based amino-functionalized porphyrins synthesized in this present work.

# CHAPTER 3. SYNTHESIS OF AMINO-FUNCTIONALIZED PORPHYRINS

As discussed in Chapter 1, porphyrins, due to their unique photochemical properties, have been recently postulated as a green alternative to the use of transition metal based photocatalysts, such as the commonly used Ru(II) and Ir(III) bipyridyl complexes. On the other hand, the synthesis of functionalized porphyrins in order to modify their properties has aroused great interest among different research groups. In 2014, we started to investigate the synthetic possibilities offered by amino-functionalized porphyrins to yield new organocatalysts; at the beginning of this PhD Thesis, we set out to explore their use as bifunctional photo-organocatalysts.

We centered our efforts on two types of porphyrin-based bifunctional catalysts: functionalized porphyrins **17**, based on MacMillan's imidazolidinones, that were designed to study the photoinduced Diels-Alder reactions in a bifunctional system (see objective [3] above), and the derivatives **18**, with the aim of being used in a bifunctional system for the study of the organophotocatalytic $\alpha$-alkylation of aldehydes (see objective [4] above).

The syntheses that we developed for these bifunctional catalysts, as well as an explanation of the key steps, are detailed below.

## 3.1. SYNTHESIS OF CATALYST 17a

For the first set of bifunctional catalysts, we decided to use imidazolidinones because of the advantages they offer from a synthetic point of view, (a) the possibility of starting from inexpensive starting materials, since the cyclization step takes place by condensation between the methylamide derived from an $\alpha$-aminoacid, which contains the $R_1$ group of the imidazolidinone, and an aldehyde, which provides the $R_2$ group of the same, in our case a porphyrin (Scheme 14), and (b) the possibility of modulating their characteristics by selecting different substituents, thus allowing the synthesis of a wide range of compounds with very different properties among them.

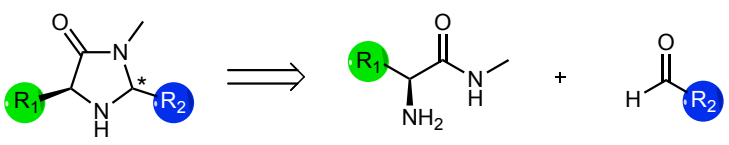


Scheme 14. Design of the photoaminocatalyst.

The preparation of porphyrin derivatives **17-I** should be relatively straightforward, since they could be obtained by condensation of 5-(4-formylphenyl)-10,15,20-triphenylporphyrin with a methylamide derivative of an α-aminoacid. In a similar way, derivatives **17-II** could arise from a similar condensation, involving 2-formyl-(5,10,15,20)-tetraphenylporphyrin:

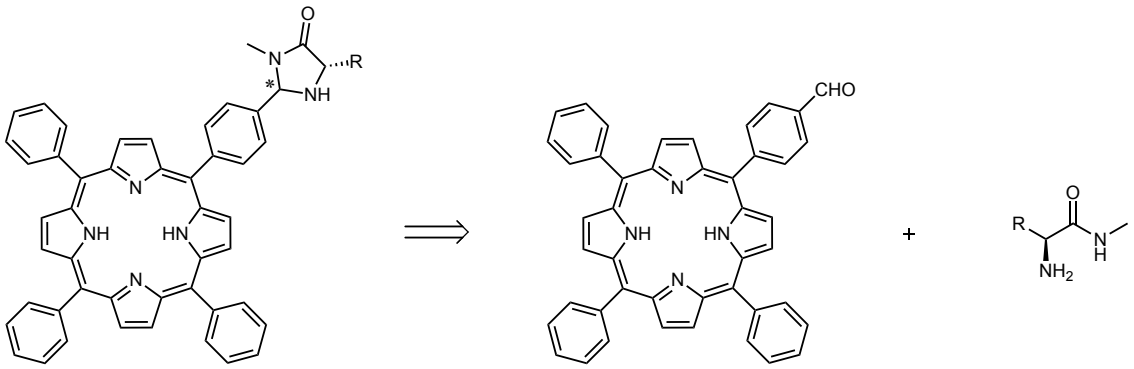


**17-I**

Scheme 15. Retrosynthetic scheme for porphyrin derivative **17-I**.

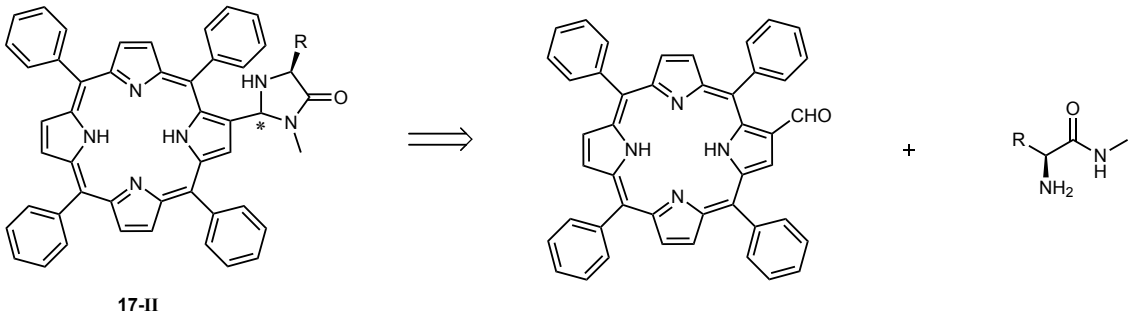


**17-II**

Scheme 16. Retrosynthetic scheme for porphyrin derivative **17-II**.

The most commonly method used for obtaining methylamides derived from *L*-α-aminoacids (Scheme 17) is based on the treatment at room temperature of the hydrochloride of the corresponding methyl ester (generally commercially available) with an excess of methylamine (40% aqueous solution).[170] The methylamide hydrochloride is obtained by elimination of the solvent and can be stored for extended periods of time. Just before the condensation with the aldehyde, the free base (more unstable) is isolated by neutralization, either with a solution of NaOH in ethanol (method A)[170] or with aqueous ammonia (method B).[116] If the methyl ester hydrochloride is not available, it can be prepared by esterification of the α-aminoacid in a methanol solution at room temperature and in presence of thionyl chloride (to generate hydrogen chloride *in situ*; Scheme 18).[171] In this way, methylamides derived from (*S*)-alanine (**23**), (*S*)-phenylalanine (**24**), glycine (**25**) and (*S*)-*tert*-leucine (**26**) have been prepared, with overall yields above 80% (except in the case of **25** and **26**, which gave moderate yields in the neutralization step).

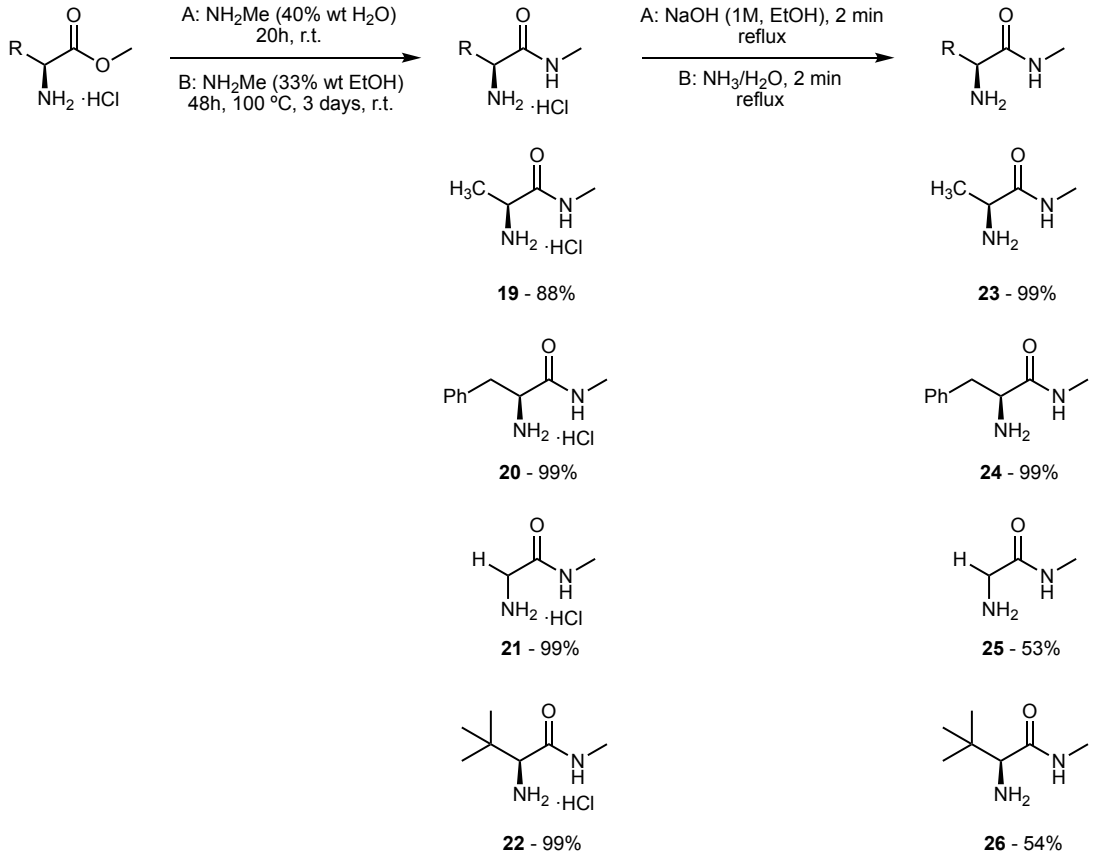


Scheme 17. Synthesis of *N*-methylamides derived from $\alpha$-aminoacids.

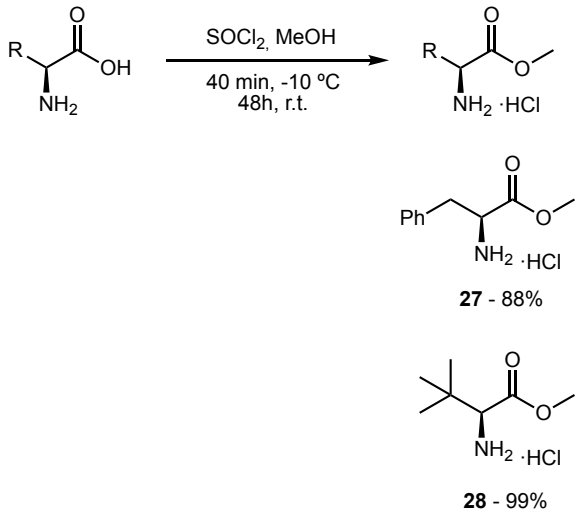


Scheme 18. Synthesis of methyl ester hydrochlorides derived from $\alpha$-aminoacids.

Regarding the porphyrincarbaldehyde components we have synthesized, following procedures described in the literature, two formylated derivatives of *meso*-tetraphenylporphyrin: 4-(10,15,20-triphenylporphyrin-5-yl) benzaldehyde **34** (and its corresponding Cu(II) metallated derivative,

**35**),[172] and 2-formyl-(5,10,15,20)-tetraphenylporphyrin **38** (in the form of Cu(II) metallated derivative).[41]

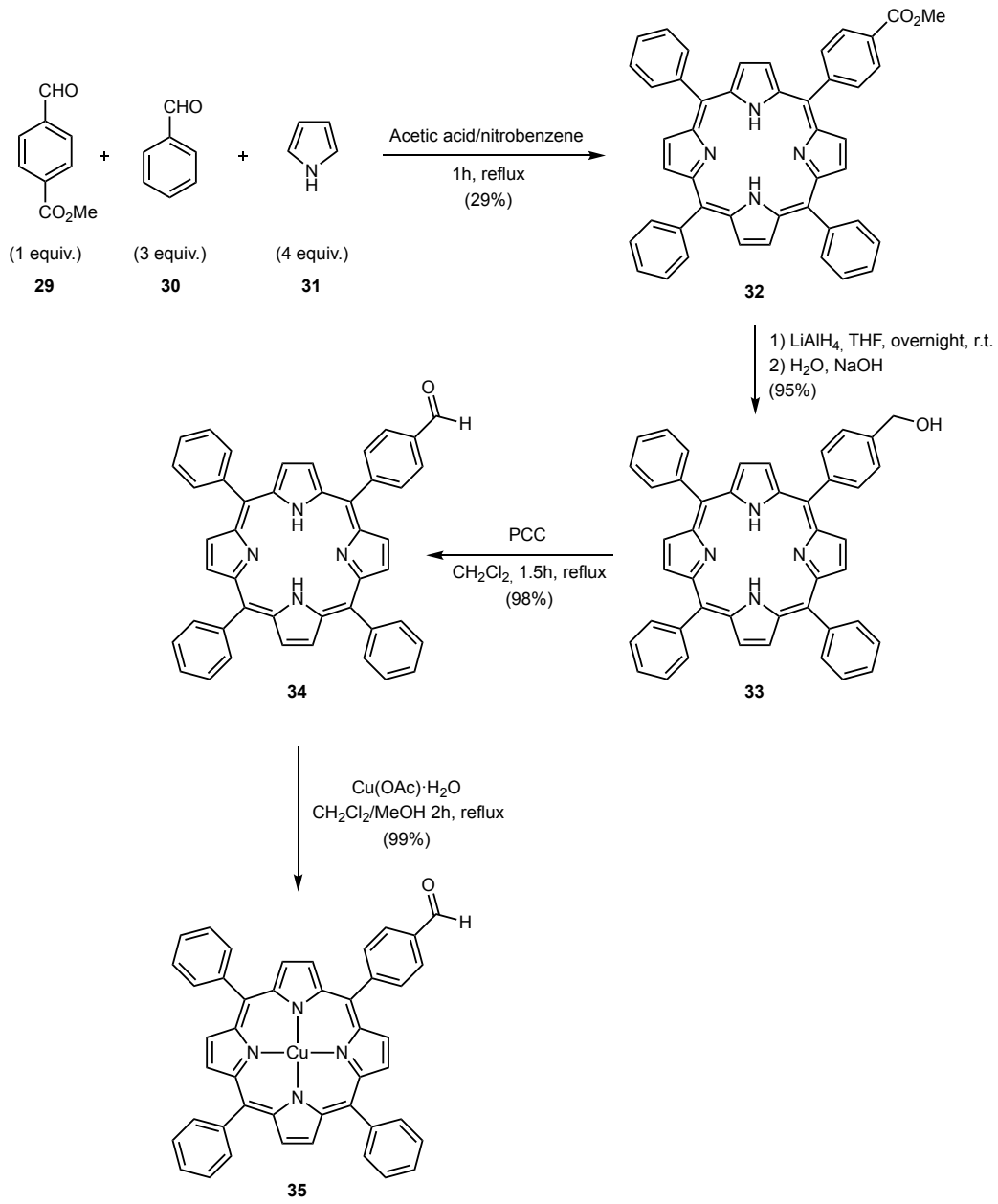


Scheme 19. Preparation of copper (II) 4-(10,15,20-triphenylporphyrin-5-yl) benzaldehyde **35**.

The synthesis of **35** begins with the obtention of porphyrin **32** by the method of Alder and Longo by the reaction of one molar equivalent of methyl 4-formylbenzoate **29** with 3 equivalents of benzaldehyde **30** and 4 equivalents of pyrrole **31**, in nitrobenzene at reflux in the presence of acetic acid.[173] After chromatographic purification, the resulting monofunctionalized porphyrin, which was obtained in remarkable yield (29%, corresponding to a 66% of the statistical yield), was reduced with lithium aluminium hydride to give the carbinol **33**,[147] whose subsequent oxidation with PCC

afforded the desired aldehyde **34** in excellent yield. Finally, by the acetate method, metallation with Cu(II) was carried out obtaining aldehyde **35** (Scheme 19).[172]

On the other hand, the synthesis of porphyrin **38** (Scheme 20) starts with the obtention of TPP **36** using the Adler and Longo method (21% yield after recrystallization).[174] Subsequently, the copper is coordinated using the acetate method and, finally, the β-formylation step is carried out.[41] Once the Vilsmeier-Haack complex has been prepared *in situ* (step 1), a solution of the copper-TPP complex **37** in 1,2-dichloroethane is added and heated at reflux for 7 hours, leading to porphyrin **38** in essentially quantitative yield.

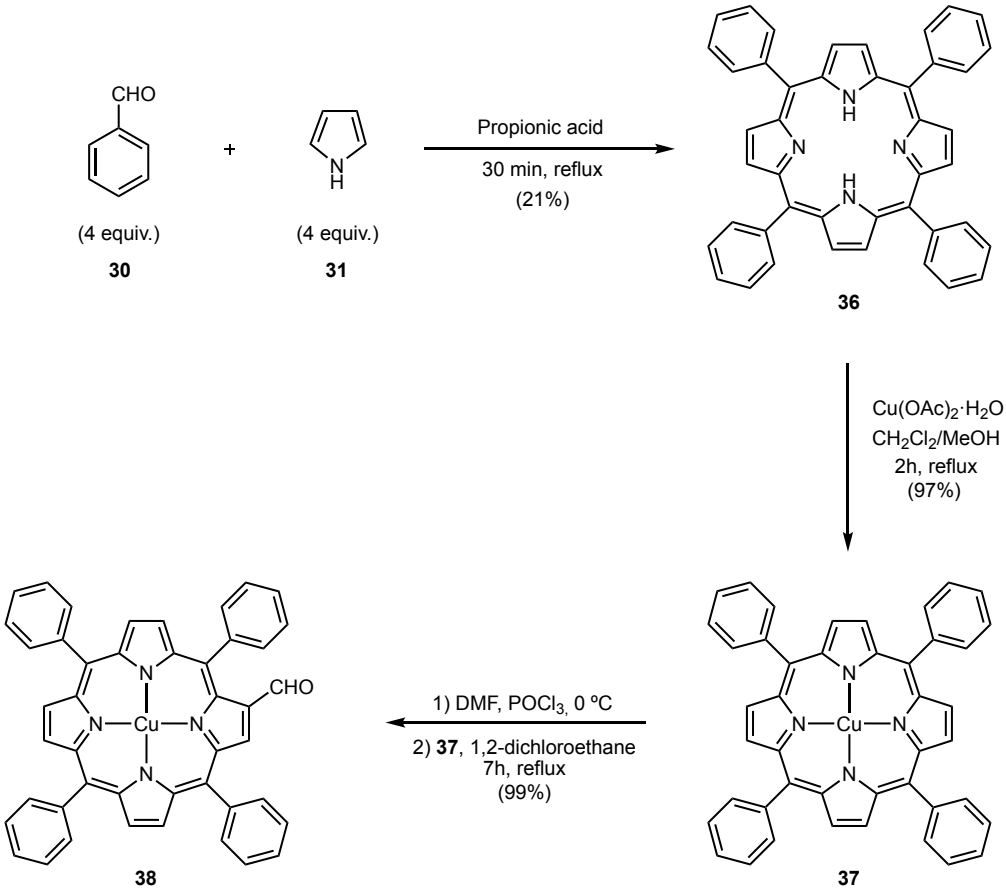


Scheme 20. Obtention of copper (II) 2-formyl-5,10,15,20-tetraphenyl porphyrin **38**.

Then, the bifunctional catalysts were prepared. With the methyl amide derivative **23** and aldehyde **35** in our hands, the imidazolidinone formation step was carried out by means of a Lewis acid catalyzed condensation reaction (Scheme 21).

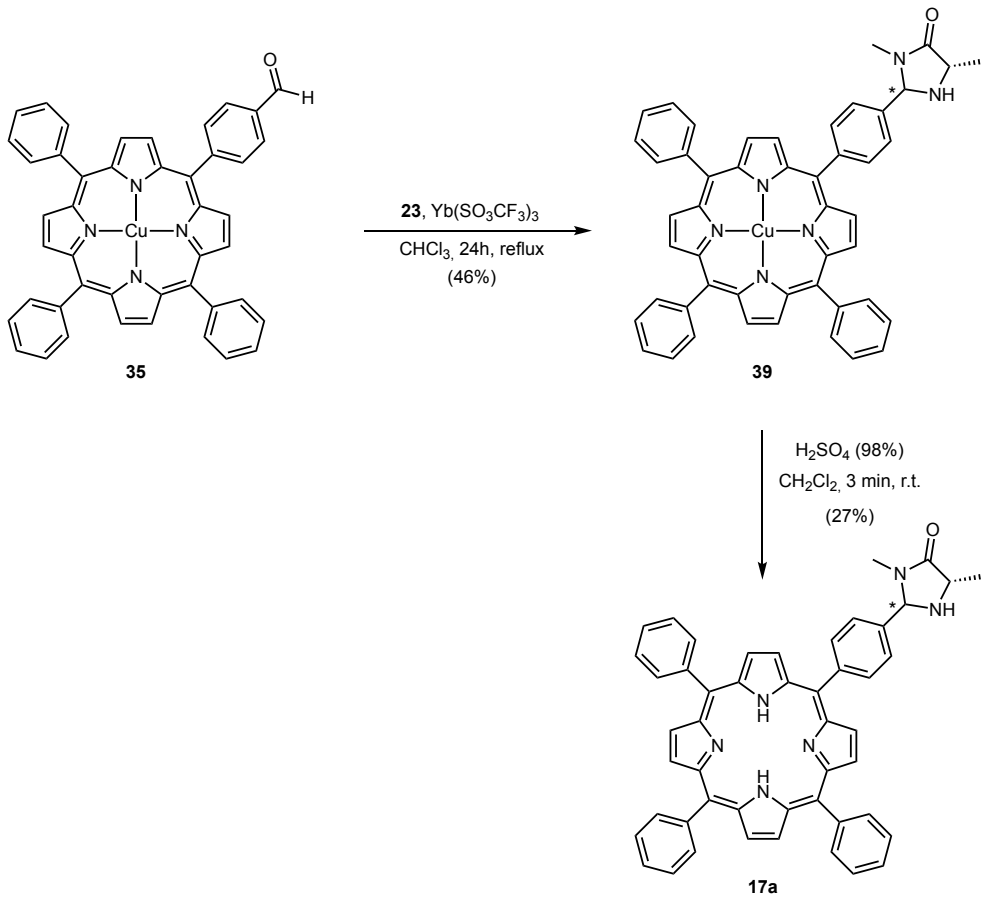


Scheme 21. Obtention of bifunctional catalyst **17a**.

The condensation between both reagents takes place at reflux in a reaction catalyzed by $Yb(SO_3CF_3)_3$, adapting the experimental procedure to that described by Alemán and co-workers.[121] Once the metallated imidazolidinone **39** is obtained, the porphyrin is demetallized in acid medium, thus obtaining the bifunctional catalyst **17a** as mixture of isomers that could not be separated by chromatography.

It is important to comment on why the use of porphyrin **35** in its metallated form is necessary. The two functions of the Ytterbium catalyst are the following, (a) to activate the carbonyl of the aldehyde to give rise to an imine intermediate, which will subsequently lead to the formation of the imidazolidinone, and (b) to coordinate with the N of the imine functional group of that intermediate, to promote the cyclization step. When the tetrapyrrole core of the porphyrin is not previously coordinated to a metal, Ytterbium is able to coordinate with the porphyrin, inhibiting the cyclization step, affording the imine intermediate as the sole product of the reaction.

This intermediate was isolated and characterized via $^{1}$H-NMR, exhibiting a singlet at a chemical shift of 8.62 ppm that corresponds to the proton of the imine group (Figure 66). Subsequent analysis of the $^{13}$C-NMR spectrum, that shows a signal at a chemical shift of 192.4 ppm, and HRMS confirmed that the isolated compound corresponded to imine **40**.

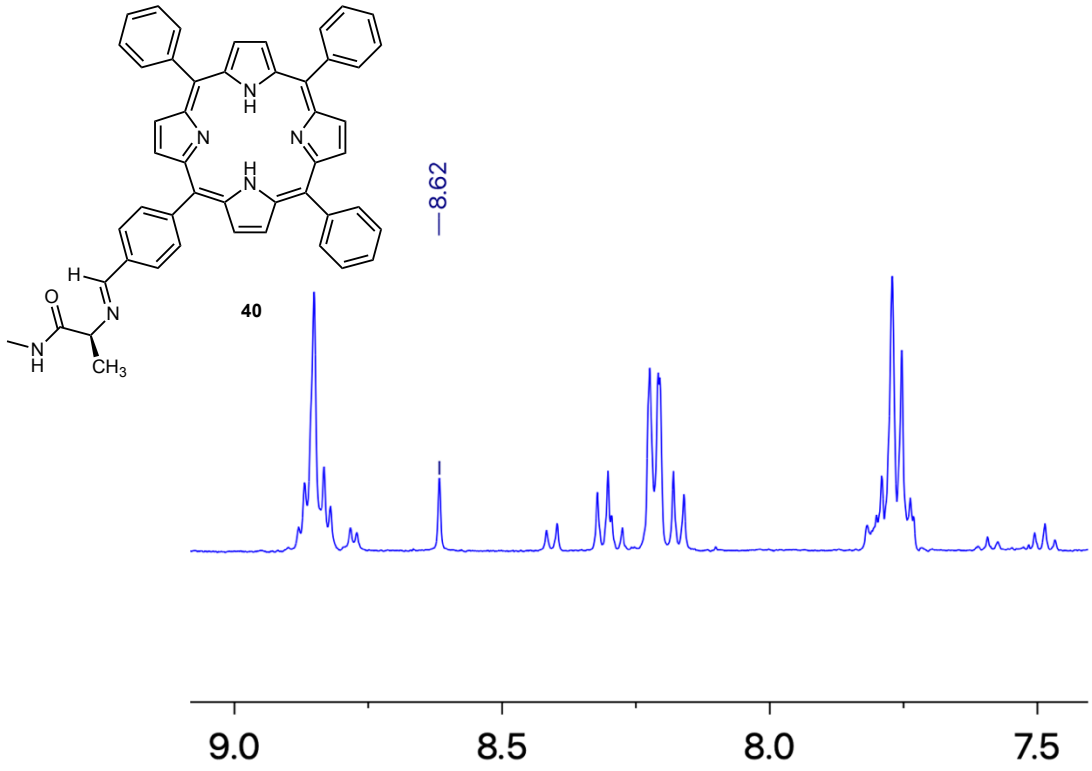


Figure 66. $^{1}$H-NMR characteristic signal for imine **40**.

The main problem observed during the synthesis of catalyst **17a** was that it could not be isolated in a pure form, since the demetallation step resulted in very complex product mixtures that were difficult to separate by column chromatography. In addition, the yields of the condensation and demetallation steps were low. Therefore, despite the development of a synthetic route to obtain it, its use in future photochemical reactions was discarded by us.

## 3.2. SYNTHESIS OF CATALYSTS 17b-d

In the light of the problems encountered during the synthesis of compound **17a**, we decided next to prepare catalysts **17b-d**, starting from porphyrin **38**, in which the formyl group is placed at a β-pyrrolic position.

Once derivatives **24**, **25** and **26** as well as porphyrin **38** were synthesized, we proceeded to the formation of imidazolidinone following the same method employed for catalyst **17a** (Scheme 22).

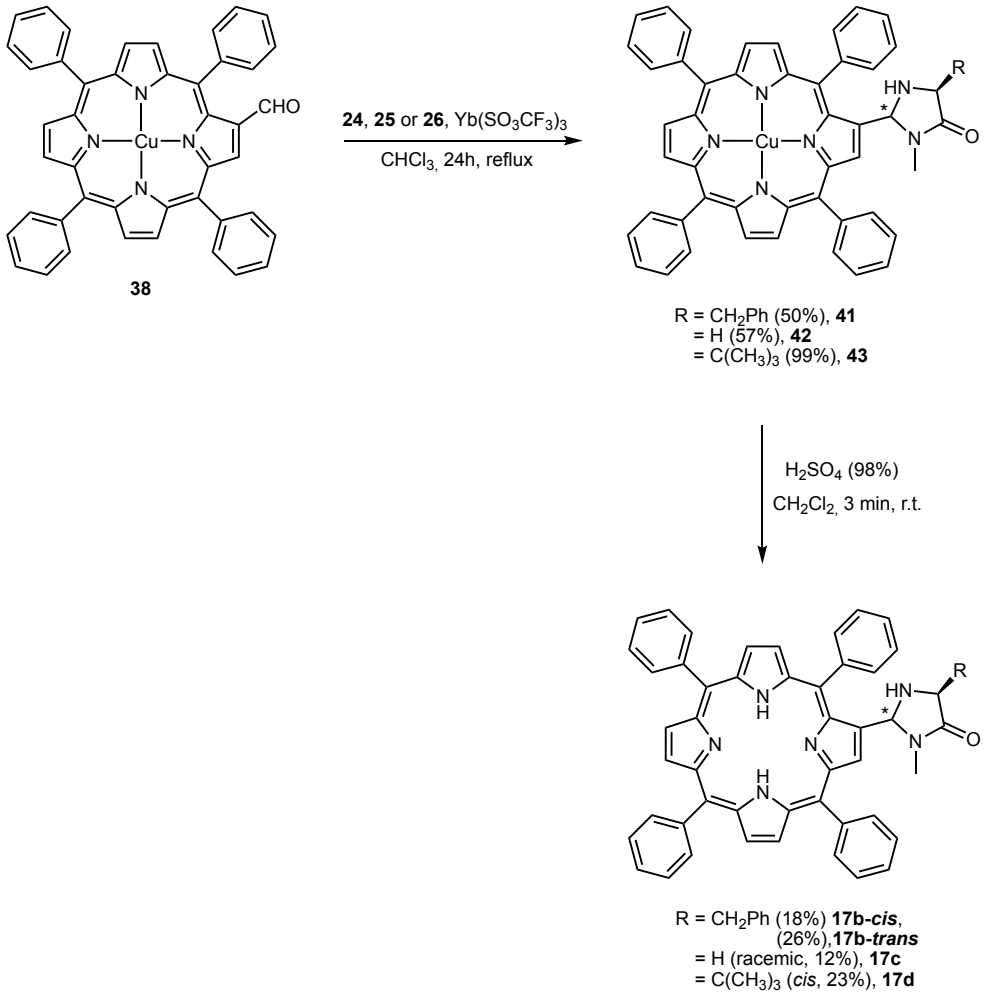


Scheme 22. Obtention of bifunctional catalysts **17b-d**.

The use of the metallated porphyrin was again crucial, since otherwise we would again obtain the imine as the final product of the reaction. After the cyclization, the demetallation in acidic medium furnished the catalysts **17b-d**.

For catalyst **17b**, a mixture of the *cis* and *trans* diastereomers was obtained, avoiding the formation of complex mixtures of products. The two isomers could be separated by column chromatography and were characterized by analysis of the $^{1}$H-NMR, $^{13}$C-NMR, $^{1}$H-$^{13}$C HSQC, $^{1}$H-$^{1}$H COSY, $^{1}$H-$^{1}$H ROESY, UV-Vis and HMRS (ESI) spectra. Assignment of the stereochemistry of both diastereomers can be made via $^{1}$H-NMR, with a different multiplicity pattern appearing at a chemical shift between 4.00 and 2.60 ppm, corresponding to the signals of the diastereotopic protons of the benzyl group (AB) and the proton at $\alpha$-position to the carbonyl (X) (Figure 67).

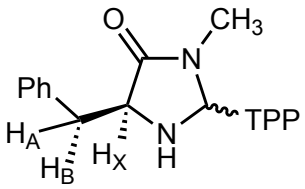


Figure 67. Simplified structure of catalyst **17b**.

For the less polar diastereomer, a first order set of signals, corresponding to the ABX system, is observed, where the $\alpha$-carbonyl proton X appears as a doublet of doublets at 3.9 ppm, giving rise to a different coupling constant with both diastereotopic protons of benzyl group A and B. It is also important to note that these A and B protons give rise to different sets of signals at a chemical shift of 3.1 and 2.8 ppm, respectively.

For the other diastereomer, the main difference observed is the appearance of a different set of signals corresponding to the ABX system. At 3.6 ppm appears a triplet corresponding to the $\alpha$-carbonyl proton X and a doublet at 3.1 ppm with an integration of 2 protons, corresponding to the benzylic protons A and B. In fact, the observed system can be mistaken for an $A_2X$ spin system.

At this point, we hypothesized that the differences observed in the $^{1}$H-NMR spectra could be due to a different degree of freedom of rotational between the two isomers. A possible explanation is that due to $\pi$-stacking attractive interactions between the benzene and the porphyrin, the *cis* isomer presents a much more restricted rotation than the *trans* isomer, and such an interaction could not occur for the latter (Figure 68).

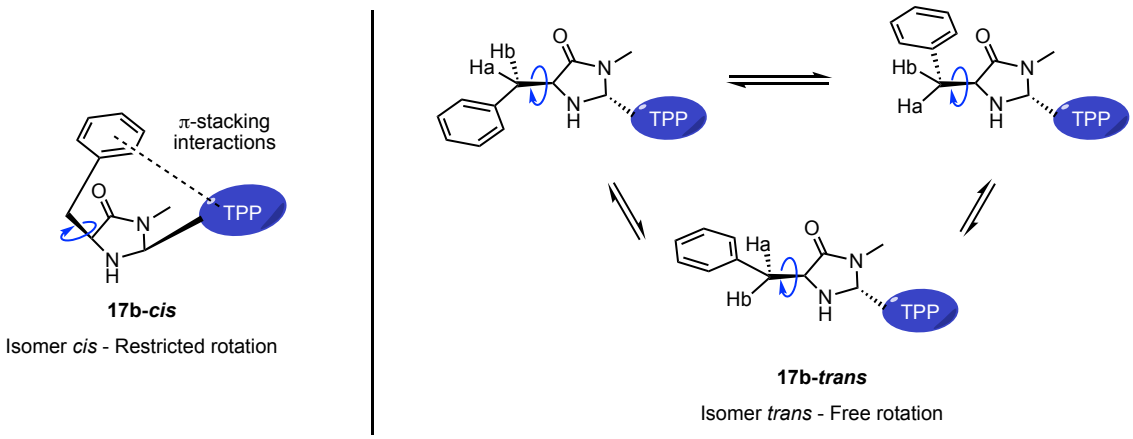


Figure 68. Comparation of the rotational freedom of the benzyl group in the *cis* and *trans* isomers.

To understand the different behavior shown by the two diastereomers, we decided to perform molecular mechanics calculations on the three lowest energy conformations of both diastereomers (Figure 69). These calculations were performed using Spartan 14 employing Monte-Carlo with the MMFF force field. Redundant conformers were manually removed. The analyses showed that, in the *cis* isomer, the benzyl group is able to interact with the π-electrons of the aromatic ring of the porphyrin, giving rise to the aforementioned π-stacking interactions which subsequently results in a rigid conformation for this isomer.

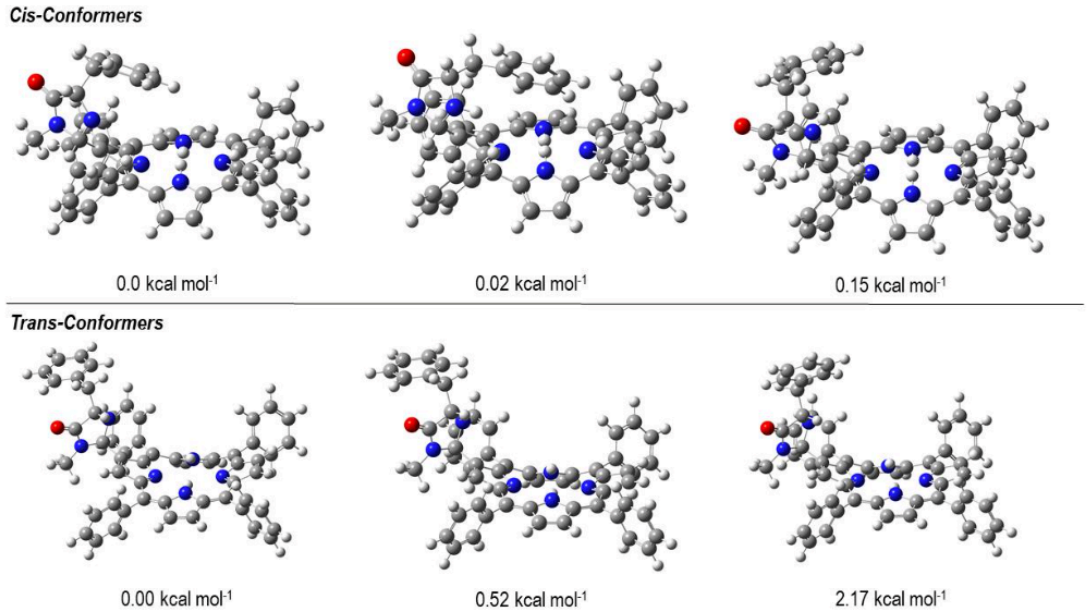


Figure 69. Three lowest energy conformers for the *cis* and *trans* isomers and their relative energies.

Accordingly, we could conclude that the isomer exhibiting an AMX subspectrum, with different chemical shifts for the two methylene protons and also with different $J_{AX}$ and $J_{MX}$ coupling constants, should therefore correspond to the *cis* isomer. Contrarywise, for the *trans* isomer the rapid conversion between the conformers with similar stabilities would result in the averaging of both the chemical shifts and of the coupling constants, leading to an ABX subspectrum in which $J_{AX} = J_{BX}$ (Figure 70).

It is worth noting that the calculations were performed at the molecular mechanics level to get a first idea of which isomer might correspond to which $^1$H-NMR spectrum. In order to determine experimentally the spatial proximity between the protons of the imidazolidinone ring and the ones of the porphyrin ring of the *cis*-isomer, both $^1$H-$^1$H NOESY and $^1$H-$^1$H ROESY spectra were performed. Unfortunately, we were unable to detect any diagnostic signal to confirm our assignment.

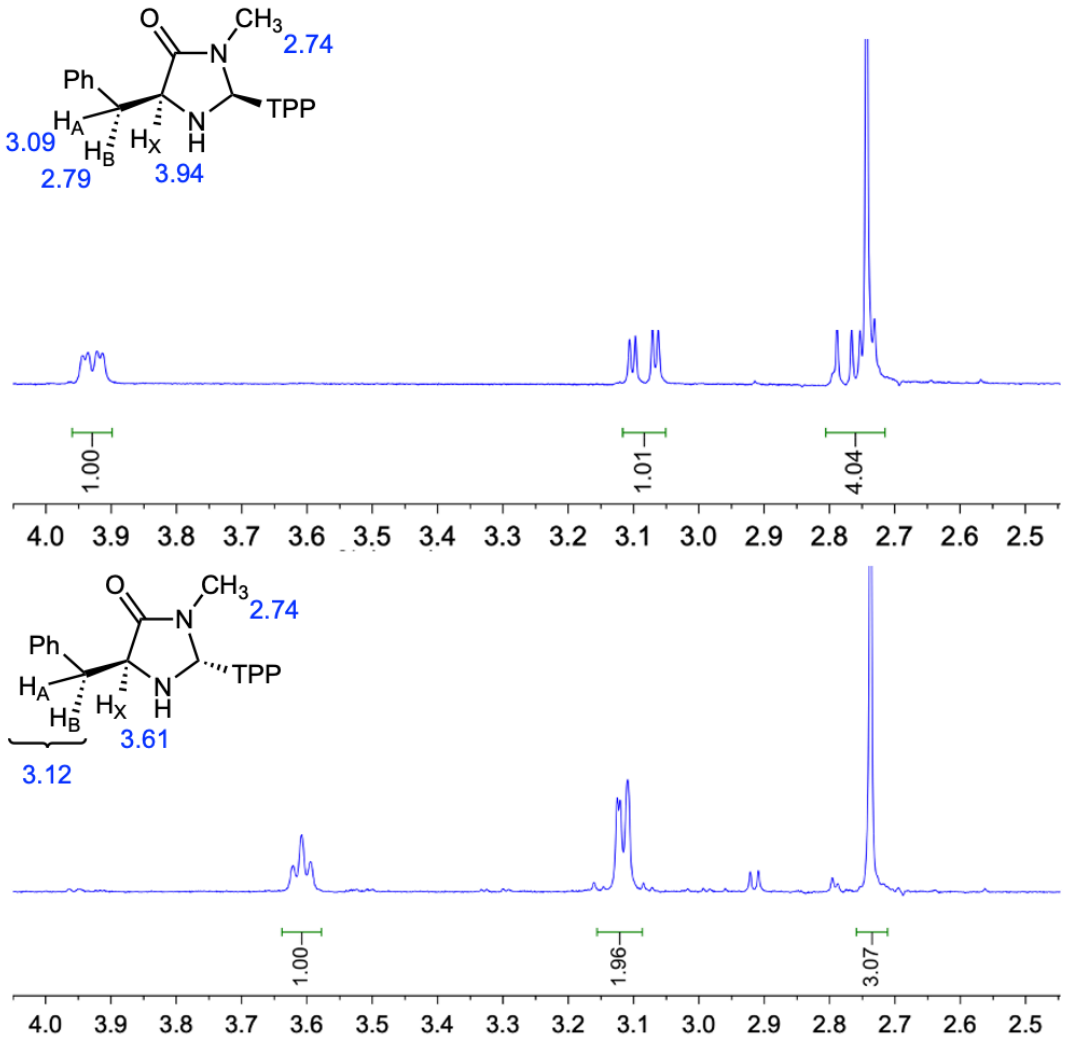


Figure 70. Assignment of the $^1$H-NMR spectra to the corresponding *cis* (top) *and trans* (bottom) diastereomers.

Catalyst **17c** was obtained in its racemic form and its use for future reactions was discarded.

Catalyst **17d** was obtained as a single diastereomer to which we assigned a *cis* configuration, assuming it to be the most stable since the imidazolidinone ring adopts an "envelope-type" conformation with both substituents in relative 1,3-diequatorial arrangement, this being more stable due to a decrease in the steric hindrance between both bulky substituents (Figure 71).

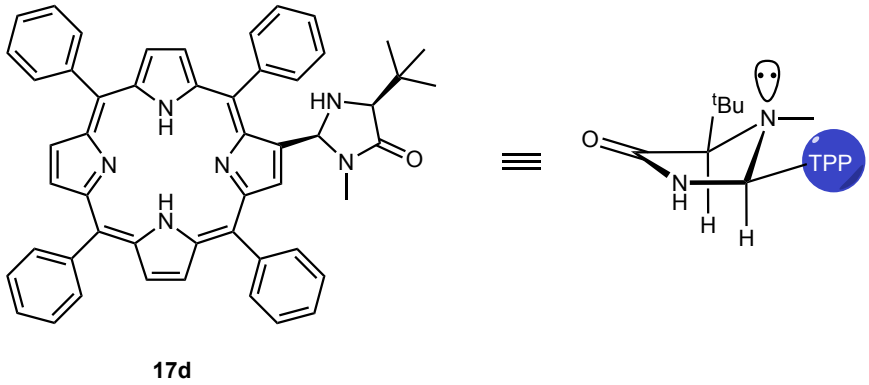


**17d**

Figure 71. "Envelope-type" conformation adopted by the *cis* isomer of catalyst **17d**.

Compounds **17b-d** were subsequently studied as organocatalysts in Diels-Alder reactions under both thermal and photochemical conditions.

## 3.3. SYNTHESIS OF CATALYST 18a

In addition to the bifunctional catalysts **17a-d**, in which a TPP unit is combined with an organocatalytic unit based on the imidazolidinone structure, we decided to prepare and study compounds **18a** and **18b**, in which the organocatalytic unit is derived from L-Proline. These chiral molecules would allow us to study asymmetric organophotocatalytic reactions of enolizable carbonyl compounds susceptible to activation by formation of an enamine (Figure 72).

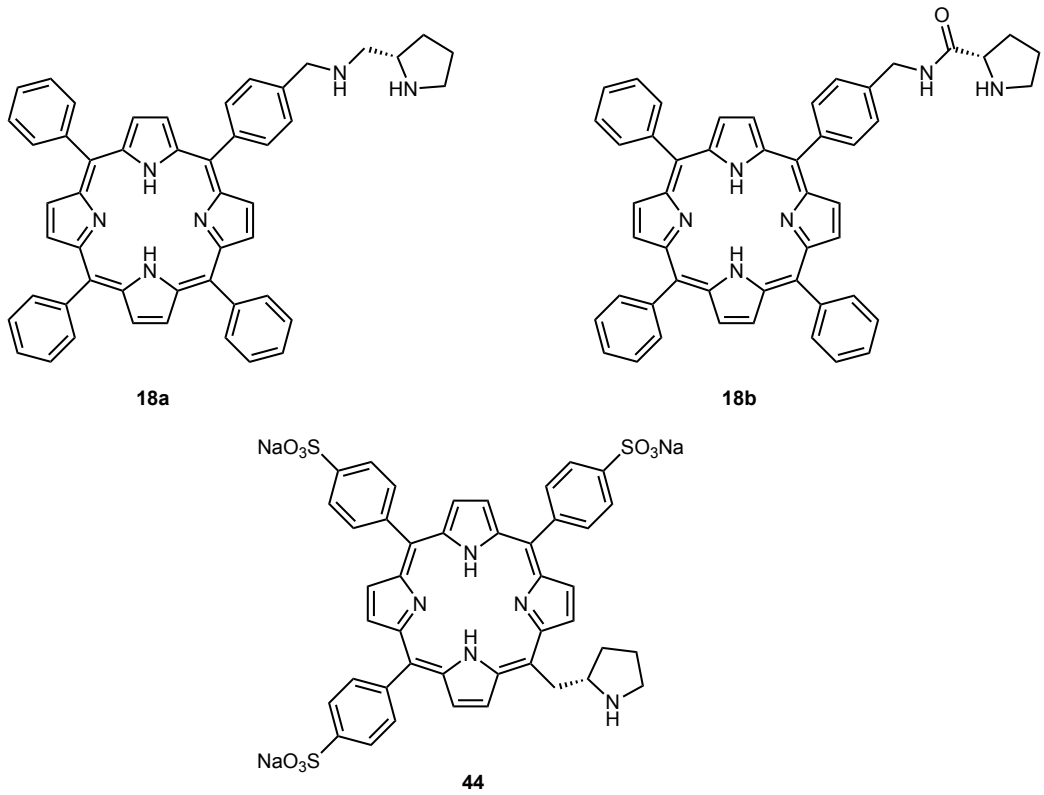


Figure 72. L-Proline-based amino-functionalized porphyrins synthesized in this present work.

Catalysts **18a** and **18b** had not been prepared previously, while the bifunctional catalyst **44** had been synthesized in the PhD Thesis of Aitor Arlegui.[54] Thus, it was necessary to design a synthetic route for the first two catalysts. The synthesis of catalyst **18a** is detailed below and, in the next section, that of catalyst **18b**.

For the synthesis of bifunctional catalyst **18a**, *N-tert*-butyloxycarbonyl (*S*)-2-aminemethylpyrrolidine **50** was prepared according to the route shown in Scheme 23, based on transformations previously described in the chemical literature.[175]

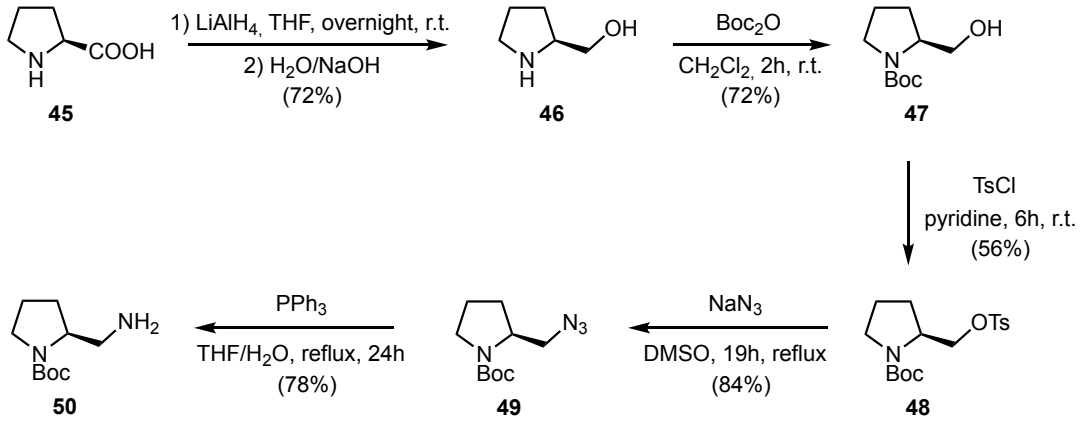


Scheme 23. Synthetic route for the preparation of *tert*-butyl (*S*)-2-aminomethyl pyrrolidine **50**.

The synthesis started with the reduction of L-Proline **45** to its corresponding alcohol **46** with lithium aluminium hydride in THF solution, followed by the subsequent protection of the amine group, obtaining the protected aminoalcohol **47**. To replace the alcohol group by the amine, the strategy followed was to transform the alcohol into a good leaving group by means of its derivatization to a tosylate by the treatment of **47** with *p*-toluenesulfonic chloride in pyridine, that afforded the compound **48**. Then, via a $S_N2$-type reaction with sodium azide under reflux of DMSO, the tosyl group was replaced by an azide group, which was subsequently reduced to a primary amine with triphenylphosphine using a mixture of water and THF (for the hydrolysis of the intermediate iminophosphorane) as solvent.

To synthesize the desired bifunctional catalyst, a strategy involving the reductive amination between *tert*-butyl (*S*)-2-aminomethylpyrrolidine **50** and aldehyde **34** was proposed. The synthesis of the aldehyde is shown in Scheme 19 above. The synthetic route developed to obtain catalyst **18a** is shown in Scheme 24.

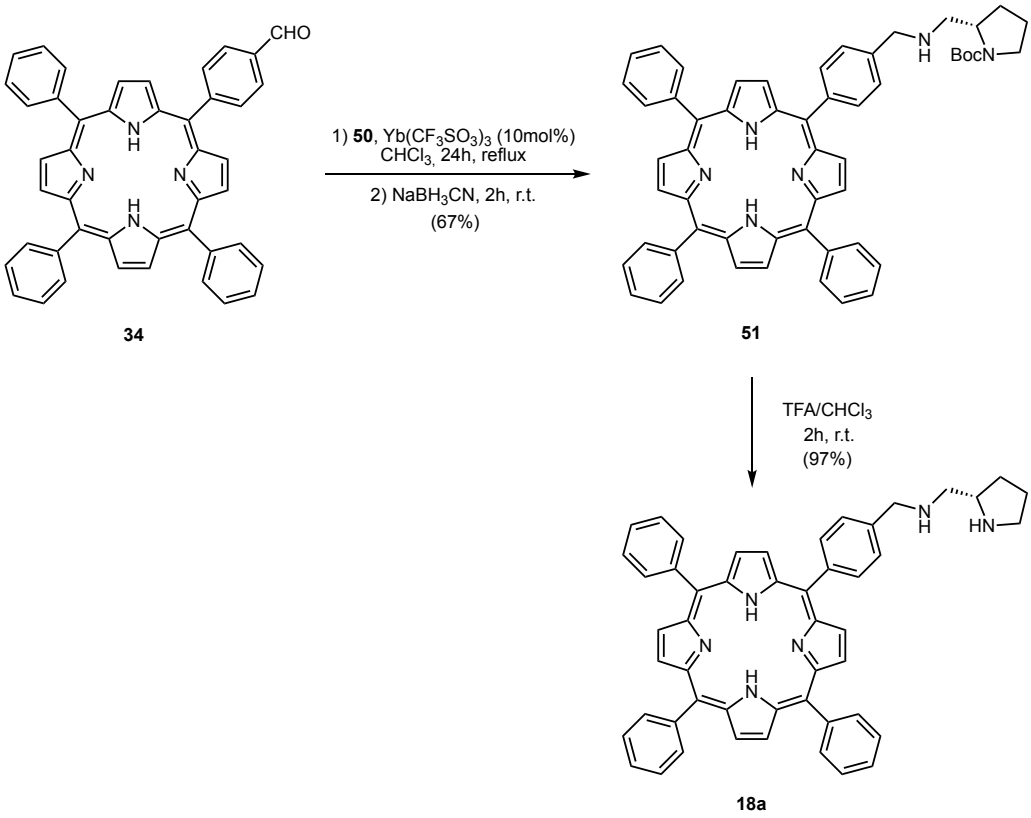


Scheme 24. Synthetic route for the preparation of bifunctional catalyst **18a**.

For the reductive amination step, different conditions were tested to see which of them gave the best results. These are shown in Table 1.

| Entry | Conditions | Yield |
|---|---|---|
| **1**[a] | MeOH/THF, $NaBH_4$, 1.5h, reflux | 0% |
| **2**[a] | THF, $NaBH_3CN$, 22h, r.t. | 0% |
| **3**[a,b] | $CHCl_3$, $Yb(SO_3CF_3)_3$, $NaBH_4$, 23h, reflux | 0% |
| **4**[b] | 1) $CHCl_3$, $Yb(SO_3CF_3)_3$, 24h, reflux 2) $NaBH_3CN$, 2h, r.t. | 67% |

Table 1. Reduction amination conditions tested. [a]The total reduction of aldehyde to alcohol was observed. [b]Readapted procedure from reference 121.

Initially, the procedure used was the same as the described in the original preparation of compound **50**,[175] so we thought that it could be a good starting point. We observed however the complete reduction of the aldehyde to alcohol, and no amine was formed (Entry 1). At this point, we drew two conclusions, (a) the solvent was not the most indicated, since this type of porphyrins presents a relatively low solubility in polar solvents such as methanol, and (b) the reducing agent used was strong enough to reduce the aldehyde to an alcohol, inhibiting the formation of the imine intermediate which gives rise to the amine through the reduction step.

We therefore decided to search the literature for reaction conditions that could be suitable for our porphyrin.[176] Using THF as a solvent in which **34** was more soluble and changing the reducing agent to a milder one such as $NaBH_3CN$, the reaction still resulted in the total reduction of the aldehyde to alcohol (Entry 2).

At this point, seeing that we always obtained the alcohol, we thought that the problem may lay in the non-formation of the imine intermediate. Given the results obtained in the parallel synthesis of the porphyrin-based bifunctional catalysts **17a-d**, when using a non-metallated porphyrin we obtained the imine, we decided to take advantage of these experimental results to access the desired product. Unfortunately, we again obtained alcohol **33** (Entry 3).

The conclusion we drew after analyzing the results obtained was that perhaps the imine formation step was in this case slower than the reduction step, so that the aldehyde and the amine would not have enough time react before the reduction of the former takes place.

To test our hypothesis, we repeated the same procedure, but introducing a change. Since it was observed that the imine was formed after 24 hours at reflux, we decided to add the reducing agent after that time and, by monitoring the evolution of the reaction by TLC, the resulting mixture was stirred at room temperature for 2 h. As shown in Table 1 (Entry 4) the desired product **51** was obtained in good yield (67%). When aldehyde **34** was substituted by the Cu(II) complex **35**, reductive amination afforded the functionalized metalloporphyrin **52** in satisfactory yield (Scheme 25).

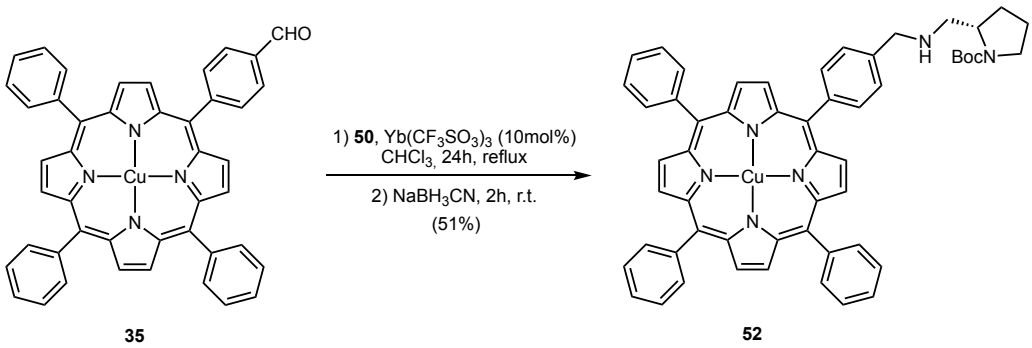


Scheme 25. Reductive amination step using metallated porphyrin **35** as starting material.

Finally, for the amine deprotection step of the pyrrolidine ring, different conditions were also tested since certain problems appeared in the course of the reaction. The different conditions that were tested are shown in Table 2.

| Entry | Conditions | Yield |
|---|---|---|
| **1**[a] | TFA, $CH_2Cl_2$, 1h, r.t. | 0% |
| **2**[a] | $H_2SO_4$ 98%, 2 min, r.t. | 0% |
| **3** | TFA, $CH_2Cl_2$, 30 min, r.t. | 0% |
| **4** | $H_3PO_4$ (aq., 85%), $CH_2Cl_2$, 3h, r.t. | 6% |
| **5** | 1) $BF_3{\cdot}Et_2O$ (0.2 equiv.), $CH_2Cl_2$, 3h, 0 ºC 2) $BF_3{\cdot}Et_2O$ (2 equiv.) 3h, r.t. | 15% |
| **6** | TFA, $CHCl_3$, 2h, r.t. | 97% |

Table 2. Boc deprotection conditions tested. [a]**52** was used as starting material.

Initially, the conditions normally used in the group for this type of deprotections (treating a dichloromethane solution of the *N*-Boc derivative with an excess of trifluoroacetic acid) were tested. To our surprise, neither the starting material **51** nor the deprotected compound **18a** were obtained, instead we observed the degradation of the starting material into a complex mixture of subproducts (Entry 1).

Because the first two conditions were tested on the metallated compound, we decided to attempt the Boc group deprotection using the same conditions as for copper decoordination.[177] Despite the fact that demetallation took place, we again observed the degradation of the starting material (Entry 2).

Because the reductive amination product **51** could perhaps decompose in a strongly acidic medium, we decided to attempt the deprotection in a milder acidic medium. Thus, we saw in the literature that both the use of a weaker Brønsted acid such as $H_3PO_4$ (aq., 85%),[178] and the use of a Lewis acid such as $BF_3$-$Et_2O$[179] gave good results. When applied on our porphyrin, what we observed was that in both cases we obtained the deprotected product **18a**, but in very low yields, not being acceptable enough for our objectives (Entries 4 and 5).

Finally, we found an article that used this type of deprotections on amino-functionalized porphyrins.[180] As can be seen in Entry 6, the only difference between the standard conditions (Entry 3) and those described in the new procedure is a change in the solvent, using $CHCl_3$ instead of $CH_2Cl_2$. In the mentioned article, the authors de not discuss why $CHCl_3$ is used as the solvent, but we believe that there is a solubility issue. When the porphyrin is protonated by the strongly acidic medium of the reaction, it becomes highly insoluble in a not too polar solvent such as $CH_2Cl_2$, but surprisingly it is still sufficiently soluble in $CHCl_3$ for the reaction to take place, obtaining very good yields (Entry 6).

At the same time, given the difficulties we were having in finding optimal conditions for the deprotection reaction, as an alternative, we decided to change the protecting group to the carbobenzyloxy group (Cbz). Following the same experimental procedures shown in Schemes 21 and 22 and knowing that to cleave the benzyl carbamate we should proceed via catalytic hydrogenation on activated palladium on carbon, these conditions should not affect the porphyrin macrocycle since its aromatic system of 18 $\pi$ electrons confers a great stability to be reduced under mild hydrogenation conditions. As for the previous protecting group, the unprotected product **18a** was not found due to the high insolubility of this type of porphyrins in solvents such as methanol or ethanol.

## 3.4. SYNTHESIS OF CATALYST 18b

We then proceeded to the synthesis of the bifunctional catalyst **18b**, which contains an amide group in its structure.

The synthesis starts with the protection with the Boc group of L-Proline (Scheme 26). Using as solvent a mixture of THF and a saturated aqueous $NaHCO_3$ solution, the protection takes place by adding the di-*tert*-butyl dicarbonate and leaving the reaction stirring at room temperature overnight, *N*-Boc-L-Proline **53** is obtained in practically quantitative yield.[181]

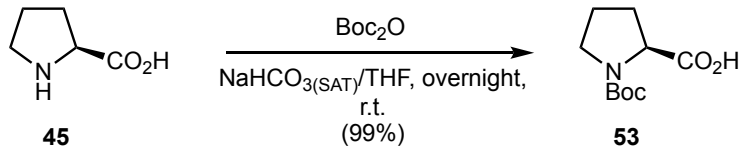


**45** **53**

Scheme 26. Obtention of precursor *N*-Boc-L-Proline **53**.

To synthesize the bifunctional catalyst **18b**, a coupling strategy between *N*-Boc-L-Proline **53** and the TPP-derivative amine **56** was proposed to form the amide group. The synthesis of **56** is shown below in Scheme 27.

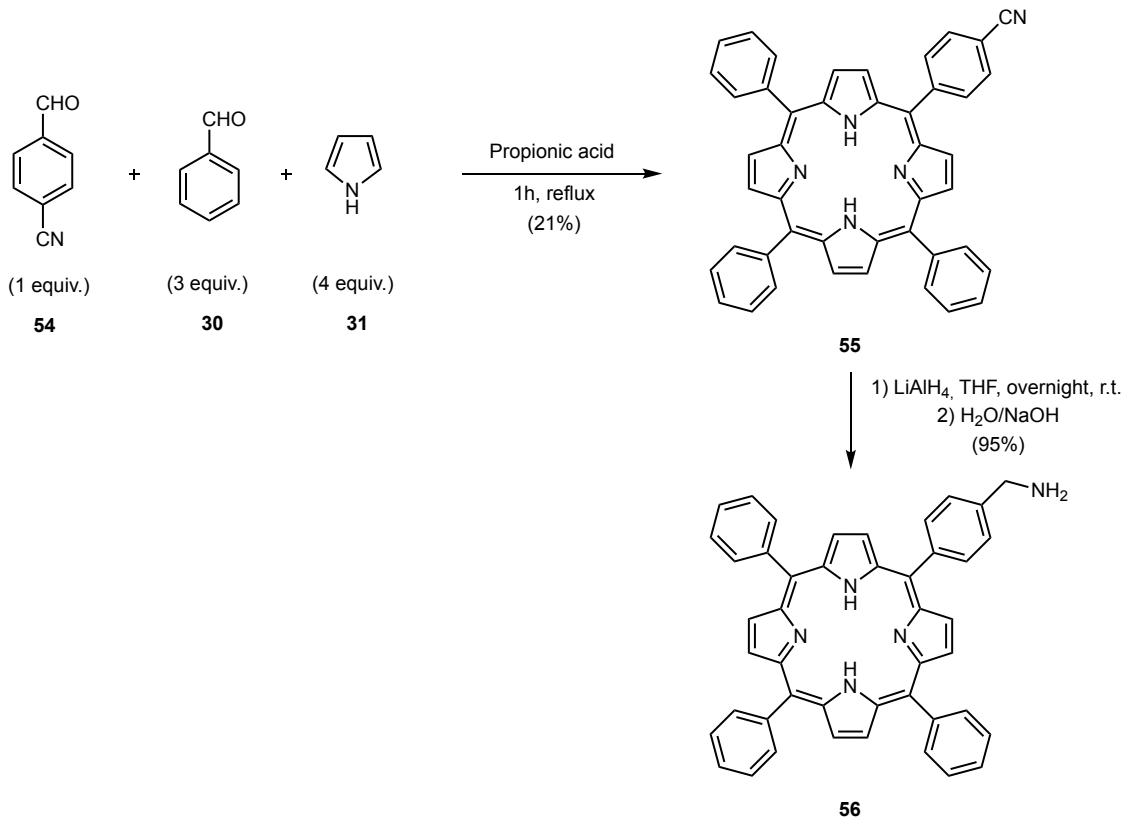


(1 equiv.) (3 equiv.) (4 equiv.)

**54** **30** **31** **55** **56**

Scheme 27. Synthesis of 4-(10,15,20-triphenylporphyrin-5-yl)methanamine **56**.

First, by the Adler and Longo method,[182] functionalized porphyrin **55**, having a nitrile group at a *para* position in one of the benzenes, was synthesized. To a solution of *p*-cyanobenzaldehyde **54** in propionic acid at reflux, benzaldehyde **30** and pyrrole **31** were added and stirred for one hour at the same temperature. After the corresponding double chromatographic purification, the desired nitrile was obtained in a 21% overall yield (48% of the statistical theoretical yield). Next, the reduction of the cyano group to amine took place by the addition of a solution of **55** in THF,[147] affording the 5-(4-aminomethylphenyl)-10,15,20-triphenyl porphyrin **56** in nearly quantitative manner.

Once both *N*-Boc-L-Proline **53** and porphyrin **56** had been synthesized, the coupling and subsequently deprotection of the Boc group was carried out. The synthetic route chosen is shown in Scheme 28.

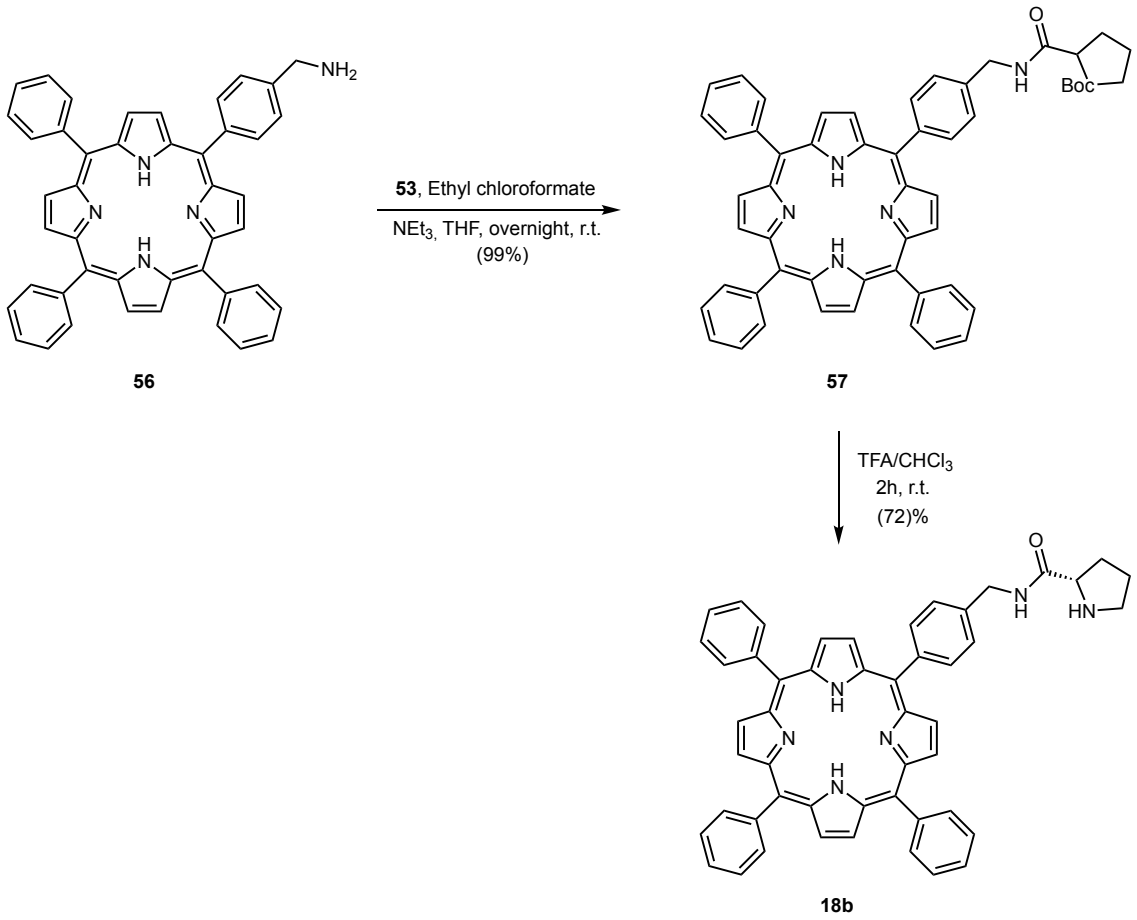


Scheme 28. Synthesis of the bifunctional catalyst **18b**.

The formation of the amide functional group took place by transformation of the carboxylic acid group of **53** into a mixed anhydride with ethyl chloroformate, that subsequently underwent a

nucleophilic attack by the amine **56**. Finally, deprotection of the Boc protecting group was performed with TFA in $CHCl_3$, using the same procedure that was employed above for the bifunctional catalyst **18a**.

# CHAPTER 4. STUDY OF THE DIELS-ALDER REACTION

Asymmetric Diels-Alder reactions have been widely studied in the field of synthetic organic chemistry.[183,184] As mentioned in the Introduction, in 2000 MacMillan and co-workers described the first Diels-Alder reaction that took place by enantioselective organocatalysis[1] bringing together two hitherto unrelated concepts, the activation of aldehydes via reversible formation of an iminium cation and asymmetric catalysis.

Before setting out to study the organocatalytic properties of amino-functionalized porphyrins **17b-*cis***, **17b-*trans***, **41** *(cis/trans* isomer mixture) and **17d** in purely photochemical cycloadditions, we decided to test their ability in the catalysis of a standard Diels–Alder cycloaddition, comparing the results obtained under purely thermal conditions with those resulting from carrying out the catalysis under irradiation with visible light. In this way, we would ascertain if these compounds were able to form efficiently the intermediate unsaturated iminium cations required in the organocatalytic cycle.

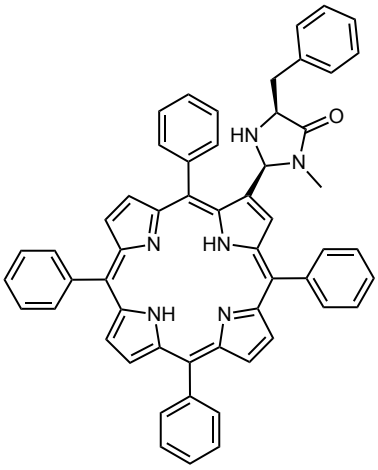


**17b-*cis***

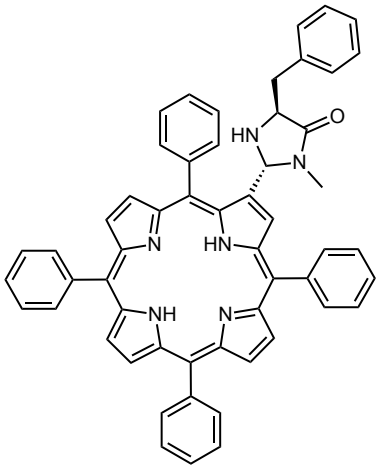


**17b-*trans***

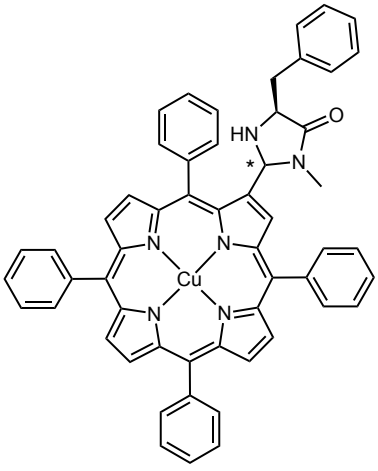


**41** (*cis/trans isomer mixture)*

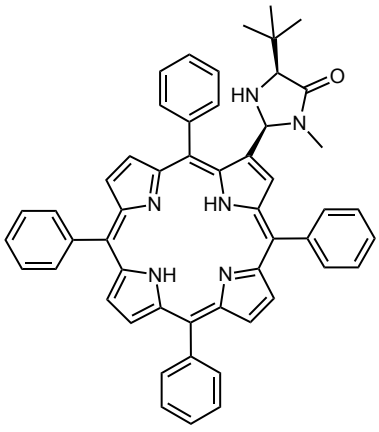


**17d**

Figure 73. Amino-functionalized porphyrins used as organocatalysts in the study of the Diels-Alder cycloaddition.

## 4.1. THERMAL DIELS-ALDER REACTIONS

The study of the Diels-Alder cycloadditions under purely thermal conditions was performed on the reaction between cinnamaldehyde **58** and cyclopentadiene **59**, adapting the conditions reported by MacMillan and co-workers.[1] For the sake of comparison, imidazolidinone **16b** was used as the reference organocatalyst. The results obtained are shown in Table 3.

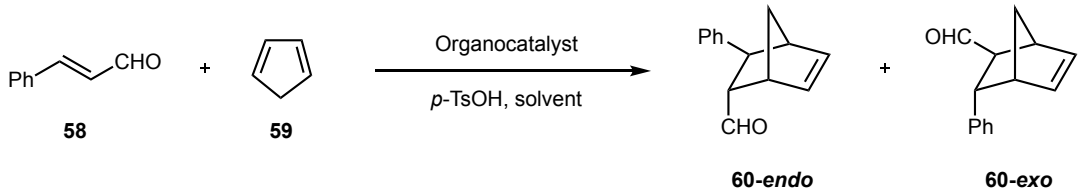


| Entry[a] | Organocatalyst | Solvent | Yield[b] | Dr (*endo*/*exo*)[c] | ee (*endo*/*exo*)[d] |
|---|---|---|---|---|---|
| **1** | **17b-*cis*** | Toluene | 9% | 75/25 | 3% (2*S*, 3*S*)/ 1% (2*S*, 3*S*) |
| **2** | **17b-*trans*** | Toluene | 27% | 68/32 | 3% (2*S*, 3*S*)/ 49% (2*S*, 3*S*) |
| **3** | **17d** | Toluene | 0% | - | - |
| **4** | **41** | MeOH/$H_2O$ (95/5) | 36% | 29/71 | 37% (2*S*, 3*S*)/ 43% (2*S*, 3*S*) |
| **5**[e] | **16b** | MeOH/$H_2O$ (95/5) | 48% | 53/47 | 71% (2*S*, 3*S*)/ 81% (2*S*, 3*S*) |

Table 3. Study of the Diels-Alder reaction between cyclopentadiene and cinnamaldehyde under thermal conditions. [a]Reaction conditions: cinnamaldehyde **58** (0.5 mmol, 1 equiv.), cyclopentadiene **59** (1.5 mmol, 3 equiv.), organocatalyst (5 mol%), *p*-TsOH (5 mol%), solvent (1 mL), r.t., 72 h. [b]Global yield of adducts **60** isolated after chromatographic purification. [c]Determined by $^1$H-NMR of the crude product mixture. [d]Determined via HPLC from the crude product mixture obtained after a reduction step with $NaBH_4$ in MeOH: Phenomenex i-cellulose 5 column; hexane/IPA 0.8%; flow rate 1 mL/min, $\lambda$ = 210 nm. [e]Reference reaction.

While the porphyrin-imidazolidinone **17b-*cis*** exhibited a poor catalytic activity (Entry 1), its isomer **17b-*trans*** triplicated the adduct yield and led to moderated enantiomeric excesses (49% ee for the *exo* diastereomer of adduct **60**, Entry 2).

When we expected to improve the diastereo- and enantiomeric excesses with catalyst **17d**, by introducing a much bulkier imidazolidinone substituent such as the *tert*-butyl group, we did not

observe the formation of the Diels-Alder adduct (Entry 3). It should be noted that, although MacMillan[1] used a mixture of water and methanol as a solvent, due to the low solubility of porphyrins in polar solvents, we decided to change the solvent to a much less polar one as toluene.

Better yields were obtained for catalyst **41**, corresponding to a metalated porphyrin, which also provided similar enantiomeric excesses, of the order of 40% ee, for both diastereomers of adduct **60** (Entry 4). The presence of the metal allowed the reaction to be carried out under MacMillan's original conditions (MeOH/$H_2O$ 95:5).

Comparing the results obtained with the reference reaction (Entry 5), which provided an approximately equimolar ratio of *exo* and *endo* adducts, a higher diastereoselectivity was observed in the reaction, with the *endo* Diels-Alder adduct being the majority with the two catalyst **17b**, while **41** showed a higher selectivity for *exo* adduct.

The determination of the diastereomeric ratios was performed directly on the reaction crudes by $^1$H-NMR, since both *endo*/*exo* diastereomers exhibit a different chemical shift for the aldehyde proton signal. The *exo* diastereomer gives rise to a doublet at a chemical shift of 9.92 ppm, whereas the *endo* diastereomer exhibits a doublet at 9.60 ppm. The doublet observed at 9.72 ppm corresponds to the unreacted starting aldehyde **58** (Figure 74).

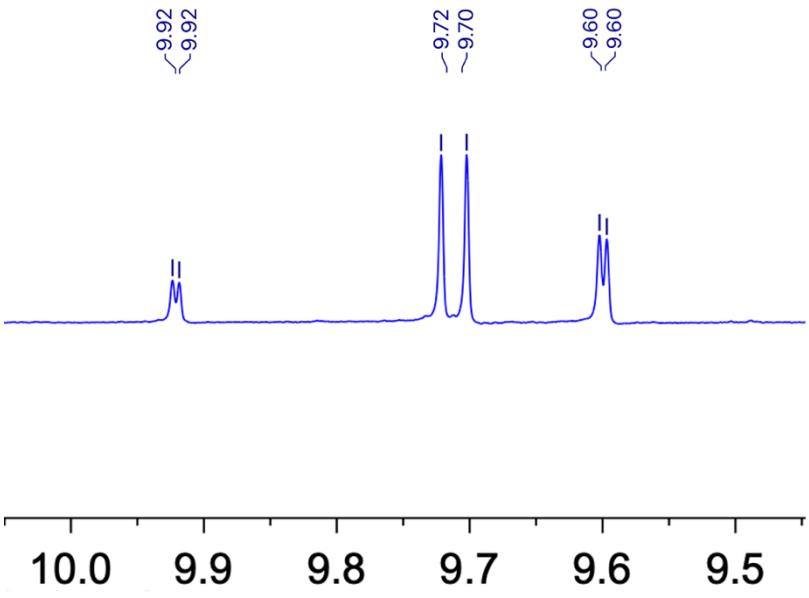


Figure 74. Determination of the Diels-Alder reaction Dr ratio via $^1$H-NMR.

The enantiomeric excess was determined via HPLC in a chiral stationary phase. For this purpose, since it was highly complicated to find optimal conditions for the separation of the four stereoisomeric aldehydes, we decided to derivatize them *in situ* to the corresponding alcohol mixture. The reduction was carried out with $NaBH_4$ in MeOH (Scheme 29).

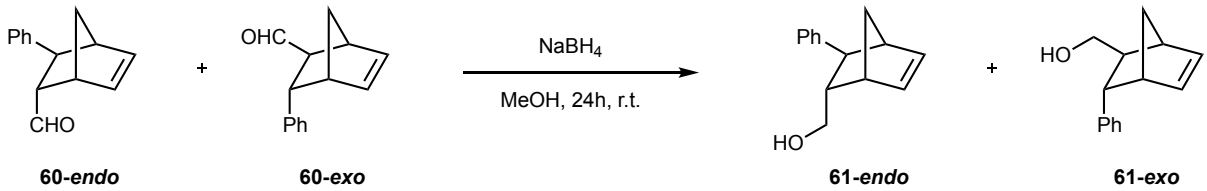


**60-*endo*** **60-*exo*** **61-*endo*** **61-*exo***

Scheme 29. Reduction of the Diels-Alder adducts **60-*endo*** and **60-*exo***.

After this reduction was performed, the enantiomeric excess was determined under the following conditions: Phenomenex i-cellulose 5 column; hexane/IPA 0.8%; flow rate 1 mL/min, $\lambda$ = 210 nm. The absolute configuration of the products was assigned in accordance with the data reported in the literature (Figure 75).[185]

From the results obtained, we concluded that the porphyrin-based catalysts **17b-*trans*** and **41** exhibited an acceptable catalytic activity in the Diels–Alder cycloaddition between cyclopentadiene and cinnamaldehyde under purely thermal conditions.

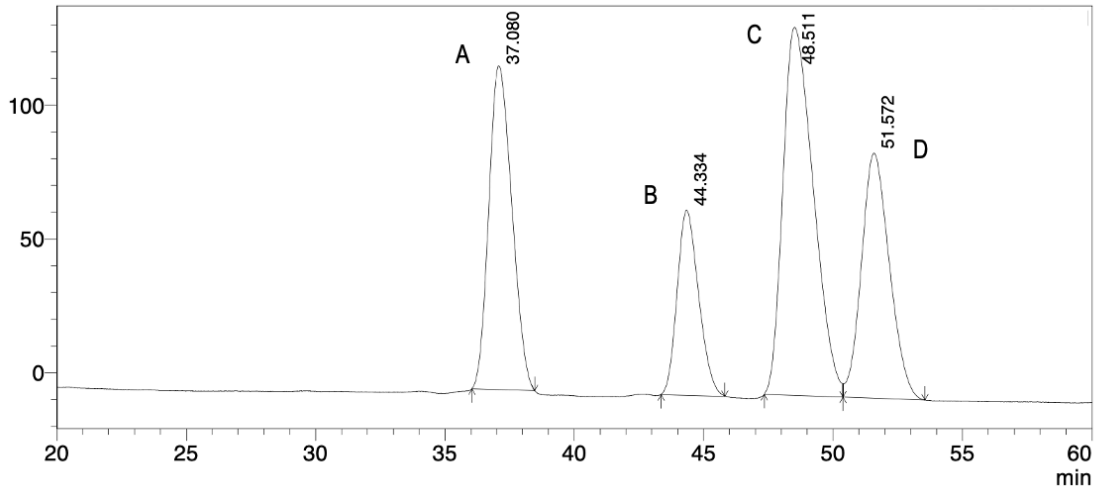


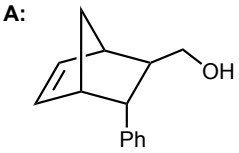


*exo*: (1*R*, 2*R*, 3*R*, 4*S*)

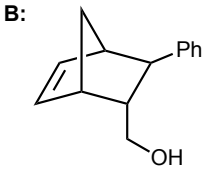


*endo*: (1*S*, 2*R*, 3*R*, 4*R*)

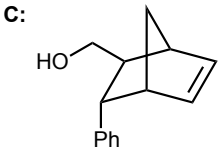


*exo*: (1*S*, 2S, 3*R*, 4*R*)

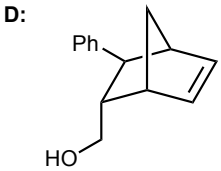


*endo*: (1*R*, 2S, 3*R*, 4*R*)

Figure 75. HPLC spectrum from a racemic mixture of the alcohol derivatization products (top). HPLC conditions: Phenomenex i-cellulose 5 column; hexane/IPA 0.8%; flow rate 1 mL/min, $\lambda$ = 210 nm. Assignment of the absolute configuration of the derivatization products (bottom).

## 4.2. PHOTOCHEMICAL DIELS-ALDER REACTIONS

### 4.2.1. CYCLOPENTADIENE AS THE DIENE MOIETY

Before using our bifunctional porphyrin derivatives as organophotochemical catalysts in Diels–Alder cycloaddition, we decided to study first a more simple dual catalysis system, in which imidazolidinones **16** would act as organocatalysts and porphyrins TPP and $TPPS_4$ (the last one both in its basic form $Na_4TPPS_4$ and in its zwitterionic form $H_2TPPS_4$) would act as photocatalysts (Figure 76).

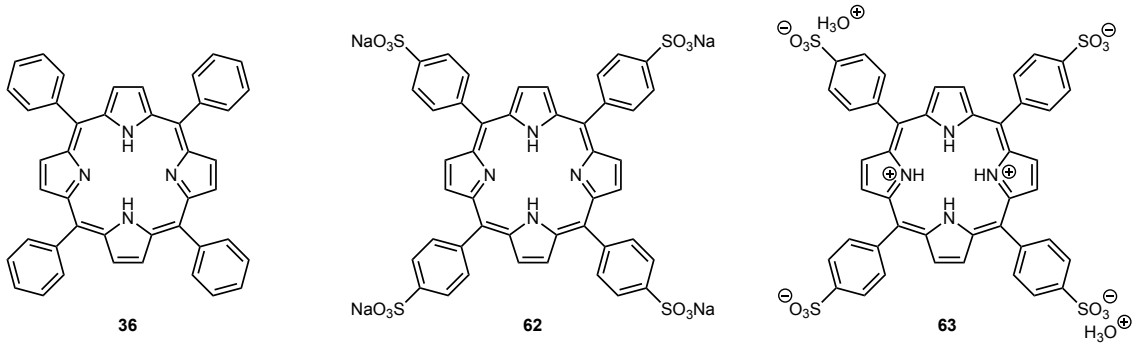


Figure 76. Structure of the different photocatalysts used for photochemical Diels-Alder reactions. The abbreviations used are as follows: TPP (photocatalyst **36**), $Na_4TPPS_4$ (photocatalyst **62**) and $H_2TPPS_4$ (photocatalyst **63**).

The use of sulfonated porphyrins was based our previous observation that in the conditions reported in MacMillan's article, (aqueous methanol),[1] neutral porphyrins such as TPP could present solubility problems.

One of the main problems in photochemistry is the reproducibility, since the experimental setup of the reaction is subject to different factors such as, for instance, the source of light irradiation, the distance between it and the reaction vial or the irradiation angle. We tried to develop a photoreactor capable of minimizing all these factors and achieving good reproducibility in the experiments performed (Figure 77). For this purpose, we placed three white LED lights (each one of them with an intensity of 450 Lumen), at an equal distance (about 5 cm) from the center of a stirring plate, where a clamp holding the reactor was located. The whole assembly was cooled by a lateral air stream.

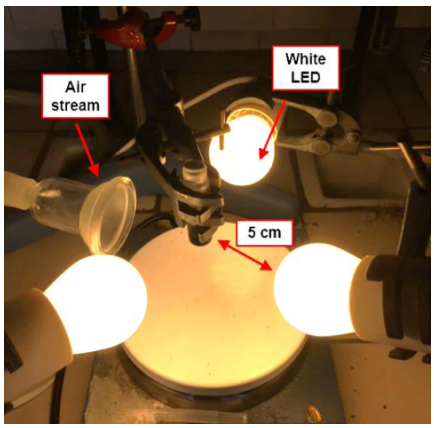


Figure 77. Experimental setting for the photocatalytic reactions (Photoreactor 1: 3 x LED, 1 LED = 450 Lm, white light).

The reaction between cyclopentadiene and cinnamaldehyde, previously performed under thermal conditions, was used as a starting point for our photochemical studies on the Diels-Alder reaction using a dual catalyst system. The results are shown in Table 4.

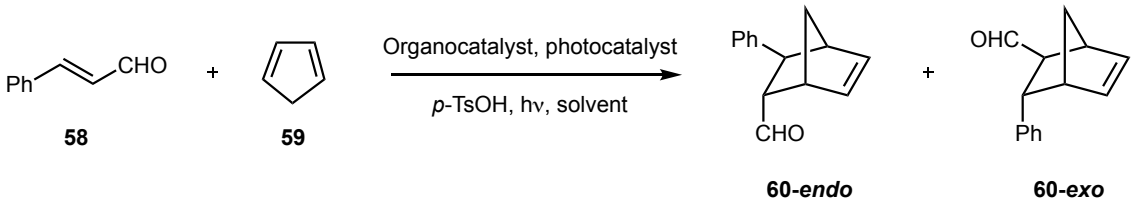


| Entry[a] | Organocat. | Photocat. | Solvent | Yield[b] | Dr (*endo*/*exo*)[c] | ee (*endo*/*exo*)[d] |
|---|---|---|---|---|---|---|
| **1** | **16a** | TPP | MeOH | 90% | 52/48 | 61% (2*S*, 3*S*)/ 67% (2*S*, 3*S*) |
| **2** | **16b** | TPP | MeOH | 99% | 53/47 | 69% (2*S*, 3*S*)/ 76% (2*S*, 3*S*) |
| **3** | **16b** | TPP | Toluene | 0% | - | - |
| **4**[e] | **16b** | $H_2TPPS_4$ | MeOH | 96% | 55/45 | 60% (2*S*, 3*S*)/ 72% (2*S*, 3*S*) |
| **5** | **16b** | $Na_4TPPS_4$ | MeOH/$H_2O$ (95/5) | 34% | 56/44 | 37% (2*S*, 3*S*)/ 24% (2*S*, 3*S*) |
| **6** | **16e** | TPP | Toluene | 0% | - | - |
| **7** | **16e** | TPP | MeOH | 0% | - | - |

Table 4. Study of Diels-Alder cycloadditions under photochemical conditions. [a]Reaction conditions: cinnamaldehyde **58** (0.5 mmol, 1 equiv.), cyclopentadiene **59** (1.5 mmol, 3 equiv.), organocatalyst (5 mol%), photocatalyst (5 mol%), *p*-TsOH (5 mol%), solvent (1 mL), 72h. [b]Global yield of adducts **60** isolated after chromatographic purification. [c]Determined by $^1$H-NMR. [d]Determined via HPLC from the crude product mixture obtained after a reduction step with $NaBH_4$ in MeOH: Phenomenex i-cellulose 5 column; hexane/IPA 0.8%; flow rate 1 mL/min, $\lambda$ = 210 nm. [e]Reaction performed without *p*-TsOH.

For both imidazolidinones **16a** (Entry 1) and **16b** (Entry 2) excellent yields were obtained with respect to the purely thermal reaction, when the reaction was carried out in methanol, even obtaining quantitatively the Diels-Alder adducts for the latter. The *endo*/*exo* diastereomeric ratio did not undergo appreciable changes, and a slight decrease in the enantiomeric excesses of both adducts was observed (compare with Table 3, Entry 5).

When the reaction was performed using toluene as solvent, the formation of the Diels-Alder adducts was not observed (Entry 3). This could explain why under purely thermal conditions, the obtained yields were so low. At this point, we decided to limit ourselves to imidazolidinone **16b** in order to study the effect that may have the other two photocatalysts to be tested. Thus, when $H_2TPPS_4$ **63** was used, the results were very similar to those obtained with TPP: excellent yields, good enantiomeric excesses, but very low diastereoselectivity (Entry 4). In contrast, when the catalyst in its basic form was used, both the yield and the enantiomeric excesses decreased considerably (Entry 5). This is consistent with the fact that the reaction needs the presence of acid catalysis to take place (formation of the iminium ion).

Finally, we decided to test imidazolidinone **16e** with the aim of improving both the diastereomeric and diastereomeric excesses by introducing a *tert*-butyl substituent, that could provide greater steric hindrance. Neither when the reaction was performed in MeOH (Entry 6) nor in toluene (Entry 7) did we observe the formation of the Diels-Alder adducts. This could be due to the steric hindrance of the *tert*-butyl group, that did not allow the formation of the iminium ion intermediate, blocking the progress of the reaction. Imidazolidinone **16d** was not tested as a catalyst because it was only obtained in its racemic form.

Both the determination of the diastereomeric ratio, via $^1$H-NMR of the crude reaction mixture, and the determination of the enantiomeric excess, via HPLC, were carried out in the same way as detailed above for the thermal reactions.

With this information, we used next the bifunctional porphyrins **17b** and **17d** in the same reaction. The results are shown in Table 5.

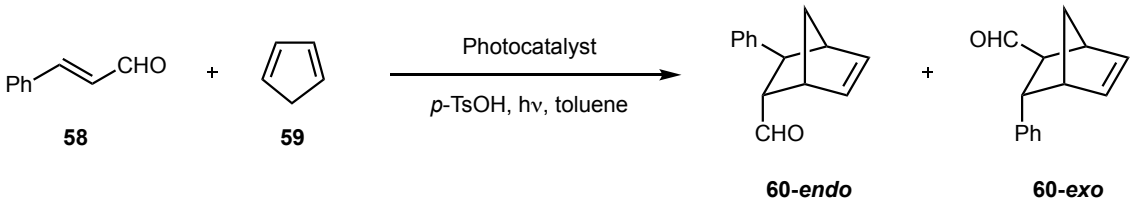


| Entry[a] | Catalyst | Yield[b] | Dr(*endo*/*exo*)[c] | ee (*endo*/*exo*)[d] |
|---|---|---|---|---|
| **1** | **17b-*cis*** | 12% | 88/12 | 1% (2*S*, 3*S*)/ 4% (2*S*, 3*S*) |
| **2** | **17b-*trans*** | 21% | 85/15 | 2% (2*S*, 3*S*)/ 2% (2*S*, 3*S*) |
| **3** | **17d** | 0% | - | - |

Table 5 Study of Diels-Alder cycloadditions under photochemical conditions. [a]Reaction conditions: cinnamaldehyde **58** (0.5 mmol, 1 equiv.), cyclopentadiene **59** (1.5 mmol, 3 equiv.), bifunctional catalyst (5 mol%), *p*-TsOH (5 mol%), toluene (1 mL), 72h. [b]Global yield of adducts **60** isolated after chromatographic purification. [c]Determined via $^1$H-NMR. [d]Determined via HPLC from the product obtained after a reduction step with $NaBH_4$ in MeOH: Phenomenex i-cellulose 5 column; hexane/IPA 0.8%; flow rate 1 mL/min, $\lambda$ = 210 nm.

The results for both bifunctional catalysts **17b-*cis*** (Entry 1) and **17b-*trans*** (Entry 2) were very similar to those obtained under thermal conditions: very poor yields and enantiomeric excesses. We were delighted to find however a much better diastereoselectivity, even higher than under thermal conditions. For the bifunctional catalyst **17d** the desired product was not observed, probably because the high steric hindrance of the *tert*-butyl group prevents the formation of the iminium ion.

Especially under photochemical conditions, using porphyrin-based imidazolidinones as bifunctional catalysts, a remarkable increase in the diastereoselectivity of the reaction is observed with respect to imidazolidinones **16**, leading to the selective formation of the *endo* adducts. However, the yield decreases considerably, and there is also a loss of the enantioselectivity, and the Diels-Alder adducts are obtained in an essentially racemic form.

Having verified that there are important differences in terms of diastereo- and enantioselectivity between photochemical and thermal conditions, we conclude that, under visible-light irradiation and in the presence of a porphyrin photocatalyst, a competition between thermal and photochemical reaction pathways may occur. Under dual catalysis conditions, where only an increase in yield is observed, a photosensitization process could be operative, in which the triplet excited porphyrin

can activate the unsaturated aldehyde (or of the intermediate iminium ion) by energy transfer, leading to an increase in the reaction rate.

For the bifunctional catalysts, however, the drastic change observed in the stereoselectivity of the cycloaddition could be due to the existence of an alternative reaction pathway. A possible photoredox mechanism of cycloaddition via oxidative quenching is shown in Scheme 30. The mechanism is described for a generic bifunctional catalytic system.

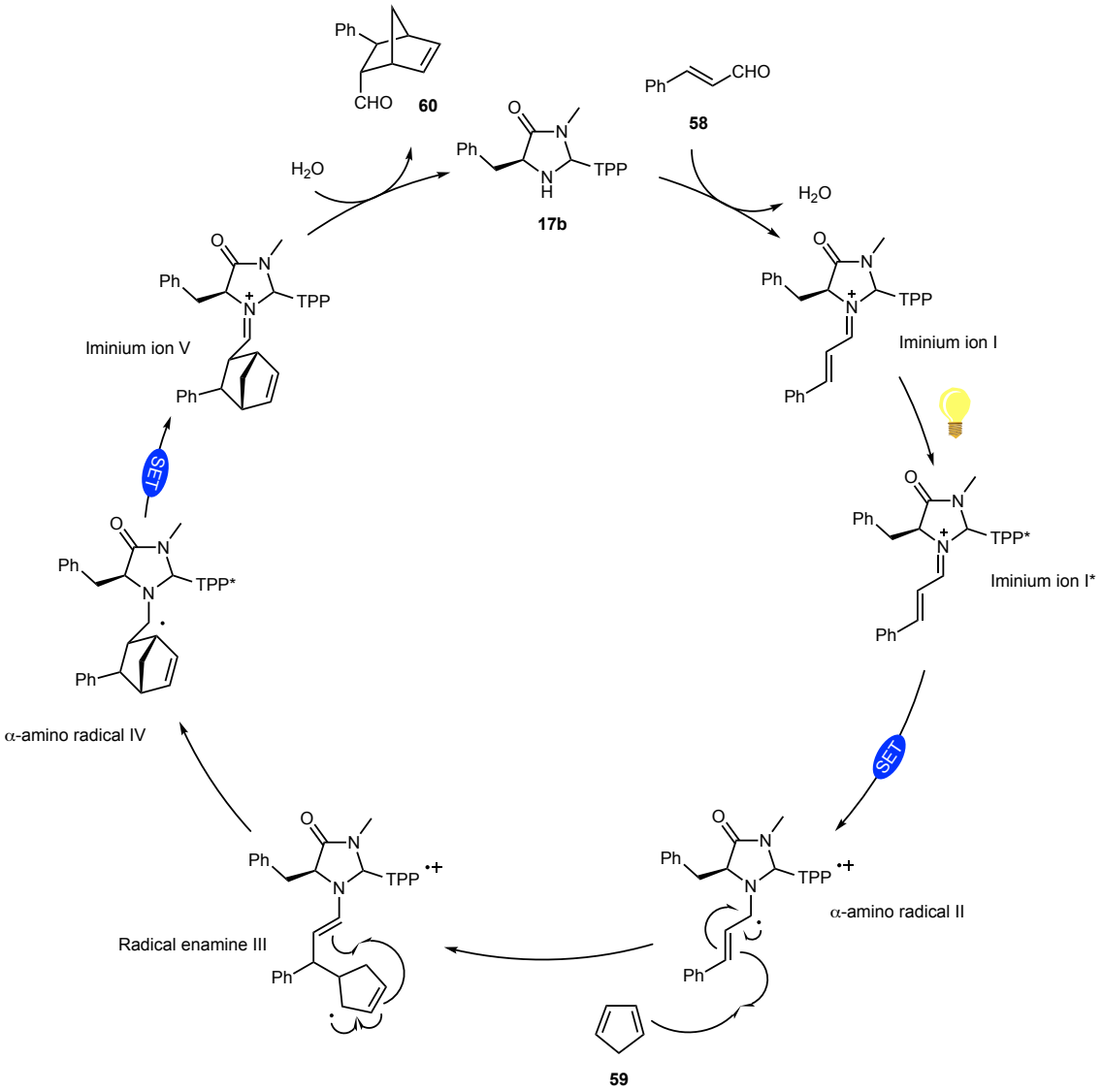


Scheme 30. Proposed mechanism for the radical Diels-Alder reaction catalyzed by **17b**.

The proposed mechanism starts with the condensation between cinnamaldehyde **58** and the bifunctional catalyst **17b**, forming the iminium ion I. The porphyrin moiety of this iminium ion can be excited when irradiated with light, giving rise to an intermediate which, via intramolecular SET reductive process, leads to the α-aminoradical II. It is the latter that reacts with cyclopentadiene **59**

via a radical [4+2] cycloaddition, forming the α-aminoradical IV, which via a SET oxidative process produces the iminium ion V. Finally, by hydrolysis, the Diels-Alder adduct **60** is obtained and the bifunctional catalyst is regenerated. In this mechanism, the selective formation of the *endo* adduct in almost racemic form might be due to the radical nature of the cyclization step.

### 4.2.2. PYRONE DERIVATIVES AS THE DIENE MOIETY

Bicyclic lactones compounds encompass a developing field of biological research being in a variety of natural products such as *scholarisine A*.[186] The structural motif of [2.2.2]-bicyclic lactone, moreover, offers the potential for decarboxylative transformations that can provide important building blocks. The basic scaffold of these compounds can arise from cycloaddition reactions of pyrones (including coumalate derivatives), that have therefore been considered as convenient and highly functionalized building blocks for the synthesis of [2.2.2]-bicyclic lactones.[187]

Lucasz, Albrecht and co-workers[187] reported the ability of pyrones to act as dienes in asymmetric organocatalytic Inverse Electronic Demand Diels-Alder (IEDDA) reactions between coumalates and dienamines, prepared *in situ* from α,β-insaturated aldehydes that can lose a proton at the γ position (Scheme 31). The distal double bond of the *in situ* formed dienamine can act as electron-rich dienophile in this type of reactions. With the readily available Jørgensen-Hayashi catalyst, good yields and enantiomeric purities could be achieved.

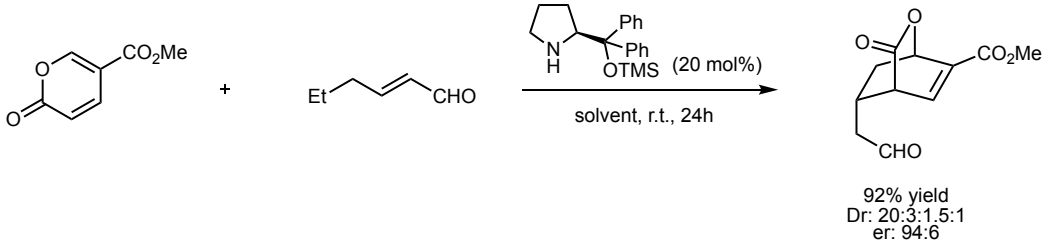


Scheme 31. Asymmetric synthesis of [2.2.2] bicyclic lactones.

Obviously, if we generated an unsaturated iminium ion from cinnamaldehyde **58** and a chiral imidazolidinone, this electron-poor intermediate would not react with a coumalate in a thermal Diels-Alder reaction. But in presence of a suitable photocatalytic system, adapting the reaction mechanism to the one proposed in the previous section (Scheme 27) to a dual catalysis scenario, the iminium ion II could be reduced by the photocatalyst via SET process giving rise to the electron-rich radical enamine III, being the latter able to react with coumalate **64**, either in a concerted

manner or in different stages, giving rise to the α-aminoradical V. Finally, this could be oxidized by the photocatalyst via SET process generating the iminium ion VI which, through a hydrolysis step, would give rise to the cycloaddition product **65** (Scheme 32).

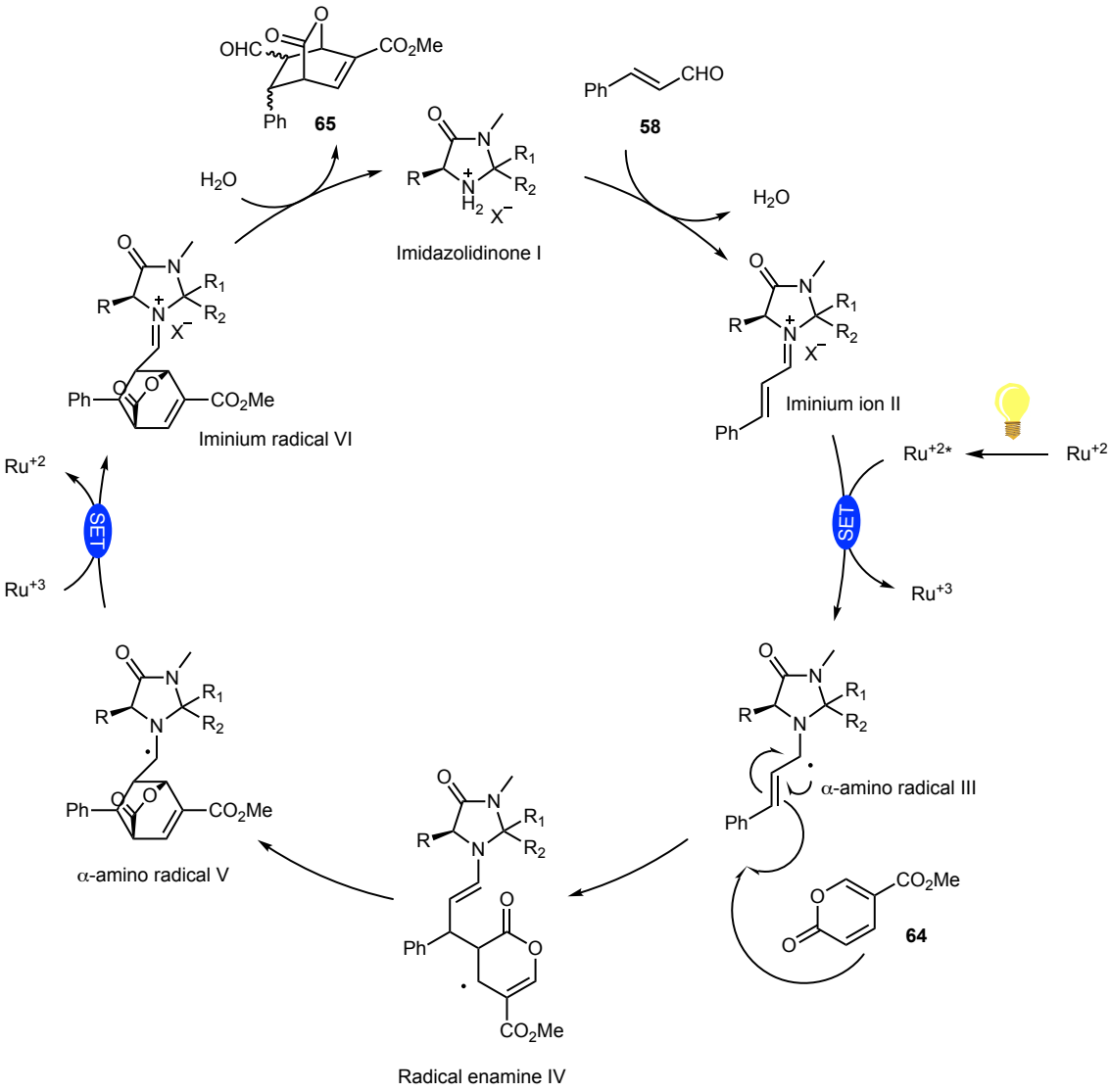


Scheme 32. Proposed photocatalytic/organocatalytic dual cycle for Diels-Alder cycloaddition between cinnamaldehyde **58** and methyl coumalate **64**.

With this idea, we decided to test the Diels-Alder reaction between cinnamaldehyde **58** and methyl coumalate **64** using imidazolidinones **16** as organocatalysts, under visible-light irradiation and in the presence of porphyrins **36**, **62** and **63**, and of $Ru(bpy)_3Cl_2$ as photocatalysts.

To carry out these experiments, we decided to modify the photoreactor (Figure 78). With this change, we intended to solve two problems encountered in the previous design, (a) the distance between the light irradiation source and the reaction vial was not exactly the same for each reaction,

which means one more unknown in the reaction set up, since the light intensity could not be the same on each side of the vial, and (b) the irradiation angle could vary from one reaction to another, depending on the height at which the reaction vial was placed. Using this new system of commercially available spiral LEDs, greater reproducibility was observed in the experiments performed. In addition, we were able to perform both white and blue light irradiation at the UV-Vis limit (395 nm).

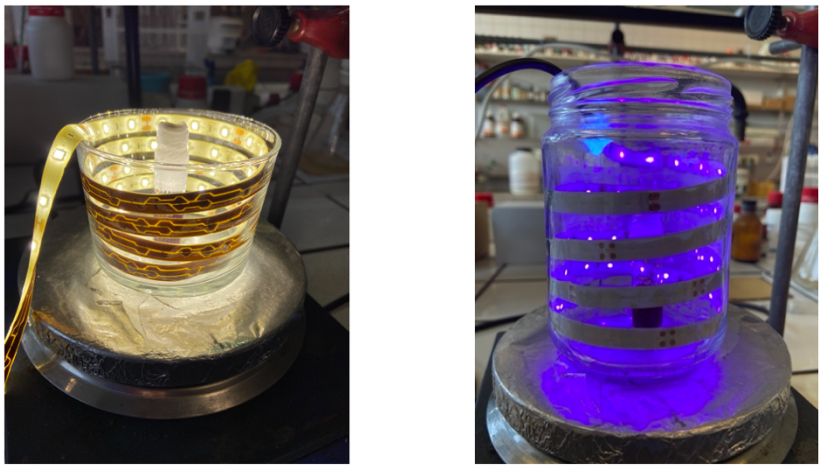

Figure 78. Experimental setting for the photocatalytic reactions. Right: Photoreactor 2, white LEDs, 18W, 1080 Lm. Left: Photoreactor 3, blue LEDS (395 nm), 18W, 1050 Lm.

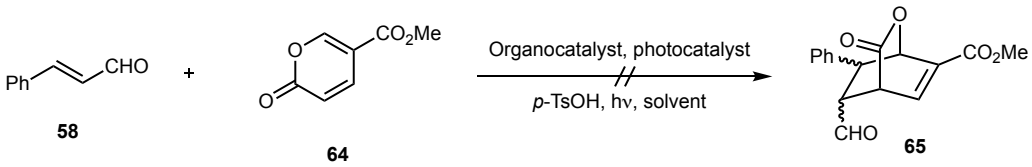


| Entry[a] | Organocatalyst | Photocatalyst | Photoreactor | Solvent |
|---|---|---|---|---|
| **1** | **16b** | TPP | 2 | Toluene |
| **2**[b] | **16b** | $H_2TPPS_4$ | 2 | MeOH |
| **3** | **16b** | $Ru(bpy)_3Cl_2$ | 3 | Toluene |
| **4** | **16b** | $Ru(bpy)_3Cl_2$ | 3 | MeOH |
| **5** | **16c** | $Ru(bpy)_3Cl_2$ | 3 | MeOH |
| **6** | **16e** | $Ru(bpy)_3Cl_2$ | 3 | MeOH |

Table 6. Study of the Diels-Alder reactions using a pyrone moiety as diene. [a]Reaction conditions: cinnamaldehyde **58** (0.5 mmol, 1 equiv.), methyl coumalate **64** (0.75 mmol, 1.5 equiv.), organocatalyst (5 mol%), photocatalyst (5 mol%), *p*-TsOH (5 mol%), solvent (1 mL), 72h. [b]Without *p*-TsOH.

To our disappointment, we were not able to detect the formation of the Diels-Alder adducts **65** in any of the conditions we tested (see Table 6). When the $Ru(bpy)_3Cl_2$ complex was used as photocatalyst, the formation of the Michael adduct **66** was observed in some instances; this compound was fully characterized via $^1$H-NMR, $^1$H-$^1$H COSY and IR (Scheme 33).

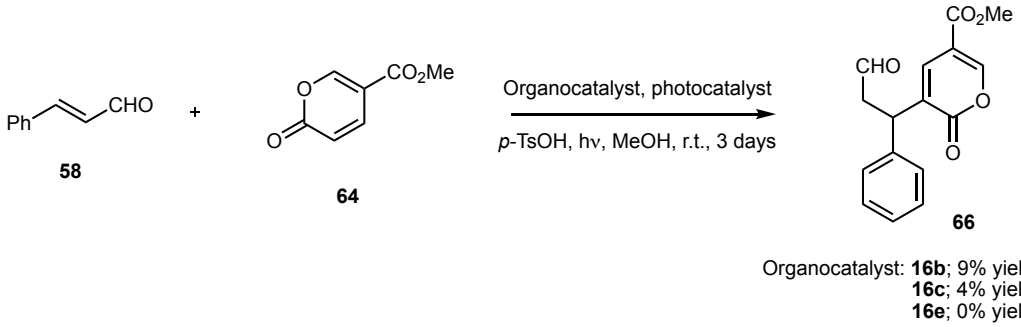


Scheme 33. Formation of Michael adduct **66**. Using $Ru(bpy)_3Cl_2$ complex as photocatalyst and MeOH as solvent.

A literature search revealed that compound **66** had been recently obtained by a thermal cross-vinylogous Rauhut-Currier (RC) reaction using secondary amines as organocatalysts.[188] To try to understand the reaction behavior a little bit more, we decided to replicate the reactions shown in Table 6 in which we observed the formation of Michael adduct **66**, but under purely thermal conditions (Table 7).

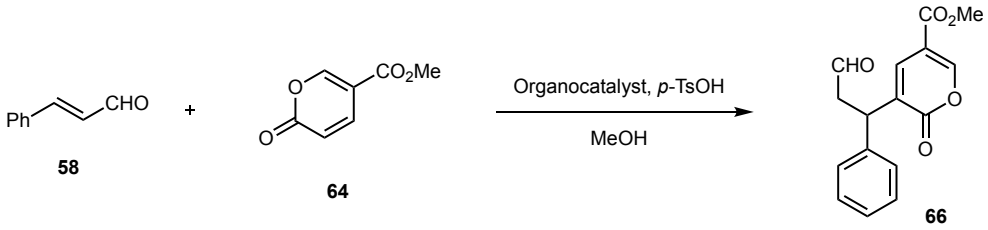


| Entry[a] | Organocatalyst | Yield[b] | Yield[c] |
|---|---|---|---|
| 1 | **16b** | 0% | 9% |
| 2 | **16c** | <2% | 4% |
| 3 | **16e** | 14% | 0% |

Table 7. Study of the formation of Michael adduct **66**. [a]Reaction conditions: cinnamaldehyde **58** (0.5 mmol, 1 equiv.), methyl coumalate **64** (0.75 mmol, 1.5 equiv.), organocatalyst (5 mol%), *p*-TsOH (5 mol%), MeOH (1 mL), r.t., 72 h. [b]Under thermal conditions. [c]Under photochemical conditions.

Under thermal conditions, Michael adduct **66** was not detected by $^1$H-NMR for imidazolidinone **16b** (Entry 1); on the other hand, the reaction with imidazolidinone **16c** gave a very low yield, but the Michael adduct could be detected by $^1$H-NMR (Entry 2). When the thermal reaction was carried

out with imidazolidinone **16e**, Michael adduct **66** could be isolated by column chromatography in a 14% yield (Entry 3).

The lack of reactivity of imidazolidinone **16b** under thermal conditions might be due to the steric hindrance of the benzyl group. Under irradiation, a small amount (9% yield) of the Michael adduct **66** was isolated. When a non-hindered imidazolidinone **16c** was used, the reaction proceeds both via thermal and photochemical pathways, but with very low yields (<2% and 4% yield, respectively).

Although the chemistry of coumalates derivatives has a wide range for inverse Diels-Alder cycloadditions, in our case, the reactivity of pyrones was not the expected one, leading to the formation of compound **66** in low yields.

# CHAPTER 5. STUDY OF THE ORGANOPHOTOCATALYTIC α-ALKYLATION OF ALDEHYDES

## 5.1. PRECEDENTS IN THE STUDY OF THE PORPHYRIN-MEDIATED PHOTOREDOX α-ALKYLATION OF ALDEHYDES

As we have described in Chapter 1 of the present PhD Thesis, MacMillan and Nicewicz, in 2008, reported the first enantioselective photochemical α-alkylation of aldehydes,[88] by using a dual catalytic system consisting of a chiral imidazolidinone, acting as an enantioselective organocatalyst, and the $Ru(bpy)_3Cl_2$ complex as a photoredox catalyst (Scheme 34). Thus, the reaction between enolizable aldehydes and electron-deficient alkyl bromides (bromomalonates, α-bromoesters, phenacyl bromide) afforded for the first time the α-alkylation products with good yields (80-93%) and enantioselectivities (up to 96% ee).

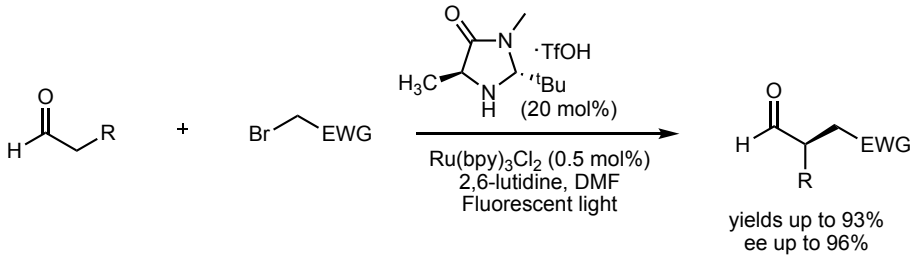


Scheme 34. Enantioselective α-alkylation of aldehydes reported by MacMillan and Nicewicz.

In the mechanism proposed by the authors, an electrophilic radical was generated by a reductive monoelectronic transfer between the excited state of the photocatalyst and the alkyl bromide; this radical stereoselectively added to the nucleophilic α carbon of the chiral enamine intermediate formed from the aldehyde and the organocatalyst. This general approach, which is known as "photoredox organocatalysis" was later extended to the α-perfluoroalkylation and the α-benzylation of aldehydes.[115,116]

More recently, Alemán and co-workers[121] have described the first bifunctional catalytic system for the enantioselective photochemical α-alkylation of aldehydes with alkyl bromides, by synthesizing catalysts having a covalent bond between a chiral imidazolidinone unit and a thioxanthone, whose photochemical activity have been previously demonstrated,[189-191] (acting as a photoredox organocatalyst) (Scheme 35).

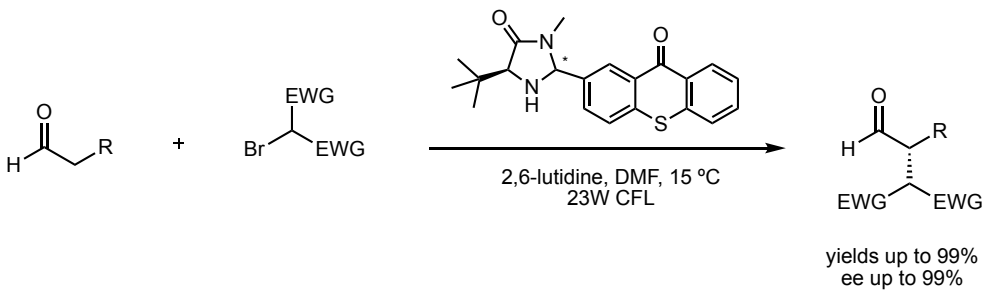


Scheme 35. Bifunctional enantioselective α-alkylation of aldehydes reported by Alemán and co-workers.

In early 2016, Gryko *et. al.* disclosed that the photocatalytic reaction of diazoacetates with enolizable aldehydes in the presence of an achiral secondary amine (morpholine or piperidine), using $Ru(bpy)_3Cl_2$ as photocatalyst, led with good yields to the α-alkylation products (Scheme 36).[192] The authors also tested the use of organic dyes as photocatalysts, but found that only Eosin Y and rose Bengal gave the alkylation products in acceptable yields.

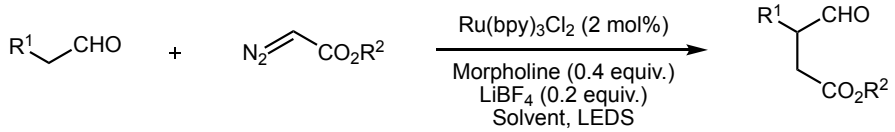


$R^1$: $CH_2Ph$; $R^2$: Et; 88% yield
$R^1$: $CH(CH_3)_2$; $R_2$: Et; 63% yield
$R^1$: $CH_2Ph$; $R^2$: $CH_2Ph$; 78% yield

Scheme 36. α-Alkylation of aldehydes reported by Gryko and co-workers, using diazo compounds as alkylating agents.

Since only the starting aldehyde was recovered when the secondary amine was replaced by a tertiary amine (triethylamine, DABCO) in the reaction, the authors proposed that the reaction proceeded via a photoredox organocatalysis of the same type as that postulated by Nicewicz and MacMillan. The formation of the enamine in the reaction medium was confirmed by proton NMR spectroscopy, gas chromatography and MS (ESI). The addition of TEMPO (a radical scavenger) completely inhibited the alkylation process, thus postulating a photoredox-type radical mechanism (also supported by RPE studies of the reaction mixture).

Later in 2016, Zawada, Kadish, Gryko and co-workers[169] reported the same photochemical α-alkylation reaction of aldehydes via diazoesters but using porphyrins (mainly *meso*-tetraphenylporphyrin TPP or its Zn complex) as photocatalysts. The hypothesis that porphyrins could be suitable organic photoredox catalysts for the C-C bond formation was supported by previous electrochemical studies that showed that TPP, in its excited state, presented a similar

reduction potential (0.91 V) to those determined for $Ru(bpy)_3^{+2}$ (0.67 V) and for Eosin Y (0.83 V). The yields obtained with 1 mol% of TPP are in general similar to those observed with $Ru(bpy)_3Cl_2$.

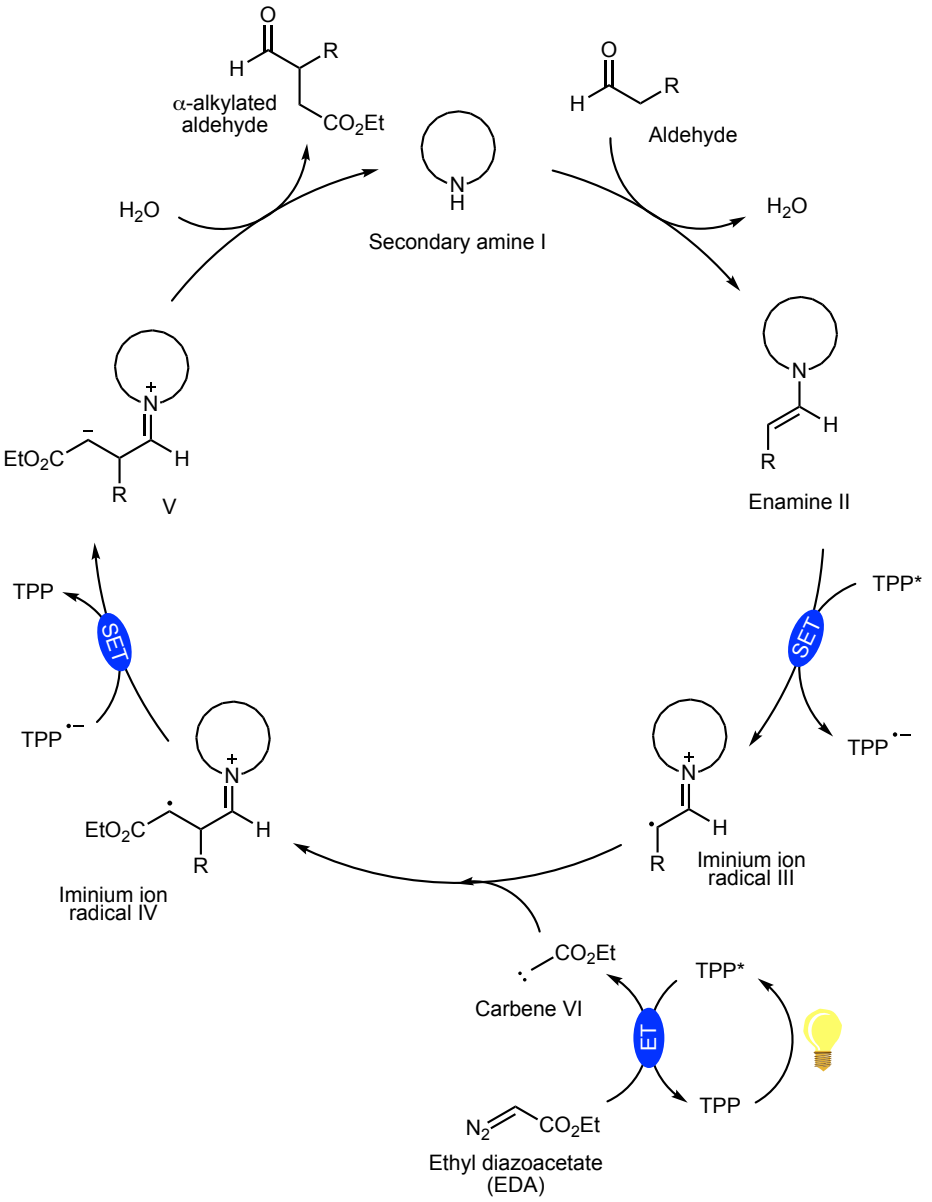


Scheme 37. Mechanism proposed by Gryko for the light-induced functionalization of aldehydes with EDA using TPP as photocatalyst.

The mechanism proposed by the authors is shown in Scheme 37 and is identical to the one they had previously described for Ru(II) catalysis (except for the nature of the photocatalyst). They postulated that the porphyrin, in its excited state, acts both as a photosensitizer and as a photoredox catalyst. The organophotocatalytic cycle begins with the condensation between the aldehyde and the secondary amine I, giving rise to enamine II. This intermediate interacts with the photoexcited porphyrin, by means of an oxidative electron transfer, in which the iminium radical ion III and the porphyrin radical anion are generated.

In parallel, the excited porphyrin (acting as a photosensitizer) generates the carbene VI (probably in the triplet state) by an energy transfer process with ethyl diazoacetate (EDA), that loses nitrogen in its excited state. At this point, the formation of the new C-C bond takes place, as the newly generated carbene reacts with the iminium radical ion III. The generated iminium radical ion IV is now reduced by the porphyrin radical-anion via reductive monoelectronic transfer, giving rise to the zwitterionic compound V (and the ground-state porphyrin). Subsequent protonation and hydrolysis of the iminium V gives rise to the α-alkylated aldehydes and the regeneration of the secondary amine I.

There is an important aspect to comment on the mechanism proposed by Gryko and co-workers and is that the authors observed that EDA quenches porphyrin luminescence. By Stern-Volmer analysis, they showed that the reaction yields were inversely proportional to the diazoester quenching rate of porphyrin fluorescence. This result was interpreted as evidence for the participation of porphyrin in both energy transfer (ET) and monoelectronic transfer (SET) processes, being both processes competitive with each other. In the light of the obtained alkylation yields (reaching 90%), the authors proposed that both processes proceeded at similar rates, because if one of the two was much faster than the other, the slower one would be inhibited, and the formation of the new C-C bond could not take place in an efficient manner.

If we compare the results obtained by the authors using TPP as photocatalyst with those obtained with $Ru(bpy)_3Cl_2$, we can see that they are practically identical, which demonstrates the effectiveness of porphyrins as photocatalysts in this type of photochemical systems. However, since only achiral secondary amines were used as organocatalysts, the α-alkylation products were obviously obtained in their racemic forms, leaving an open window to explore the possibility for an enantioselective version of the reaction.

## 5.2. STUDY OF THE α-ALKYLATION OF ALDEHYDES EMPLOYING A DUAL PHOTOCATALYTIC SYSTEM

In the context of the use of porphyrins as catalysts in enantioselective photochemical processes that we had explored (both in the dual and bifunctional catalysis modes) in Chapter 4 of the present PhD Thesis, we decided to focus our efforts on the development of an asymmetric version of the photocatalytic alkylation of aldehydes with α-diazoesters.

As a first step, we decided to reproduce the reaction between 3-phenylpropionaldehyde **67** and EDA **68**, using as photocatalyst TPP **36**, and various achiral secondary amines (piperidine, morpholine, pyrrolidine) in a DMSO solution and in the presence of an acidic co-catalyst (to promote enamine formation). These reaction conditions had provided the best yields according to the investigations of Gryko and co-workers.[169] The results are shown in Table 8.

By $^1$H-NMR analysis of the reaction crudes, the degree of formation of the desired α-alkylated product, as well as the overall conversion of the reaction can be clearly evaluated, since both aldehydes, starting aldehyde **67** and α-alkylated aldehyde **69**, give rise to different signals for the aldehydic protons. The starting aldehyde **67** presents a triplet with a chemical shift of 9.83 ppm, while the proton of the α-alkylated aldehyde **69** appears as a doublet at 9.80 ppm (Figure 79).

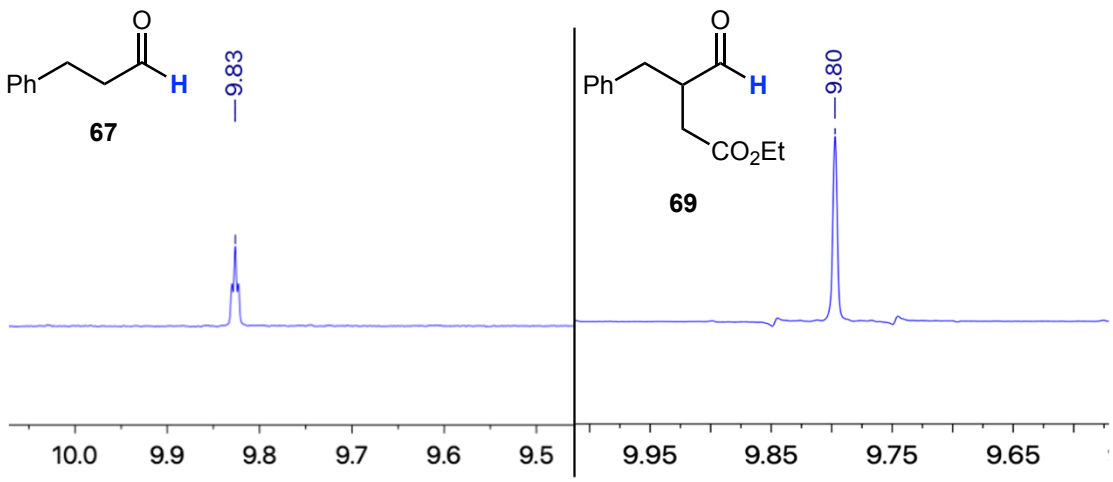


Figure 79. Difference in the aldehyde proton signal between 3-phenylpropionaldehyde **67** (left) and ethyl-3-benzyl-4-oxobutanoate **69** (right).

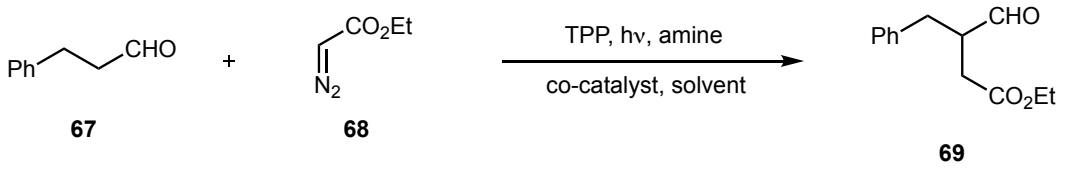


| Entry[a] | Equiv. EDA | Amine | Co-catalyst | Solvent | Yield[b] |
|---|---|---|---|---|---|
| **1** | 1 | Piperidine | - | DMSO/Buffer pH 4 (9/1) | 0% |
| **2**[d] | 1[c] | Piperidine | AcOH | DMSO | 0% |
| **3**[d] | 1 | Piperidine | AcOH | DMSO | 21% |
| **4** | 1 | Piperidine | - | DMSO | 0% |
| **5** | 1 | Morpholine | $LiBF_4$ | DMSO | 0% |
| **6** | 1 | Piperidine | $LiBF_4$ | DMSO | 29% |
| **7** | 1.2 | Piperidine | $LiBF_4$ | DMSO | 42% |
| **8** | 1.2 | Morpholine | $LiBF_4$ | DMSO | 0% |
| **9** | 1.2 | Pyrrolidine | $LiBF_4$ | DMSO | 0% |

Table 8. Reproducibility and optimization studies. [a]Reaction conditions: 3-phenylpropionaldehyde **67** (0.5 mmol, 1 equiv.), EDA **68**, TPP (1 mol%), amine (0.4 equiv.), co-catalyst (0.2 equiv.), solvent (5 mL), light (Photoreactor 1: 3 x LED, LED = 450 Lm, white light), 5 h. [b]Yield of **69** isolated after chromatographic purification. [c]EDA was added in two fractions. [d]The aldol self-condensation product was obtained.

In our first attempt, we slightly modified the conditions reported in the article by changing the amine used (piperidine instead of morpholine). Instead of an acidic co-catalyst, a 9:1 mixture of DMSO and an aqueous buffer solution of pH = 4 was used as the reaction medium. Under these conditions, we did not observe the formation of the α-alkylated product (Entry 1).

Acetic acid (AcOH) was then added to act as a co-catalyst (20 mol%) and the pH 4 buffer solution was removed from the solvent (Entry 2). Also, EDA **68** was added in two portions, the second after 2.5 h of reaction, to avoid the polymerization of the carbene in excess. By $^1$H-NMR analysis of the reaction crude, we did not observe the formation of the α-alkylation product, although no unreacted starting aldehyde remained. Instead, we observed the appearance of a new set of signals, most notably a singlet with a chemical shift of 9.44 ppm. Further analysis of the $^1$H-NMR spectrum complemented by an MS (ESI) revealed that the newly formed product corresponded to the aldol self-condensation product **70**, following Knoevenagel conditions (Figure 80).

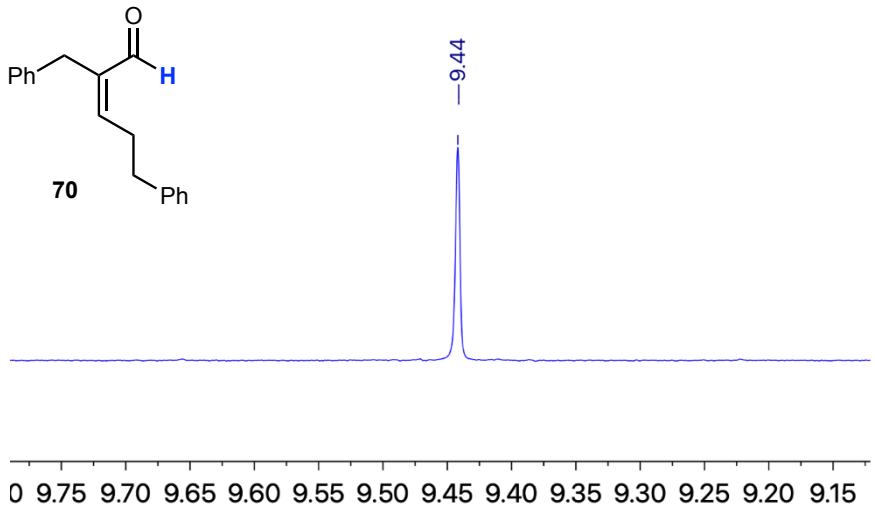


Figure 80. Characteristic signal of the aldehyde proton of the aldolic self-condensation product **70**.

At this point, we decided to set up two more reactions (Entry 3 and 4). In these, EDA was added in one portion, after concluding that its deficit favored the aldol self-condensation reaction over the photochemical α-alkylation. The desired α-alkylated product was only observed in the first one (Entry 3, with acetic acid as co-catalyst), but with very poor yields. In the absence of acetic acid, no reaction was observed. These two results confirmed the importance of the co-catalyst in the reaction.

Since adding a Brønsted acid as a co-catalyst favored the aldolic selfcondensation reaction, we decided to replace it with a Lewis acid, that should be also capable of performing the activation of the carbonyl in the enamine formation step. We decided to use $LiBF_4$ as co-catalyst, as described by Gryko.[169,192] Entry 5 shows exactly the same reported conditions, but, for our surprise, we did not observe the formation of the α-alkylation product (Gryko and co-workers reported a 90% yield).[169] In view of this problem, we switched from morpholine to piperidine, obtaining in this case a higher yield, although still low (Entry 6). Morpholine had been reported as the secondary amine that gave the best yields,[169,192] but in our case, only with piperidine we observed the formation of the alkylated product.

After analyzing the results obtained, we put forward a second hypothesis. A slight excess of EDA could positively affect the reaction yield by minimizing the formation of the aldol self-condensation by-product **70**. Thus, 1.2 equivalents of EDA were added in one portion and, in order to choose the most suitable secondary amine for our system, piperidine (Entry 7), morpholine (Entry 8) and pyrrolidine (Entry 9) were used. The results showed that as expected, (a) the addition of 1.2

equivalents of EDA improved the overall reaction yields when using piperidine as the organocatalyst (see entries 6 and 7), (b) both for morpholine and for pyrrolidine, the formation of the desired product was not observed, and (c) the secondary amine that best suited our photochemical system was piperidine.

Once both the EDA equivalents and the secondary amine were optimized, we decided to test different photocatalysts. The main problem we had encountered while performing the first optimization studies was that the chromatographic separation of the α-alkylation product from the photocatalyst always led to a partial degradation. We therefore decided to resort to the use of the water-soluble porphyrins shown in Figure 76 which should be easier to remove from the reaction crude, also facilitating $^1$H-NMR analysis. We also tested the three secondary amines used previously as organocatalysts. The results are shown in Table 9.

The yields of the alkylation product **69** were calculated either from the weight of the crude obtained after aqueous work-up and extraction with ethyl acetate, or when conversion was not complete, from the weight of product **69** isolated after chromatographic purification. Contrary to the reports by Gryko,[169] when we attempted a further purification of the α-alkylated aldehyde by silica gel column chromatography of the crude product, we always observed a very low recovery of compound **69**.

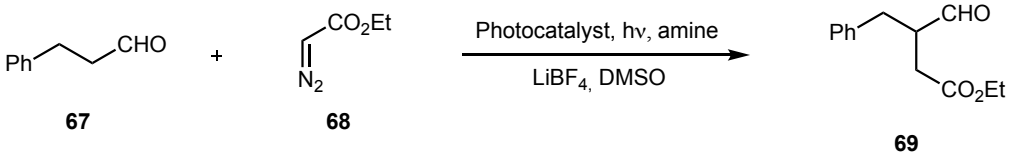


**67** **68** **69**

| Entry[a] | Amine | Photocatalyst | Conversion[b] | Yield[c] |
|---|---|---|---|---|
| **1** | Piperidine | $Na_4TPPS_4$ | 100% | 84% |
| **2** | Morpholine | $Na_4TPPS_4$ | 53% | 30%[d] |
| **3** | Pyrrolidine | $Na_4TPPS_4$ | 0% | 0% |
| **4** | Piperidine | $H_2TPPS_4$ | 100% | 63% |
| **5** | Morpholine | $H_2TPPS_4$ | 0% | 0% |
| **6** | Pyrrolidine | $H_2TPPS_4$ | 0% | 0% |

Table 9. Photocatalyst optimization studies. [a]Reaction conditions: 3-phenylpropionaldehyde **67** (0.25 mmol, 1 equiv.), EDA **68** (0.30 mmol, 1.2 equiv.), photocatalyst (1 mol%), amine (0.4 equiv.), $LiBF_4$ (0.2 equiv.), DMSO (2 mL), light (Photoreactor 2: white LEDs, 18 W, 1080 Lm), 5 h. [b]Calculated as explained above in Table 8. [c]Estimated by $^1$H-NMR analysis of the crude reaction mixture obtained after aqueous work-up. Corresponding to the weight of the crude reaction product. [d]After chromatographic purification.

Best results were obtained when using $Na_4TPPS_4$ **62** (1 mol%) as the photocatalyst and piperidine (40 mol%) as the organocatalyst (Entry 1 of Table 9). In these conditions, complete conversion was achieved after 5 h of irradiation, and only **69** was detected in the reaction crude by $^1H$ NMR analysis. We selected therefore an irradiation time of 5 h for the remaining experiments. When morpholine was used as the organocatalyst (Entry 2 in Table 9), the α-alkylated aldehyde was obtained in a 53% conversion (30% isolated yield), showing the $^1H$-NMR of the crude the recovery of the starting aldehyde. In the presence of pyrrolidine (Entry 3), no alkylation product was formed, recovering in its totality the starting aldehyde. When we used the dual catalytic system formed by the zwitterionic form $H_2TPPS_4$ **63** and by piperidine, although conversion was again complete after 5 h (Entry 4), the yield of **69** decreased to 63%, due to the competing formation of the Knoevenagel self-condensation product **70**. With this photocatalyst, neither morpholine (Entry 5) nor pyrrolidine (Entry 6) promoted the formation of the alkylation product, obtaining a mixture of the starting aldehyde **67** and the Knoevenagel self-condensation product **70**.

When the reaction was set up with 0.2 equivalents of piperidine, to see the effect of a decrease in the amount of amine, we observed that, after 5 h of reaction, the conversion of the initial aldehyde was 89%, and that the estimated yield by NMR of **69** decreased to 67%.

Thus, these optimization studies revealed that the best conditions for our photocatalytic system were aldehyde (0.25 mmol, 1 equiv.), EDA **68** (0.30, 1.2 equiv.), $Na_4TPPS_4$ **62** (1 mol%), piperidine (0.4 equiv.), $LiBF_4$ (0.2 equiv.), under white light irradiation (Photoreactor 2: LEDs, 18 W, 1080 Lm), 5 h.

As the next step, we set out to expand the photocatalytic system to other aldehydes, thus evaluating the scope of the reaction (always with 0.4 equivalents of piperidine as the organocatalyst and 1 mol% of $Na_4TPPS_4$ as the photocatalyst, in degassed DMSO and in the presence of 0.2 equivalents of $LiBF_4$, with an irradiation time of 5 h). The results are shown in Table 10. The yields were calculated from the weight of the crude alkylated products and from analysis of the $^1H$ NMR spectra as explained above. It is worth noting that under these work-up conditions, only alkylated product was obtained.

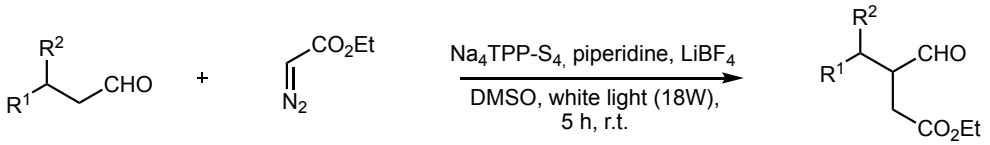


**67, 71-78** **68** **69, 79-86**

| Entry[a] | Aldehyde | $R^1$ | $R^2$ | Product | Yield[b] |
|---|---|---|---|---|---|
| **1** | **67** | Ph | H | **69** | 84% |
| **2** | **71** | H | H | **79** | 75% |
| **3** | **72** | $CH_3$-$(CH_2)_2$ | H | **80** | 45% |
| **4** | **73** | $CH_3$-$(CH_2)_4$ | H | **81** | 51% |
| **5** | **74** | Ph-$CH_2$-O | H | **82** | 0% |
| **6** | **75** | (4-$CH_3O$)Ph | H | **83** | 53% |
| **7** | **76** | (3-Cl)Ph | H | **84** | 48% |
| **8** | **77** | Cy | H | **85** | 37% |
| **9[c]** | **78** | $CH_3$ | $CH_3$ | **86** | 60% |

Table 10. Reaction scope. [a]Reaction conditions: aldehyde **67**, **71-78** (0.25 mmol, 1 equiv.), EDA **68** (0.30 mmol, 1.2 equiv.), $Na_4TPPS_4$ (1 mol%), piperidine (0.4 equiv.), $LiBF_4$ (0.2 equiv.), DMSO (2 mL), light (Photoreactor 2: white LEDs, 18 W, 1080 Lm), 5 h. [b]Corresponding to the weight of the reaction product not purified chromatographically. [c]Compound **89l-rac** was used as organocatalyst since complex product mixtures were obtained with piperidine.

Entry 1 of Table 10 corresponds to 3-phenylpropionaldehyde and is therefore identical to entry 1 of Table 9. When we changed the aromatic substituent to a saturated chain, we saw a linearly inverse dependence between the yield of the alkylated product and the chain length of the starting aldehyde, with total conversion of the starting aldehyde to the corresponding α-alkylated product (Entries 2, 3 and 4). When we introduced a benzyloxy group instead of the saturated chain, the α-alkylation product could not be detected (Entry 5), recovering the starting aldehyde.

Returning to the 3-phenylpropionaldehyde skeleton, we observed that the introduction of a *p*-methoxy (Entry 6) or of a *m*-chloro substituent in the phenyl ring (Entry 7) resulted in a moderate decrease of the reaction yield. On the other hand, the replacement of the phenyl group by a cyclohexyl one (Entry 8) led to a much lower yield. Finally, we saw that the substitution at the β-position to the aldehyde does not significantly hinder alkylation at the α-position. When the reaction was carried out with isovaleraldehyde (Entry 9), the yield was superior to those obtained with *n*-hexanal (Entry 3) and with *n*-octanal (Entry 4).

To conclude the scope investigation for aldehydes, we decided to try the reaction with a dialdehyde, such as glutaraldehyde **87**, to see if we could obtain the monoalkylation product or, if, on contrary, the dialkylation product (Scheme 38). Unfortunately, we did not detect either the mono- or the di-alkylation product.

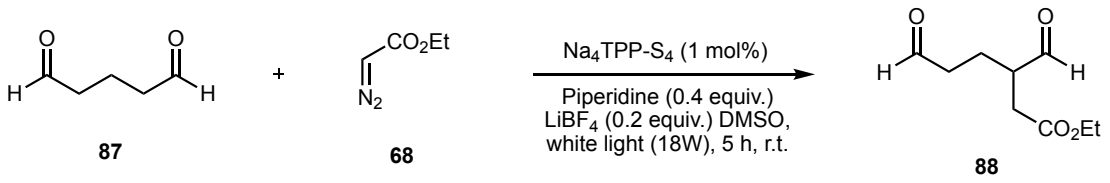


Scheme 38. Attempt of the α-alkylation reaction with glutaraldehyde **87**.

Having evaluated the extent of the reaction with respect to the aldehyde structure, we initiated chirality induction studies on the reaction. To perform such studies, various chiral pyrrolidines derived from L-Proline, organocatalysts **89a-l**, were used as a secondary amine organocatalyst. Since the alkylation of 3-phenylpropionaldehyde **67** gave very good results, we decided to use it as the reference reaction (Table 11).

The enantiomeric excess of **69** was determined via HPLC in a chiral stationary phase. For this purpose, since we could not find suitable conditions for the separation of the two enantiomeric aldehydes, we decided to derivatize them to the unsaturated ester **91** via Wittig reaction with (carbethoxymethylene)triphenylphosphorane **90** (Scheme 39). The racemic compound **91** was prepared by derivatization of the racemic aldehyde **69** obtained with piperidine.

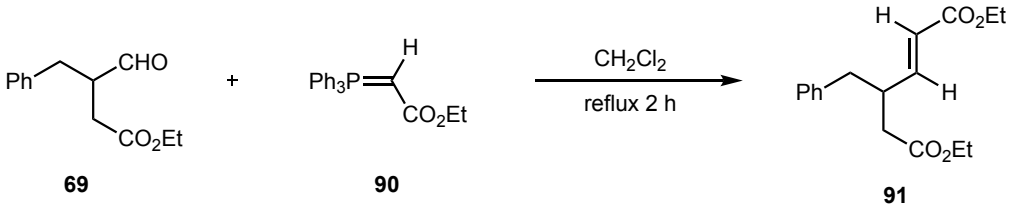


Scheme 39. Wittig derivatization of α-alkylated aldehyde **69**.

While organocatalysts **89a-c** were commercially available, the remaining ones (**89d-l**) were synthesized by us. Catalysts **89d** and **89g-l** are relatively simple amides from L-Proline.

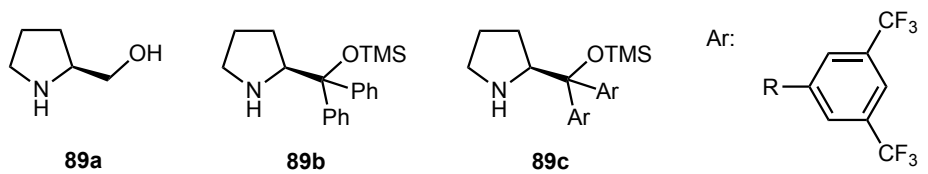


Figure 81. Chemical structure of organocatalysts **89a-c**.

A commonly used method for the formation of the amide bond is the coupling between an amine and a carboxylic acid, in this case *N*-Boc-L-Proline **53** (see Scheme 26 for its preparation), by reaction with ethyl chloroformate in the presence of triethylamine. The resulting mixed anhydride intermediate is not isolated, and is submitted to the nucleophilic attack of the amine.[193] Subsequent cleavage of the *tert*-butylcarbamate afforded the required amides. In this way, organocatalysts **89d** and **89g-l** were prepared with overall yields above 75%, except for the deprotections of precursors **94** and **97** (Scheme 40).

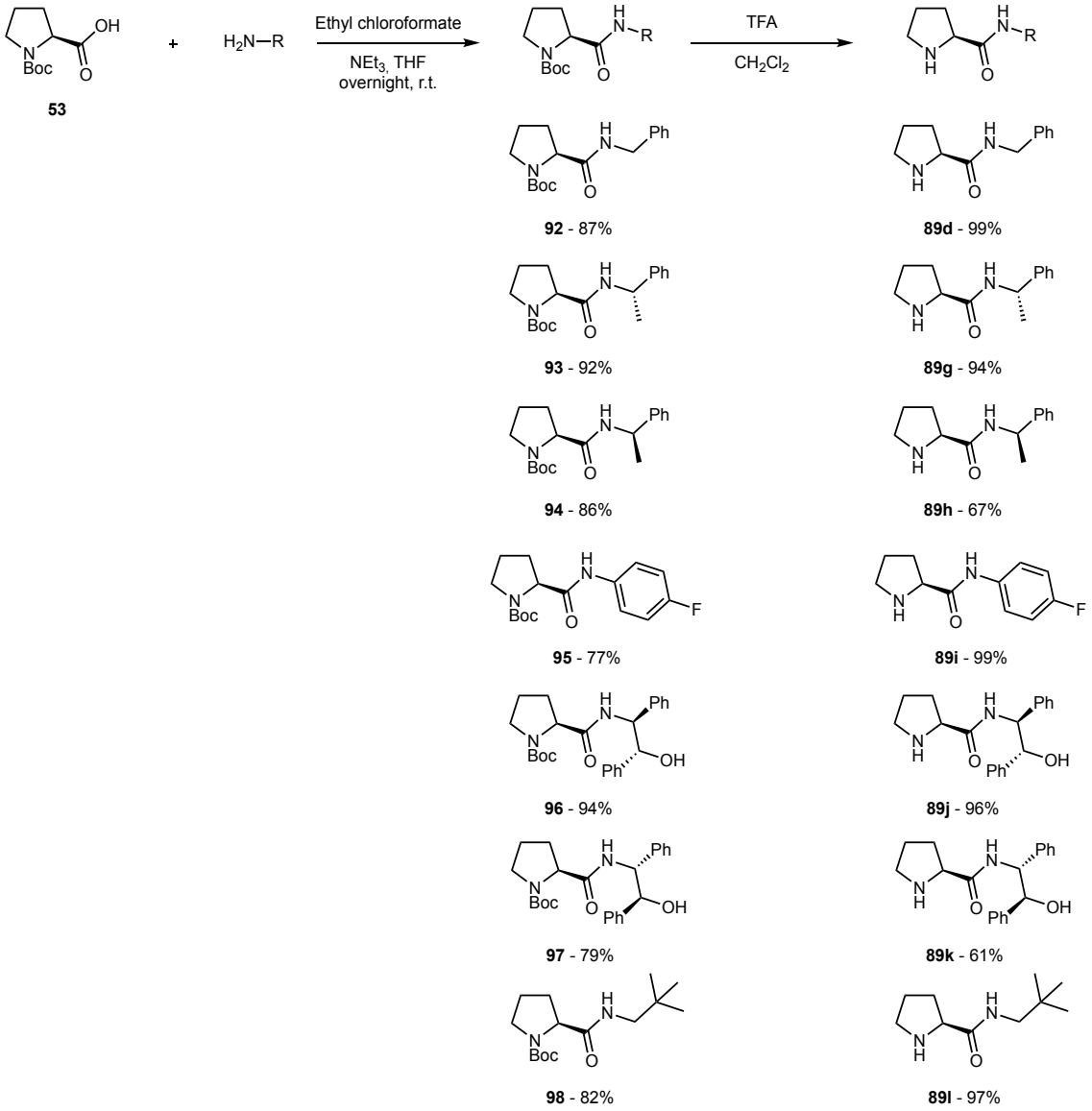


Scheme 40. Synthetic route for the obtention of L-Proline-based organocatalysts **89d-l**.

The synthesis of organocatalyst **89e** is based on the same coupling strategy shown in Scheme 42, being the amine in this case the (*S*)-2-aminomethylpyrrolidine, that can be readily obtained from L-Proline. For this purpose, the coupling between 2-phenylacetic acid and *N*-*tert*-butoxycarbonyl (*S*)-2-aminomethylpyrrolidine **50** (whose synthesis has been discussed above, see Scheme 23)

was carried out, obtaining excellent yields for both the coupling and the deprotection steps (Scheme 41).

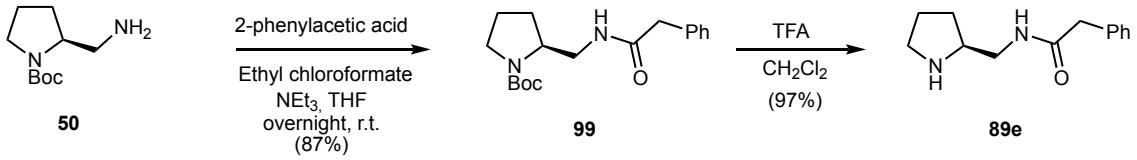


Scheme 41. Synthetic route for the obtention of L-Proline-based organocatalyst **89e**.

Finally, to synthesize organocatalyst **89f**, which presents the thioamide group in its structure, the oxygen of the carbonyl functional group was substituted by the sulfur in an extra step between the coupling and the deprotection steps (Scheme 42). The yield of both the substitution with Lawesson's reagent and the deprotection steps were moderate.

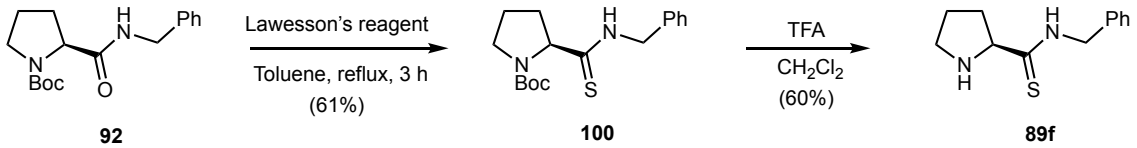


Scheme 42. Synthetic route for the obtention of L-Proline-based organocatalyst **89f**.

The results obtained with the different organocatalysts (0.4 equivalents), using the tetrasodium salt of 5,10,15,20-(*p*-sulfonatophenyl)-porphyrin **62** (1 mol%) as photocatalyst in degassed DMSO as solvent are shown in Table 11, detecting only the expected signals for the α-alkylation product, except for organocatalyst **89c**, where the $^{1}$H-NMR analysis of the crude showed the formation of an unidentified aldehyde derivate.

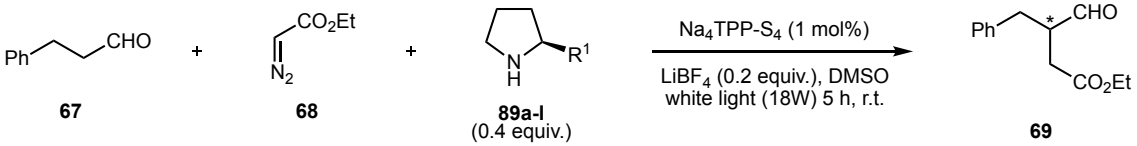


| Entry[a] | $R^1$ | Organocatalyst | Yield[b] | ee[c] |
|---|---|---|---|---|
| 1 | $CH_2OH$ | **89a** | 62% | 8% |
| 2 | $CPh_2OTMS$ | **89b** | 47% | 2% |
| 3 | $CAr_2OTMS$ | **89c** | 0%[d] | - |
| 4 | 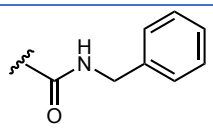 | **89d** | 88% | 29% |
| 5 | 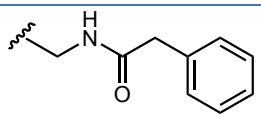 | **89e** | 96% | 0% |
| 6 | 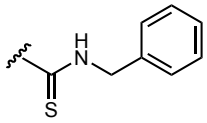 | **89f** | -[e] | - |
| 7 | 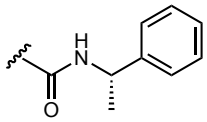 | **89g** | 90% | 5% |
| 8 | 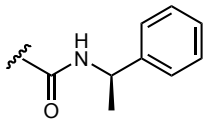 | **89h** | 91% | 4% |
| 9 | 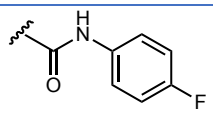 | **89i** | 40% | 28% |
| 10 | 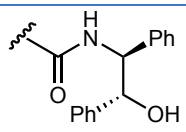 | **89j** | 90% | 27% |
| 11 | 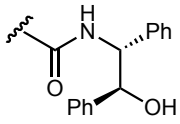 | **89k** | 68% | 23% |
| 12 | 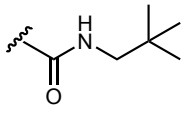 | **89l** | 97% | >99% |

Table 11. Chirality induction studies. [a]Reaction conditions: aldehyde **67** (0.25 mmol, 1 equiv.), EDA **68** (0.30 mmol, 1.2 equiv.), $Na_4TPP\text{-}S_4$ (1 mol%), organocatalyst **89a-l** (0.4 equiv.), $LiBF_4$ (0.2 equiv.), DMSO (2 mL), light (Photoreactor 2: white LEDs, 18 W, 1080 Lm), 5 h. [b]Corresponding to the weight of the reaction product not purified chromatographically. [c]Determined via chiral HPLC after derivatization to **91**: Phenomenex i-cellulose 5 column; Hexane/IPA 1%; 1 mL/min flow rate; λ = 218 nm, being enantiomer (*S*) the major enantiomer in all cases. [d]The formation of an unidentified aldehyde derivate was observed. [e]Imidazolidinethione is formed exclusively.

Our initial idea was to test L-Proline as a chiral organocatalyst, but during the system optimization studies we saw that the addition of acidic medium to the reaction gave rise to the aldolic selfcondensation product, so we decided to start with the simplest neutral derivative of this compound, (*S*)-prolinol **89a**. As shown in Table 11, a moderate yield of **69** was obtained. We were pleased to find that the product was not obtained in racemic form, albeit with a very low enantiomeric excess (Entry 1).

In the light of this finding, we decided to continue the study with the Hayashi-Jørgensen **89b** (Entry 2) and Jørgensen **89c** (Entry 3) catalysts (hoping that an increase of the steric hindrance at the chiral center of the catalyst would improve the enantioselectivity of the process), but the results were worse than those obtained for organocatalyst **89a**. With **89b**, a strong diminution of the reaction yield took place, and the product was formed in essentially racemic form. With **89c**, the $^1$H-NMR analysis of the crude showed the formation of an unidentified aldehyde derivate. These results showed two important experimental facts: a) that a bulky pyrrolidine substituent hinders the reaction, and b) the necessity to place a hydrogen bond donor group on the pyrrolidine substituent. Thus, organocatalysts **89d-l**, with an amide group in their structure, which should form stronger hydrogen bonds than those of the hydroxyl group of **89a**, were synthesized as explained above.

The first one of these amides to be tested was organocatalyst **89d**, which resulted in better yields and enantiomeric excesses, even though the enantiomeric excess (29% ee) was still quite poor (Entry 4). At this point, we set out to evaluate the effect of placing the amide carbonyl group further away from the pyrrolidine unit by synthesizing compound **89e**. Despite obtaining an excellent yield, the α-alkylation product was obtained in its racemic form (Entry 5).

To further test our hypothesis that the enantiomeric excess could have a directly proportional relationship to the acidic character of the hydrogen bond donor group, we synthesized organocatalyst **89f**, exchanging the amide functional group for a thioamide, with an even more acidic NH (Entry 6). By $^1$H-NMR analysis of the reaction crude we only observed however the exclusive formation of imidazolidinethione **101**, and we were able to separate its two diastereomers *exo* and *endo* (Figure 82). This result is discussed in more detail in Appendix I.

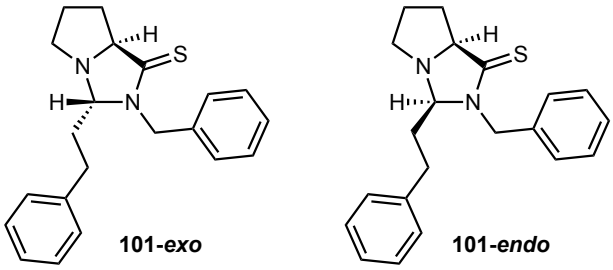


Figure 82. *Exo*/*endo* diastereomers of imidazolidinethione **101**.

In organocatalysts **89g** and **89h**, a methyl group was introduced at the benzyl position, with the idea that the additional chiral center might help to improve the enantioselectivity of the reaction. To our surprise, despite the fact that the α-alkylation product **69** was obtained in excellent yield with both catalysts, we saw a significant decrease in the enantiomeric excess (Entry 7 and 8). It is important to comment the fact that the major enantiomer in both cases was the same, indicating that the configuration of the additional chiral center did not have a relevant impact on the enantioselective course of the reaction.

In the light of the results obtained, organocatalyst **89i** (an amide derived from 4-fluoroaniline) was synthesized, with the idea that the aromatic system could interact with the carbon-carbon double bond of the enamine, through π-stacking type interactions as in the case of organocatalyst **89d**, and increase the poor enantiomeric excesses obtained previously. Despite obtaining similar enantiomeric excesses, the yield declined considerably (Entry 9).

Even if the presence of a substituent at the α' position to the nitrogen had negative effects on the reaction yield, we thought that placing a hydroxyl group at the β' position the enantioselectivity of the reaction could be improved, due to the possibility of forming hydrogen bonds with the substrate. The results showed an increase in the reaction yield, but the enantiomeric excesses remained slightly below the 30% for both organocatalysts **89j** (Entry 10) and **89k** (Entry 11).

Seeing that the course of the reaction stereochemistry was not controlled by π-stacking type interactions between the aldehyde and the organocatalyst, we thought of modifying the steric hindrance of the amine moiety by placing the bulky substituent one carbon away from the pyrrolidine chiral center. To that end, we synthesized the prolinamide **89l** with a neopentyl group attached to the nitrogen atom. We were delighted to find that both the yield and the enantiomeric

excess obtained when using **89l** as an organocatalyst were excellent (Entry 12). With this compound, only one peak in the chiral HPLC chromatogram of the derivative **91** (Figure 83) was observed.

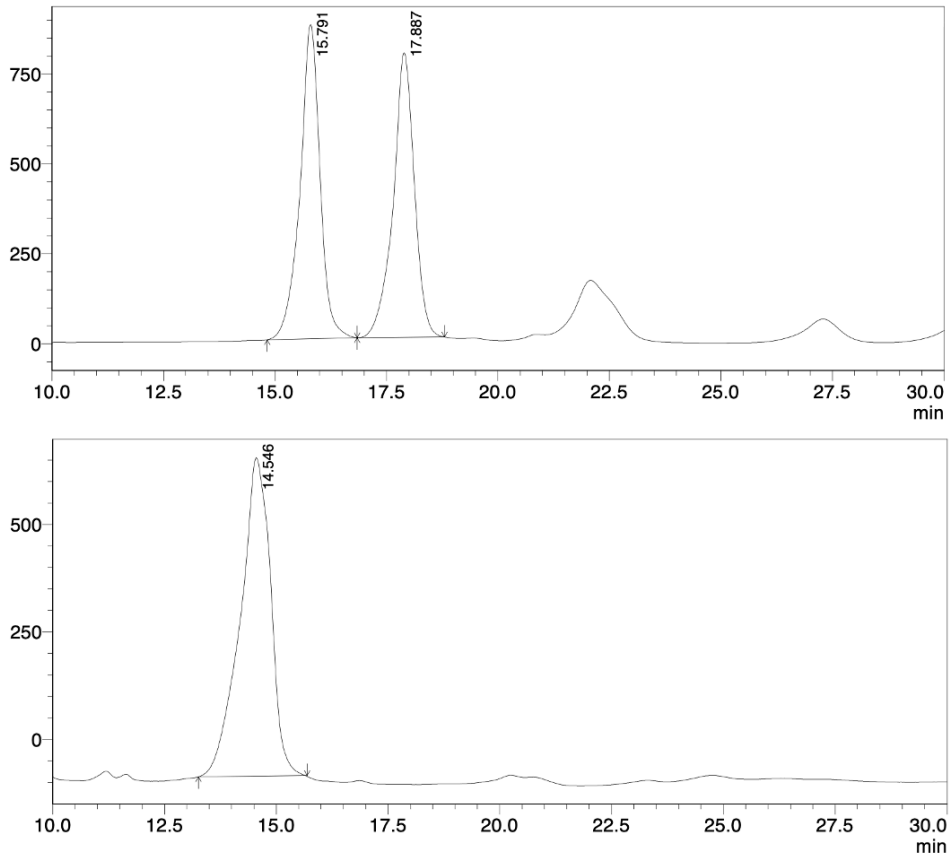


Figure 83. HPLC chromatograms of Wittig derivative **91** of a racemic sample (top) and enantiopure (bottom).

The determination of the absolute configuration of the major enantiomer of the α-alkylated aldehyde **69** was performed by chemical correlation. For this purpose, and since compound **69** had not been previously synthesized in its enantiopure form, we decided to carry out a literature search to find out whether the absolute configuration and specific rotation of any of its derivatives had been previously described. In 2004, Robins and co-workers reported the synthesis of diol (*R*)-**102** in non-racemic form, along with the value of its specific rotation.[195] In light of this precedent, the enantiopure aldehyde **69** was reduced to alcohol **102** by reaction with $LiAlH_4$ in THF for 24 h at room temperature (Scheme 43). When we measured the specific rotation of the diol **102** obtained by us, we observed that this compound was levorotatory, contrary to the dextrorotatory character[195] of (*R*)-**102** (we have no explanation for the discrepancy between the absolute values, beyond that in our case the enantiomeric purity was essentially complete).

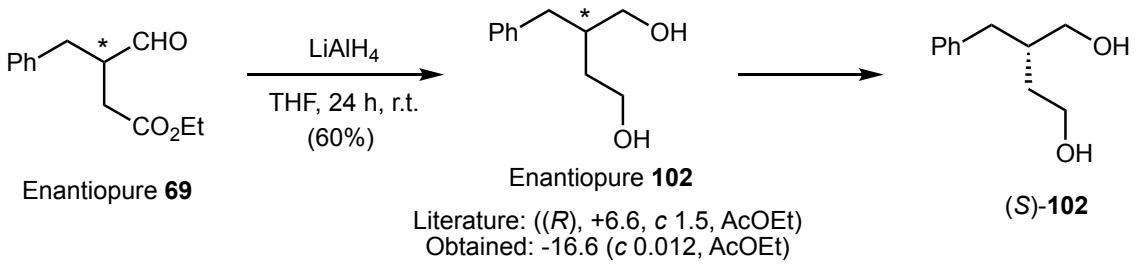


Enantiopure **69**

Enantiopure **102**

Literature: ((*R*), +6.6, *c* 1.5, AcOEt)
Obtained: -16.6 (*c* 0.012, AcOEt)

(*S*)-**102**

Scheme 43. Reduction of aldehyde **69** to diol **102**.

The specific rotation measurements thus established unambiguously an absolute (*S*)-configuration for diol **102** and, consequently, also for the α-alkylated aldehyde **69**. The obtained absolute configuration fits perfectly with a mechanistic model involving a hydrogen bond between the NH group of the intermediate (*E*)-enamine radical cation and the carbonyl oxygen of the carbene, leading to the enantiopure (*S*)-**69** compound (Scheme 44).

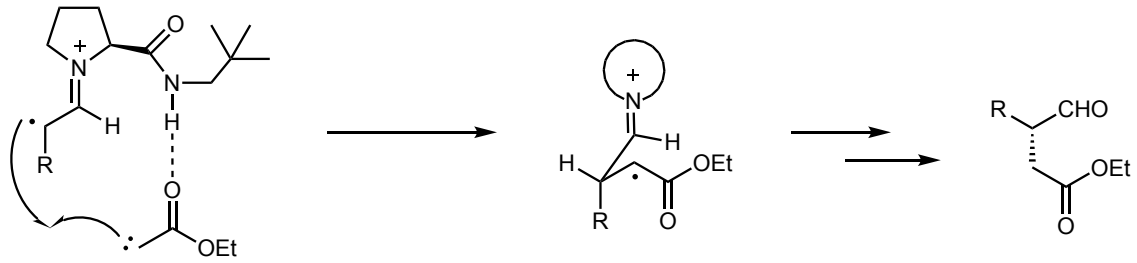


Scheme 44. Mechanistic model for the obtention of (*S*)-**69** aldehyde.

In the light of the excellent results obtained for organocatalyst **89l** in the alkylation of **67**, we decided to evaluate the enantioselectivity of the reaction of some of the aldehydes that had given the best yields in the reaction catalyzed by piperidine (see Table 10). The results are given in Table 12.

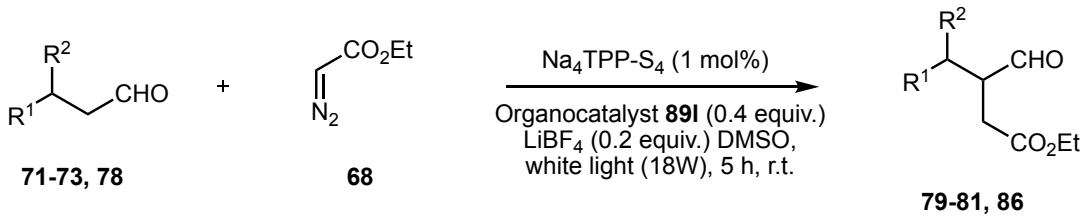


| Entry[a] | Aldehyde | $R^1$ | $R^2$ | Product | Yield[b] | ee[c] |
|---|---|---|---|---|---|---|
| **1**[d] | **67** | Ph | H | **69** | 97% | >99% |
| **2** | **71** | H | H | **79** | 0% | - |
| **3** | **72** | $CH_3$-$(CH_2)_2$ | H | **80** | 95% | 44% |
| **4** | **73** | $CH_3$-$(CH_2)_4$ | H | **81** | 90% | 84% |
| **5** | **78** | $CH_3$ | $CH_3$ | **86** | 99% | 66% |

Table 12. Enantioselectivity studies. [a]Reaction conditions: aldehyde (0.25 mmol, 1 equiv.), EDA **68** (0.30 mmol, 1.2 equiv.), $Na_4TPP\text{-}S_4$ **62** (1 mol%), organocatalyst **89I** (0.4 equiv.), $LiBF_4$ (0.2 equiv.), DMSO (2 mL), light (white LEDs, 18 W, 1080 Lm), 5h. [b]According to the weight of the product, without chromatographic purification. [c]Determined by chiral HPLC from the Wittig derivative product: Phenomenex i-cellulose 5 column; Hexane/IPA 1% ; flow rate 1 mL/min; λ = 218 nm), being enantiomer (*S*) the major enantiomer in all cases. [d]Shown in Table 13 to compare the results obtained for the other aldehydes.

As it can be seen, good to excellent yields were obtained for aldehydes with saturated alkyl substituents except for propanal **71** (Entry 2) for which we did not observe the formation of the desired product. Instead, the $^1$H-NMR analysis of the crude showed the formation of an unidentified aldehyde derivate.

For *n*-octanal **73** (Entry 4), a very good enantioselectivity (84% ee) was obtained, contrary to what was observed with *n*-hexanal **72** (Entry 3), whose alkylation took place with much lower enantioselectivity (44% ee); this indicates that the longer the saturated chain length is, the better the enantiomeric excesses are obtained. The introduction of a methyl substituent at the β-position of the aldehyde has a significant influence on the enantioselectivity of the reaction since we observed a 66% ee in the alkylation of isovaleraldehyde **78** (Entry 5).

In the reaction conditions we used a relatively high amount of the chiral organocatalyst (0.4 equivalents to aldehyde), since as mentioned before we could not achieve complete conversion of the starting aldehyde **67** when using 0.2 equivalents of piperidine. To gain some insight into this issue, Mario Jiménez in his Master's work studied the kinetics of the reaction between 3-phenylpropanal **67** and EDA **68** using both 0.4 equivalents and 0.2 equivalents of organocatalyst

**89l**.[196] The results are shown in Figure 84. The studies were carried out by analyzing the reaction crudes at different times through gas chromatography (GC).

As it can be seen, when the reaction was set up with 0.4 equivalents of organocatalyst **89l**, we observed by GC complete conversion of the starting aldehyde **67** after 180 min of reaction (in full agreement with the $^1$H NMR spectrum of the reaction crude). On the contrary, when we performed the reaction with 0.2 equivalents of the organocatalyst, conversion was not complete (*ca.* 80% according to both by GC and $^1$H-NMR) even after 5 h of reaction.

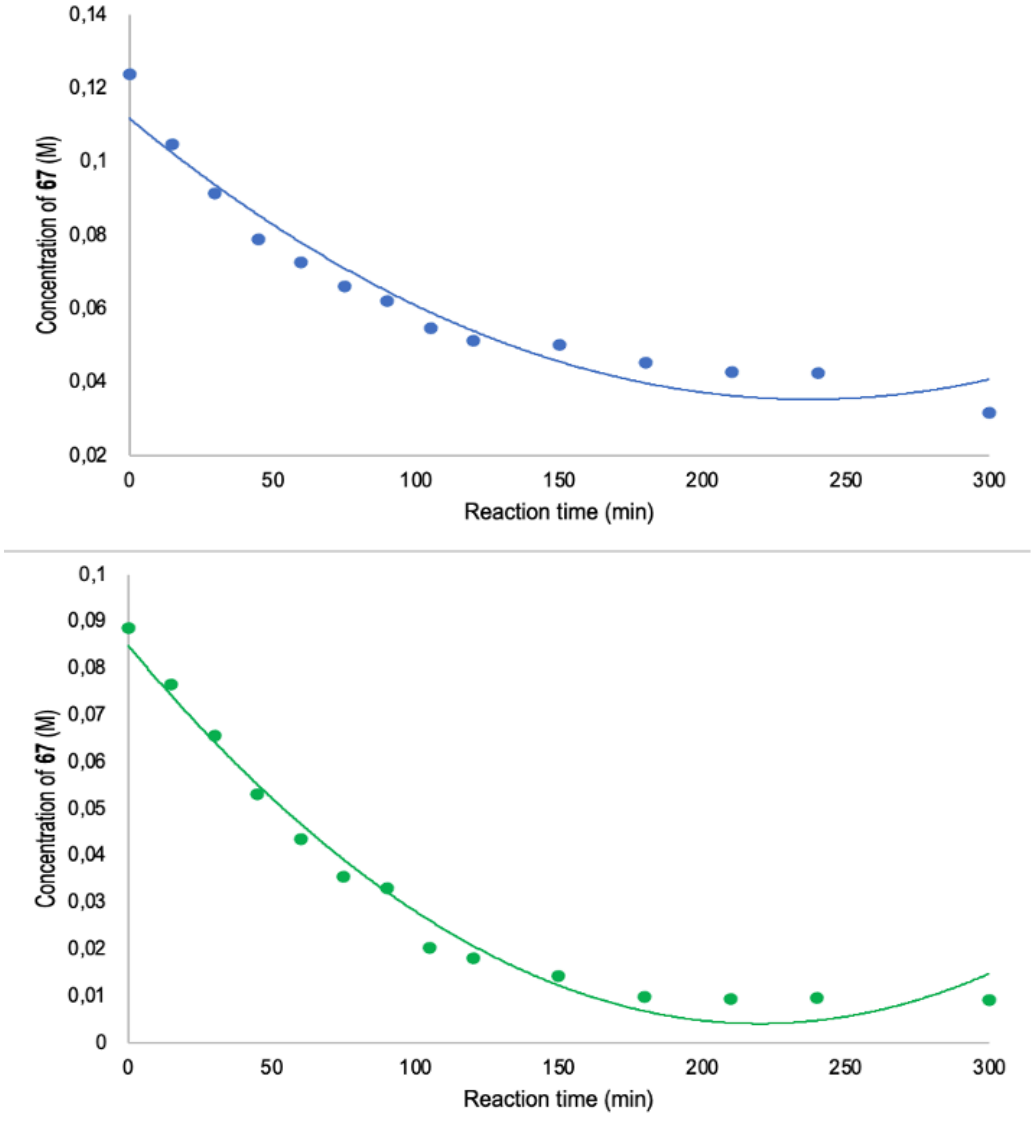


Figure 84. Kinetics studies for the photochemical α-alkylation reaction between 3-phenylpropionaldehyde **67** and EDA **68** using 0.2 equivalents (top) and 0.4 equivalents (bottom) of organocatalyst **89l**. Conditions: CP7503 CP-Chirasil DEX CB 25m, 0.32 mm, 0.25 μm column, 250 ºC injector temperature, 50 to 250 ºC (with a rate of 10 ºC/min) column temperature.

In the light of this result, we decided to test a reaction under the same conditions (aldehyde **67**, 1.2 equiv. of EDA, 0.2 equiv. of $LiBF_4$, DMSO, white light (photoreactor 2: 18W LEDs), 5 h, r.t.), but in the absence of the organocatalyst, to ascertain whether the starting aldehyde **67** underwent some competitive degradation process. To our surprise, **67** reacted completely after 5 h of irradiation, and we observed the essentially quantitative formation of a new product **103** (Scheme 45).

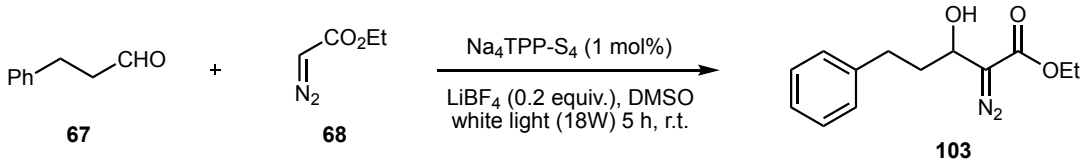


Scheme 45. Photochemical reaction set up without the organocatalyst.

This compound was purified by flash column chromatography through silica gel, using a mixture of hexane/AcOEt (4/1) to (3/1) as eluent, and according to its spectral data ($^1$H-NMR, $^{13}$C-NMR, $^1$H-$^1$H COSY and MS (ESI)) was identified as the α-diazo-β-hydroxyester **103**. The aldol-type nucleophilic addition of EDA **68** to different types of aldehydes has been described under thermal conditions,[197,198] but always needs the presence of a strong base. To confirm this unexpected result, we carried out the same photoinduced aldol addition on a non-enolizable aldehyde, such as benzaldehyde, and we isolated the aldol **104** in quantitative yield (Scheme 46).

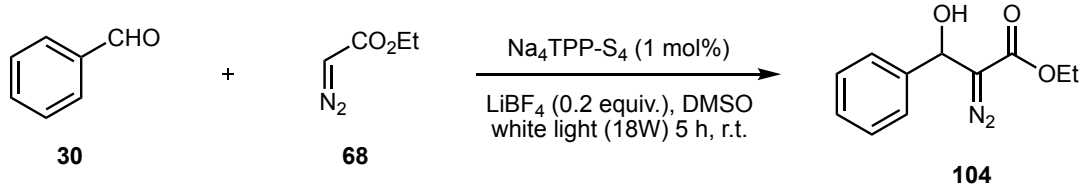


Scheme 46. Formation of α-diazo-β-hydroxyester **104** under photochemical conditions.

This transformation is currently being studied in our research group, since the photoinduced formation of the aldol does not fit with the mechanism proposed by Gryko and co-workers (Scheme 33). In it, the authors propose that the interaction between the excited photocatalyst and the EDA leads to the formation of the carbene via an energy transfer process. Following this mechanism, the aldol addition product could not be formed, due to two main reasons, (a) the carbene formation step is much faster than the nucleophilic addition of the diazocompounds, and (b) as can be seen, the compounds keeps the $N_2$ fragment in its structure, if such photosensitization process really took place at the time of the attack, it should have already been released in the form of nitrogen gas. On the other hand, it is important to note that the presence of a secondary or of a tertiary amine, in

sub-stoichiometric amounts, totally inhibits this reaction leading to the formation of the α-alkylation product or the recovery of the starting aldehyde, respectively.

As a conclusion, we can say that it we have developed a suitable dual organophocatalytic system for aldehyde α-alkylation reactions that allowed us to study the enantioselectivity of the reaction by using the L-Proline-derivatives as organocatalysts **89a-l**.

The formation of the aldol addition subproduct **103** suggests that the reaction could go through a mechanism different from that disclosed by Gryko and co-workers (Scheme 33), although further studies are needed to be able to propose an alternative mechanism.

## 5.3. STUDY OF THE α-ALKYLATION OF ALDEHYDES EMPLOYING A BIFUNCTIONAL PHOTOCATALYTIC SYSTEM

In the light of the results obtained for the dual catalysis photochemical system, we set out to ascertain the viability of a bifunctional catalysis photochemical system for the same reaction, using the L-Proline-based amino-functionalized porphyrins **18** and **44** as bifunctional catalysts (Figure 85).

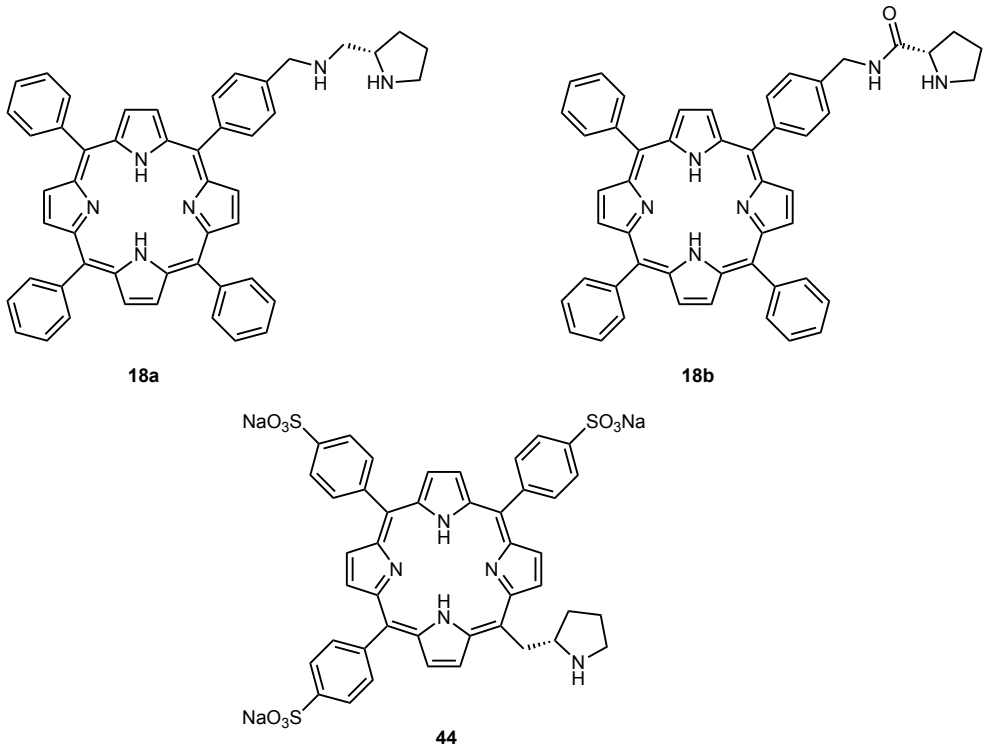


Figure 85. L-Proline-based amino-functionalized porphyrins **18** and **44**.

Given the good results obtained in terms of enantioselectivity and yield for organocatalysts **89d-l** and that for organocatalyst **89e** the α-alkylated product was obtained in its racemic form (Entry 5 in Table 11), we decided not to use compound **18a** as a platform for the development of the bifunctional system, since its structure presents many similarities with the aforementioned organocatalyst **89e**.

Thus, we decided to study the reaction between 3-phenylpropionaldehyde **67** and EDA **68** as a starting point to achieve our goal. Firstly, we decided to test bifunctional catalyst **18b**, due to the fact that, like organocatalysts **89d-l**, it presents an amide group in its structure (Table 11 shows the high yields obtained by those organocatalysts with the amide group), expecting to obtain similar

results. For this purpose, since in the dual system the photocatalyst and the organocatalyst were added in different proportions, we first decided to study the reaction for different molar ratios of the bifunctional catalyst, showing the results in Table 13.

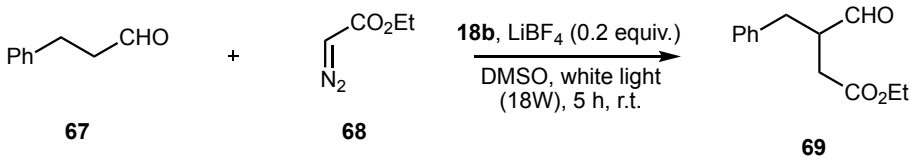


**67** **68** **69**

| Entry[a] | Molar ratio of 18b | Conversion[b] |
|---|---|---|
| **1** | 1 mol% | 38% |
| **2** | 5 mol% | 40% |
| **3**[c] | 10 mol% | 27% |
| **4** | 20 mol% | 38% |

Table 13. Development of the bifunctional photocatalytic system. [a]Reaction conditions: aldehyde **67** (0.25 mmol, 1 equiv.), EDA **68** (0.30 mmol, 1.2 equiv.), bifunctional catalyst **18b**, $LiBF_4$ (0.2 equiv.), DMSO (2 mL), light (white LEDs, 18 W, 1080 Lm), 5h. [b]Determined via $^1$H-NMR. [c]The aldolic selfcondensation product **70** was obtained in a 49% of conversion.

As can be seen in Table 13, very similar, although relatively low conversions were obtained in each test performed, demonstrating the capacity of the bifunctional catalyst to induce α-alkylation. It should be noted that when compound **18b** was added at a molar ratio of 10 mol% (Entry 3), the aldol selfcondensation product was obtained as the major compound. Looking at the results obtained, we can say that bifunctional catalyst **18b** presents promising preliminary results in the absence of optimizing the system in terms of conversion of the starting aldehyde and purity of the α-alkylation product, since it could not be adequately purified due to the appearance of a reaction subproduct that we were unable to separate from the desired product (this subproduct gives rise to a doublet at a chemical shift of 9.72 ppm in the $^1$H-NMR spectrum).

In parallel, the same experiments were performed, but using the amino-functionalized porphyrin **44** as a bifunctional catalyst, showing the results in Table 14.

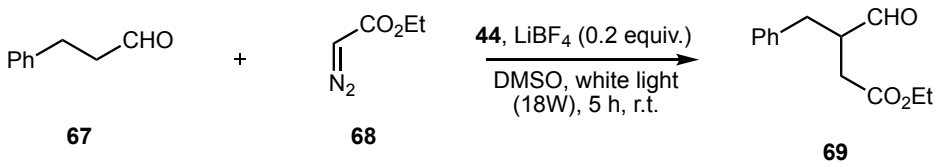


| Entry[a] | Molar ratio of 44 | Conversion[b] |
|---|---|---|
| **1** | 1 mol% | - |
| **2** | 5 mol% | 8% |
| **3** | 10 mol% | 42% |
| **4** | 20 mol% | 7% |

Table 14. Development of the bifunctional photocatalytic system. [a]Reaction conditions: aldehyde **67** (0.25 mmol, 1 equiv.), EDA **68** (0.30 mmol, 1.2 equiv.), bifunctional catalyst **44**, $LiBF_4$ (0.2 equiv.), DMSO (2 mL), light (white LEDs, 18 W, 1080 Lm), 5h. [b]Determined via $^1$H-NMR.

When only a 1 mol% of the catalyst was used (Entry 1), no alkylation product could be detected by $^1$H-NMR. An 8% conversion was observed for a 5 mol% (Entry 2). Best results were obtained for a 10 mol% of the catalyst, we obtained the best results, reaching a 42% of conversion of the starting aldehyde (Entry 3). Despite using in this case a sulfonated porphyrin (soluble in polar solvents such as water), which should facilitate the purification step, we were unable to purify the starting product due to again the formation of the unidentified subproduct giving rise to the doublet at 9.72 ppm.

It should be mentioned that due to the complexity of the reaction crudes, it was not possible to obtain satisfactorily the Wittig **91** adducts, so we have not been able to evaluate the enantioselectivity provided by these bifunctional catalysts.

Given the results obtained for both bifunctional catalysts **18b** and **44**, we can conclude that these amino-functionalized porphyrins present an acceptable catalytic activity in the developed photochemical system, but that a dual organophotocatalytic system appears to be a more convenient alternative.

# CHAPTER 6. CONCLUSIONS

The objectives that were initially set out in this Thesis have been explored. The work developed and its conclusions are summarized in the following sections.

[1]. By using chiral imidazolidinones as organocatalysts and amphiphilic porphyrins as photocatalysts, we have developed a dual catalysis photochemical system. When applied to the visible-light promoted Diels-Alder cycloaddition reaction between cinnamaldehyde and cyclopentadiene, we have observed, in comparison to the same reaction under purely thermal conditions, a substantial increase in yields (from 48% to values between 90-99%), with similar values of both diastereomeric ratio and enantiomeric excess.

[2]. When a methyl coumalate was used as a diene moiety in an inverse electronic demand Diels-Alder reaction with cinnamaldehyde, under the same conditions, the Michael adduct formation was observed, a process which also takes place under thermal conditions.

[3]. We have developed a suitable synthetic route for the synthesis of porphyrin-derived imidazolidinones. When these were used as bifunctional catalysts in the Diels-Alder cycloaddition reaction between cinnamaldehyde and cyclopentadiene, we observed, both under thermal and photochemical conditions, a remarkable increase in the diastereoselectivity of the reaction, although with very poor yields and enantiomeric excesses compared to those obtained with chiral imidazolidinones, under dual catalysis conditions.

[4]. We have shown that in the organophotocatalytic reaction of $\alpha$-alkylation of aldehydes with diazoesters, the use of the tetrasodium salt of 5,10,15,20-tetrakis(4-sulfonatophenyl)porphyrin as photocatalyst, presents numerous advantages over conventional photocatalysts. A simple aqueous treatment allows the complete removal of the two catalysts, avoiding chromatographic purification of the reaction crude.

[5]. By using chiral pyrrolidines derived from L-Proline, we have performed chirality induction studies in the organophotocatalytic reaction of $\alpha$-alkylation of 3-phenylpropionaldehyde with ethyl diazoacetate. We have observed that the presence of a hydrogen-bond donor group in the organocatalyst, such as the amide group, enhanced the enantioselectivity of the reaction. By using the chiral amide derived from L-Proline and neopentylamine, we obtained the $\alpha$-alkylation product in excellent yield and in enantiomerically pure form. An initial exploration of the scope of this enantioselective version of the reaction has been performed.

[6]. The absolute configuration of the alkylation product of 3-phenylpropionaldehyde with ethyl diazoacetate has been determined by chemical correlation, through its reduction to the corresponding diol. The absolute (*S*)-configuration obtained fits perfectly with a mechanistic model involving a hydrogen- bond between the NH group of the (*E*)-enamine radical cation intermediate and the carbonyl oxygen of the carbene derived from ethyl diazoacetate.

[7]. We have developed suitable synthetic routes for the synthesis of several L-Proline-derived amino-functionalized porphyrins. When two of them were used as bifunctional catalysts in the organophotocatalytic $\alpha$-alkylation reaction of 3-phenylpropionaldehyde with ethyl diazoacetate, we saw that these presented an acceptable catalytic activity with conversions between 30% and 40%. Due to the complexity of the reaction crude, the enantioselectivity of the reaction could not be evaluated.

# CHAPTER 7. EXPERIMENTAL SECTION

## 7.1. GENERAL METHODS

Some solvents were distilled when anhydrous conditions were required, such as dichloromethane (from $CaH_2$) and tetrahydrofuran (from Na/benzophenone). Other solvents, such as hexane and ethyl acetate for column chromatography, were used directly without any purification beyond that already applied by the supplier (VWR and Merck Life Science, mostly).

Deuterated solvents were supplied by Merck Life Science.

For normal phase HPLC chromatography, HPLC grade solvents (hexane and isopropyl alcohol) were used directly without any purification beyond that already applied by the supplier (VWR). For reverse phase HPLC, HPLC grade methanol and a pH = 6.8 aqueous buffer solution were used as the mobile phase.

The follow-up of all the reactions has been performed by thin layer chromatography (TLC) using TLC-aluminium sheets, Merck 60 $f_{254}$. For the visualization of the TLC, UV light and chemical revelators ($KMnO_4$, *p*-anisaldehyde, phosphomolybdic acid and DNP) were used.

Column chromatographic purifications were performed under pressurized air in a column filled with 60 Å pore size and 40-63 μm particle size silica gel, as stationary phase, and solvent mixtures (hexane, ethyl acetate, dichloromethane, and methanol) as eluents.

$^{1}H$ and $^{13}C$ NMR spectra were recorded at room temperature on a Varian Mercury 400 instrument. 2D NMR spectra were recorded also at room temperature on a Varian Mercury 500 or on a Varian Mercury Bruker 400 instrument. $^{1}H$-NMR spectra were referenced to TMS ($\delta$ = 0 ppm) or to residual non-deuterated solvent peaks as internal standards. $^{13}C$-NMR were referenced to solvent peaks. Multiplicities are reported as follows: s = singlet, br = broad signal, d = doublet, t = triplet, q = quartet, quint = quintuplet, sext = sextuplet, m = multiplet or unresolved and combinations of these multiplicities (e. g. dd, dt, td, etc.). Coupling constants *J* are given in Hz.

HRMS spectra were recorded using a Bruker MicroTOF electrospray ionization spectrometer (ESI).

Normal phase HPLC analyses were performed on a Shimadzu instrument comprising a LC-20-AD solvent delivery unit, a DGU-20As degasser unit and an SPD-M20A UV/Vis Photodiode Array Detector; with chiral stationary phase using Daicel Chiralpak® IB, Daicel Chiralcel® AS-H columns and Phenomenex LC Columns 250 x 4.6 mm Lux® (5 μm i-Cellulose 5, 5μm i-Cellulose 3 and 5 μm i-Amylose 1).

Reverse phase HPLC analyses were performed using a C18 250 mm x 4 mm column (Nucleosil 120-5, Scharlab) equipped with an analytic precolumn (Resolve C18, Waters) on a Shimadzu instrument equipped with a UV-Vis detector, two LC-10 AS pumps and a Shimadzu Class VP programmer.

UV-Vis spectra were recorded at room temperature on a double beam spectrophotometer: Cary-Varian 5E, which uses the software Scan Varian. For the measurements, quartz Suprasil cells were used with optical path 10 mm x 10 mm.

A Rotofix 32 A from Hettich was used to centrifuge the aggregate samples of sulphonated porphyrins.

The lyophilized samples were prepared at a vacuum pump cooled with an immersion cooler Cryocool CC-100 II, filled with acetone at -80ºC.

Specific rotation measurements ($[\alpha]_D$) were obtained in a Perkin-Elmer 241 MC polarimeter, at the sodium D line (589 nm), at room temperature in a cuvette with a 10 cm optical path. Concentrations are expressed in g/100 mL.

Photoredox reactions were performed in different homemade photoreactors, as described in Chapter 4 (Figures 77 and 78).

## 7.2. SYNTHESIS OF SODIUM 4,4',4'',4'''-(PORPHYRIN-5,10,15,20-TETRAYL) TETRABENZENESULFONATE (62) AND 5,10,15,20-TETRAKIS(4-SULFOPHENYL)PORPHYRIN (63)

### 5,10,15,20-TETRAPHENYL PORPHYRIN (36)[174]

A 500 mL round-bottomed flask, equipped with magnetic stirring and a Liebig reflux condenser was filled in with 300 mL of propionic acid and heated until reflux. At this point, freshly distilled pyrrole (5.4 mL, 77.6 mmol) and benzaldehyde (7.92 mL, 77.8 mmol) were added simultaneously through the condenser, so that any momentary excess of one of the reactants in the reaction mixture is avoided. The reaction mixture was stirred for 30 min under reflux and cooled down to room temperature. Then, the resulting suspension was filtered in a Büchner funnel and the collected solid was washed with MeOH until the washings were colorless. The solid was dried under vacuum in the desiccator to obtain the porphyrin as a purple crystalline solid (2.52 g, 21% yield).

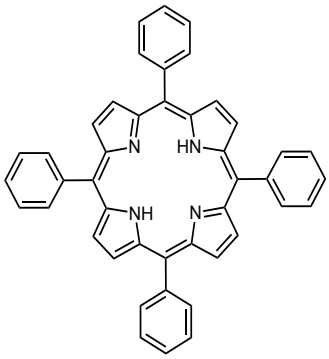


**$^1$H-NMR** ($CDCl_3$, 400 MHz): $\delta$ = 8.85 (s, 8H), 8.25-8.20 (dd, *J* = 7.5 Hz, *J'* = 1.5 Hz, 8H), 7.82-7.72 (m, 12H), -2.77 (br, 2H) ppm. **UV-Vis** [$CH_2Cl_2$, $\lambda_{max}$ nm ($\varepsilon$), c = 2.05 x $10^{-6}$ M]: 417 (488000), 517 (16000), 549 (9600), 591 (6900), 649 (4600).

### SODIUM 4,4',4'',4'''-(PORPHYRIN-5,10,15,20-TETRAYL)TETRABENZENESULFONATE (62)[199]

In a 100 mL round-bottomed flask, equipped with magnetic stirring and a Dimroth reflux condenser, 5,10,15,20-tetraphenyl porphyrin (1.00 g, 1.6 mmol) and concentrated $H_2SO_4$ (98 %, 55 mL) were added sequentially, and the resulting mixture was stirred and heated up to 100 ºC. Stirring at 100 ºC was maintained for 6 h, the mixture was then cooled down to room temperature and stirred overnight. At this point, the resulting green suspension was carefully poured over $H_2O$ MilliQ (15 mL), was distributed in 25 mL vials, and centrifuged to 6000 rpm for 40 minutes to obtain the porphyrin's J-aggregate as a dark green precipitate; the supernatant liquid was removed by decantation and the remaining solid was dispersed in a small amount of water. The suspension

was carefully basified with solid $Na_2CO_3$ until the solution changed its color from green to red. At this point, the solvent was removed under vacuum and the resulting purple solid was dissolved in the minimum amount of MeOH, heated up to reflux and allowed to cool down to room temperature to precipitate the inorganic salts. This process was repeated twice. Then, the solvent was removed under vacuum and the resulting solid was, first, redissolved in water and then lyophilized for 2 days, affording the desired porphyrin sodium salt as a purple solid (1.33 g, 88% yield). The purity was then analyzed by UV-Vis.

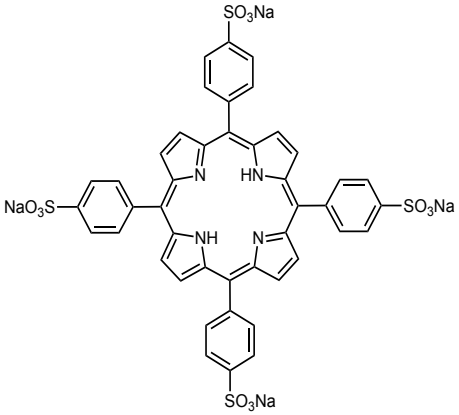


**$^1$H-NMR** (DMSO-$d_6$, 400 MHz): $\delta = 8.86$ (s, 8H), 8.19 (d, $J$ = 8.1 Hz, 8H), 8.06 (d, $J$ = 8.0 Hz, 8H), -2.96 (br, 2H) ppm.

**5,10,15,20-TETRAKIS(4-SULFOPHENYL)PORPHYRIN (63)[54]**

In a 100 mL round-bottomed flask, equipped with magnetic stirring and a Dimroth reflux condenser, 5,10,15,20-tetraphenyl porphyrin (500 mg, 0.8 mmol) and concentrated $H_2SO_4$ (98 %, 7 mL) were added sequentially, and the resulting mixture was stirred and heated up to 100 ºC. Stirring at 100 ºC was maintained for 6 h, the mixture was then cooled down to room temperature and stirred overnight. At this point, the resulting green suspension was carefully poured over $H_2O$ MilliQ (15 mL), was distributed in 25 mL vials, and centrifuged to 6000 rpm for 40 minutes to obtain the porphyrin's J-aggregate as a dark green precipitate; the supernatant is carefully separated and the precipitate is washed again with 15 mL more of $H_2O$ MilliQ. This process is repeated until the pH of the supernatant liquid is constant, with a value close to 1.5. Then, it is washed with an aqueous solution of 0.1M HCl and two more times with $H_2O$ MilliQ. Finally, the product is lyophilized for 2 days, affording the desired porphyrin in its zwitterionic form as a green solid (480 mg, 63% yield).

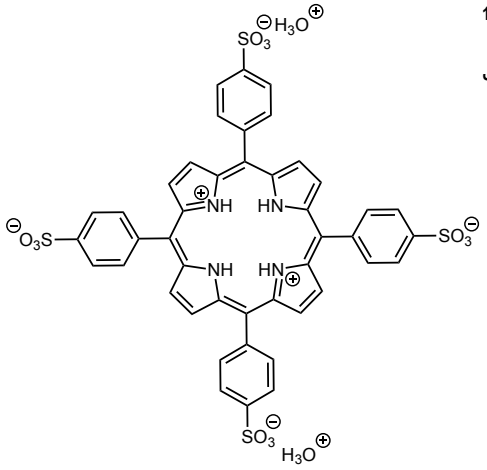

**$^1$H-NMR** (DMSO-$d_6$, 400 MHz): $\delta$ = 8.79 (s, 8H), 8.69 (d, *J* = 7.8 Hz, 8H), 8.32 (d, *J* = 8.1 Hz, 8H) ppm.

## 7.3. SYNTHESIS OF SODIUM (*S*)-4,4',4''-(20-(PYRROLIDIN-2-YLMETHYL) PORPHYRIN-5,10,15-TRIYL) TRIBENZENESULFONATE (44)

### (*S*)-PROLINOL (46)[200]

In a 500 mL round-bottomed flask, equipped with magnetic stirring and a reflux condenser, 200 mL of anhydrous commercial THF were introduced. Then, $LiAlH_4$ (6.89 g, 181.5 mmol) was carefully added, followed by the portion wise addition of L-Proline (6.97g, 60.5 mmol), noticing intense bubbling. The resulting grey suspension was vigorously stirred at room temperature for 24 h. At this point, 10 mL of $H_2O$ were carefully added to the reaction mixture, followed by the slow sequential addition of 10 mL of a 15 % (w/v) NaOH aqueous solution and by 10 mL of $H_2O$. At this point, the precipitate color change from grey to white was observed. Once the color change was complete, 200 mL of diethyl ether were added, and the resulting white crystalline solid was filtered out and washed with 3 x 50 mL of ethyl acetate. The combined organic layers were concentrated under vacuum to afford a yellowish oil (4.38 g, 72% yield), that was directly used in the next step without further purification.

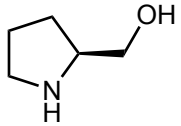

**$^1$H-NMR** ($CDCl_3$, 400 MHz): $\delta$ = 3.53 (q, *J* = 6.6 Hz, 1H C**H**–N), 3.33 (m, 2H, C**H$_2$**OH), 2.96-2.76 (m + br, 4H), 1.87-1.67 (m, 3H), 1.45-1.37 (m, 1H) ppm.

**_N_-BOC-(_S_)-PROLINOL (47)[201]**

To a magnetically stirred solution of (*S*)-Prolinol **46** (4.38 g, 43.4 mmol) in DCM (125 mL), triethylamine (21.7 mL, 156.1 mmol) was added, followed by di(*tert*-butyl)dicarbonate (11.36 g, 52.0 mmol). The mixture was stirred for 2 h at room temperature. At this point, 50 mL of $H_2O$ were added, and the two layers were separated. The organic phase was washed with 2 x 20 mL of $H_2O$, dried over anhydrous $Na_2SO_4$ and concentrated under vacuum to afford a red oil. The crude product was purified by flash column chromatography through deactivated silica gel (2.5% v/v $NEt_3$) and using an eluent gradient from hexane/AcOEt (5/1) to hexane/AcOEt (1/1), to give the protected prolinol as a yellowish oil (3.65 g, 72% yield).

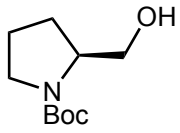


**$^1$H-NMR** ($CDCl_3$, 400 MHz): $\delta$ = 4.75 (br, 1H O**H**), 3.97 (m, 1H C**H**–N), 3.66-3.55 (m, 2H C**$H_2$**OH), 3.48-3.42 (m, 1H), 3.34-3.28 (m, 1H), 2.01 (sext, *J* = 5.5 Hz, 1H), 1.81 (m, 3H), 1.47 (s, 9H) ppm.

**_N_-BOC-(_S_)-PROLINAL (105)[202]**

In a 100 mL round-bottomed flask equipped with magnetic stirring, oxalyl chloride (2.33 mL, 27.2 mmol) was added at -78 ºC under Ar atmosphere. Then, a solution of anhydrous DMSO (3.0 mL, 42.2 mmol) in dry DCM (7 mL) was added and the resulting mixture was stirred for 20 minutes at -78 ºC. At this point, a solution of *N*-Boc-(*S*)-prolinol **47** (3.65 g, 18.1 mmol) in dry DCM (25 mL) was added and the reaction mixture was stirred for 20 more additional minutes, when triethylamine (10.10 mL, 72.5 mmol) was added. The reaction mixture was stirred for 2h at -78 ºC and stirring was maintained overnight at room temperature. At this point, 20 mL of a 10 % aqueous solution of ammonium chloride were added to quench the reaction, and the two layers were separated. The aqueous layer was washed with 3 x 10 mL of DCM and the combined organic layers were washed with 4 x 20 mL of a saturated solution of $NaHCO_3$, dried over anhydrous $Na_2SO_4$ and concentrated under vacuum to afford the crude aldehyde as a yellowish oil (3.50 g, 97% yield), that was not submitted to further purification.

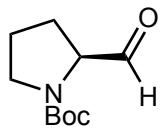


**$^1$H-NMR** ($CDCl_3$, 400 MHz; *ca.* 1:1 rotamer mixture): $\delta$ = 9.56 (br, 1H C**H**=O), 9.47 (d, *J* = 2.9 Hz, 1H C**H**=O), 4.21-4.04 (m, 2H), 3.59-3.25 (m, 4H), 2.20-1.86 (m, 8H), 1.48 (s, 9H), 1.47 (s, 9H) ppm.

### *N*-BOC-(*S*)-2-(2-METHOXYVINYL) PYRROLIDINE (106)[203]

In a 250 mL round-bottomed flask equipped with magnetic stirring, the phosphonium salt $Ph_3PCH_2(COMe)Cl$ (12.50 g, 35.1 mmol) was added and the flask was purged with Ar. Then, anhydrous commercial THF (67 mL) was added via syringe and the reaction vas cooled to -78 ºC. Next, KHDMS (44 mL of a 1 M solution in THF, 44.0 mmol) was added dropwise and the mixture was stirred for 30 minutes at -78 ºC and for 30 additional minutes at 0 ºC, bringing about a reaction color change from yellow to orange, indicative of the ylide formation. At this point a solution of *N*-Boc-(*S*)-prolinal **105** (3.49 g, 17.6 mmol) in anhydrous commercial THF (60 mL) was added dropwise, and the reaction mixture was stirred for two additional hours at 0 ºC and, subsequently, overnight at room temperature. The reaction was quenched by the addition of 30 mL of $H_2O$ and extracted with 30 mL of diethyl ether. The organic layer was cooled down to -30 ºC for 10 min, to eliminate the phosphine oxide formed, and the supernatant solution was decanted. Then, this organic layer was concentrated under vacuum and the residue was purified by flash column chromatography (Hexane/AcOEt (7/3)) to afford the pyrrolidine **106** as a yellowish oil (3.20 g, 80% yield).

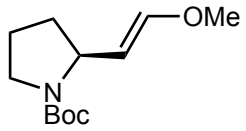


**$^1$H-NMR** ($CDCl_3$, 400 MHz): $\delta$ = 6.40 (d, *J* = 12.2 Hz, 1H =C**H**–OMe), 4.64 (m, 1H C**H**=CH–OMe), 3.51 (s, 3H OC**H$_3$**), 2.08-1.98 (m, 2H), 1.92-1.76 (m, 3H), 1.69-1.64 (m, 2H), 1.45 (s, 9H) ppm.

### *N*-BOC-(*S*)-HOMOPROLINAL (107)[203]

The pyrrolidine **106** (3.20 g, 14.0 mmol) was dissolved in acetone (33 mL) in a round-bottomed flask. Then, 2 M aqueous HCl (13 mL) was added and the mixture was stirred at room temperature for 40 minutes. At this point, to quench the reaction, aqueous saturated $NaHCO_3$ was added dropwise until no bubbling was observed, and the resulting aqueous solution was extracted with 2 x 20 mL of diethyl ether. The combined organic layers were dried with anhydrous $Na_2SO_4$ and concentrated under vacuum. The crude product was purified by flash column chromatography (hexane/AcOEt 7% v/v) to obtain the desired aldehyde **107** as a yellowish oil (0.923 g, 31% yield).

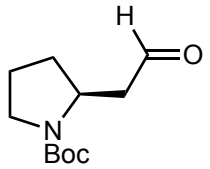


**$^1$H-NMR** ($CDCl_3$, 400 MHz): $\delta$ = 9.78 (t, *J* = 2.1 Hz, 1H C**H**=O), 4.29 (m, 1H C**H**–N), 3.40-3.32 (m, 3H), 2.87 (m, 1H), 2.47 (dd, *J* = 14.4 Hz, *J'* = 7.2 Hz, 1H), 2.15-2.08 (m, 1H), 1.85 (quint, *J* = 7.2 Hz, 2H), 1.46 (s, 9H) ppm.

## *TERT*-BUTYL-(*S*)-2-((10, 15, 20-TRIPHENYLPORPHYRIN-5-YL) METHYL) PYRROLIDINE-1-CARBOXYLATE (108)[54]

In a 2 L three-necked, round-bottomed flask equipped with magnetic stirring and a Dimroth condenser, commercial non-distilled DCM (1 L) was added, and the system was purged with Ar. *N*-Boc-(*S*)-homoprolinal **107** (496 mg, 2.3 mmol), benzaldehyde (714 μL, 7.0 mmol) and freshly distilled pyrrole (647 μL, 9.3 mmol) were then added sequentially. After 5 min stirring, $BF_3{\cdot}Et_2O$ (118 μL, 0.9 mmol) was added, and the reaction flask was covered with black paper and left stirring for 3h at room temperature. After this time, *p*-chloranil (1.72 g, 7.0 mmol) was added in one portion and the stirred mixture was heated to reflux for 1h. After cooling to room temperature, the reaction mixture was concentrated under vacuum until approximately 100 mL of solvent were remaining in the flask. The crude mixture of porphyrins was purified by two consecutive flash column chromatographies. In the first one, using DCM as the eluent, the less polar TPP was separated from the mixture of substituted porphyrins, that was submitted to a second chromatographic purification eluting with a mixture of hexane/DCM (1/4) to afford the desired monosubstituted porphyrin as a purple solid (0.543 g, 73% of the maximum statistical yield).

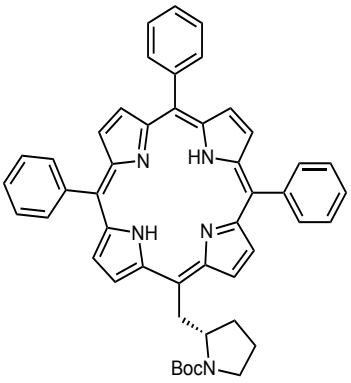


**$^1$H-NMR** ($CDCl_3$, 400 MHz): $\delta$ = 9.87 (m, 1H), 9.64 (m, 1H), 8.96 (d, *J* = 7.6 Hz, 2H), 8.80 (s, 4H), 8.20-8.17 (m, 6H), 7.77-7.73 (m, 9H), 5.78-5.75 (m, 1H), 5.62-5.58 (m, 1H), 5.02 (m, 1H), 4.83-4.74 (m, 1H), 3.84-3.79 (m, 1H), 3.72-3.59 (m, 1H), 3.51-3.41 (m, 1H), 2.37-2.17 (m, 1H), 1.93-1.82 (m, 2H), 1.64 (s, 9H), -2.75 (bs, 2H) ppm. **$^{13}$C-NMR** ($CDCl_3$, 400 MHz) $\delta$ = 155.12, 143.14, 142.53, 142.13, 134.72, 127.83, 126.88, 126.78, 119.87, 118.99, 116.32, 115.79, 80.56, 79.52, 63.42, 62.77, 47.28, 38.86, 38.02, 29.89, 28.98, 23.71, 22.87. **HRMS** ($ESI^+$) *m/z*: calculated for $C_{48}H_{44}N_5O_2$ $[M+H]^+$, 722.3495; found 722.3489. **UV-Vis** [$CH_2Cl_2$, $\lambda_{max}$ nm ($\varepsilon$), c = 3.43 x $10^{-5}$ M]: 417 (400000), 516 (14600), 551 (7000), 591 (4500), 647 (3800).

**SODIUM (*S*)-4,4',4''-(20-(PYRROLIDIN-2-YLMETHYL) PORPHYRIN-5,10,15-TRIYL) TRIBENZENESULFONATE (44)[54]**

The procedure described above for the obtention of sodium 4,4',4'',4'''-(porphyrin-5,10,15,20-tetrayl)tetrabenzenesulfonate **62** was followed, affording the desired porphyrin as a purple solid. Starting from 170 mg (0.23 mmol) of *tert*-butyl-(*S*)-2-((10,15,20-triphenylporphyrin-5-yl)methyl pyrrolidine-1-carboxylate **108**, 178 mg (0.19 mmol) of the desired porphyrin were obtained with an 82% yield.

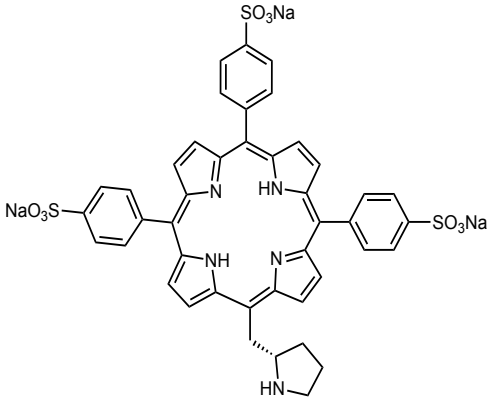


**$^1$H-NMR** (DMSO-$d_6$, 400 MHz): $\delta$ = 9.85 (br, 1H), 9.63 (br, 1H), 8.90 (m, 2H), 8.80 (s, 4H), 8.19 (m, 6H), 7.75 (m, 6H), 4.23 (s, 1H), 3.34 (m, 3H), 3.00-2.80 (dd, 1H), 2.50-2.40 (dd, 1H), 2.11 (m, 1H) 1.90-1.80 (m, 2H), 1.65 (m, 2H), -2.96 (bs, 2H) ppm. **HRMS** (ESI$^-$) *m/z*: calculated for $C_{43}H_{32}N_5O_9S_3^{-3}$ [M-3Na]$^{-3}$/3, 286.0454; found 286.0454.

## 7.4. SYNTHESIS OF IMIDAZOLIDINONES 16a-e

**L-PHENYLALANINE METHYL ESTER HYDROCHLORIDE (27)[171]**

In a 100 mL round-bottomed flask, equipped with magnetic stirring, 25 mL of absolute MeOH were introduced and cooled down to -10 ºC (salt water/ice bath). At this point, $SOCl_2$ (7 mL, 96 mmol) was added via syringe and the reaction mixture was stirred for 10 min at the same temperature. Then, L-phenylalanine (1.65 g, 10.0 mmol) was added, and the solution was stirred for 40 additional minutes at -10 ºC and 48 h at room temperature. Next, the reaction mixture was concentrated under reduced pressure, 15 mL of MeOH were added to the residue, and the resulting solution was concentrated under reduced pressure. Addition of MeOH (15 mL) and concentration under vacuum were repeated, 50 mL of diethyl ether were added, and the resulting precipitate was filtered and recrystallized from MeOH/$Et_2O$ to afford the methyl ester hydrochloride as a colorless solid (1.97 g, 88% yield), that was subsequently used without further purification.

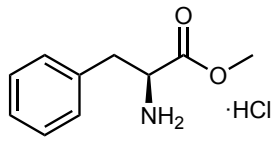


**L-*TERT*-LEUCINE METHYL ESTER HYDROCHLORIDE (28)[116]**

In a 25 mL round-bottomed flask, equipped with magnetic stirring and a Dimroth reflux condenser, L-*tert*-leucine (760 mg, 5.9 mmol) was dissolved in absolute MeOH (6 mL) and the reaction was cooled down to -10 ºC (salt water/ice bath). At this point, $SOCl_2$ (0.90 mL, 12.4 mmol) was added dropwise, and the mixture was stirred for 10 min at -10 ºC and for 6 h under reflux. After this time, the mixture was allowed to cool down to room temperature and concentrated under reduced pressure to give a solid, that was mixed with 10 mL of toluene and again removed under reduced pressure in order to remove traces of water that could remain in the reaction crude. This process was repeated three times before drying the crude product under vacuum overnight to afford the methyl ester hydrochloride (1.03 g, quantitative yield) as a yellowish solid, that was subsequently used without further purification.

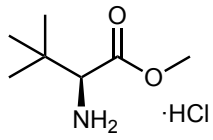


**GENERAL PROCEDURE FOR THE OBTENTION OF *N*-METHYL-α-AMINOAMIDE HYDROCHLORIDES[170]**

In a 10 mL round-bottomed flask, equipped with magnetic stirring, the suitable α-aminoacid methyl esther hydrochloride was added to an aqueous solution of methylamine (2.0 mL, 40 wt. %, 23.1 mmol) and the resulting mixture was stirred at room temperature for 20 h. Then, absolute ethanol (20 mL) was added, and the solution was concentrated under reduced pressure. This process was repeated three times in order to remove the excess of methylamine and water. Finally in order to remove traces of water that could remain in the crude, the solid was mixed with toluene and evaporated under vacuum, affording the corresponding methylamide hydrochloride as a colorless solid, that was subsequently used without further purification.

## L-ALANINE METHYLAMIDE HYDROCHLORIDE (19)

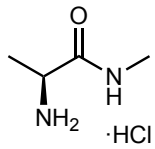

Commercial L-alanine methyl ester hydrochloride (16.2 mmol) was used in the reaction. White solid, 1.97 g, 88% yield.

## L-PHENYLALANINE METHYLAMIDE HYDROCHLORIDE (20)

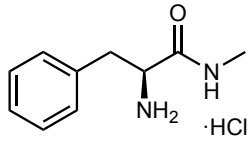

Yellowish solid, 1.30 g, quantitative yield (from 5.80 mmols of **27**).

## GLYCINE METHYLAMIDE HYDROCHLORIDE (21)

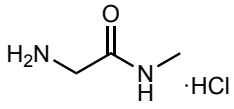

Commercial glycine methyl esther hydrochloride (12.0 mmol) was used in the reaction. Colorless solid, 1.62 g, quantitative yield.

## L-*TERT*-LEUCINE METHYLAMIDE HYDROCHLORIDE (22)[116]

In a thick-wall glass reaction tube equipped with magnetic stirring and a screw top, L-*tert*-leucine methyl ester hydrochloride **28** (1.03 g, 5.7 mmol) was added to a solution of methylamine in EtOH (7.00 mL, 33% wt. , 54.5 mmol). Then, the reaction tube was tightly sealed, and heated up to 100 ºC for 48 h, and subsequently stirred for 3 days at room temperature. At this point, the solution was transferred to a round-bottomed flask and concentrated under reduced pressure to afford the desired methylamide hydrochloride as a yellowish solid (1.00 g, quantitative yield), that was not characterized and was used without further purification in subsequent reactions.

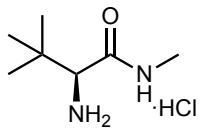

## GENERAL PROCEDURE FOR THE OBTENTION OF *N*-METHYL-α-AMINOAMIDES[170]

In a 10 mL round-bottomed flask, equipped with magnetic stirring and a Dimroth reflux condenser, the suitable α-aminoacid methylamide hydrochloride was added to a 1 M solution of NaOH in EtOH (3 mL) and heated up to reflux for 2 min. Then, a digestion of the crude was carried out with EtOAc to insolubilize the formed NaCl. At this point, the suspension was filtered through a cotton plug in a Pasteur pipette and evaporated *in vacuo* to afford the desired α-aminoacid methylamide, that was not characterized and was directly used in the next reaction without further purification.

### L-ALANINE METHYLAMIDE (23)

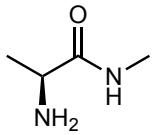

Pale orange solid, 408 mg, quantitative yield (from 1.80 mmol of hydrochloride **19**)

### L-PHENYLALANINE METHYLAMIDE (24)

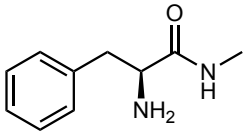

Yellowish oil, 370 mg, quantitative yield (from 2.27 mmol of hydrochloride **20**).

### GLYCINE METHYLAMIDE (25)

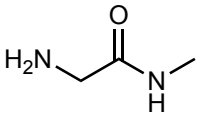

Colorless oil, 190 mg, 53% yield (from 4.02 mmol of hydrochloride **21**).

### L-*TERT*-LEUCINE METHYLAMIDE (26)[116]

In a 10 mL round-bottomed flask, equipped with a magnetic stirrer, L-*tert*-leucine methylamide hydrochloride **22** (285 mg, 1.6 mmol) was dissolved in a mixture of water (3 mL) and concentrated $NH_3$ (0.15 mL, 2.5 mmol). Once the solid was completely dissolved, the solution was extracted with

a 20 % mixture of 2-propanol in DCM (5 x 20 mL). Then, the organic phase was dried over $MgSO_4$ and concentrated under reduced pressure to give a solid, that was mixed with 10 mL of toluene and again evaporated under reduced pressure in order to remove traces of water that could remain in the reaction crude. This process was repeated three times before drying the crude reaction product to afford an orange solid (123 mg, 54% yield), that was not characterized and was directly used in next reaction without further purification.

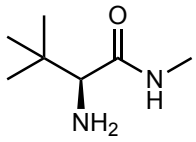

**PREPARATION OF (*S*)-2,2,3,5-TETRAMETHYLIMIDAZOLIDIN-4-ONE (16a)[204]**

A 10 mL round-bottomed flask, equipped with magnetic stirring and containing a solution of L-alanine methylamide **23** (200 mg, 2.0 mmol) in anhydrous MeOH (6 mL), was purged with Ar. Then, acetone (0.75 mL, 10.2 mmol) was added and the mixture was heated up to reflux overnight. At this point, the reaction was allowed to cool down to room temperature and concentrated under reduced pressure to afford the desired product (220 mg, 79% yield) as an off-white solid.

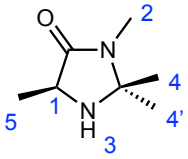

**$^1$H-NMR** ($CDCl_3$, 400 MHz): $\delta$ = 3.67 (q, *J* = 6.9 Hz, $1H_1$), 2.80 (s, $3H_2$), 2.06 (br, $1H_3$), 1.51 (s, $3H_{4/4'}$), 1.43 (d, *J* = 6.9 Hz, $3H_5$), 1.39 (s, $3H_{4'/4}$) ppm.

**PREPARATION OF (*S*)-5-BENZYL-2,2,3-TRIMETHYLIMIDAZOLIDIN-4-ONE (16b)[204]**

A 10 mL round-bottomed flask, equipped with magnetic stirring and containing a solution of L-phenylalanine methylamide **24** (160 mg, 0.9 mmol) in anhydrous MeOH (4.8 mL), was purged with Ar. Then, acetone (0.35 mL, 4.70 mmol) was added and the mixture was heated up to reflux overnight. At this point, the reaction was allowed to cool down to room temperature and concentrated under reduced pressure to afford the desired product (189 mg, 90% yield) as a yellowish oil.

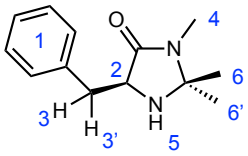

**$^1$H-NMR** ($CDCl_3$, 400 MHz): δ = 7.26 (m, $5H_1$), 3.80 (dd, *J* = 6.9 Hz, *J'* = 4.7 Hz, $1H_2$), 3.15 (dd, *J* = 14.1 Hz, *J'* = 4.7 Hz, $1H_3$), 3.01 (dd, *J* = 14.1 Hz, *J'* = 6.9 Hz, $1H_{3'}$), 2.76 (s, $3H_4$), 1.78 (br, $1H_5$), 1.26 (s, $3H_6$), 1.16 (s, $3H_{6'}$) ppm.

## PREPARATION OF 2,2.3-TRIMETHYLIMIDAZOLIN-4-ONE (16c)[205]

In a 10 mL round-bottomed flask, equipped with magnetic stirring, containing activated molecular sieves (0.8 g, 4 Å) and glycine methylamide hydrochloride **21** (508 mg, 4.1 mmol), acetone (1.50 mL, 20.2 mmol) and $NEt_3$ (0.60 mL, 4.3 mmol) were added, and the resulting mixture was heated up to reflux for 3h. Then, the reaction mixture was treated with 3 mL of AcOEt and 0.1 mL of $NEt_3$. The resulting suspension was filtered, and the filtrates were concentrated under reduced pressure to afford the desired imidazolidinone (0.385 g, 75% yield) as an orange oil.

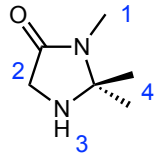

**$^1$H-NMR** ($CDCl_3$, 400 MHz): δ = 3.47 (s, $3H_1$), 2.79 (s, $2H_2$), 1.78 (br, $1H_3$) 1.37 (s, $6H_4$) ppm.

## PREPARATION OF *rac*-2-(*TERT*-BUTYL)-3-METHYLIMIDAZOLIDIN-4-ONE (16d)[170]

In a 25 mL round-bottomed flask, equipped with magnetic stirring and Dimroth reflux condenser, containing glycine methylamide **25** (160 mg, 1.8 mmol), dry $CHCl_3$ (15 mL) was added. Once the amide was completely dissolved, pivaldehyde (395 μL, 313 mg, 3.6 mmol) and $(CF_3SO_2)_3Yb$ (10 mg, 0.016 mmol, 10 mol%) were added sequentially, and the mixture was heated up to reflux for 8h. After cooling to room temperature, the solvent was evaporated under reduced pressure and the crude product was purified via flash column chromatography through silica gel, using AcOEt/MeOH 2% v/v as eluent, to afford the desired imidazolidinone (0.221 g, 78% yield) as a yellowish oil.

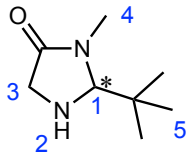

**$^1$H-NMR** ($DMSO\text{-}d_6$, 400 MHz): δ = 4.04 (s, $1H_1$), 3.36 (br, $1H_2$), 3.20 (s, $2H_3$), 2.81 (s, $3H_4$), 0.88 (s, $9H_5$) ppm.

**PREPARATION OF (2*S*,5*S*)-5-BENZYL-2-*TERT*-BUTYL-3-METHYLIMIDAZOLIN-4-ONE (16e)[116]**

In a 50 mL round-bottomed flask, equipped with magnetic stirring and Dimroth reflux condenser, and containing L-phenylalanine methylamide **24** (1.05 g, 5.6 mmol), $CHCl_3$ (15 mL) was added. Once the oil was completely dissolved, pivaldehyde (1.30 mL, 1.03 g, 12 mmol) and $(CF_3SO_2)_3Yb$ (72 mg, 0.12 mmol, 20 mol%) were added sequentially, and the mixture was heated up to reflux overnight. After cooling to room temperature, the reaction mixture was evaporated under reduced pressure and the residue was purified via flash column chromatography through silica gel, using hexane/AcOEt (1/3) as eluent, to afford the desired product (157 mg, 15% yield) as a colorless solid.

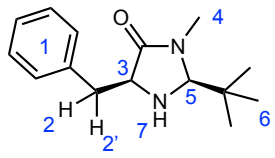


**$^1$H-NMR** ($CDCl_3$, 400 MHz): $\delta$ = 7.29-7.13 (m, $5H_1$), 4.02 (s, $1H_5$), 3.67 (dd, $J$ = 7.4 Hz, $J'$ = 3.6 Hz, $1H_3$), 3.12 (dd, $J$ = 13.3 Hz, $J'$ = 3.6 Hz, $1H_2$), 2.93 (dd, $J$ = 13.3 Hz, $J'$ = 7.4 Hz, $1H_{2'}$), 2.88 (s, $3H_4$), 2.01 (br, $1H_7$), 0.80 (s, $9H_6$) ppm.

## 7.5. SYNTHESIS OF PORPHYRIN-DERIVED IMIDAZOLIDINONES

**PREPARATION OF COPPER (II) *MESO*-TETRAPHENYL PORPHYRIN (37)[159]**

In a 250 mL round-bottomed flask, equipped with magnetic stirring and a Dimroth reflux condenser, 5,10,15,10-tetraphenyl porphyrin **36** (450 mg, 0.7 mmol) was dissolved in DCM (60 mL). Once all the solid was dissolved, MeOH (20 mL) and $Cu(OAc)_2 \cdot H_2O$ (243 mg, 1.2 mmol) were added and the reaction mixture was heated up to reflux and stirred for 2 h until all the starting material was consumed (one spot in TLC, Hexane/DCM (1/1)). Then, the solvent was removed by distillation under reduced pressure, the residue was redissolved in the minimum amount of DCM and filtered through a short plug of silica gel using DCM as eluent. After filtration, the solvents were evaporated under reduced pressure to afford the desired compound as a purple solid (432 mg, 97% yield), that was not characterized.

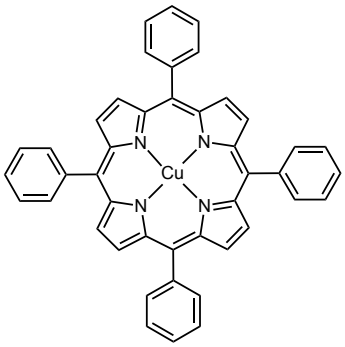


**PREPARATION OF COPPER(II) 2-FORMYL-5,10,15,20-TETRAPHENYL PORPHYRIN (38)[41]**

In a 500 mL round-bottomed flask, equipped with magnetic stirring and a Liebig reflux condenser, under Ar atmosphere, dry *N,N*-dimethylformamide (11.1 mL, 154 mmol) was added and cooled down in an ice-water bath. Then, phosphorous oxychloride (8.5 mL, 91.8 mmol) was added slowly, showing the formation of the Vilsmeier-Haack complex as a viscous golden mixture. In another 500 mL round-bottomed flask, equipped with magnetic stirring, copper(II) *meso*-tetraphenyl porphyrin **37** (1.37 g, 2.0 mmol) was added, and was purged with Ar. At this point, dry 1,2-dichloroethane (210 mL) was added and the resulting suspension was stirred in an ice-water bath until no solid was remaining. Then, the porphyrin solution was added via cannula to the Vilsmeier-Haack complex and the resulting mixture was heated up to reflux for 7 h and stirred overnight at room temperature. The reaction mixture was poured into an aqueous solution of NaOAc (105 g in 500 mL) and stirred for 10 min. After this time, the green two-phase mixture was transferred to a separatory funnel and extracted with an aqueous solution of NaOH (36 g in 1.25 L) until no green color was observed. Then, the aqueous phase was extracted with $CHCl_3$ (3 x 200 mL) and the combined organic layers were washed with an aqueous saturated solution of $NaHCO_3$ (2 x 500 mL), dried over anhydrous $MgSO_4$ and evaporated under reduced pressure. The residue was redissolved in the minimum amount of DCM and filtered through a short plug of silica gel using DCM as eluent, to afford the desired product (1.60 g, quantitative yield) as a purple solid, that was not characterized.

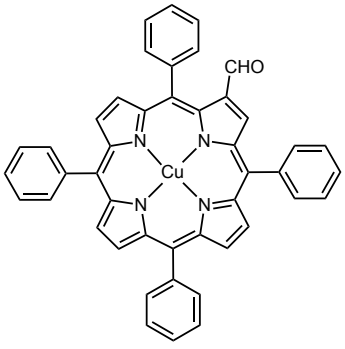

**PREPARATION OF METHYL 4-(10,15,20-TRIPHENYLPORPHYRIN-5-YL) BENZOATE (32)[173]**

In a 500 mL round-bottomed flask, equipped with magnetic stirring and a Liebig reflux condenser, a mixture of AcOH (glacial, 200 mL) and nitrobenzene (150 mL) was heated up to reflux, and methyl 4-formylbenzoate (1.44 g, 8.8 mmol) was added in one portion. When all the solid was dissolved, benzaldehyde (2.25 mL, 21.9 mmol) and freshly distilled pyrrole (2.00 mL, 29.4 mmol) were added, and the mixture was stirred at reflux for 1h. At this point, the solvents were distilled *in vacuo* and the remaining purple paste was purified via flash column chromatography using Hexane/DCM (7/3) as eluent, to afford the desired porphyrin (781 mg, 29% yield) as a purple solid.

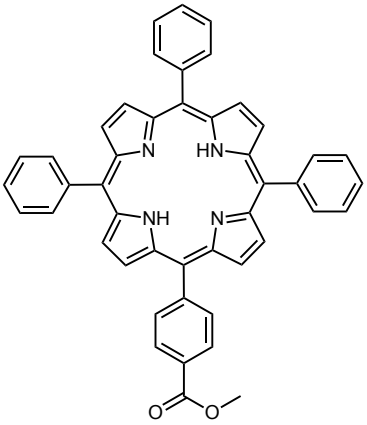


**$^1$H-NMR** (CDCl3, 400 MHz): $\delta$ = 8.87-8.78 (m, 8H), 8.42 (d, *J* = 8.9 Hz, 2H), 8.29 (d, *J* = 8.9 Hz, 2H), 8.22-8.20 (d, *J* = 7.4Hz, 6H), 7.79-7.72 (m, 9H), 4.10 (s, 3H), -2.77 (br, 2H N**H**) ppm.

**PREPARATION OF (4-(10,15,20-TRIPHENYLPORPHYRIN-5-YL)PHENYL) METHANOL (33)[147]**

In a 500 mL round-bottomed flask, equipped with magnetic stirring, $LiAlH_4$ (296 mg, 7.8 mmol) was added and the system was purged with Ar. Then, dry THF (6.1 mL) was added and, subsequently, a solution of methyl 4-(10,15,20-triphenylporphyrin-5-yl) benzoate **32** (1.32 g, 1.9 mmol) in dry THF (155 mL) was added via syringe. The reaction mixture was stirred at room temperature for 1 h. At this point, the reaction was quenched with HCl 1% (211 mL) and the resulting green solution was transferred to a separatory funnel and extracted with DCM until the aqueous phase became colorless. The combined organic layers were treated with a 32% w/w aqueous solution of $NH_3$ noticing the changing of color from green to purple, and the aqueous phase was extracted with DCM (3 x 50 mL). The combined organic layers were dried over $NaSO_4$ and concentrated under reduced pressure to give a purple solid, that was purified via flash column chromatography, using hexane/DCM (1/1) as eluent. The desired porphyrin (1.19 g, 95% yield) was obtained as a purple solid.

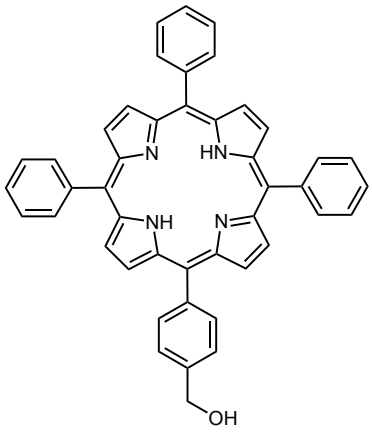


**$^1$H-NMR** (CDCl3, 400 MHz): $\delta$ = 8.85 (s, 8H), 8.82 (d, *J* = 8.0 Hz, 8H), 7.78-7.73 (m, 11H), 5.30 (s, 2H), -2.77 (br, 2H N**H**) ppm.

**PREPARATION OF 4-(10,15,20-TRIPHENYLPORPHYRIN-5-YL) BENZALDEHYDE (34)[172]**

In a 500 mL round-bottomed flask equipped with magnetic stirring, (4-(10,15,20-triphenylporphyrin-5-yl)phenyl) methanol **33** (395 mg, 0.60 mmol) was dissolved in freshly distilled DCM (255 mL). Then, pyridinium chlorochromate (395 mg, 1.8 mmol) was added, noticing a change of color from purple to dark green, and the reaction was stirred for 1h at room temperature. At this point, silica gel (60 mL) was added to the reaction crude and the solvent was evaporated under reduced pressure. The resulting dark grey solid, was purified via flash column chromatography, using DCM as eluent, to afford the desired product (390 mg, quantitative yield) as a purple solid

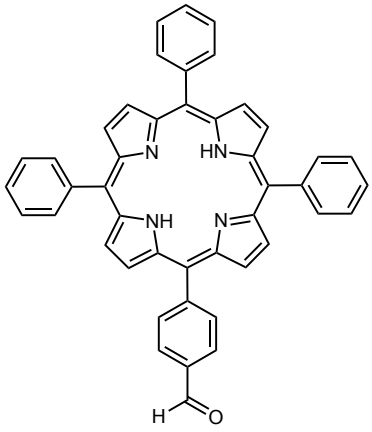


**$^1$H-NMR** ($CDCl_3$, 400 MHz): $\delta$ = 10.39 (s, 1H, C**H**=O), 8.88 (AB system (part A), *J* = 4.8 Hz, 2H), 8.85 (s, 4H), 8.79 (AB system (part B), *J* = 4.8 Hz, 2H) 8.42 (d, *J* = 7.8 Hz, 2H), 8.29 (d, *J* = 7.8 Hz, 2H), 8.22 (d, *J* = 6.4 Hz, 6H), 7.82-7.73 (m, 9H), -2.77 (br, 2H N**H**) ppm.

**PREPARATION OF COPPER (II) 4-(10,15,20-TRIPHENYLPORPHYRIN-5-YL) BENZALDEHYDE (35)[172]**

In a 50 mL round-bottomed flask, equipped with magnetic stirring and a Dimroth reflux condenser, 4-(10,15,20-triphenylporphyrin-5-yl)benzaldehyde **34** (140 mg, 0.22 mmol) was dissolved in DCM (11 mL). Then, MeOH (4 mL) and $Cu(OAc)_2 \cdot H_2O$ (79 mg, 0.39 mmol) were added

and the resulting solution was heated up to reflux for 2 h. After this time, the solvents were evaporated under reduced pressure; the residue was redissolved in the minimum amount of DCM and filtered through a short plug of silica gel using DCM as eluent, to afford the desired product (151 mg, quantitative yield) as a purple solid.

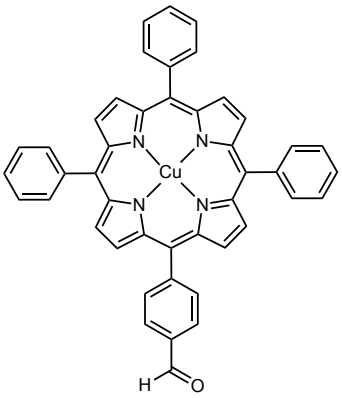

**UV-Vis** [$CH_2Cl_2$, $\lambda_{max}$ nm ($\varepsilon$), c = 4.59 x $10^{-5}$ M]: 412 (479894), 537 (15831)

**PREPARATION OF COPPER (II) (5*S*)-3,5-DIMETHYL-2-(4-(10,15,20-TRIPHENYLPORPHYRIN-5-YL)PHENYL)IMIDAZOLIDIN-4-ONE (39)[121]**

In a 25 mL round-bottomed flask, equipped with magnetic stirring and a Dimroth reflux condenser, L-alanine methylamide **24** (30 mg, 0.22 mmol) was introduced. Then, a solution of copper(II) 4-(10,15,20-triphenylporphyrin-5-yl)benzaldehyde **35** (81 mg, 0.11 mmol) in $CHCl_3$ (6 mL) and $Yb(SO_3CF_3)_3$ (0.62 mg, 1 mol%) were added sequentially. The stirred mixture was heated up to reflux for 24 h. After cooling to room temperature, the solvent was evaporated under reduced pressure and the residue was purified via flash column chromatography through $Et_3N$-pretreated silica gel (2.5% v/v $NEt_3$) using mixtures of DCM/MeOH (from 1% v/v to 5% v/v) as eluents. The fast-running red band containing unreacted starting material was not collected. Compound **39** (40 mg, 46% yield) was obtained as a diastereomeric mixture (two spots in TLC, DCM/MeOH 0.5%), that was not characterized.

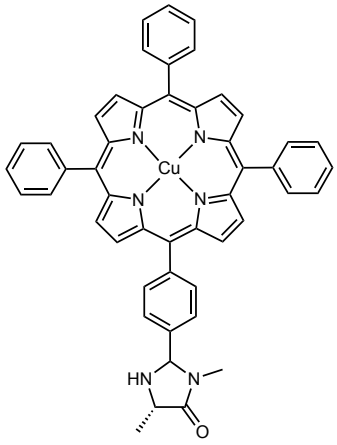

**PREPARATION OF (5*S*)-3,5-DIMETHYL-2-(4-(10,15,20-TRIPHENYLPORPHYRIN-5-YL)PHENYL)IMIDAZOLIDIN-4-ONE (17a)**

In a 25 mL round-bottomed flask, equipped with magnetic stirring, 40 mg (0.05 mmol) of metalated porphyrin **39** were dissolved in DCM (5 mL). $H_2SO_4$ (0.7 mL, 98%) was added and the resulting green mixture was vigorously stirred for 3 min. Then, the two-phase mixture was poured over a cold aqueous NaOH solution (1 g in 340 mL), transferred to a separatory funnel and shaken until no green color was observed in the organic layer. The aqueous phase was extracted with DCM (3 x 50 mL) and the combined organic layers were washed with an aqueous saturated solution of $NaHCO_3$ (2 x 100 mL), dried over $Na_2SO_4$ and the solvent was evaporated under reduced pressure. Finally, the obtained crude product was purified via flash column chromatography through $Et_3N$-pretreated silica gel (2.5% $NEt_3$) using DCM/MeOH 2% as eluent, affording a complex diastereomeric mixture that could not be separated. The purple solid (10 mg, 27% yield) obtained was not characterized.

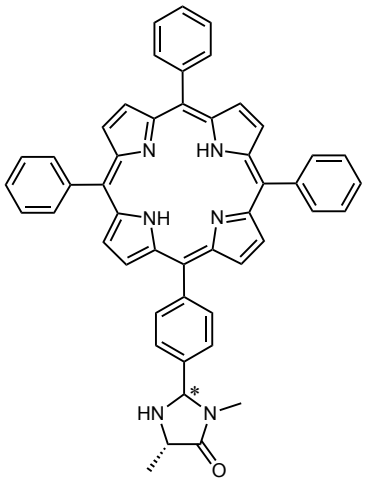


**PREPARATION OF COPPER(II) (5*S*)-5-BENZYL-3-METHYL-2-(5,10,15,20-TETRAPHENYL PORPHYRIN-2-YL)IMIDAZOLIDIN-4-ONE (41)[121]**

In a 25 mL round-bottomed flask, equipped with magnetic stirring and a Dimroth reflux condenser, L-phenylalanine methylamide **24** (198 mg, 1.11 mmol) was introduced. Then, a solution of copper(II) 2-formyl-5,10,15,20-tetraphenyl porphyrin **34** (960 mg, 1.36 mmol) in $CHCl_3$ (12 mL) and $Yb(SO_3CF_3)_3$ (6.0 mg, 0.010 mmol, 1 mol%) were added sequentially. The stirred mixture was heated up to reflux for 24 h. After cooling to room temperature, the solvent was evaporated under reduced pressure and purified via flash column chromatography through $Et_3N$-pretreated silica gel

(2.5% v/v $NEt_3$) using a mixture of DCM/MeOH 0.5% v/v as eluent. The fast-running red band containing unreacted starting material was not collected. Compound **41** (purple solid, 481 mg, 50% yield ) was obtained as a diastereomeric mixture (two spots in TLC, DCM/MeOH 0.5%), that was not characterized.

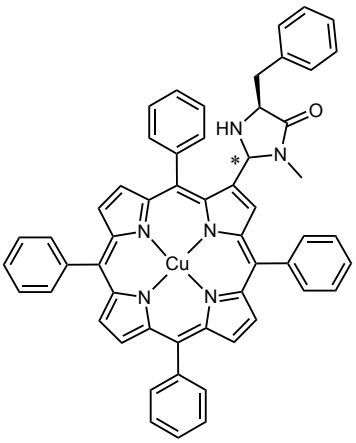


**PREPARATION OF (2*S*,5*S*)-5-BENZYL-3-METHYL-2-(5,10,15,20-TETRAPHENYL PORPHYRIN-2-YL)IMIDAZOLIDIN-4-ONE (17b-*cis*) AND (2*S*,5*S*)-5-BENZYL-3-METHYL-2-(5,10,15,20-TETRAPHENYL PORPHYRIN-2-YL)IMIDAZOLIDIN-4-ONE (17b-*trans*)**

In a 50 mL round-bottomed flask, equipped with magnetic stirring, 312 mg (0.36 mmol) of metalated porphyrin **41** were dissolved in DCM (20 mL). Concentrated $H_2SO_4$ (5 mL, 98%) was added and the resulting green mixture was vigorously stirred for 4 min. Then, the two-phase mixture was poured over an ice-cold aqueous NaOH solution (9 g in 300 mL), transferred to a separatory funnel, and shaken until no green color was observed. The aqueous phase was extracted with DCM (3 x 100 mL) and the combined organic layers were washed with an aqueous saturated solution of $NaHCO_3$ (2 x 100 mL) and dried over $MgSO_4$. The solvent was evaporated under reduced pressure to afford the crude product was purified via flash column chromatography through $Et_3N$-pretreated silica gel (2.5% v/v $NEt_3$) using DCM/MeOH 2% as eluent. In this way, the pure *cis* (purple solid, 82 mg, 18% yield) and *trans* (purple solid, 116 mg, 26% yield.) isomers of **17b** could be isolated.

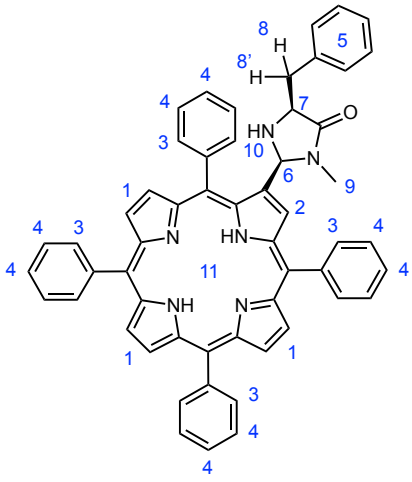

**17b-*cis***. **$^{1}$H-NMR** ($CDCl_3$, 400 MHz): $\delta$ = 8.81 (m, $3H_1$), 8.77 (d, $J$ = 4.8 Hz, $2H_1$), 8.65 (d, $J$ = 4.8 Hz, $1H_1$), 8.61 (s, $1H_2$), 8.26 (d, $J$ = 7.4 Hz, $1H_3$), 8.18 (d, $J$ = 6.4 Hz, $4H_3$), 8.13 (m, $2H_3$), 8.10 (d, $J$ = 7.4 Hz, $1H_3$), 7.81-7.69 (m, $11H_4$), 7.68 (dd, $J$ = 7.6 Hz, $J'$ = 1.3 Hz, $1H_4$), 7.33-7.19 (m, $5H_5$), 5.34 (s, $1H_6$), 3.93 (dd, $J$ = 9.1 Hz, $J'$ = 3.6 Hz, $1H_7$), 3.08 (dd, $J$ = 14.0 Hz, $J'$ = 3.6 Hz, $1H_8$), 2.78 (dd, $J$ = 14.0 Hz, $J'$ = 9.1 Hz, $1H_{8'}$), 2.74 (s, $3H_9$), 2.16 (br, $1H_{10}$), -2.73 (br, $2H_{11}$) ppm. **$^{13}$C-NMR** ($CDCl_3$, 400 MHz): $\delta$ = 174.6, 142.2, 142.1, 142.0, 141.9, 141.82, 142.76, 138.2, 134.8 (2C), 134.73 (4C), 134.67 (3C), 134.6, 134.57, 133.6, 129.6 (2C), 128.9, 128.7, 128.6, 128.4, 128.04, 127.96 (2C), 126.95 (5C), 126.9 (3C), 126.8, 126.7 (2C), 120.7, 120.6, 120.5, 119.4 77.4, 77.3, 77.0, 76.6, 71.5, 59.6, 58.2, 37.2, 29.9, 28.2, 8.2 ppm. **HRMS (ESI)**: *m/z* calculated for $C_{55}H_{43}N_6O$ $[M+H]^+$, 803.3493; found 803.3468. **UV-Vis** [$\lambda_{max}$ nm ($\varepsilon$), c = 2.810 x $10^{-6}$ M, $CH_2Cl_2$]: 421 (178091), 451 (173314), 517 (202137), 552 (80789), 593 (63249), 650 (50866).

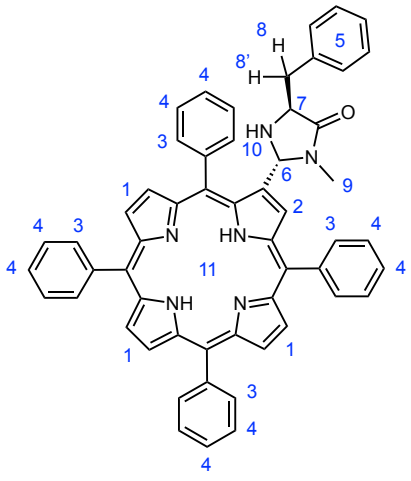

**17b-*trans***. **$^{1}$H-NMR** ($CDCl_3$, 400 MHz): $\delta$ = 8.82 (m, $3H_1$), 8.77 (d, $J$ = 4.7 Hz, $2H_1$), 8.67 (d, $J$ = 4.6 Hz, $1H_1$), 8.38 (s, $1H_2$), 8.32 (d, $J$ = 7.5 Hz, $1H_3$), 8.30-8.03 (m, $5H_3$), 8.01 (d, $J$ = 7.5 Hz, $2H_3$), 7.86-7.70 (m, $10H_4$), 7.67 (q, $J$ = 7.6 Hz, $2H_4$), 7.12-6.99 (m, $5H_5$), 5.08 (s, $1H_6$), 3.60 (t, $J$ = 5.6 Hz, $1H_7$), 3.11 (dd, $J$ = 5.4 Hz, $J'$ = 1.7 Hz, $2H_{8,8'}$), 2.73 (s, $3H_9$), 1.89 (bs, $1H_{10}$), -2.73 (bs, $2H_{11}$) ppm. **$^{13}$C-NMR** ($CDCl_3$, 400 MHz): $\delta$ = 174.1, 142.5, 142.2, 142.1, 141.94, 141.88, 139.5, 139.3, 134.9, 134.8 (2C), 134.72 (4C), 134.68 (2C), 134.63, 134.58, 134.5, 133.0, 132.5, 130.0, 129.2, 128.8, 128.7, 128.5, 128.3, 128.08, 128.05, 128.0, 127.1, 126.98 (4C), 126.96 (3C), 126.92 (2C), 126.86, 120.7, 118.5, 77.4, 77.3, 77.0, 76.7, 58.0, 42.8, 40.9, 29.8, 28.2, 27.9, 8.1 ppm. **HRMS (ESI):** *m/z* calculated for $C_{55}H_{43}N_6O$ $[M+H]^+$, 803.3493; found 803.3458. **UV-Vis** [$\lambda_{max}$ nm ($\varepsilon$), c = 1.338 x $10^{-6}$ M, $CH_2Cl_2$]: 422 (131748), 519 (171251), 553 (78959), 595 (63186), 655 (72072).

**PREPARATION OF COPPER (II) 3-METHYL-2-(5,10,15,20-TETRAPHENYLPORPHYRIN-7-YL)IMIDAZOLIDIN-4-ONE (42)[121]**

In a 25 mL round-bottomed flask, equipped with magnetic stirring and a Dimroth reflux condenser, glycine methylamide **25** (80 mg, 0.91 mmol) was introduced. Then, a solution of copper(II) 2-formyl-5,10,15,20-tetraphenyl porphyrin **34** (450 mg, 0.64 mmol) in $CHCl_3$ (5 mL), and $Yb(SO_3CF_3)_3$ (5.0 mg, 0.008 mmol, 1 mol%) were added sequentially. The stirred mixture was heated up to reflux for 24 h. After cooling to room temperature, the solvent was evaporated under reduced pressure and the residue was purified via flash column chromatography through $Et_3N$-pretreated silica gel (2.5% v/v $NEt_3$) using a mixture of DCM/MeOH 0.5% v/v as eluent. The fast-running red band containing unreacted starting material was not collected. Racemic compound **42** (282 mg, 57% yield) was obtained as a purple solid that was not characterized.

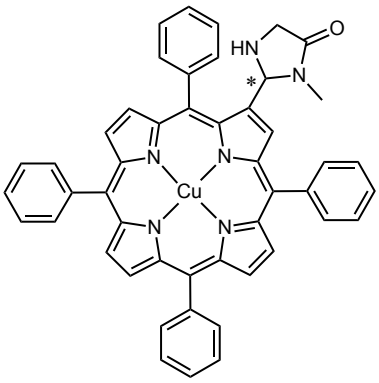


**PREPARATION OF 3-METHYL-2-(5,10,15,20-TETRAPHENYLPORPHYRIN-7-YL)IMIDAZOLIDIN-4-ONE (17c)**

In a 50 mL round-bottomed flask, equipped with magnetic stirring, 282 mg (0.36 mmol) of the copper porphyrin **42** were dissolved in DCM (20 mL). Concentrated $H_2SO_4$ (5 mL, 98%) was added and the resulting green mixture was vigorously stirred for 4 min. Then, the two-phase mixture was carefully poured into a cold aqueous NaOH solution (10 g in 300 mL), transferred into a separatory funnel, and shaken until no green color was observed. The aqueous phase was extracted with DCM (3 x 100 mL) and the combined organic layers were washed with an aqueous saturated solution of $NaHCO_3$ (2 x 100 mL), dried over $MgSO_4$ and the solvent was evaporated under reduced pressure. Finally, the obtained crude product was purified via flash column chromatography through $Et_3N$-pretreated silica gel (2.5% v/v $NEt_3$) using DCM/AcOEt (1/1) as eluent. Racemic compound **17c** (30 mg, 12% yield) was obtained as a purple solid.

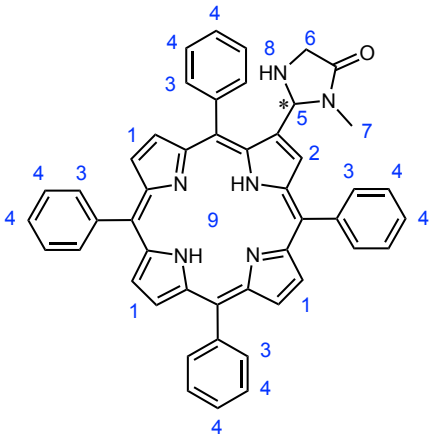

**$^1$H-NMR** ($CDCl_3$, 400 MHz): $\delta$ = 8.92-8.74 (m, $6H_1$), 8.71 (s, $1H_2$), 8.38 (d, *J* = 7.5 Hz, $1H_3$), 8.28-8.14 (m, $6H_3$), 8.11 (d, *J* = 7.5 Hz, $1H_3$), 7.85-7.65 (m, $12H_4$), 5.31 (s, $1H_5$), 3.67 (d, *J* = 16.4 Hz, $1H_6$), 3.39 (d, *J* = 16.4 Hz, $1H_6$), 2.78 (s, $3H_7$), 2.07 (br, $1H_8$), -2.67 (br, $2H_9$) ppm. **HRMS (ESI):** *m/z* calculated for $C_{48}H_{37}N_6O$ $[M+H]^+$, 713.3016; found 713.3023.

## PREPARATION OF COPPER (II)(5*S*)-5-(*TERT*-BUTYL)-3-METHYL-2-(5,10,15,20-TETRAPHENYLPORPHYRIN-2-YL)IMIDAZOLIDIN-4-ONE (43)[121]

In a 25 mL round-bottomed flask, equipped with magnetic stirring and a Dimroth reflux condenser, L-*tert*-leucine methylamide **26** (85 mg, 0.59 mmol) was introduced. Then, a solution of copper(II) 2-formyl-5,10,15,20-tetraphenyl porphyrin **38** (318 mg, 0.45 mmol) in $CHCl_3$ (4.4 mL), and $Yb(SO_3CF_3)_3$ (3.00 mg, 0.005 mmol, 1 mol%) were added sequentially. The stirred mixture was heated up to reflux for 24 h. After cooling to room temperature, the solvent was evaporated under reduced pressure and the residue was purified by flash column chromatography through $Et_3N$-pretreated silica gel (2.5% v/v $NEt_3$) using a mixture of DCM/MeOH 0.5% v/v as eluent. The fast-running red band containing unreacted starting material was not collected. Compound **43** (purple solid, 385 mg, quantitative yield) was obtained as a diastereomeric mixture (two spots in TLC, DCM/MeOH 0.5% v/v), that was not characterized.

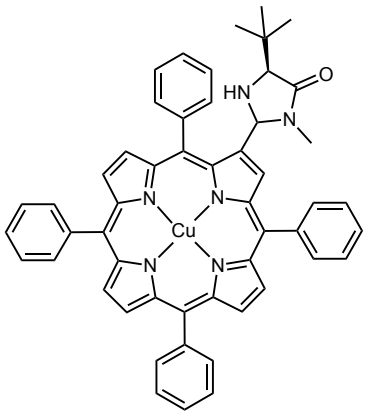

**PREPARATION OF (2*R*,5*S*)-5-(*TERT*-BUTYL)-3-METHYL-2-(5,10,15,20-TETRAPHENYLPORPHYRIN-2-YL)IMIDAZOLIDIN-4-ONE (17d)**

In a 25 mL round-bottomed flask, equipped with magnetic stirring, 385 mg (0.46 mmol) of the copper porphyrin **43** were dissolved in DCM (5 mL). Concentrated $H_2SO_4$ (6.5 mL, 98%) was added and the resulting green mixture was vigorously stirred for 4 min. Then, the two-phase mixture was poured over an ice-cold aqueous NaOH solution (9 g in 300 mL), transferred to a separatory funnel, and shaken until no green color was observed. The aqueous phase was extracted with DCM (3 x 100 mL) and the combined organic layers were washed with an aqueous saturated solution of $NaHCO_3$ (2 x 100 mL), dried over $MgSO_4$ and the solvent was evaporated under reduced pressure. Finally, the crude product was purified by flash column chromatography through $Et_3N$-pretreated silica gel (2.5% v/v $NEt_3$) using DCM/MeOH 3% v/v as eluent. Compound **17d** (purple solid, 85 mg, 23% yield) was obtained as a single diastereomer.

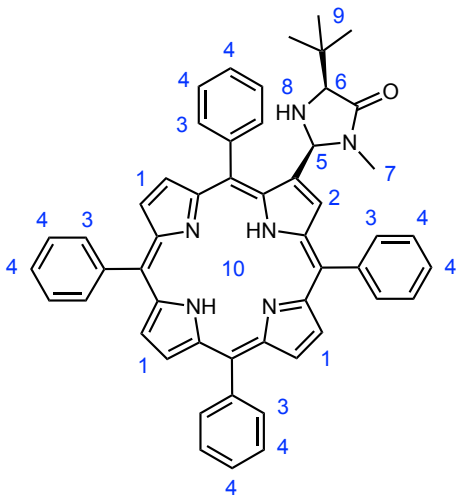


**$^1$H-NMR** ($CDCl_3$, 400 MHz): $\delta$ = 8.82 (m, $3H_1$), 8.77 (d, $J$ = 4.8 Hz, $2H_1$), 8.69 (s, $1H_2$), 8.62 (d, $J$ = 4.9 Hz, $1H_1$), 8.34 (d, $J$ = 6.8 Hz, $1H_3$), 8.24-8.10 (m, $7H_3$), 7.83-7.38 (m, $12H_4$), 5.47 (s, $1H_5$), 3.41 (s, $1H_6$), 2.69 (s, $3H_7$), 2.24 (br, $1H_8$), 0.95 (s, $9H_9$), -2.69 (br, $2H_{10}$) ppm. **HRMS (ESI):** *m/z* calculated for $C_{52}H_{45}N_6O$ $[M+H]^+$, 769.3649; found 769.3618. **UV-Vis** [$\lambda_{max}$ nm ($\varepsilon$), c = 2.948 x $10^{-6}$ M, $CH_2Cl_2$]: 420 (284484), 518 (14123), 552 (5829), 593 (4313), 650 (3216).

## 7.6. SYNTHESIS OF (*S*)-1-(PYRROLIDIN-2-YL)-*N*-(4-(10,15,20-TRIPHENYL PORPHYRIN-5-YL)BENZYL)METHANAMINE (18a)

**PREPARATION OF *N*-BOC-(*S*)-2-(4-TOLUENSULFONYLOXY)-METHYLPYRROLIDINE (48)[175]**

To an ice-cold solution of *N*-Boc-L-prolinol **47** (2.93 g, 14.6 mmol) in pyridine (23 mL), placed in a 250 mL round-bottomed flask equipped with magnetic stirring, 4-toluensulfonyl chloride (4.70 g, 24.7 mmol) was added and the resulting mixture was stirred for 6 h at room temperature. At this point, $Et_2O$ (200 mL) was added and the two-phase mixture was transferred to a separatory funnel.

The organic phase was washed successively with HCl 10% (2 x 50 mL), a saturated aqueous solution of $NaHCO_3$ (3 x 50 mL) and brine (3 x 50 mL), dried over $Na_2SO_4$ and concentrated under reduced pressure. The resulting orange solid was purified via flash column chromatography through silica gel using Hex/AcOEt (3/2) as eluent, affording the desired product (2.91 g, 56% yield) as a yellowish oil.

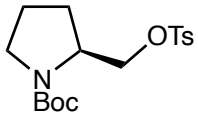


**$^1$H-NMR** ($CDCl_3$, 400 MHz): $\delta$ = 7.76 (d, *J* = 8.2 Hz, 2H), 7.73 (d, *J* = 8.2 Hz, 2H), 3.93 (m, 2H), 3.28 (m, 3H), 2.44 (s, 3H), 1.84 (m, 4H), 1.47 (s, 9H) ppm.

**PREPARATION OF *N*-BOC-(*S*)-2-AZIDOMETHYLPYRROLIDINE (49)[175]**

In a 250 mL round bottomed flask, equipped with magnetic stirring and a Dimroth reflux condenser, *N*-Boc-(*S*)-2-(4-toluensulfonyloxy)-methylpyrrolidine **48** (2.914 g, 8.2 mmol) was dissolved in anhydrous DMSO (87 mL). Then, sodium azide (3.195 g, 49.1 mmol) was added and the mixture was stirred for 19 h at 64 ºC. At this point, it was allowed to cool down until room temperature, diluted with $Et_2O$ (166 mL) and transferred to a separatory funnel. The organic phase was washed with water (3 x 120 mL) and brine (1 x 60 mL), dried with $Na_2SO_4$ and concentrated under reduced pressure. The desired product (1.556 g, 84% yield) was obtained as a yellowish oil, that did not require further purification.

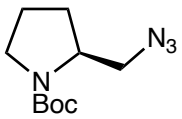


**$^1$H-NMR** ($CDCl_3$, 400 MHz): $\delta$ = 4.00-3.80 (m, 1H), 3.37 (m, 4H), 1.86 (m, 4H), 1.47 (s, 9H) ppm.

**PREPARATION OF *TERT*-BUTYL (*S*)-2-AMINOMETHYLPYRROLIDINE-1-CARBOXYLATE (50)[175]**

In a 250 mL round bottomed flask, equipped with magnetic stirring and a Dimroth reflux condenser, *N*-Boc-(*S*)-2-azidomethylpyrrolidine **49** (1.556 g, 6.9 mmol) was dissolved in THF (59 mL). Then, triphenylphosphine (3.609 g, 13.8 mmol) and $H_2O$ (0.3 mL) were added and the resulting mixture was heated up to reflux for 24 h. After cooling down to room temperature, the solvents were evaporated under reduced pressure and the resulting oil was redissolved in $Et_2O$

(125 mL); the solution's pH was then adjusted to pH = 2 with 1 M aqueous HCl. Then, the aqueous phase was washed with $Et_2O$ (2 x 25 mL), the pH was brought to 12 with aqueous 2 M NaOH and extracted with DCM (6 x 20 mL). The combined organic layers were dried with $Na_2SO_4$ and concentrated under reduced pressure to afford a yellowish oil (1.070 g, 78% yield), that did not require further purification.

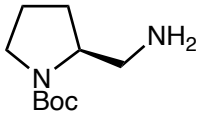


**$^1$H-NMR** ($CDCl_3$, 400 MHz): $\delta$ = 3.75 (m, 2H), 3.26 (m, 2H), 2.77 (m, 1H), 2.62 (m, 1H), 1.75 (m, 3H), 1.49 (br, 2H), 1.40 (s, 9H) ppm.

## PREPARATION OF *TERT*-BUTYL (*S*)-2-(((4-(10,15,20-TRIPHENYLPORPHYRIN-5-YL)BENZYL)AMINO)METHYL)PYRROLIDINE-1-CARBOXYLATE (51)

In a 25 mL round-bottomed flask, equipped with magnetic stirring and a Dimroth reflux condenser, *N*-Boc-(*S*)-2-aminomethylpyrrolidine **50** (72 mg, 0.36 mmol) was introduced. Then, a solution of 4-(10,15,20-triphenylporphyrin-5-yl) benzaldehyde **34** (115 mg, 0.18 mmol) in $CHCl_3$ (8 mL) and $Yb(SO_3CF_3)_3$ (2.8 mg, 0.0045 mmol, 1.2 mol%) were added sequentially. The stirred mixture was heated up to reflux for 24 h. After cooling to room temperature, $NaBH_3CN$ (22.6 mg, 0.36 mmol) was added in one portion and the reaction mixture was stirred for 1 h at room temperature and quenched with $H_2O$ (15 mL). Then, the aqueous phase was separated and extracted with DCM (3 x 10 mL), and the combined organic layers were dried over $Na_2SO_4$ and concentrated under reduced pressure. The resulting purple solid was purified via flash column chromatography using a mixture of DCM/MeOH (from 1 to 5%) as eluent, affording the desired product (100 mg, 67% yield) as a purple solid.

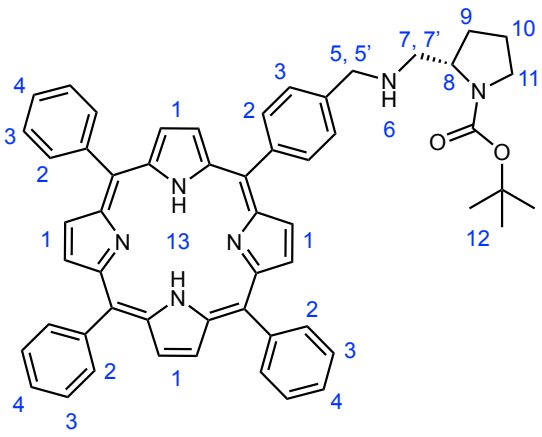


**$^1$H-NMR** ($CDCl_3$, 400 MHz): $\delta$ = 8.84 (s, 8$H_1$), 8.21 (d, $J$ = 7.7 Hz, 8$H_2$), 7.76 (m, 11$H_{3,4}$), 4.34-4.17 (m, 2$H_{5, 5'}$), 3.51-3.38 (m, 2$H_{7, 7'}$), 3.10-3.03 (m, 1$H_8$), 2.20 (m, 2$H_{11}$), 1.95-1.86 (m, 3H, $H_6$ + 2$H_{10}$), 1.51 (s, 11H, 2$H_9$ + 9$H_{12}$), -2.77 (br, 2$H_{13}$) ppm. **HRMS (ESI):** *m/z* calculated for $C_{55}H_{50}N_6O_2$ $[M+H]^+$, 827.3995.; found 827.4057.

**PREPARATION OF (*S*)-1-(PYRROLIDIN-2-YL)-*N*-(4-(10,15,20-TRIPHENYL PORPHYRIN-5-YL)BENZYL)METHANAMINE (18a)**

In a 25 mL round-bottomed flask, equipped with magnetic stirring, *tert*-butyl (*S*)-2-(((4-(10,15,20-triphenylporphyrin-5-yl)benzyl)amino)methyl)pyrrolidine-1-carboxylate **51** (100 mg, 0.12 mmol) was dissolved in $CHCl_3$ (6 mL). Then, trifluoroacetic acid (6 mL) was added and the resulting green solution was stirred for 2 h at room temperature. At this point, the reaction was concentrated under reduced pressure, redissolved in $CHCl_3$ (10 mL) and an aqueous solution of NaOH (3.454 g in 100 mL) was added, noticing a change of color from green to purple. The aqueous phase was separated and extracted with DCM (10 mL portions) until colorless; the combined organic phases were dried over $Na_2SO_4$ and concentrated under reduced pressure, affording a purple solid that was purified via flash column chromatography through silica gel, using a mixture of DCM/MeOH (from 0.5 to 10%) to give the desired porphyrin (84 mg, 97% yield) as a purple solid.

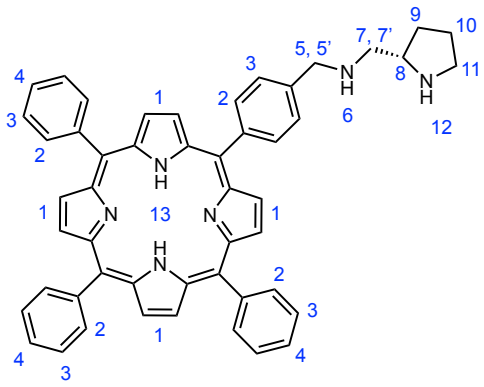

**$^1$H-NMR** ($CDCl_3$, 400 MHz): $\delta$ = 8.82 (s, $8H_1$), 8.20-8.16 (m, $8H_2$), 7.76-7.69 (m, $11H_{3,4}$), 4.41-4.27 (m, $2H_{5,5'}$), 3.49-3.34 (m, 3H, $2H_{7,7'} + H_{12}$), 2.32 (m, $1H_8$), 2.17-2.07 (m, $2H_{11}$), 1.82 (br, $1H_6$), 1.31-1.25 (m, $2H_{10}$), 0.88 (m, $2H_9$) ppm. **HRMS (ESI):** *m/z* calculated for $C_{50}H_{42}N_6$ $[M+H]^+$, 727.3471; found 727.3549. **UV-Vis** [$\lambda_{max}$ nm ($\varepsilon$), 1.382 x $10^{-6}$ M, $CH_2Cl_2$]: 418 (533734), 515 (49241), 549 (22161), 590 (5295), 647 (5057).

## 7.7. SYNTHESIS OF (*S*)-*N*-(4-(10,15,20-TRIPHENYLPORPHYRIN-5-YL)BENZYL) PYRROLIDINE-2-CARBOXAMIDE (18b)

**PREPARATION OF *N*-BOC-L-PROLINE (53)[181]**

In a 50 mL round-bottomed flask, equipped with magnetic stirring, L-Proline (1.00 g, 8.7 mmol) was dissolved in an aqueous saturated solution of $NaHCO_3$ (13 mL), and cooled down to 0 ºC with an ice-water bath. Then, di-*tert*-butyl dicarbonate (2.09 g, 9.6 mmol) was dissolved in THF (5 mL) and added dropwise to the cold solution. The resulting mixture was stirred for 19 h at room temperature. At this point, THF was removed under reduced pressure and, after cooling down to 0

ºC, the aqueous solution was acidified to pH = 2 with 3 M aqueous HCl (2.7 + 13.3 mL). The aqueous phase was extracted with AcOEt (3 x 15 mL) and the combined organic layers were dried over $Na_2SO_4$ and concentrated under reduced pressure, to afford the desired product (1.87 g, quantitative yield) as a white solid, that was not characterized and was subsequently used without further purification.

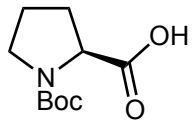


**PREPARATION OF 4-(10,15,20-TRIPHENYLPORPHYRIN-5-YL)BENZONITRILE (55)[182]**

In a 500 mL round-bottomed flask, equipped with magnetic stirring and a Liebig reflux condenser, propionic acid (350 mL) and 4-cyanobenzaldehyde (1.928 g, 14.7 mmol) were added sequentially. Once all the of aldehyde was dissolved, the mixture was heated up to reflux and benzaldehyde (4.5 mL, 44.1 mmol) and freshly distilled pyrrole (4.1 mL, 58.8 mmol) were added and the black reaction mixture was stirred for 1 h under reflux, protected from light. After this time, the reaction mixture was cooled down to room temperature and the solvent was removed via vacuum distillation. Next, the obtained purple paste was purified by flash column chromatography through silica gel, using DCM as eluent. In this way, the less polar TPP could be separated from another fraction containing the substituted porphyrins. After elimination of the solvent, the crude mixture was purified again by flash column chromatography in silica gel, using DCM/Hexane (4/1) as eluent, affording the desired product (868 mg, 21% yield) as a metallic purple solid.

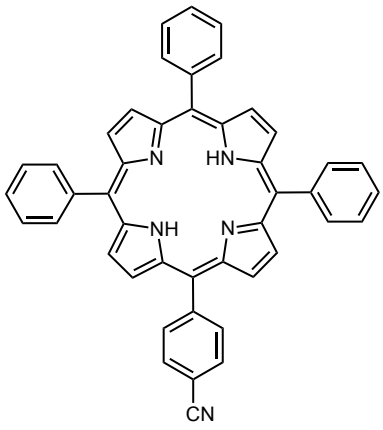


**$^1$H-NMR** ($CDCl_3$, 400 MHz): $\delta$ = 8.89-8.72 (m, 8H), 8.33 (d, *J* = 7.9 Hz, 2H), 8.21 (m, 6H), 8.06 (d, *J* = 8.2 Hz, 2H), 7.76 (m, 9H), -2.77 (br, 2H) ppm.

**PREPARATION OF 4-(10,15,20-TRIPHENYLPORPHYRIN-5-YL)METHANAMINE (56)[182]**

In a 500 mL round-bottomed flask, equipped with magnetic stirring, $LiAlH_4$ (310 mg, 8.2 mmol) was introduced, and the system was purged with Ar. Then, dry THF (6.1 mL) was added and, subsequently, a solution of 4-(10,15,20-triphenylporphyrin-5-yl) benzonitrile **55** (868 mg, 1.4 mmol) in dry THF (155 mL) was added via syringe. The reaction mixture was stirred at room temperature for 1 h. At this point, the reaction was quenched with aqueous 1% HCl (211 mL) and the resulting green solution was transferred to a separatory funnel and extracted with DCM until colorless. The combined organic layers were treated with a 32% (w/w) aqueous solution of $NH_3$, that brought about a change of color from green to purple, and the aqueous phase was separated and extracted with DCM (3 x 50 mL). The combined organic layers were dried over $NaSO_4$ and concentrated under reduced pressure to afford a purple solid, that was purified via flash column chromatography through silica gel, using a mixture of DCM/MeOH (from 2 to 5%) as eluent. The desired porphyrin (618 mg, 71% yield) was obtained as a purple solid.

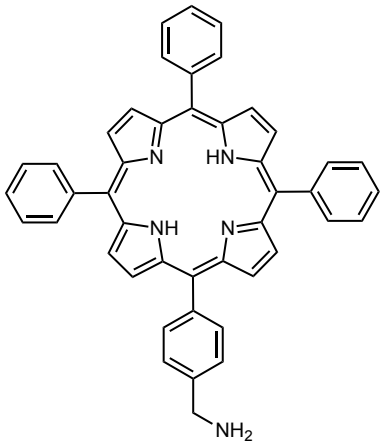


**$^1$H-NMR** ($CDCl_3$, 400 MHz): $\delta$ = 8.83 (m, 8H), 8.26 (br, 2H) 8.18 (m, 8H), 7.74 (m, 11H), 4.25 (s, 2H), -2.67 (br, 2H) ppm.

**PREPARATION OF *TERT*-BUTYL (*S*)-2-((4-(10,15,20-TRIPHENYLPORPHYRIN-5-YL)BENZYL) CARBAMOYL)PYRROLIDINE-1-CARBOXYLATE (57)**

In a 25 mL round-bottomed flask, equipped with magnetic stirring, a solution of *N*-Boc-L-Proline **53** (251 mg, 1.2 mmol) and $NEt_3$ (270 μL, 2.1 mmol) in dry THF (2.1 mL) was cooled down to -15 ºC. Then, a solution of ethyl chloroformate (110 μL, 125 mg, 1.15 mmol) in dry THF (1.6 mL) was added, and the mixture was stirred for 30 minutes at -15 ºC. Next, a solution of 4-(10,15,20-triphenylporphyrin-5-yl)methanamine **56** (618 mg, 0.96 mmol) in dry THF (5.1 mL) was added dropwise, and the reaction mixture was stirred overnight at room temperature. At this point, DCM

(15 mL) was added and the organic phase was washed with $NaHCO_3$ (15 mL) and brine (15 mL), dried over $NaSO_4$ and concentrated under reduced pressure, affording a purple solid that was purified by flash column chromatography through silica gel, using a mixture of DCM/MeOH (from 0.5 to 2%) as eluent. The desired porphyrin (806 mg, quantitative yield) was obtained as a purple solid.

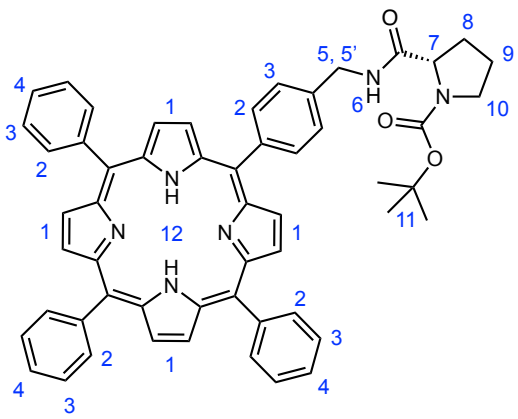

**$^1$H-NMR** ($CDCl_3$, 400 MHz): $\delta$ = 8.84 (s, $8H_1$), 8.22-8.16 (m, $8H_2$), 7.76-7.63 (m, $11H_{3,4}$), 4.93 (dd, $J$ = 10.2 Hz, $J'$ = 6.4 Hz, $1H_5$), 4.48 (m, $1H_{5'}$), 3.55 (m, $2H_{10}$), 2.54-2.28 (m, $1H_7$), 2.06-1.99 (m, 3H, $H_6$ + $2H_9$), 1.49 (s, $9H_{11}$), 0.88 (m, $2H_8$), -2.78 (br, $2H_{12}$) ppm.

## PREPARATION OF (*S*)-*N*-(4-(10,15,20-TRIPHENYLPORPHYRIN-5-YL)BENZYL) PYRROLIDINE-2-CARBOXAMIDE (18b)

In a 250 mL round-bottomed flask, equipped with magnetic stirring, *tert*-butyl (*S*)-2((4-(10,15,20-triphenylporphyrin-5-yl)benzyl)carbamoyl)pyrrolidine-1-carboxylate **57** (806 mg, 0.96 mmol) was dissolved in $CHCl_3$ (51 mL). Then, trifluoroacetic acid (51 mL) was added and the resulting green solution was stirred for 2 h at room temperature. At this point, the reaction was concentrated under reduced pressure, the residue was redissolved in $CHCl_3$ (50 mL); an aqueous solution of NaOH (7.639 g in 200 mL) was added, noticing a change of color from green to purple. The aqueous phase was extracted with DCM until colorless, dried over $Na_2SO_4$ and concentrated under reduced pressure, affording a purple solid that was purified via flash column chromatography through silica gel, using a mixture of DCM/MeOH (from 0.5 to 5%), to afford the desired porphyrin (541 mg, 72% yield) as a purple solid.

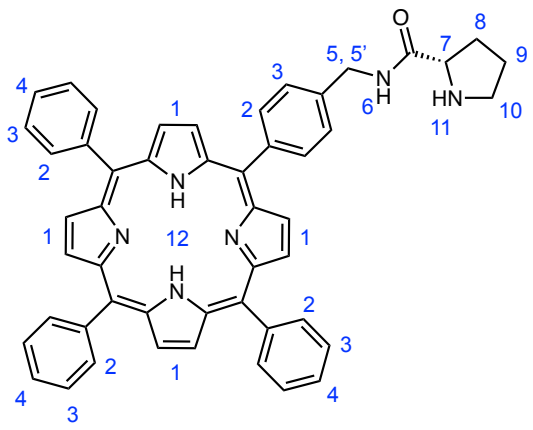

**$^1$H-NMR** ($CDCl_3$, 400 MHz): $\delta$ = 9.09 (br, $1H_6$), 8.82 (s, $8H_1$), 8.21-8.14 (m, $8H_2$), 7.74-7.65 (m, $11H_{3,4}$), 4.97 (dd, *J* = 10.2 Hz, *J'* = 6.4 Hz, $1H_5$), 4.79 (m, $1H_{5'}$), 3.29 (m, $2H_{10}$), 2.60 (br, $1H_{11}$), 2.02 (m, 3H, $H_7$ + $2H_9$), 1.66 (m, $2H_8$), -2.79 (br, $2H_{12}$). **HRMS (ESI):** *m/z* calculated for $C_{50}H_{40}N_6O_2$ $[M+H]^+$, 741.3264; found 741.3332. **UV-Vis** [$\lambda_{max}$ nm ($\varepsilon$), c = 3.892 x $10^{-6}$ M, $CH_2Cl_2$]: 418 (562430), 515 (49153), 550 (22271), 590 (6971), 646 (5823).

## 7.8. SYNTHESIS OF ORGANOCATALYSTS DERIVED FROM L-PROLINE 89d-l[193]

L-Proline-derived organocatalysts **89a-c** were commercially available.

### PREPARATION OF *TERT*-BUTYL (*S*)-2-(BENZYLCARBAMOYL)PYRROLIDINE-1-CARBOXYLATE (92)[193]

In a 50 mL round-bottomed flask, equipped with magnetic stirring, *N*-Boc-L-Proline **53** (500 mg, 2.33 mmol) and $NEt_3$ (390 μL, 283 mg, 2.8 mmol) were dissolved in dry THF (4.5 mL) and the resulting mixture was cooled down to -15 ºC. Then, a solution of ethyl chloroformate (225 μL, 256 mg, 2.36 mmol) in dry THF (3.2 mL) and a solution of benzylamine (510 μL, 500 mg, 4.66 mmol) in dry THF (1.2 mL) were added sequentially at the same temperature, and the reaction mixture was stirred overnight at room temperature. Next, the reaction mixture was diluted with DCM (20 mL) and was washed successively with citric acid (50 mL, 30% w/v), brine (50 mL) and a saturated aqueous solution of $NaHCO_3$ (50 mL). The organic phase was separated, dried over $Na_2SO_4$ and concentrated under vacuum to afford a yellowish oil (615 mg, 87% yield) that was used without further purification.

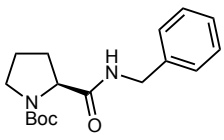

**$^1$H-NMR** ($CDCl_3$, 400 MHz): $\delta$ = 7.36-7.18 (m, 5H), 6.36 (br, 1H N**H**), 4.45 (dd, *J* = 15.2 Hz, *J'* = 6.2 Hz, 1H N–C**H**H'–Ph), 4.30 (dd, *J* = 15.2 Hz, *J'* = 5.9 Hz, 1H N–CH**H'**–Ph), 4.15 (m, 1H), 3.50-3.26 (m, 2H), 2.48-1.87 (m, 4H), 1.39 (s, 9H) ppm.

**PREPARATION OF (*S*)-*N*-BENZYLPYRROLIDINE-2-CARBOXAMIDE (89d)[193]**

In a 50 mL round-bottomed flask, equipped with magnetic stirring, a solution of *N*-Boc-L-proline benzylamide **92** (615 mg, 2.02 mmol) in DCM (5 mL) was cooled down to 0 ºC with an ice-water bath. Then, trifluoroacetic acid (3.9 mL) was added dropwise and the resulting mixture was stirred at 0 ºC for 1 h. After this time, the solvents were evaporated under vacuum, an aqueous solution of NaOH (2.268 g in 15 mL) was added and the aqueous phase was extracted with DCM (3 x 20 mL). The combined organic layers were dried over $Na_2SO_4$ and concentrated under reduced pressure to afford a yellowish oil (412 mg, quantitative yield), that did not require any further purification.

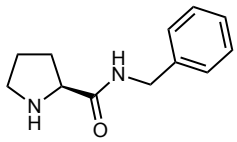

**$^1$H-NMR** ($CDCl_3$, 400 MHz): $\delta$ = 7.95 (br, 1H N**H**–CO),7.34-7.25 (m, 5H Ph), 4.44 (d, *J* = 6.1 Hz, 2H C**H$_2$**–NHCO), 3.79 (dd, *J* = 9.2 Hz, *J'* = 5.3 Hz, 1H), 3.03-2.84 (m, 2H), 2.22-2.12 (m, 1H), 1.96 (sext, *J* = 6.8 Hz, 1H), 1.87 (br, 1H N**H**), 1.74-1.67 (m, 2H) ppm.

**PREPARATION OF *TERT*-BUTYL (*S*)-2-((2-PHENYLACETAMIDO)METHYL)PYRROLIDINE-1-CARBOXYLATE (99)**

In a 25 mL round-bottomed flask, equipped with magnetic stirring, 2-phenylacetic acid (123 mg, 0.90 mmol) and $NEt_3$ (160 μL, 116 mg, 1.15 mmol) were dissolved in dry THF (2 mL) and the resulting mixture was cooled down to -15 ºC. Then, a solution of ethyl chloroformate (86 μL, 98 mg, 0.90 mmol) in dry THF (1.5 mL) and a solution of *tert*-butyl (*S*)-2-aminomethylpyrrolidine-1-carboxylate **50** (223 mg, 1.12 mmol) in dry THF (0.5 mL), were sequentially added at the same temperature, and the reaction mixture was stirred overnight at room temperature. After this time, the reaction mixture was diluted with DCM (25 mL) and was washed with aqueous citric acid (20 mL, 30% w/w), with brine (20 mL) and with a saturated aqueous solution of $NaHCO_3$ (20 mL). After drying over $Na_2SO_4$, the solvent was concentrated under vacuum to afford a yellowish oil (249 mg, 87% yield), that was subsequently used without further purification.

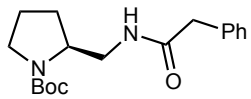

**$^1$H-NMR** ($CDCl_3$, 400 MHz): $\delta$ = 7.34-7.27 (m, 5H Ph), 4.15 (q, *J* = 7.1 Hz, 2H), 3.61 (s, 2H), 1.98-1.85 (m, 2H), 1.66 (br, 1H), 1.47 (s, 9H), 1.25 (t, *J* = 7.1 Hz, 3H) ppm.

**PREPARATION OF (*S*)-2-PHENYL-*N*-(PYRROLIDIN-2-YLMETHYL)ACETAMIDE (89e)**

In a 25 mL round-bottomed flask, equipped with magnetic stirring, *tert*-butyl (*S*)-2-((2-phenylacetamido)methyl)pyrrolidine-1-carboxylate **99** (249 mg, 0.78 mmol) was dissolved in DCM (2.3 mL) and the solution was cooled down to 0 ºC with an ice-water bath. Then, trifluoroacetic acid (1.8 mL) was added and the resulting mixture was stirred for 1h at 0 ºC. After this time, the solvents were evaporated under vacuum, an aqueous solution of NaOH (1.052 g in 15 mL) was added and the aqueous phase was extracted with DCM (3 x 20 mL). The combined organic layers were dried over $Na_2SO_4$ and concentrated under reduced pressure to afford a partially solidified yellowish oil (672 mg, 97% yield), that was subsequently used without further purification.

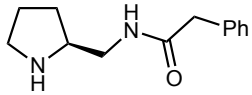

**$^1$H-NMR** ($CDCl_3$, 400 MHz): $\delta$ = 7.34-7.28 (m, 5H Ph), 4.15 (q, *J* = 7.16 Hz, 2H), 3.61 (s, 2H), 2.49-2.44 (dd, *J* = 12.4 Hz, *J'* = 6.8 Hz, 1H), 1.78-1.68 (m, 4H), 1.46 (br, 2H), 1.25 (t, *J* = 7.2 Hz, 3H) ppm. **$^{13}$C-NMR** ($CDCl_3$, 400 MHz): $\delta$ = 171.6, 134.2, 129.3, 129.2, 127.0, 60.8, 46.2, 43.7, 41.4, 28.7, 14.2 ppm. **HRMS (ESI):** *m/z* calculated for $C_{13}H_{18}N_2O$ $[M+H]^+$, 218.1419; found 218.1425.

**PREPARATION OF *TERT*-BUTYL (*S*)-2-(BENZYLCARBAMOTHIOYL)PYRROLIDINE-1-CARBOXYLATE (100)[17]**

In a 100 mL round-bottomed flask, equipped with magnetic stirring and a Dimroth reflux condenser, *tert*-butyl (*S*)-2-(benzylcarbamoyl)pyrrolidine-1-carboxylate **92** (633 mg, 2.08 mmol) and Lawessons's reagent (460 mg, 1.04 mmol) were dissolved in toluene (27 mL) and the resulting mixture was heated up to reflux and stirred for 3 h. Then, it was allowed to cool down to room temperature and the solvent was evaporated under reduced pressure. The resulting yellowish solid was purified via flash column chromatography using hexane/AcOEt (3/1) as eluent, to afford the desired product (403 mg, 61% yield) as a white solid.

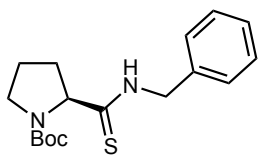

**$^1$H-NMR** ($CDCl_3$, 400 MHz): $\delta$ = 7.34-7.29 (m, 5H Ph), 5.02 (br, 1H CS–N**H**), 4.74 (m, 2H), 3.51-3.40 (m, 2H), 2.33 (m, 2H), 1.87 (m, 2H), 1.39 (s, 9H), 1.26 (m, 1H) ppm.

**PREPARATION OF (*S*)-*N*-BENZYLPYRROLIDINE-2-CARBOTHIOAMIDE (89f)[17]**

*Tert*-Butyl (*S*)-2-(benzylcarbamothioyl)pyrrolidine-1-carboxylate **100** (403 mg, 1.26 mmol) was dissolved in DCM (2.7 mL) in a 25 mL round-bottomed flask, equipped with magnetic stirring, and the system was purged with Ar. Then, TFA (1.25 mL) and $Et_3SiH$ (1.5 mL, 3.03 mmol) were added via syringe and the resulting solution was stirred for 90 min at room temperature. After this time, the solvents were eliminated under reduced pressure and the resulting paste was treated with $Et_2O$ (15 mL), observing the formation of a precipitate, that was filtered out and redissolved in $CHCl_3$ (15 mL). At this point, the organic solution was washed with a saturated aqueous solution of $NaHCO_3$ (2 x 15 mL), dried over $MgSO_4$ and concentrated under reduced pressure to afford the desired product (166 mg, 60% yield) as a white solid.

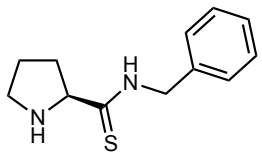

**$^1$H-NMR** ($CDCl_3$, 400 MHz): $\delta$ = 10.08 (br, 1H CS–N**H**), 7.37-7.29 (m, 5H Ph), 4.87 (d, *J* = 4.9 Hz, 2H), 4.26 (dd, *J* = 9.0 Hz, *J'* = 5.6 Hz, 1H), 3.08-2.88 (m, 2H), 2.46-2.37 (m, 1H), 2.07 (sext, *J* = 6.2 Hz, 1H), 1.75-1.56 (m, 3H, 2H + N**H** pyrrolidine) ppm.

**PREPARATION OF *TERT*-BUTYL (*S*)-2-(((*S*)-1-PHENYLETHYL)CARBAMOYL)PYRROLIDINE-1-CARBOXYLATE (93)[206]**

In a 50 mL round-bottomed flask, equipped with magnetic stirring, *N*-Boc-L-Proline **53** (500 mg, 2.33 mmol) and $NEt_3$ (390 μL, 283 mg, 2.8 mmol) were dissolved in dry THF (4.5 mL) and the resulting mixture was cooled down to -15 ºC. Then, a solution of ethyl chloroformate (225 μL, 257 mg, 2.36 mmol) in dry THF (3.2 mL) and, subsequently, a solution of (*S*)-1-phenylethan-1-amine (600 μL, 578 mg, 4.77 mmol) in THF (1.2 mL) were added at the same temperature, and the reaction mixture was stirred overnight at room temperature. At this point, the reaction mixture was diluted with DCM (20 mL) and the organic phase was washed successively with citric acid (50 mL, 30% w/v), brine (50 mL) and a saturated aqueous solution of $NaHCO_3$ (50 mL). After drying over $Na_2SO_4$, the solvent was concentrated under vacuum to afford the desired product (677 mg, 92% yield) as a yellowish oil, that did not require any further purification.

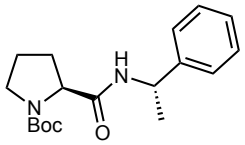

**$^1$H-NMR** ($CDCl_3$, 400 MHz): $\delta$ = 7.32 (m, 5H Ph), 6.24 (br, 1H N**H**–CO), 5.17-5.03 (m, 1H), 4.31-4.20 (m, 1H), 3.49-3.30 (m, 2H), 2.39-2.13 (m, 1H), 1.88 (m, 3H), 1-47-1.45 (br, 12H, 3H $CH_3$ + 9H $C(CH_3)_3$) ppm

**PREPARATION OF (*S*)-*N*-((*S*)-1-PHENYLETHYL)PYRROLIDINE-2-CARBOXAMIDE (89g)[206]**

In a 50 mL round-bottomed flask, equipped with magnetic stirring, (*S*)-*N*-Boc-(*S*)-prolinemethylbenzylamide **93** (677 mg, 2.13 mmol) was dissolved in DCM (5.3 mL) and the solution was cooled down to 0 ºC with an ice-water bath. Then, trifluoroacetic acid (4.1 mL) was added and the resulting mixture was stirred for 1 h at 0 ºC. After this time, the solvents were evaporated under vacuum, an aqueous solution of NaOH (2.385 g in 15 mL) was added and the aqueous phase was extracted with DCM (3 x 20 mL). The combined organic layers were dried over $Na_2SO_4$ and concentrated under reduced pressure to afford a yellowish oil (434 mg, 94% yield), that did not require any further purification.

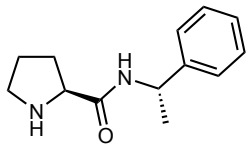

**$^1$H-NMR** ($CDCl_3$, 400 MHz): $\delta$ = 7.90 (br, 1H N**H**–CO), 7.33-7.30 (m, 5H Ph), 5.10 (quint, *J* = 6.9 Hz, 1H C**H**–NCO), 3.71 (dd, *J* = 9.1 Hz, *J'* = 5.4 Hz, 1H), 3.04-2.88 (m, 2H), 2.19-2.09 (m, 1H), 1.95 (sext, *J* = 6.8 Hz, 1H), 1.87 (br, 1H N**H**), 1.73 (m, 2H), 1.48 (d, *J* = 6.9 Hz, 3H) ppm.

**PREPARATION OF *TERT*-BUTYL (*S*)-2-(((*R*)-1-PHENYLETHYL)CARBAMOYL)PYRROLIDINE-1-CARBOXYLATE (94)[206]**

In a 50 mL round-bottomed flask, equipped with magnetic stirring, *N*-Boc-L-Proline **53** (500 mg, 2.33 mmol) and $NEt_3$ (390 μL, 283 mg, 2.8 mmol) were dissolved in THF (4.5 mL) and the resulting mixture was cooled down to -15 ºC. Then, a solution of ethyl chloroformate (225 μL, 257 mg, 2.36 mmol) in dry THF (3.2 mL) and a solution of (*R*)-1-phenylethan-1-amine (600 μL, 578 mg, 4.77 mmol) in dry THF (1.2 mL) were added sequentially at the same temperature, and the reaction mixture was stirred overnight at room temperature. At this point, the reaction mixture was diluted with DCM (20 mL) and was washed with an aqueous solution of citric acid (50 mL, 30% w/w), with brine (50 mL) and with a saturated aqueous solution of $NaHCO_3$ (50 mL). After drying over $Na_2SO_4$,

the solvent was removed by rotary evaporation to afford the *N*-protected amide (638 mg, 86% yield) as a yellowish oil, that did not require any further purification.

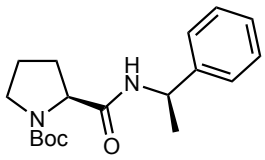

**$^1$H-NMR** ($CDCl_3$, 400 MHz): $\delta$ = 7.50 (br, 1H N**H**–CO), 7.32-7.24 (m, 5H Ph), 5.10 (m, 1H C**H**–NCO), 4.29 (m, 1H), 3.35 (m, 2H), 2.40-2.06 (m, 1H), 1.85 (m, 3H), 1.47 (br m, 12H, 3H $CH_3$ + 9H $C(CH_3)_3$) ppm.

**PREPARATION OF (*S*)-*N*-((*R*)-1-PHENYLETHYL)PYRROLIDINE-2-CARBOXAMIDE (89h)[206]**

In a 50 mL round-bottomed flask, equipped with magnetic stirring, the *N*-Boc-prolineamide **94** (638 mg, 2.0 mmol) was dissolved in DCM (5 mL) and the solution was cooled down to 0 ºC with an ice-water bath. Then, trifluoroacetic acid (3.9 mL) was added and the resulting mixture was stirred for 1 h at 0ºC. After this time, the solvents were evaporated under vacuum, an aqueous solution of NaOH (2.385 g in 15 mL) was added to the residue and the aqueous phase was extracted with DCM (3 x 20 mL). The combined organic layers were dried over $Na_2SO_4$ and were concentrated under reduced pressure to afford the desired amide (293 mg, 67% yield) as a yellowish oil, that was subsequently used without further purification.

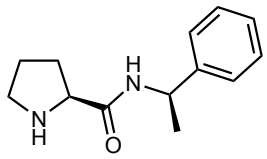

**$^1$H-NMR** ($CDCl_3$, 400 MHz): $\delta$ = 7.94 (br, 1H N**H**–CO), 7.34-7.22 (m, 5H Ph), 5.09 (quint, *J* = 7.1 Hz, 1H C**H**–NCO), 3.74 (dd, *J* = 9.2 Hz, *J'* = 5.2 Hz, 1H), 3.02-2.83 (m, 2H), 2.16-2.07 (m, 1H), 1.94-1.85 (m, 2H), 1.67 (quint, *J* = 6.7 Hz, 2H), 1.48 (d, *J* = 7.0 Hz, 3H C**H$_3$**) ppm.

**PREPARATION OF *TERT*-BUTYL (*S*)-2-((4-FLUOROPHENYL)CARBAMOYL)PYRROLIDINE-1-CARBOXYLATE (95)[207]**

In a 50 mL round-bottomed flask, equipped with magnetic stirring, *N*-Boc-L-Proline **53** (500 mg, 2.33 mmol) and $NEt_3$ (390 μL, 283 mg, 2.8 mmol) were dissolved in dry THF (4.5 mL) and the resulting mixture was cooled down to -15 ºC. Then, a solution of ethyl chloroformate (225 μL, 257 mg, 2.36 mmol) in dry THF (3.2 mL) and a solution of *p*-fluoroaniline (450 μL, 528 mg, 4.75 mmol) in dry THF (1.2 mL) were sequentially added at the same temperature, and the reaction mixture was stirred overnight at room temperature. At this point, the reaction mixture was diluted with DCM

(20 mL) and was successively washed with an aqueous solution of citric acid (50 mL, 30% w/w), with brine (50 mL) and with a saturated aqueous solution of $NaHCO_3$ (50 mL). After drying over $Na_2SO_4$, the solvent was removed by rotary evaporation, to afford a white solid (553 mg, 77% yield), that was used in the next step without further purification.

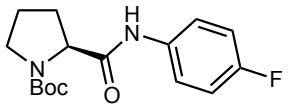

**$^1$H-NMR** ($CDCl_3$, 400 MHz): $\delta$ = 9.50 (br, 1H N**H**–CO), 7.49-7.45 (m, 2H Ph), 7.02-6.97 (m, 2H Ph), 4.51-4.38 (m, 1H), 3.48-3.29 (m, 2H), 2.60-2.47 (m, 1H), 2.01-1.83 (m, 3H), 1.49 (s, 9H) ppm.

**PREPARATION OF (*S*)-*N*-(4-FLUOROPHENYL)PYRROLIDINE-2-CARBOXAMIDE (89i)[207]**

In a 50 mL round-bottomed flask, equipped with magnetic stirring, *tert*-butyl (*S*)-2-((4-fluorophenyl)carbamoyl)pyrrolidine-1-carboxylate **95** (553 mg, 1.79 mmol) was dissolved in DCM (5.3 mL) and the solution was cooled down to 0 ºC with an ice-water bath. Then, trifluoroacetic acid (4.1 mL) was added and the resulting mixture was stirred for 1 h at 0ºC. After this time, the solvents were evaporated under vacuum, an aqueous solution of NaOH (2.385 g in 15 mL) was added and the aqueous phase was extracted with DCM (3 x 20 mL). The combined organic layers were dried over $Na_2SO_4$ and concentrated under reduced pressure to afford the desired amide (373 mg, quantitative yield) as an orange oil, that was not purified.

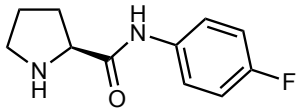

**$^1$H-NMR** ($CDCl_3$, 400 MHz): $\delta$ = 9.72 (br, 1H N**H**–CO), 7.58-7.54 (m, 2H Ph), 7.02-6.98 (m, 2H Ph), 3.86 (dd, *J* = 9.2 Hz, *J'* = 5.2 Hz, 1H), 3.12-2.95 (m, 2H), 2.26-2.17 (m 1H), 2.04 (m, 2H), 1.79-1.72 (m, 2H) ppm.

**PREPARATION OF *TERT*-BUTYL (*S*)-2-(((1*S*,2*R*)-2-HYDROXY-1,2-DIPHENYLETHYL) CARBAMOYL)PYRROLIDINE-1-CARBOXYLATE (96)[16]**

In a 25 mL round-bottomed flask, equipped with magnetic stirring, a solution of *N*-Boc-L-Proline **53** (100 mg, 0.47 mmol) and of $NEt_3$ (80 μL, 58 mg, 0.57 mmol) in dry THF (0.9 mL) was cooled down to -15 ºC. Then, a solution of ethyl chloroformate (45 μL, 51 mg, 0.47 mmol) in dry THF (0.7 mL) and a solution of (1*R*,2*S*)-2-amino-1,2-diphenylethan-1-ol (199 mg, 0.94 mmol) in dry THF (0.3 mL) were added sequentially at the same temperature, and the reaction mixture was stirred

overnight at room temperature. Then, the reaction mixture was diluted with DCM (10 mL) and was washed successively washed with aqueous citric acid (25 mL, 30% w/w), brine (25 mL) and a saturated aqueous solution of $NaHCO_3$ (25 mL). After drying over $Na_2SO_4$, the solvent was removed by evaporation under vacuum to afford a white solid (181 mg, 94% yield), that was used without purification in the next step.

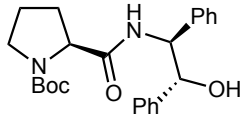

**$^1$H-NMR** ($CDCl_3$, 400 MHz): $\delta$ = 7.91 (br, 1H N**H**–CO), 7.20 (m, 6H Ph), 7.05-7.01 (m, 4H Ph), 5.24 (dd, *J* = 8.5 Hz, *J'* = 4.1 Hz, 1H), 5.11 (d, *J* = 4.1 Hz, 1H), 3.36-3.27 (m, 2H), 2.24 (br, 1H O**H**), 1.86-1.82 (m, 2H), 1.57 (m, 3H), 1.47 (s, 9H) ppm.

## PREPARATION OF (*S*)-*N*-((1*S*,2*R*)-2-HYDROXY-1,2-DIPHENYLETHYL)PYRROLIDINE-2-CARBOXAMIDE (89j)[16]

In a 10 mL round-bottomed flask, equipped with magnetic stirring, *tert*-butyl (*S*)-2-(((1*S*,2*R*)-2-hydroxy-1,2-diphenylethyl)carbamoyl)pyrrolidine-1-carboxylate **96** (181 mg, 0.44 mmol) was dissolved in DCM (1.3 mL) and the solution was cooled down to 0 ºC with an ice-water bath. Then, trifluoroacetic acid (1.0 mL) was added and the resulting mixture was stirred for 1 h at 0ºC. Then, the solvents were evaporated under vacuum, an aqueous solution of NaOH (0.585 g in 5 mL) was added and the aqueous phase was extracted with DCM (3 x 10 mL). The combined organic layers were dried over $Na_2SO_4$ and concentrated under reduced pressure to afford a white solid (131 mg, 96% yield), that was subsequently used without further purification.

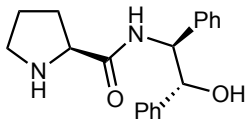

**$^1$H-NMR** ($CDCl_3$, 400 MHz): $\delta$ = 8.45 (br, 1H N**H**–CO), 7.24-7.22 (m, 6H Ph), 7.04-7.00 (m, 4H Ph), 5.28 (dd, *J* = 8.4 Hz, *J'* = 4.1 Hz, 1H), 5.05 (d, *J* = 4.1 Hz, 1H), 3.78 (dd, *J* = 9.2 Hz, *J'* = 5.2 Hz, 1H), 3.27 (br, 1H), 3.03-2.82 (m, 2H), 2.10 (br, 1H), 1.84 (sext, *J* = 6.6 Hz, 1H), 1.64 (quint, *J* = 6.6 Hz, 3H) ppm.

**PREPARATION OF *TERT*-BUTYL (S)-2-(((1*R*,2*S*)-2-HYDROXY-1,2-DIPHENYLETHYL) CARBAMOYL)PYRROLIDINE-1-CARBOXYLATE (97)[16]**

In a 25 mL round-bottomed flask, equipped with magnetic stirring, *N*-Boc-L-Proline **53** (299 mg, 1.39 mmol) and $NEt_3$ (233 μL, 169 mg, 1.67 mmol) were dissolved in dry THF (2.7 mL) and the resulting mixture was cooled down to -15 ºC. Then, a solution of ethyl chloroformate (133 μL, 152 mg, 1.40 mmol) in dry THF (1.9 mL) and a solution of (1*S*,2*R*)-2-amino-1,2-diphenylethan-1-ol (355 mg, 1.67 mmol) in dry THF (0.8 mL) were added sequentially at the same temperature, and the reaction mixture was stirred overnight at room temperature. Next, the reaction mixture was diluted with DCM (10 mL) and was washed successively with aqueous citric acid (25 mL, 30% w/w), with brine (25 mL) and with a saturated aqueous solution of $NaHCO_3$ (25 mL). After drying over $Na_2SO_4$, the solvent was eliminated under vacuum to afford a yellowish oil (446 mg, 79% yield), that was used without purification in the next step.

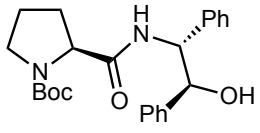


**$^1$H-NMR** ($CDCl_3$, 400 MHz): δ = 7.91 (br, 1H N**H**–CO), 7.20 (m, 6H Ph), 7.05-6.99 (m, 4H Ph), 5.25 (dd, *J* = 8.5 Hz, *J'* = 4.1 Hz, 1H), 5.11 (d, *J* = 4.1 Hz, 1H), 3.49-3.33 (m, 3H), 2.41 (br, 1H OH), 1.94-1.83 (m, 4H), 1.47 (s, 9H) ppm.

**PREPARATION OF (*S*)-*N*-((1*R*,2*S*)-2-HYDROXY-1,2-DIPHENYLETHYL)PYRROLIDINE-2-CARBOXAMIDE (89k)[16]**

In a 10 mL round-bottomed flask, equipped with magnetic stirring, a solution of *tert*-butyl (*S*)-2-(((1*R*,2*S*)-2-hydroxy-1,2-diphenylethyl)carbamoyl)pyrrolidine-1-carboxylate **97** (148 mg, 0.36 mmol) in DCM (1.3 mL) was cooled down to 0 ºC with an ice-water bath. Then, trifluoroacetic acid (1.0 mL) was added and the resulting mixture was stirred for 1 h at 0ºC. After this time, the solvents were evaporated under vacuum, an aqueous solution of NaOH (0.585 g in 5 mL) was added, and the aqueous phase was extracted with DCM (3 x 10 mL). The combined organic layers were dried over $Na_2SO_4$ and concentrated under reduced pressure to afford a white solid (207 mg, 61% yield), that was subsequently used without further purification.

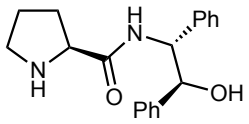

**$^1$H-NMR** ($CDCl_3$, 400 MHz): $\delta$ = 8.46 (br, 1H N**H**–CO), 7.27-7.21 (m, 6H Ph), 7.04-7.01 (m, 4H Ph), 5.28 (dd, *J* = 8.5 Hz, *J'* = 4.1 Hz, 1H), 5.06 (d, *J* = 4.1 Hz, 1H), 3.79-3.75 (m, 1H), 3.02-2.82 (m, 2H), 2.14-2.04 (m, 2H), 1.86-1.79 (m, 1H), 1.64 (quint, *J* = 6.7 Hz, 2H), 1.44 (d, *J* = 11.6 Hz, 1H) ppm.

## PREPARATION OF *TERT*-BUTYL (*S*)-2-(NEOPENTYLCARBAMOYL)PYRROLIDINE-1-CARBOXYLATE (98)

In a 50 mL round-bottomed flask, equipped with magnetic stirring, *N*-Boc-L-Proline **53** (1.00 g, 4.66 mmol) and $NEt_3$ (650 μL, 472 mg, 4.66 mmol) were dissolved in dry THF (9 mL) and the resulting mixture was cooled down to -15 ºC. Then, a solution of ethyl chloroformate (445 μL, 507 mg, 4.67 mmol) in dry THF (6.4 mL) and a solution of neopentyl amine (655 μL, 485 mg, 5.56 mmol) in dry THF (2.4 mL) were added sequentially at the same temperature, and the reaction mixture was stirred overnight at room temperature. Then, the reaction mixture was diluted with DCM (25 mL) and was washed successively with aqueous citric acid (50 mL, 30% w/w), brine (50 mL) and with a saturated aqueous solution of $NaHCO_3$ (50 mL). After drying over $Na_2SO_4$, the solvent was concentrated under vacuum to afford a yellowish oil (1.080 g, 82% yield), that was used without purification in the next step.

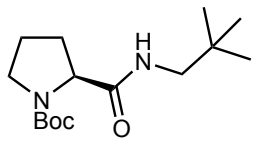

**$^1$H-NMR** ($CDCl_3$, 400 MHz): $\delta$ = 7.05 (br, 1H N**H**–CO), 4.30 (m, 1H), 3.42-3.34 (m, 3H), 3.08-3.01 (m, 2H), 1.88 (m, 3H), 1.47 (s, 9H), 0.90 (s, 9H) ppm.

## PREPARATION OF (*S*)-*N*-NEOPENTYLPYRROLIDINE-2-CARBOXAMIDE (89l)

In a 100 mL round-bottomed flask, equipped with magnetic stirring, *tert*-butyl (*S*)-2-(neopentylcarbamoyl)pyrrolidine-1-carboxylate **98** (1.080 g, 3.79 mmol) was dissolved in DCM (11.2 mL) and the solution was cooled down to 0 ºC with an ice-water bath. Then, trifluoroacetic acid (8.8 mL) was added and the resulting mixture was stirred for 1 h at 0ºC. After this time, the solvents were evaporated under vacuum, an aqueous solution of NaOH (5.113 g in 25 mL) was added and the aqueous phase was extracted with DCM (3 x 30 mL). The combined organic layers were dried over $Na_2SO_4$ and concentrated under reduced pressure to afford a partially solidified oil (672 mg, 97% yield), that was not purified.

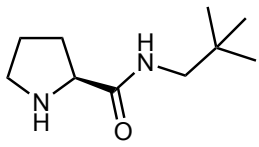

**$^{1}$H-NMR** ($CDCl_3$, 400 MHz): $\delta$ = 7.79 (bs, 1H N**H**–CO), 3.76 (dd, *J* = 9.2 Hz, *J'* = 5.1 Hz, 1H), 3.12 (dd, *J* = 13.2 Hz, *J'* = 7.2 Hz, 1H), 3.03 (m, 1H), 2.96-2.88 (m, 2H), 2.19-2.09 (m, 1H), 1.97-1.90 (m, 2H, 1H + N**H** pyrrolidine), 1.75-1.68 (m, 2H), 0.90 (s, 9H) ppm. **$^{13}$C-NMR** ($CDCl_3$, 400 MHz): $\delta$ = 174.9, 60.7, 50.0, 47.3, 31.9, 30.9, 27.2, 26.2 ppm. **HRMS (ESI):** *m/z* calculated for $C_{10}H_{21}N_2O$ $[M+H]^+$, 185.1648; found 185.1649. **$[\alpha]_D$:** -0.55 (c 0.98, $CHCl_3$).

## 7.9. AMINE-CATALYZED DIELS-ALDER REACTIONS

### GENERAL PROCEDURE FOR THE AMINE-CATALYZED DIELS-ALDER CYCLOADDITION OF (*E*)-CINNAMALDEHYDE AND CYCLOPENTADIENE UNDER THERMAL CONDITIONS[208]

The corresponding catalyst (0.025 mmol, 5 mol%), *p*-toluenesulfonic acid monohydrate (5 mg, 0.026 mmol, 5 mol%) and 1 mL of solvent[a] were placed in a 3 mL vial, equipped with magnetic stirring, and the resulting mixture was stirred for 10 min. At this point, (*E*)-cinnamaldehyde (63 μL, 66 mg, 0.50 mmol) and, after 30 min, freshly distilled cyclopentadiene (125 μL, 98 mg, 1.48 mmol) were added and the reaction mixture was stirred for 72 h at room temperature. The mixture was then poured over DCM (10 mL) and washed with an aqueous saturated solution of $NaHCO_3$ (2 x 30 mL) until no green color remained or reappeared. The organic layer was dried over $MgSO_4$ and concentrated under reduced pressure. The *endo*/*exo* ratio of the Diels-Alder adducts was determined via $^1$H-NMR analysis of the crude.

When using MeOH as solvent, the Diels-Alder adduct was obtained in its acetal form, that was no further purified and, subsequently, the deprotection was performed. The crude was diluted with DCM (2 mL) and TFA (1 equivalent) and $H_2O$ (1 equivalent) were added. After stirring for 2 h at room temperature, the mixture was diluted with DCM and washed with an aqueous saturated solution of $NaHCO_3$ and brine. The organic layer was dried over $MgSO_4$ and concentrated under reduced pressure to obtain the corresponding aldehyde adducts.

When using toluene as solvent, the Diels-Alder adducts were purified via flash column chromatography on silica gel using hexane/DCM (1/1) as eluent.

The aldehyde adducts were derivatized by reduction with excess of $NaBH_4$ in MeOH (10 mL) to obtain the alcohol adducts to determine the enantiomeric rate through HPLC.

[a] MeOH or Toluene

**GENERAL PROCEDURE FOR THE AMINE-CATALYZED DIELS-ALDER CYCLOADDITION OF (*E*)-CINNAMALDEHYDE AND CYCLOPENTADIENE UNDER PHOTOCHEMICAL CONDITIONS**

In a 3 mL vial, equipped with magnetic stirring, (*E*)-cinnamaldehyde (63 μL, 66 mg, 0.50 mmol), freshly distilled cyclopentadiene (125 μL, 98 mg, 1.48 mmol), *p*-toluenesulfonic acid monohydrate (5 mg, 0.026 mmol, 5 mol%) and the corresponding catalyst (0.025 mmol, 5 mol %)[a] were dissolved in 1 mL of previously degassed solvent[b]. The vial was closed with a septum, a high vacuum was applied for 10 minutes and the vial was backfilled with Ar. The process was repeated for 3 times in order to remove all the dissolved gasses. At this point, the vial was sealed with Parafilm®, placed in the corresponding photoreactor[c] and stirred for 72 h. A fan placed above the photoreactor was used for cooling the system. The mixture was then diluted with DCM (10 mL) and washed with an aqueous saturated solution of $NaHCO_3$ (2 x 30 mL) until no green color remained or reappeared. The organic layer was dried over $MgSO_4$ and concentrated under reduced pressure. The *endo*/*exo* ratio of the Diels-Alder adducts was determined via $^1$H-NMR analysis of the crude.

When using MeOH as solvent, the Diels-Alder adduct was obtained in its acetal form, that was no further purified and, subsequently, the deprotection was performed following the procedure explained above.

When using toluene as solvent, the Diels-Alder adducts were purified via flash column chromatography on silica gel using hexane/DCM (1/1) as eluent.

The aldehyde adducts were derivatized by reduction with excess of $NaBH_4$ in MeOH (10 mL) to obtain the alcohol adducts to determine the enantiomeric rate through HPLC.

[a] Employing bifunctional catalytic system: 0.025 mmol of catalyst (5 mol%); employing dual catalytic system: 0.025 mmol of $Na_4TPPS_4$ or $H_2TPPS_4$ as photocatalyst (5 mol%) and 0.025 of imidazolidinone as organocatalyst (5 mol%).

[b] Employing **17b-*cis***, **17b-*trans***, **17d** and TPP **36** as photocatalyst: Toluene; employing $Na_4TPPS_4$: MeOH/$H_2O$ (95/5); employing $H_2TPPS_4$: MeOH.

[c] Photoreactor 1: 3 white LEDs, 1 x LED = 450 Lumens, 4 W (Figure 86, left)

Photoreactor 2: white LEDs, 18 W (Figure 86, right)

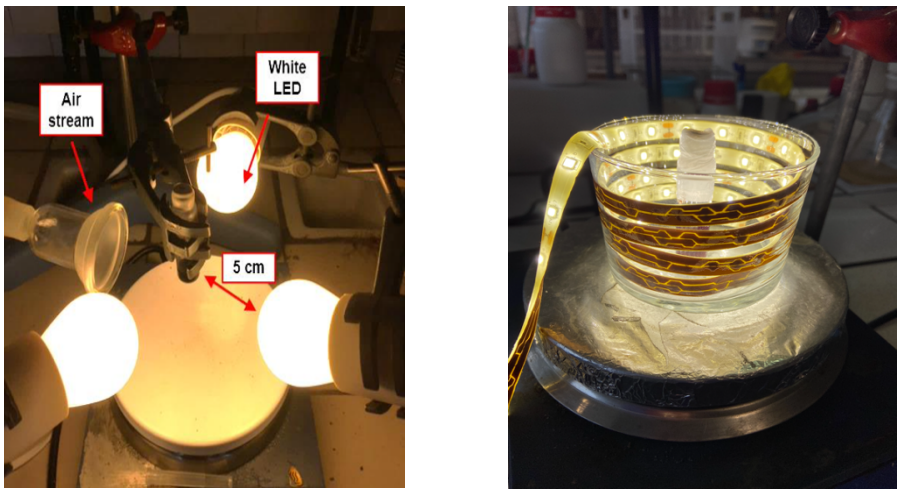


Figure 86. Experimental setting for the photocatalytic reactions, photoreactor 1 (left) and photoreactor 2 (right).

## (1*R**,2*S**,3*S**,4*S**)-3-PHENYLBICYCLO[2.2.1]HEPT-5-ENE-2-CARBALDEHYDE ($60_{ENDO}$)[208]

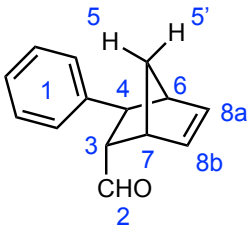


Yellowish oil. **$^1$H-NMR** ($CDCl_3$, 400 MHz): δ = 9.60 (d, *J* = 2.2 Hz, $1H_2$), 7.36-7.12 (m, $5H_1$), 6.42 (dd, *J* = 5.5 Hz, *J'* = 3.4 Hz, $1H_{8a/8b}$), 6.18 (dd, *J* = 5.5 Hz, *J'* = 2.7 Hz, $1H_{8b/8a}$), 3.34 (m, $1H_{6/7}$), 3.13 (m, $1H_{7/6}$), 3.09 (d, *J* = 4.7 Hz, $1H_4$), 2.98 (m, $1H_3$), 1.81 (d, *J* = 9.2 Hz, $1H_5$), 1.62 (dm, *J* = 9.2 Hz, $1H_{5'}$) ppm. **HPLC** (Phenomenex i-cellulose 5 column; hexane/IPA 0.8%; flow rate 1 mL/min; 210 nm) $t_R$ = 40.5 min (2*R*,3*R*), 46.3 min (2*S*,3*S*). After converting the product to the corresponding alcohol with excess of $NaBH_4$ in MeOH.

## (1S*,2S*,3S*,4R*)-3-PHENYLBICYCLO[2.2.1]HEPT-5-ENE-2-CARBALDEHYDE ($60_{EXO}$)[208]

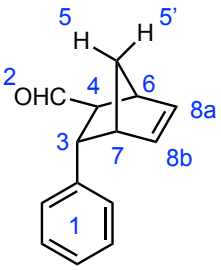


Yellowish oil. **$^1$H-NMR** ($CDCl_3$, 400 MHz): δ = 9.92 (d, *J* = 2 Hz, $1H_2$), 7.36-7.12 (m, $5H_1$), 6.34 (dd, *J* = 5.8 Hz, *J'* = 3.4 Hz, $1H_{8a/8b}$), 6.08 (dd, *J* =5.4 Hz, *J'* = 2.8 Hz, $1H_{8b/8a}$), 3.73 (t, *J* = 3.9 Hz, $1H_{6,7}$), 3.22 (m, $1H_{7/6}$), 3.09 (d, *J* = 4.7 Hz, $1H_4$), 2.98 (m, $1H_3$), 2.59 (dm, *J* = 4.9 Hz, $1H_5$), 1.42 (dm, *J* = 9.2 Hz, $1H_{5'}$) ppm. **HPLC** (Phenomenex i-cellulose 5 column; hexane/IPA 0.8%; flow rate 1 mL/min; 210 nm) $t_R$ = 33.6 min (2*R*,3*R*), 43.4 (2*S*,3*S*). After converting the product to the corresponding alcohol with excess of $NaBH_4$ in MeOH.

## 7.10. ORGANOCATALYTIC PHOTOREDOX α-ALKYLATION OF ALDEHYDES

### GENERAL PROCEDURE FOR THE DUAL ORGANOCATALYTIC PHOTOREDOX α-ALKYLATION OF ALDEHYDES WITH ETHYL DIAZOACETATE[169]

Sodium 4,4',4'',4'''-(porphyrin-5,10,15,20-tetrayl)tetrabenzenesulfonate **62** (2.6 mg, 0.0025 mmol), $LiBF_4$ (4.7 mg, 0.05 mmol), the corresponding organocatalyst (0.10 mmol, 0.40 equiv.) and the suitable aldehyde (0.25 mmol) were introduced in a 3 mL glass vial, equipped with magnetic stirring. Then, previously degassed DMSO (2 mL) was added via syringe, the vial was tightly stoppered with a rubber septum, and a high vacuum was applied for 5-10 min. At this point, the vial was backfilled with Ar, in order to remove all the dissolved gases, and ethyl diazoacetate (32 μL, 35 mg, 0.30 mmol, 1.2 equivs.) was added via syringe. The vial was placed in the photoreactor set up (Figure 86, right) and the reaction mixture was stirred for 5 h at room temperature under visible light irradiation (white LEDs, 18 W). A fan placed above the photoreactor was used for cooling the system. After this time, the light was turned off and the mixture was diluted with AcOEt (5 mL) and transferred to a separatory funnel. The organic phase was extracted with water (3 x 10 mL), dried over $Na_2SO_4$ and the solvent was removed under reduced pressure, to give the corresponding crude α-alkylated aldehyde as a yellow oil, that was characterized via $^1$H-NMR and was submitted to derivatization by Wittig reaction with ethyl triphenylphosphoranyl acetate without further purification.

### REPRESENTATIVE PROCEDURE FOR THE BIFUNCTIONAL ORGANOCATALYTIC PHOTOREDOX α-ALKYLATION OF ALDEHYDES WITH ETHYL DIAZOACETATE

The bifunctional catalyst[a], $LiBF_4$ (4.7 mg, 0.05 mmol) and 3-phenylpropionaldehyde **67** (34 μL, 34 mg, 0.25 mmol) were introduced in a 3 mL glass vial, equipped with magnetic stirring. Then, previously degassed DMSO (2 mL) was added via syringe, the vial was tightly stoppered with a rubber septum, and a high vacuum was applied for 5-10 min. At this point, the vial was backfilled with Ar in order to remove all the dissolved gases, and ethyl diazoacetate (32 μL, 35 mg, 0.30 mmol, 1.2 equivalents) was added via syringe. The vial was placed in the photoreactor set up (Figure 86, right) and the reaction mixture was stirred for 5 h at room temperature under visible-light irradiation (white LEDs, 18 W). A fan placed above the photoreactor was used for cooling the system. After this time, the light was turned off and the mixture was diluted with AcOEt (5 mL) and

transferred to a separatory funnel. The organic phase was extracted with water (3 x 10 mL), dried over $NaSO_4$ and the solvent was removed under reduced pressure, obtaining the corresponding crude $\alpha$-alkylated aldehyde as a yellow oil, that was characterized via $^1$H-NMR.

[a] Bifunctional catalyst employed: (*S*)-N-(4-(10,15,20-triphenylporphyrin-5-yl)benzyl)pyrrolidine-2-carboxamide **18b** and sodium (*S*)-4,4',4''-(20-(pyrrolidine-2-ylmethyl)porphyrin-5,10,15-triyl)tribenzenesulfonate **44**. Quantities used: 1, 5, 10 and 20 mol%.

### (*S*)-ETHYL 3-BENZYL-4-OXOBUTANOATE (69)

The racemic compound **69** was synthesized as explained above, but using piperidine (0.10 mmol, 0.40 equiv.) as organocatalyst.

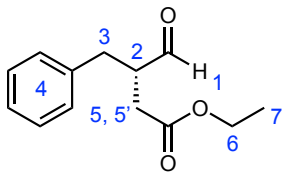


Yellow oil (97% yield). **$^1$H-NMR** ($CDCl_3$, 400 MHz): $\delta$ = 9.79 (br, $1H_1$), 7.30-7.16 (m, $5H_4$), 4.11 (q, *J* = 7.1 Hz, $2H_6$), 3.17-3.08 (m, $2H_3$), 2.77-2.71 (m, $1H_2$), 2.67-2.61 (m, $1H_5$), 2.40 (dd, *J* = 16.7 Hz, *J'* = 4.9 Hz, $1H_{5'}$), 1.23 (t, *J* = 7.1 Hz, $3H_7$) ppm. **$^{13}$C-NMR** ($CDCl_3$, 400 MHz): $\delta$ = 202.4, 171.8, 137.8, 129.1, 128.8, 126.8, 60.8, 49.3, 34.7, 37.8, 15.2 ppm.

### ETHYL 3-METHYL-4-OXOBUTANOATE (79)

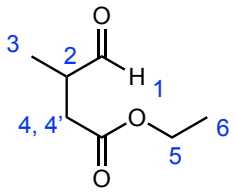


Yellow oil (75% yield). **$^1$H-NMR** ($CDCl_3$, 400 MHz): $\delta$ = 9.70 (br, $1H_1$), 4.14 (q, *J* = 7.1 Hz, $2H_5$), 2.86 (m, $1H_2$), 2.74 (dd, *J* = 16.4 Hz, *J'* = 7.0 Hz, $1H_4$), 2.39 (dd, *J* = 16.4 Hz, *J'* = 6.3 Hz, $1H_{4'}$), 1.26 (t, *J* = 7.1 Hz, $3H_6$), 1.20 (d, *J* = 7.3 Hz, $3H_3$) ppm.

### ETHYL 3-FORMYLHEPTANOATE (80)

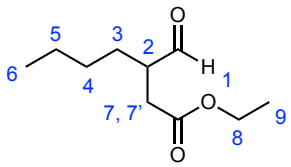


Yellow oil (95% yield, 44 %ee). **$^1$H-NMR** ($CDCl_3$, 400 MHz): $\delta$ = 9.72 (br, $1H_1$), 4.15 (q, *J* = 7.1 Hz, $2H_8$), 2.82 (m, $1H_2$), 2.71 (dd, *J* = 16.4 Hz, *J'* = 8.1 Hz, $1H_7$), 2.42 (dd, *J* = 16.4 Hz, *J'* = 5.2 Hz, $1H_{7'}$), 1.72 (m, $2H_3$), 1.34 (m, $4H_{4,5}$), 1.26 (t, *J* = 7.1 Hz, $3H_9$), 0.91 (t, *J* = 6.8 Hz, $3H_6$) ppm. **$^{13}$C-NMR** ($CDCl_3$, 400 MHz): $\delta$ = 203.1, 172.0, 60.8, 47.7, 33.2, 28.9, 28.3, 27.2, 22.7, 13.8 ppm.

## ETHYL 3-FORMYLNONANOATE (81)

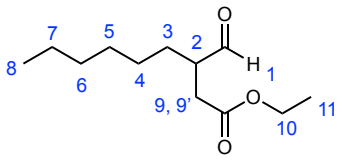

Yellow oil (90% yield, 84% ee). **$^1$H-NMR** ($CDCl_3$, 400 MHz): $\delta$ = 9.72 (br, $1H_1$), 4.15 (q, *J* = 7.2 Hz, $2H_{10}$), 2.82 (m, $1H_2$), 2.71 (dd, *J* = 16.4 Hz, *J'* = 8.2 Hz, $1H_9$), 2.41 (dd, *J* = 16.4 Hz, *J'* = 5.3 Hz, $1H_{9'}$), 1.30-1.24 (m, 13H, $10H_{3\text{-}7}$ + $3H_{11}$), 0.88 (m, $3H_8$) ppm. **$^{13}$C-NMR** ($CDCl_3$, 400 MHz): $\delta$ = 203.1, 172.0, 60.8, 47.8, 33.2, 31.6, 29.3, 28.6, 27.2, 26.7, 22.5, 14.0 ppm.

## ETHYL 3-FORMYL-4-(4-METHOXYPHENYL)BUTANOATE (83)

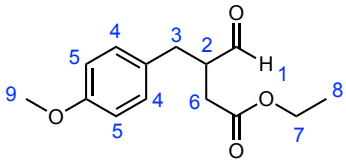

Yellow oil (88% yield). **$^1$H-NMR** ($CDCl_3$, 400 MHz): $\delta$ = 9.78 (d, *J* = 0.4 Hz, $1H_1$), 7.09 (d, *J* = 8.7 Hz, $2H_5$), 6.85 (d, *J* = 8.7 Hz, $2H_4$), 4.09 (q, *J* = 7.2 Hz, $2H_7$), 3.78 (s, $3H_9$), 3.07 (m, $2H_3$), 2.72-2.60 (m, 2H, $1H_2$ + $1H_6$), 2.40 (dd, *J* = 16.8 Hz, *J'* = 5.2 Hz, $1H_6$) ppm.

## ETHYL 3-(3-CHLOROPHENYL)-4-OXOBUTANOATE (84)

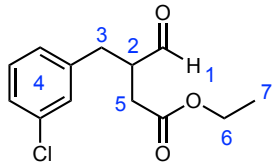

Yellow oil (79% yield). **$^1$H-NMR** ($CDCl_3$, 400 MHz): $\delta$ = 9.78 (s, $1H_1$), 7.24-7.07 (m, $4H_4$), 4.12 (q, *J* = 7.1 Hz, $2H_6$), 3.09 (m, $2H_3$), 2.75-2.61 (m, 2H, $1H_2$ + $1H_5$), 2.40 (dd, *J* = 16.8 Hz, *J'* = 5.1 Hz, $1H_5$), 1.24 (t, *J* = 7.1 Hz, $3H_7$) ppm.

## ETHYL 4-CYCLOHEXYL-3-FORMYLBUTANOATE (85)

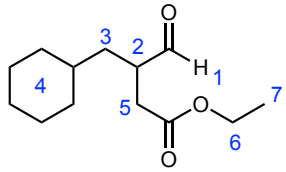

Yellow oil (88% yield). **$^1$H-NMR** ($CDCl_3$, 400 MHz): $\delta$ = 9.70 (d, *J* = 1.2 Hz, $1H_1$), 4.15 (q, *J* = 7.1 Hz, $2H_6$), 2.89 (m, $1H_2$), 2.67 (dd, *J* = 16.6 Hz, *J'* = 8.3 Hz, $1H_5$), 2.40 (dd, *J* = 16.6 Hz, *J'* = 5.1 Hz, $1H_5$), 2.32 (m, $1H_3$), 1.25 (m, 15H, $1H_3$, + $11H_4$ + $3H_7$) ppm.

**ETHYL 3-FORMYL-4-METHYLPENTANOATE (86)**

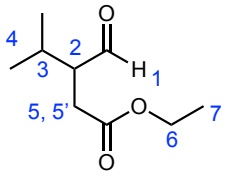


Yellow oil (99% yield, 66% ee). **$^{1}$H-NMR** ($CDCl_3$, 400 MHz): $\delta$ = 9.76 (s, $1H_1$), 4.13 (q, $J$ = 7.2 Hz, $2H_6$), 2.98-2.80 (m, 2H, $1H_2$ + $1H_5$), 2.75-2.69 (m, $1H_3$), 2.33 (dd, $J$ = 16.6 Hz, $J'$ = 4.1 Hz, $1H_{5'}$), 1.26 (t, $J$ = 7.2 Hz, $3H_7$), 0.90 (d, $J$ = 8.2 Hz, $6H_4$) ppm. **$^{13}$C-NMR** ($CDCl_3$, 400 MHz): $\delta$ = 203.4, 172.5, 60.7, 53.6, 29.8, 27.2, 20.2, 19.2 ppm.

When using compound **89f** as organocatalyst, a different product from the $\alpha$-alkylated was obtained in both thermal and photochemical conditions. The photochemical procedure is the same as explained before for the other organocatalysts. The thermal procedure is explained below.

(*S*)-*N*-benzylpyrrolidine-2-carbothioamide **89f** (22.01 mg, 0.10 mmol), $LiBF_4$ (4.7 mg, 0.05 mmol) and 3-phenylpropionaldehyde (14 $\mu$L, 010 mmol) were introduced in a 3 mL glass vial, equipped with magnetic stirring and left stirring for 3 h at room temperature. At this point, the reaction mixture was diluted with AcOEt (5 mL) and transferred to a separatory funnel. The organic phase was extracted with water (3 x 10 mL), dried over $NaSO_4$ and the solvent was removed under reduced pressure, obtaining the corresponding crude, that was purified via flash chromatography through silica gel, using a mixture of hexane/AcOEt (from 8/1 to 3/1) as eluent. The *endo*/*exo* ratio was determined via $^{1}$H-NMR analysis of the reaction crude and the determination of each diastereomer was carried out through $^{1}$H-$^{1}$H COSY, HSQC and $^{1}$H-NOESY experiments.

**(3*R*,7a*S*)-2-BENZYL-3-PHENETHYLHEXAHYDRO-1H-PYRROLO [1,2-c]IMIDAZOLE-1-THIONE ($101_{EXO}$)**

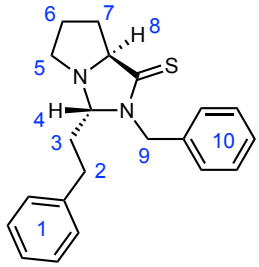


Yellow oil (7 mg, 21% yield). **$^{1}$H-NMR** ($CDCl_3$, 400 MHz): $\delta$ = 7.38-7.06 (m, 10H, $5H_1$ + $5H_{10}$), 5.71 (d, $J$ = 14.7 Hz, $1H_9$), 4.29 (t, $J$ = 6.6 Hz, $1H_4$), 4.20 (d, $J$ = 8.6 Hz, $1H_8$), 4.08 (d, $J$ = 14.7 Hz, $1H_{9'}$), 3.09-3.04 (m, $1H_5$), 2.80-2.75 (m, $1H_2$), 2.66-2.58 (m, $2H_{2'}$), 2.34 (q, $J$ = 7.2 Hz, $2H_3$), 2.23 (q, $J$ = 8.8 Hz, $1H_{5'}$), 2.04-1.97 (m, $1H_7$), 1.83-1.66 (m, 3H, $2H_6$ + $1H_{7'}$) ppm. **$^{13}$C-NMR** ($CDCl_3$, 400 MHz): $\delta$ = 205.9 (C=S), 140.8, 134.8, 128.9 (2C), 128.5 (2C), 128.2 (2C), 128.1 (2C), 126.1, 85.8 ($C_8$), 76.4 ($C_4$), 55.9 ($C_5$), 48.7 ($C_9$), 34.6 ($C_7$), 30.9 ($C_2$), 30.6 ($C_3$), 24.7 ($C_6$) ppm. **MS (ESI):** *m/z* calculated for $C_{21}H_{24}N_2S$ $[M+H]^+$, 337.17; found 337.17.

**(3*S*,7a*S*)-2-BENZYL-3-PHENETHYLHEXAHYDRO-1H-PYRROLO [1,2-c]IMIDAZOLE-1-THIONE ($101_{ENDO}$)**

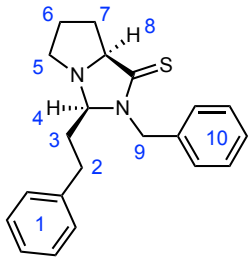


Yellow oil (13 mg, 39% yield). **$^1$H-NMR** ($CDCl_3$, 400 MHz): $\delta$ = 7.32-7.06 (m, 10H, $5H_1$ + $5H_{10}$), 5.23 (d, *J* = 15.1 Hz, $1H_9$), 4.79 (d, *J* = 15.1 Hz, $1H_{9'}$), 4.68 (dd, *J* = 11.3 Hz, *J'* = 3.0 Hz, $1H_4$), 4.07 (dd, *J* = 9.2 Hz, *J'* = 3.4 Hz, $1H_8$), 2.95 (t, *J* = 7.0 Hz, $1H_5$), 2.89-2.83 (m, $1H_2$), 2.71-2.63 (m, $1H_{2'}$), 2.58-2.51 (m, $1H_7$), 2.44-2.36 (m, 2H, $1H_{5'}$ +$1H_{7'}$), 2.24-2.16 (m, $1H_3$), 1.92-1.83 (m, 3H, $1H_{3'}$ + $2H_6$) ppm. **$^{13}$C-NMR** ($CDCl_3$, 400 MHz): $\delta$ = 206.0 (C=S), 140.8, 134.8, 128.9 (2C), 128.5 (2C), 128.2 (2C), 128.1 (2C), 126.1, 82.0 ($C_4$), 76.6 ($C_8$), 48.7 ($C_9$), 45.6 ($C_5$), 31.6 ($C_2$), 30.1 ($C_3$), 28.4 ($C_7$), 24.3 ($C_6$) ppm. **MS (ESI):** *m/z* calculated for $C_{21}H_{24}N_2S$ $[M+H]^+$, 337.17; found 337.17.

**GENERAL PROCEDURE FOR THE WITTIG DERIVATIZATION OF THE ALKYLATED ALDEHYDES**

In a 25 mL round-bottomed flask, equipped with magnetic stirring and a Dimroth reflux condenser, the corresponding crude alkylated aldehyde (0.25 mmol, 1.0 equivalent) and ethyl (triphenylphosphoranylidene) acetate (0.75 mmol, 3 equivalents) were dissolved in freshly distilled DCM (5-7 mL) and the resulting solution was heated up to reflux and stirred for 2 h. After cooling to room temperature, the organic phase was washed with aqueous 1 M HCl (15 mL) and the aqueous phase was extracted with DCM (3 x 15 mL). The combined organic layers were washed with a saturated aqueous solution of $NaHCO_3$ (2 x 15 mL). The new aqueous phase was extracted with DCM (3 x 15 mL) and the combined organic layers were dried over $Na_2SO_4$ and concentrated under vacuum to afford a yellow solid that was purified via flash column chromatography on silica gel using hexane/AcOEt (5/1) as eluent, affording a yellowish oil.

## DIETHYL (*E*)-4-BENZYLHEX-2-ENEDIOATE (91)

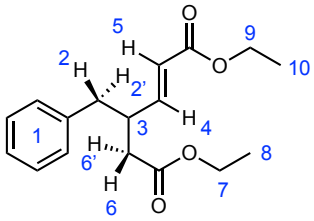

Yellow oil. **$^1$H-NMR** ($CDCl_3$, 400 MHz): δ = 7.28-7.15 (m, $5H_1$), 6.86 (dd, *J* = 15.7 Hz, *J'* = 8.2, $1H_4$), 5.79 (d, *J* = 15.7 Hz, $1H_5$), 4.17 (q, *J* = 6.1 Hz, $2H_7$), 4.10 (q, *J* = 6.6 Hz, $2H_9$), 3.25 (m, $1H_3$), 2.99 (dd, *J* = 12.8 Hz, *J'* = 8.1 Hz, $1H_2$), 2.73 (dd, *J* = 12.8 Hz, *J'* = 8.1 Hz, $1H_{2'}$), 2.61 (dd, *J* = 15.6 Hz, *J'* = 8.2 Hz, $1H_6$), 2.37-2.28 (m, $1H_{6'}$), 1.30-1.21 (m, 6H, $3H_8$ + $3H_{10}$) ppm. **HPLC** (Phenomenex i-cellulose 5 column; Hexane/IPA 1%; flow rate 1 mL/min; 218 nm) $t_R$ = 15.8 min (*S*), 17.9 min (*R*).

## DIETHYL (*E*)-4-BUTYLHEX-2-ENEDIOATE (109)

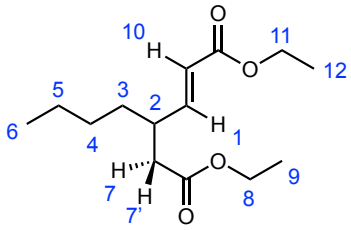

Yellow oil. **$^1$H-NMR** ($CDCl_3$, 400 MHz): δ = 6.85 (dd, *J* = 15.7 Hz, *J'* = 8.7 Hz, $1H_1$), 5.85 (d, *J* = 15.7 Hz, $1H_{10}$), 4.21-4.08 (m, 4H, $2H_8$ + $2H_{11}$), 2.70 (m, $1H_2$), 2.45-2.32 (m, $2H_{7, 7'}$), 1.33-1.22 (m, 6H, $3H_9$ + $3H_{12}$), 0.92-0.87 (m, $9H_{3-6}$) ppm. **HPLC** (Phenomenex i-cellulose 5 column; Hexane/IPA 1%; flow rate 1 mL/min; 218 nm) $t_R$ = 20.4 min (*S*), 21.9 min (*R*).

## DIETHYL (*E*)-4-HEXYLHEX-2-ENEDIOATE (110)

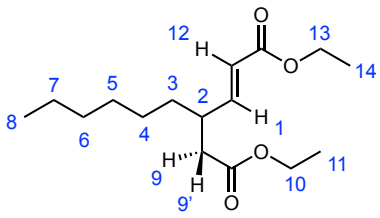

Yellow oil. **$^1$H-NMR** ($CDCl_3$, 400 MHz): δ = 6.77 (dd, *J* = 15.7 Hz, *J'* = 8.7 Hz, $1H_1$), 5.85 (d, *J* = 15.7 Hz, $1H_{12}$), 4.20-4.09 (m, 4H, $2H_{10}$ + $2H_{13}$), 2.71 (m, $1H_2$), 2.44-2.31 (m, $2H_{9, 9'}$), 1.32-1.22 (m, 6H, $3H_{11}$ + $3H_{14}$), 0.90-0.86 (m, $13H_{3-8}$) ppm. **HPLC** (Phenomenex i-cellulose 5 column; Hexane/IPA 1%; flow rate 1 mL/min; 218 nm) $t_R$ = 20.6 min (*S*), 22.0 min (*R*).

**DIETHYL (*E*)-4-ISOPROPYLHEX-2-ENEDIOATE (111)**

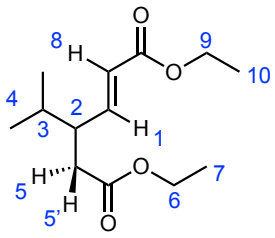

Yellow oil. **$^1$H-NMR** ($CDCl_3$, 400 MHz): δ = 6.81 (dd, *J* =15.8 Hz, *J'* = 9.3 Hz, $1H_1$), 5.84 (d, *J* = 15.6 Hz, $1H_8$), 4.20-4.09 (m, 4H, $2H_9$ + $2H_6$), 2.60 (m, $1H_2$), 2.50 (dd, *J* = 15.1 Hz, *J'* = 9.2 Hz, $1H_5$), 2.35 (dd, *J* = 15.1 Hz, *J'* = 9.2 Hz, $1H_{5'}$), 1.74 (m, *J* = 6.8 Hz, $1H_3$), 1.30-1.21 (m, 6H, $3H_{10}$ + $3H_7$), 0.93-0.88 (d, *J* = 6.8 Hz, $6H_4$) ppm. **HPLC** (Phenomenex i-cellulose 5 column; Hexane/IPA 1%; flow rate 1 mL/min; 218 nm) $t_R$ = 20.3 min (*S*), 21.9 min (*R*).

**(*S*)-2-BENZYLBUTANE-1,4-DIOL (102)[195]**

In a 50 mL round-bottomed flask, equipped with magnetic stirring, the enantiopure aldehyde **69** (74.8 mg, 0.34 mmol) was dissolved in dry THF (3 mL). Then, $LiAlH_4$ (51.6 mg, 1.36 mmol) was added and the system was filled with Ar and left stirring for 24 h. At this point, 75 μL of $H_2O$ were carefully added to the reaction mixture, followed by the slow sequential addition of 75 μL of a 15 % (w/v) NaOH aqueous solution and by 75 μL of $H_2O$. At this point, the precipitate color change from grey to white was observed. Once the color change was complete, 3 mL of diethyl ether were added and the aqueous phase was extracted several times with AcOEt, dried over $MgSO_4$, filtered and evaporated under reduced pressure to obtain a yellowish oil, that was purified via flash chromatography through silica gel, using a mixture of hexane/AcOEt as eluent, affording the desired product (37 mg, 60% yield) as a yellowish oil.

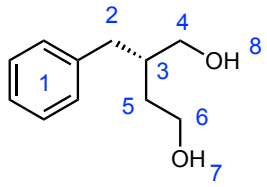

Yellowish oil. **$^1$H-NMR** ($CDCl_3$, 400 MHz): δ = 7.29-7.16 (m, $5H_1$), 3.76-3.49 (m, 4H, $2H_4$ + $2H_6$), 3.04 (m, $1H_3$), 2.65 (m, $2H_2$), 1.99 (br, 2H, $1H_7$ + $1H_8$), 1.81-1.61 (m, $2H_5$) ppm. **$[\alpha]_D$:** -16.6 (c 0.012, AcOEt). [Literature: **$[\alpha]_D$:** +6.6 (c 1.5, EtOAc) for the (*R*)-enantiomer).[195]

# APPENDICES

# APPENDIX 1: IMIDAZOLIDINETHIONES FROM THE REACTION BETWEEN PROLINETHIOAMIDE 89f AND ALDEHYDES

In the light of the results obtained for organocatalyst **89d** (see Chapter 5, Table 11, Entry 4), we hypothesized that the enantiomeric excess could have a directly proportional relationship to the acidic character of the hydrogen bond donor group. Chiral prolinethioamide derivatives had previously been used in the group as asymmetric organocatalysts in aldol reactions,[194] and to validate our hypothesis, we decided to use compound **89f** as the chiral catalyst, changing the amide group for a thioamide one.

The $^1$H-NMR analysis of the crude reaction showed the appearance of a new set of signals at a chemical shift between 5.71 and 4.05 ppm, while neither the $\alpha$-alkylated product **69** nor the aldol self-condensation product **70** could be detected. After chromatographic purification of the reaction crude, we could isolate two different compounds in a 2:1 ratio, that on the basis their $^1$H NMR spectra appeared to be cyclic imidazolidinethiones arising from the condensation of the starting aldehyde **67** with the prolinethioamide **89f**.

In fact, a literature search revealed[17] that although the thioamide group can generate a stronger hydrogen bond with an aldehyde than an amide group, it can also promote a faster competitive secondary reaction leading to the formation of the corresponding imidazolidinethione by condensation with the aldehyde (Scheme 47).

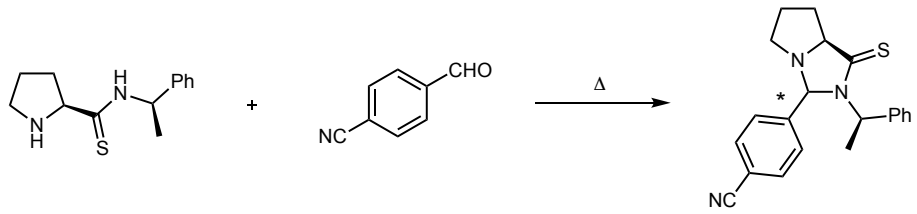


Scheme 47. Reported thermal formation of an imidazolidinethione by condensation of a thioamide organocatalyst with an aldehyde.

The two new compounds isolated could correspond therefore to the pair of *exo*/*endo* diastereomers of a cyclic imidazolidinethione, according to both the different multiplicity and chemical shift of the $^1$H-NMR signals observed. After performing a deeper $^1$H-NMR analysis, complemented by an IR spectrum, a $^{13}$C-NMR and a MS (ESI) for both compounds (Figures 87

and 88), the formation of the two possible diastereomers of imidazolidinethione **101** was fully confirmed.

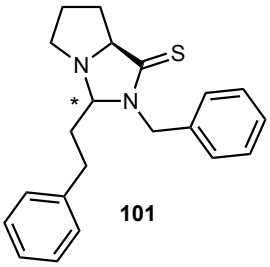


**101**

$^{13}$C-NMR: $\delta$ = 205.1 ppm
IR: $\nu$ = 1494.88 cm$^{-1}$
1471.21 cm$^{-1}$
EM (ESI): *m/z* = 337.17 (MH$^{+}$)

Figure 87. Key signals observed in the spectroscopical characterization of the two diastereomers of imidazolidinethione **101**.

Among other signals, the $^{13}$C-NMR spectra showed a signal corresponding to a quaternary carbon at a chemical shift of 205.1 ppm, corresponding to the thioamide carbon. The presence of a thioamide was subsequently confirmed by the IR spectra, that exhibited two bands at 1495 cm$^{-1}$ and at 1471 cm$^{-1}$, corresponding to the C=S and C-S stretchings, respectively. The MS (ESI) spectra showed exactly the calculated molecular mass of imidazolidinethione **101** for both compounds. Finally, the assignments of the *exo*/*endo* diastereomers to each $^{1}$H-NMR spectra were performed through $^{1}$H-$^{1}$H COSY, HSQC and $^{1}$H-$^{1}$H NOESY (Figure 88).

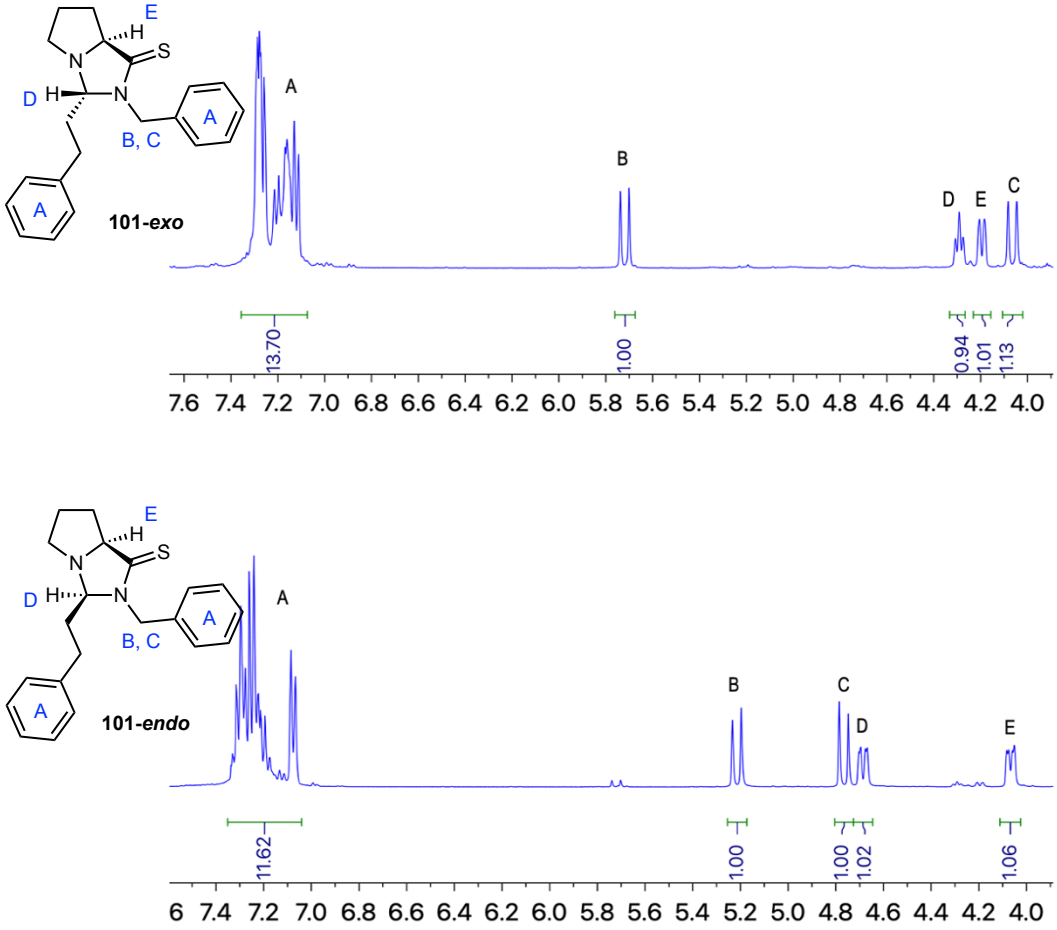


Figure 88. Assignment of the $^{1}$H-NMR spectra to the corresponding *exo* (top) and *endo* (bottom) diastereomers.

The assignments of the *exo*/*endo* diastereomers to each $^{1}$H-NMR spectra was performed through the $^{1}$H-$^{1}$H COSY spectra, since $H_D$ and $H_E$ can only be correlated in the *endo* diastereomer.

To confirm the formation of the imidazolidinethione, we decided to carry out the condensation reaction with an aldehyde not capable of giving rise the $\alpha$-alkylation product, choosing pivalaldehyde **112** for this purpose. Thus, the two possible products to be obtained should be (a) the unreacted starting aldehyde and (b) the corresponding imidazolidinethione. The reaction was carried out under both thermal (Scheme 48a) and photochemical (Scheme 48b) conditions, obtaining in both cases the corresponding imidazolidinethione as a single diastereomer (*exo*).

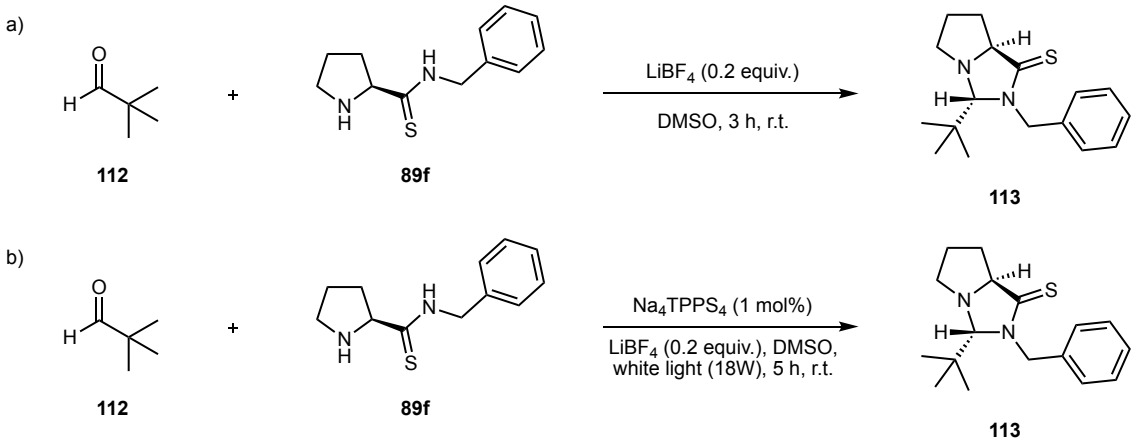


Scheme 48. Imidazolidine reaction between pivaldehyde **112** and organocatalyst **89f** under a) thermal and b) photochemical conditions.

Finally, when the reaction was carried out with aldehydes **67** and **71-73** in both thermal and photochemical conditions, we observed that the *endo* diastereomer was in general the major one and that its proportion in the mixture always increased when the reaction was carried out under photochemical conditions (Table 15).

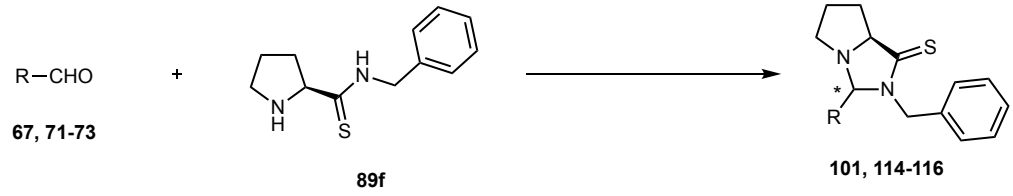


| Entry[a] | Aldehyde | Dr (*exo*/*endo*)[b] | Dr (*exo*/*endo*)[c] |
|---|---|---|---|
| **1** | **67** | 1/1 | 1/2 |
| **2** | **71** | 1/1.6 | 1/2.6 |
| **3** | **72** | 1/1.4 | 1/2.5 |
| **4** | **73** | 1/1.9 | 1/2 |

Table 15. Imidazolidinethione formation studies. [a]Reaction conditions. Thermal conditions: aldehyde (0.25 mmol, 1 equiv.), organocatalyst **89f** (0.25 mmol, 1 equiv.), $LiBF_4$ (0.2 equiv.), DMSO (2 mL), r.t., 3 h. Photochemical conditions: aldehyde (0.25 mmol, 1 equiv.), organocatalyst **89f** (0.25 mmol, 1 equiv.), $Na_4TPP\text{-}S_4$ (1 mol%), $LiBF_4$ (0.2 equiv.), DMSO (2 mL), light (white LEDs, 18 W, 1080 Lm), 5 h [b]Under thermal conditions (determined via $^1$H-NMR). [c]Under photochemical conditions (determined via $^1$H-NMR).

# APPENDIX 2: STRUCTURE INDEX

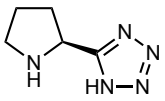

**1**

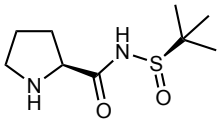

**2**

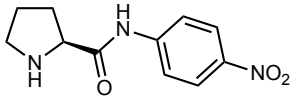

**3**

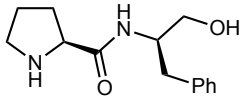

**4**

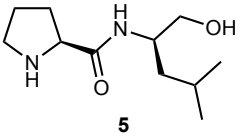

**5**

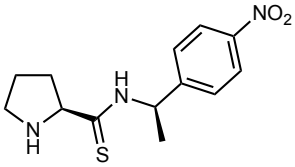

**6**

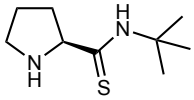

**7**

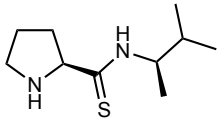

**8**

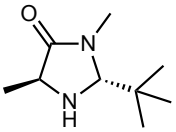

**9**

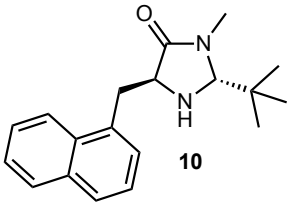

**10**

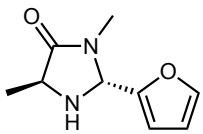

**11**

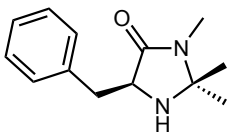

**12**

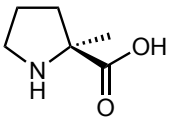

**13**

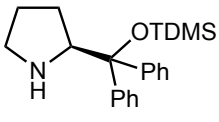

**14**

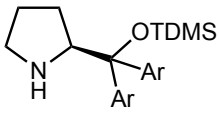

**14**

Ar:

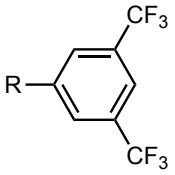

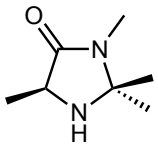

**16a**

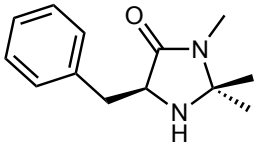

**16b**

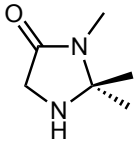

**16c**

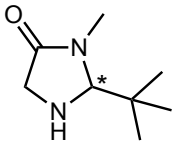

**16d**

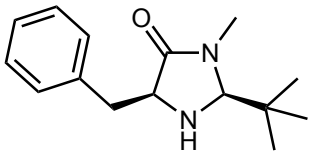

**16e**

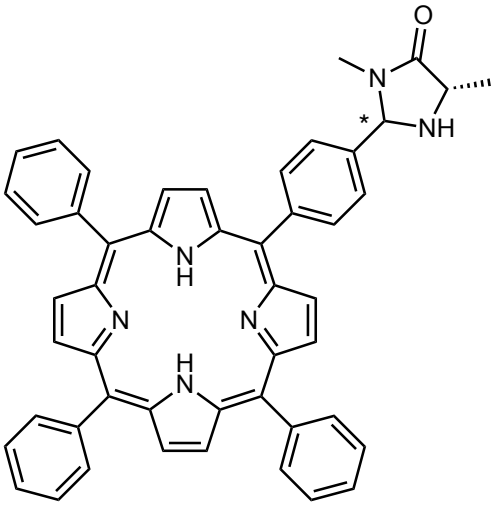

**17a**

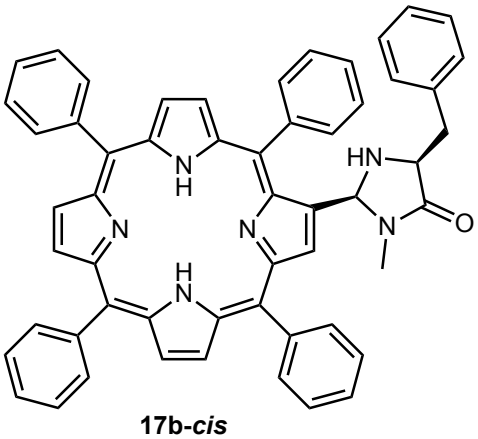

**17b-*cis***

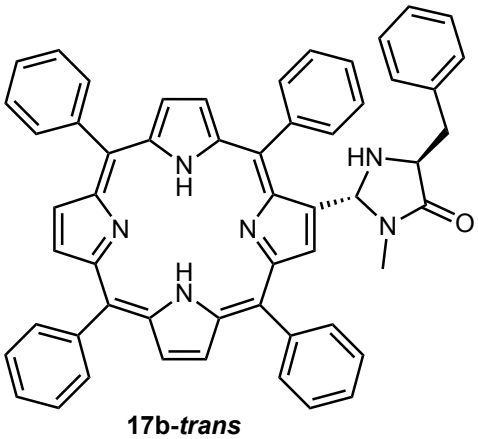

**17b-*trans***

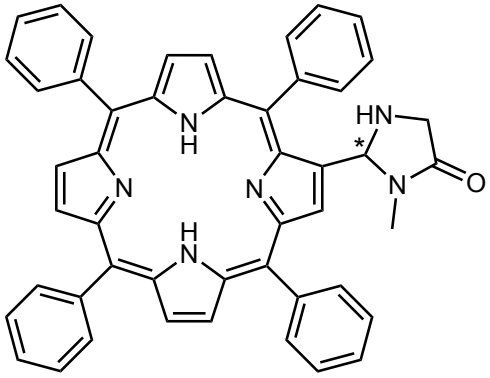

**17c**

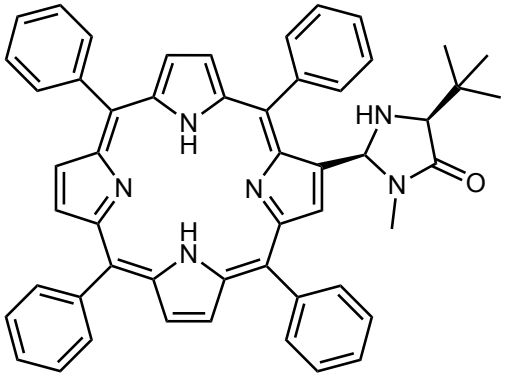

**17d**

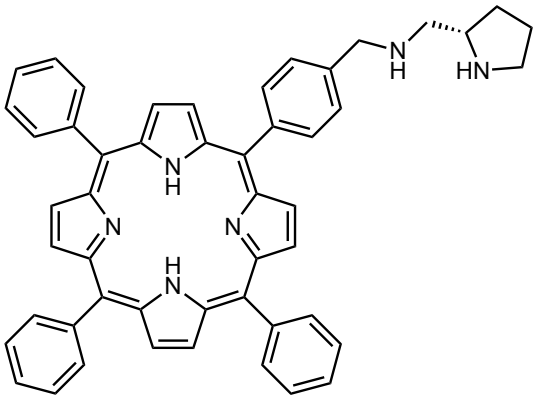

**18a**

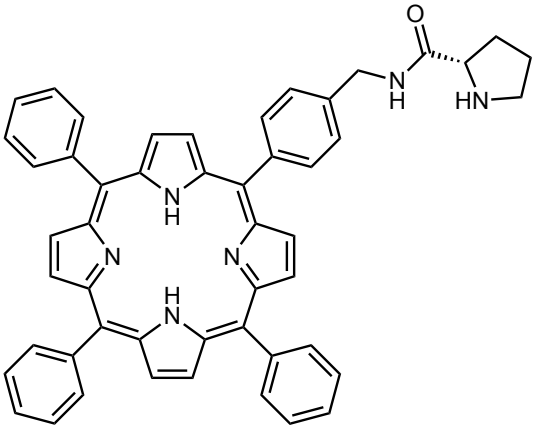

**18b**

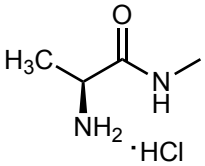

**19**

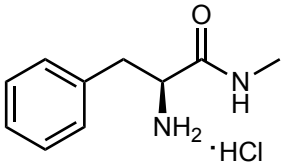

**20**

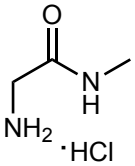

**21**

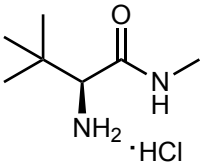

**22**

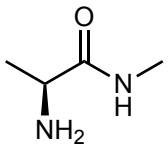

**23**

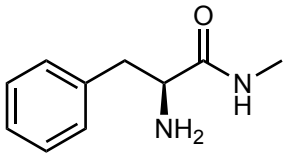

**24**

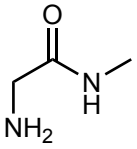

**25**

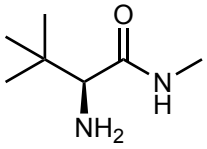

**26**

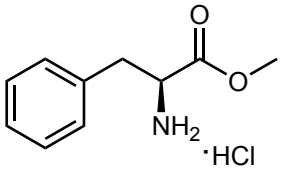

**27**

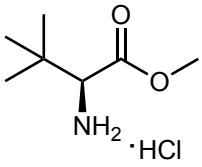

**28**

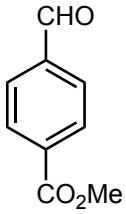

**29**

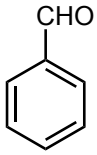

**30**

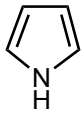

**31**

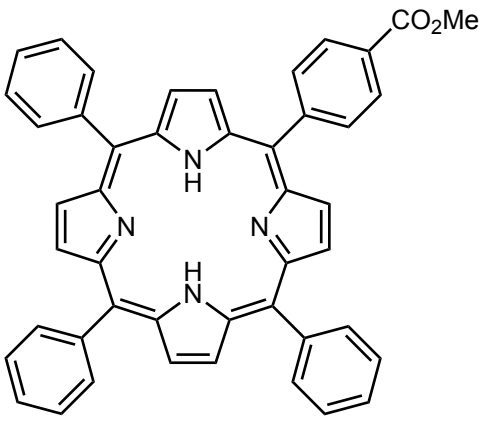

**32**

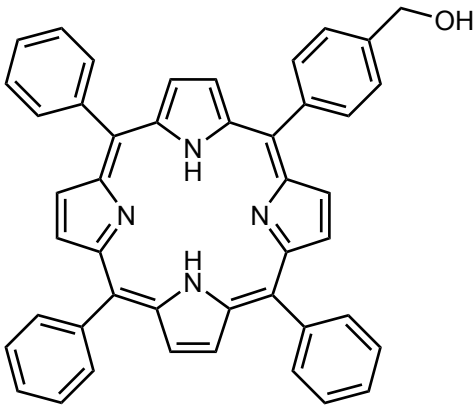

**33**

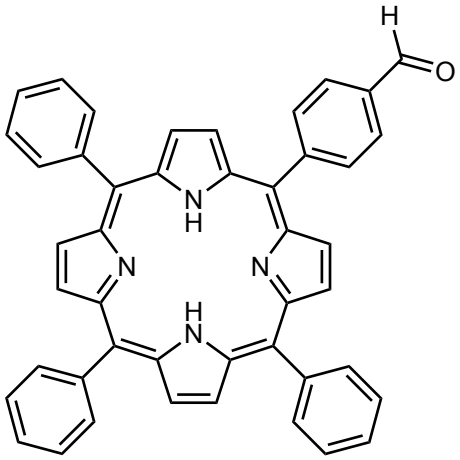

**34**

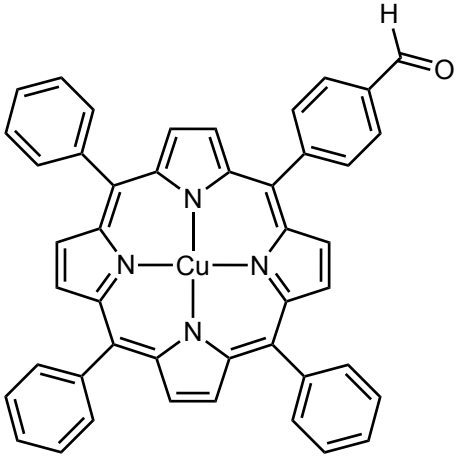

**35**

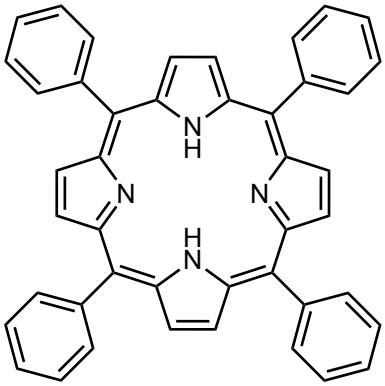

**36**

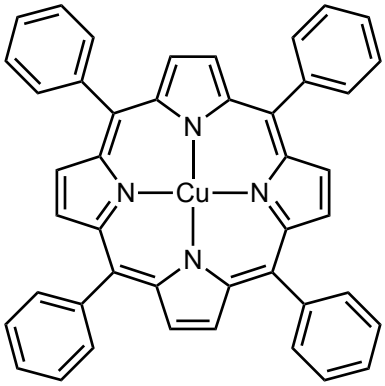

**37**

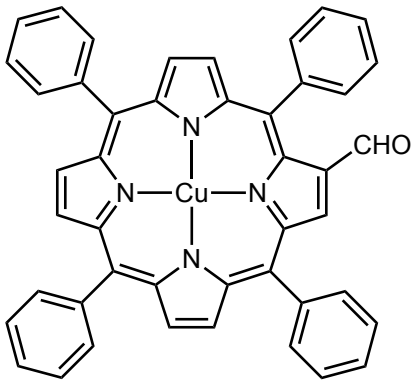

**38**

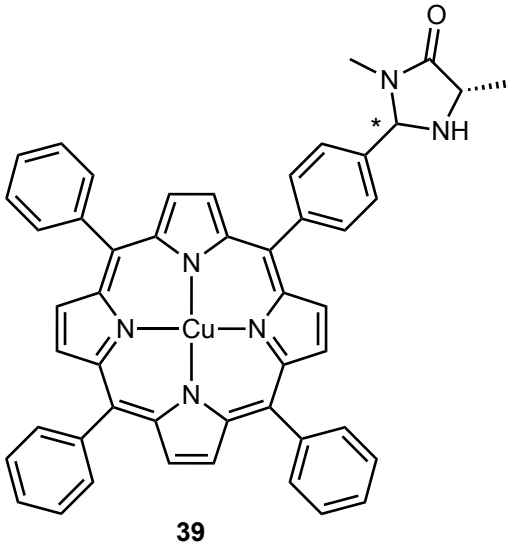

**39**

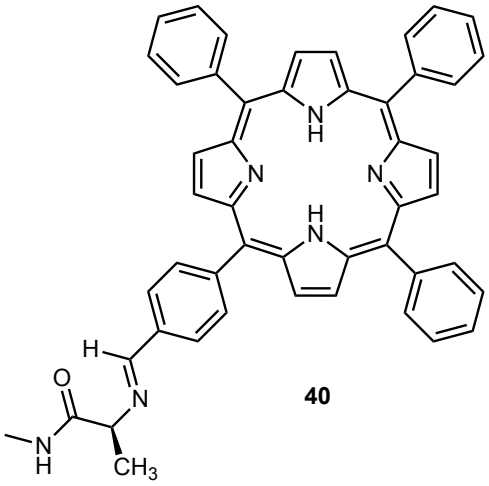

**40**

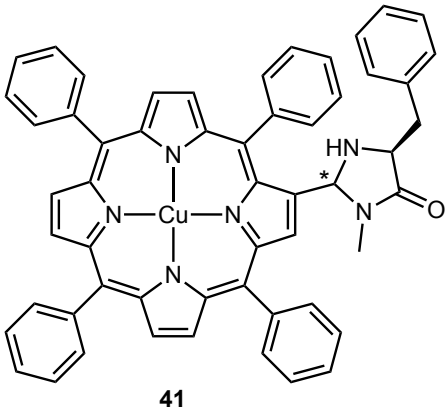

**41**

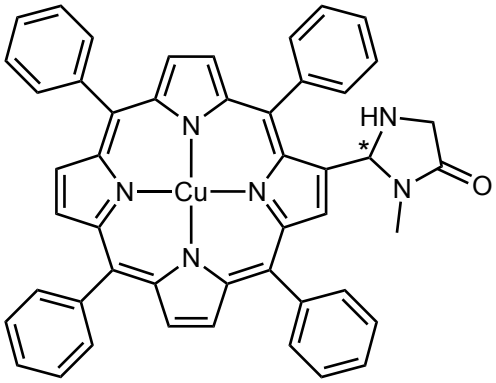

**42**

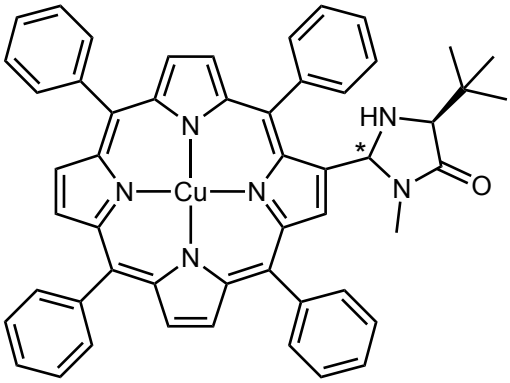

**43**

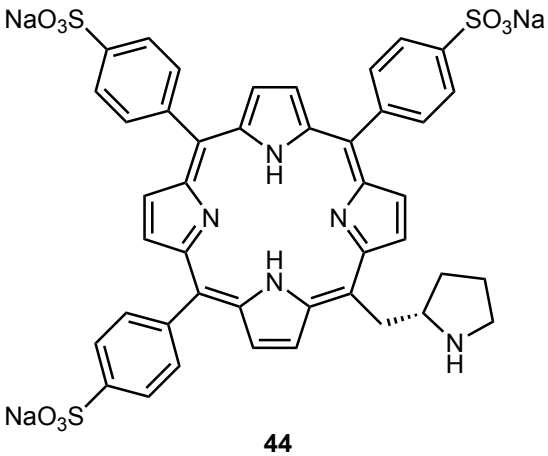

**44**

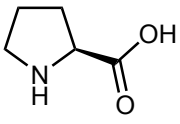

**45**

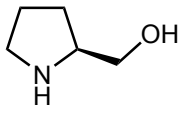

**46**

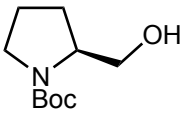


**47**

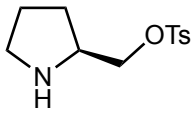


**48**

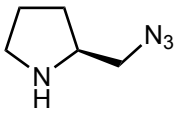


**49**

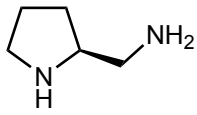


**50**

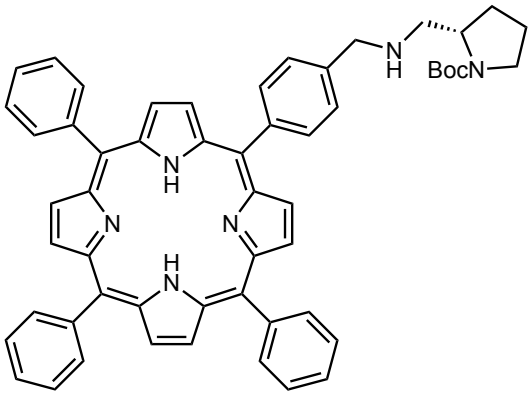


**51**

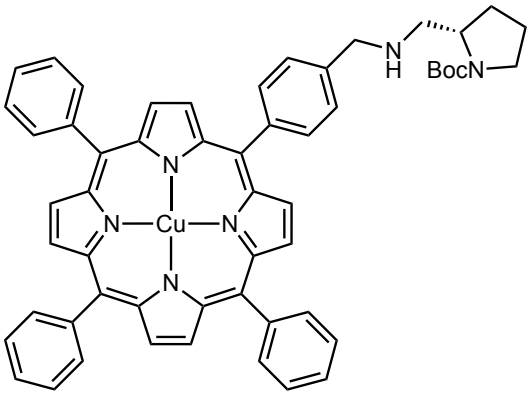


**52**

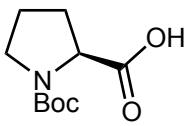


**53**

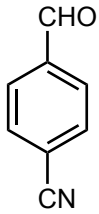


**54**

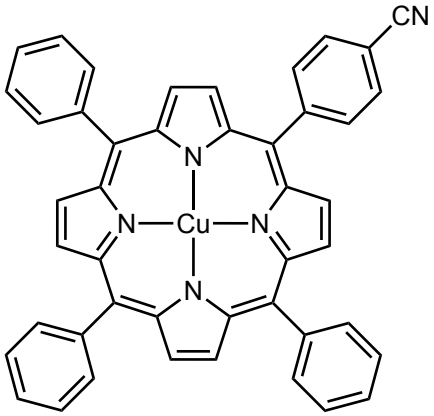


**55**

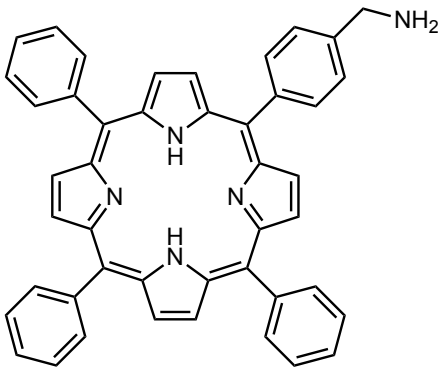


**56**

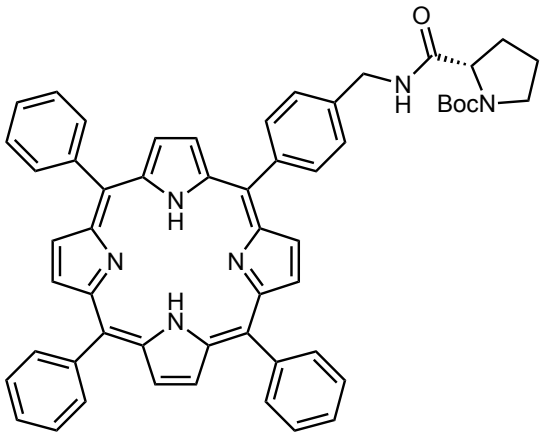


**57**

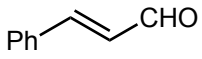


**58**

**59**

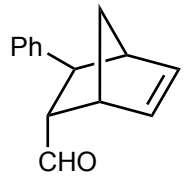


**60-*endo***

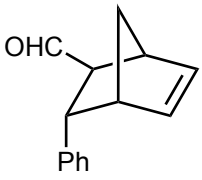


**60-*endo***

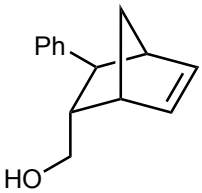


**61-*endo***

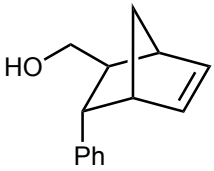


**61-*endo***

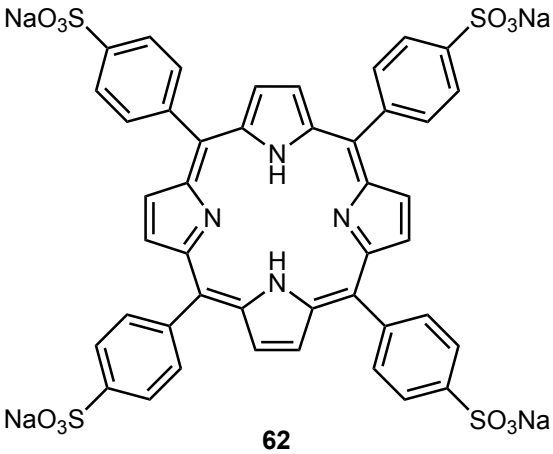


**62**

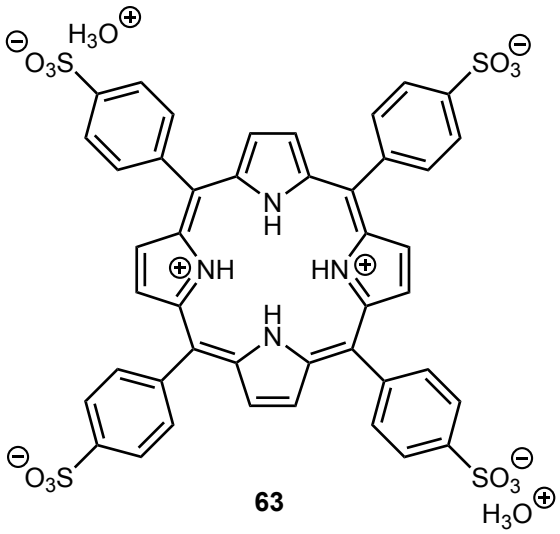


**63**

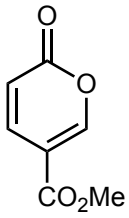


**64**

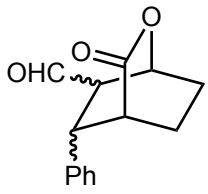


**65**

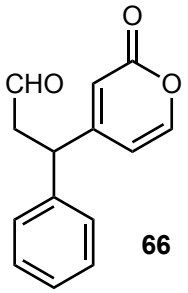


**66**

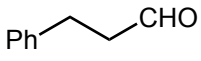


**67**

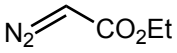


**68**

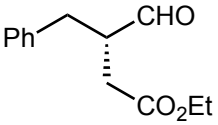


**69**

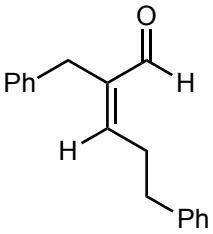


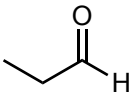


**71**

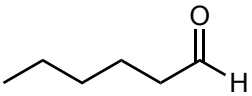


**72**

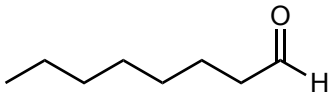


**73**

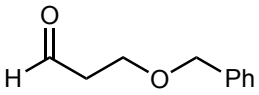


**74**

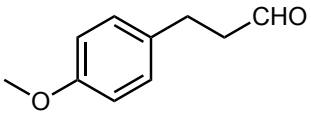


**75**

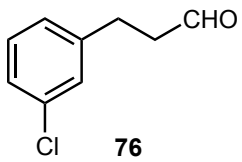


**76**

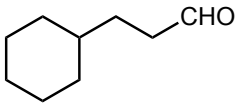


**77**

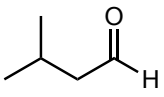


**78**

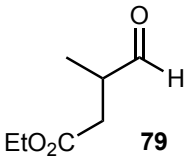


**79**

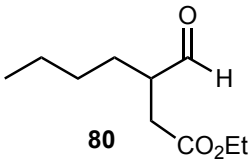


**80**

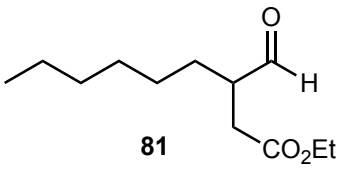


**81**

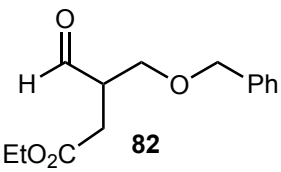


**82**

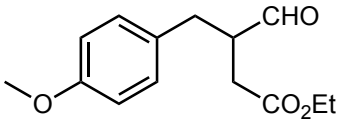


**83**

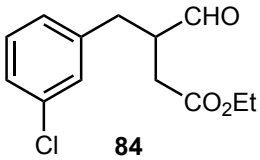


**84**

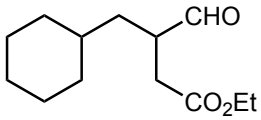


**85**

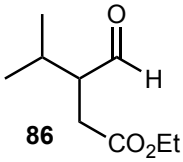


**86**

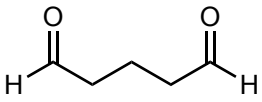


**87**

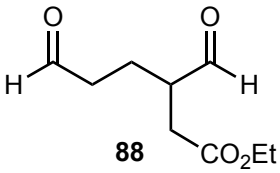


**88**

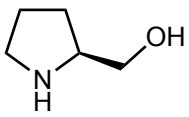


**89a**

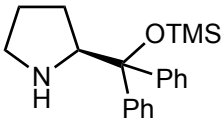


**89b**

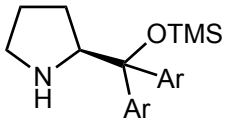


**89c**

Ar:

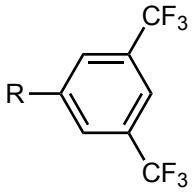

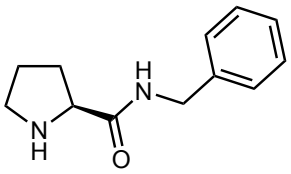

**89d**

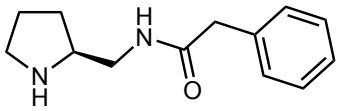

**89e**

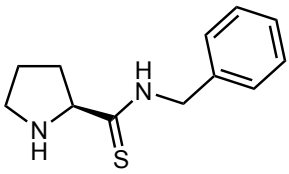

**89f**

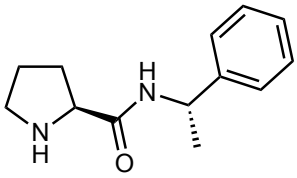

**89g**

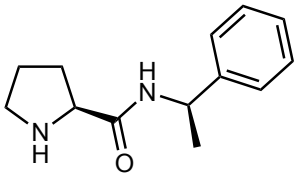

**89h**

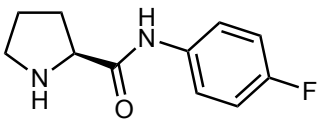

**89i**

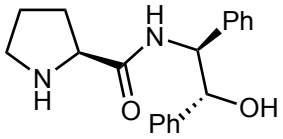

**89j**

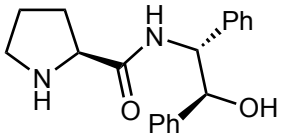

**89k**

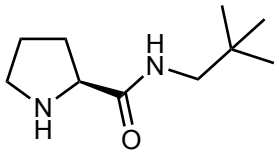

**89l**

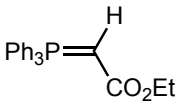

**90**

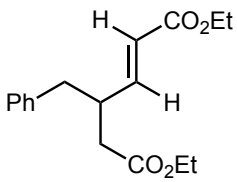

**91**

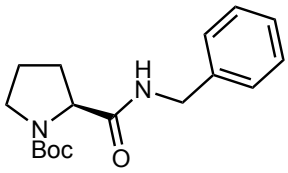

**92**

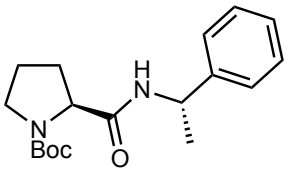

**93**

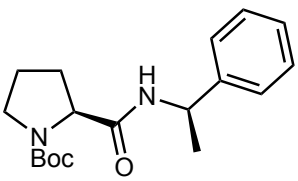

**94**

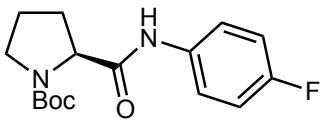

**95**

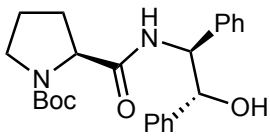

**96**

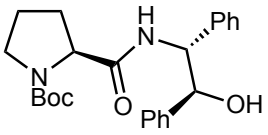

**97**

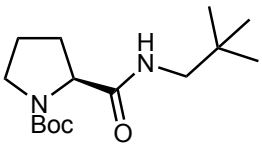

**98**

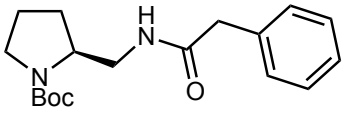

**99**

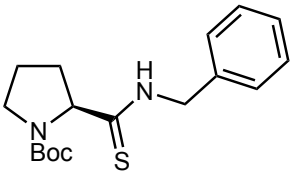

**100**

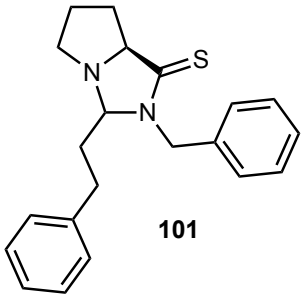

**101**

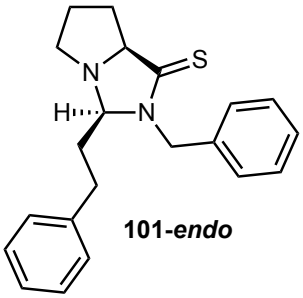

**101-*endo***

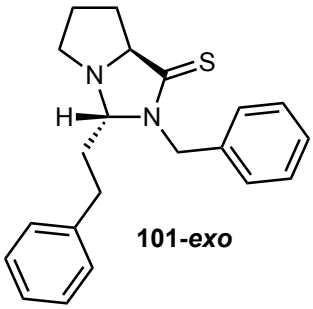

**101-*exo***

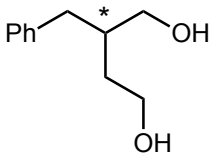

**102**

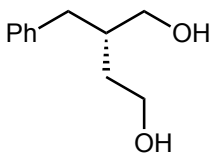

(*S*)-**102**

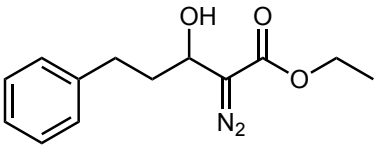

**103**

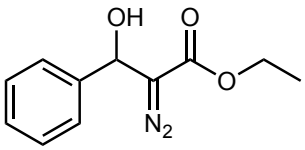

**104**

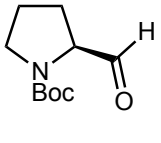

**105**

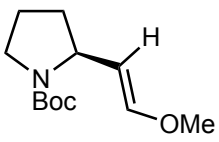


**106**

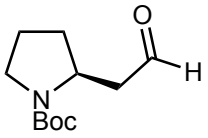


**107**

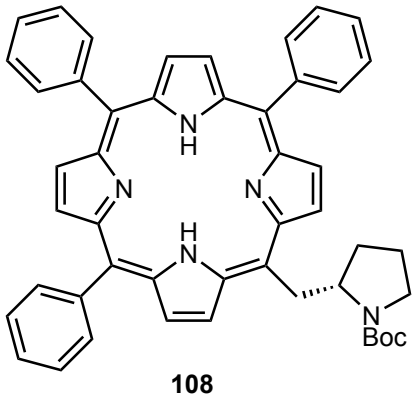


**108**

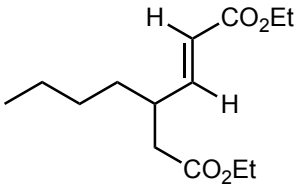


**109**

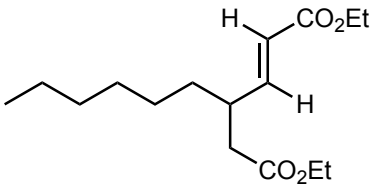


**110**

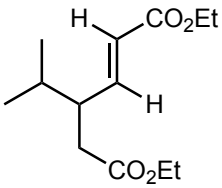


**111**

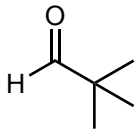


**112**

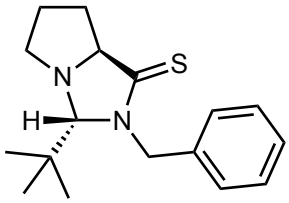


**113**

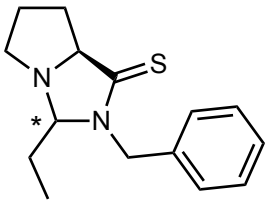


**114**

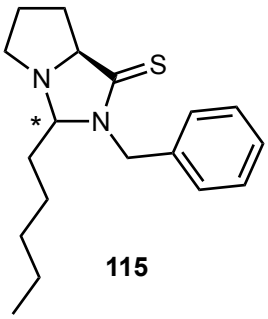


**115**

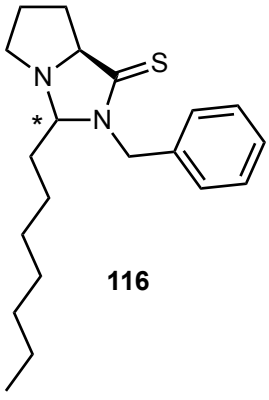


**116**

# APPENDIX 3: NMR SPECTRA

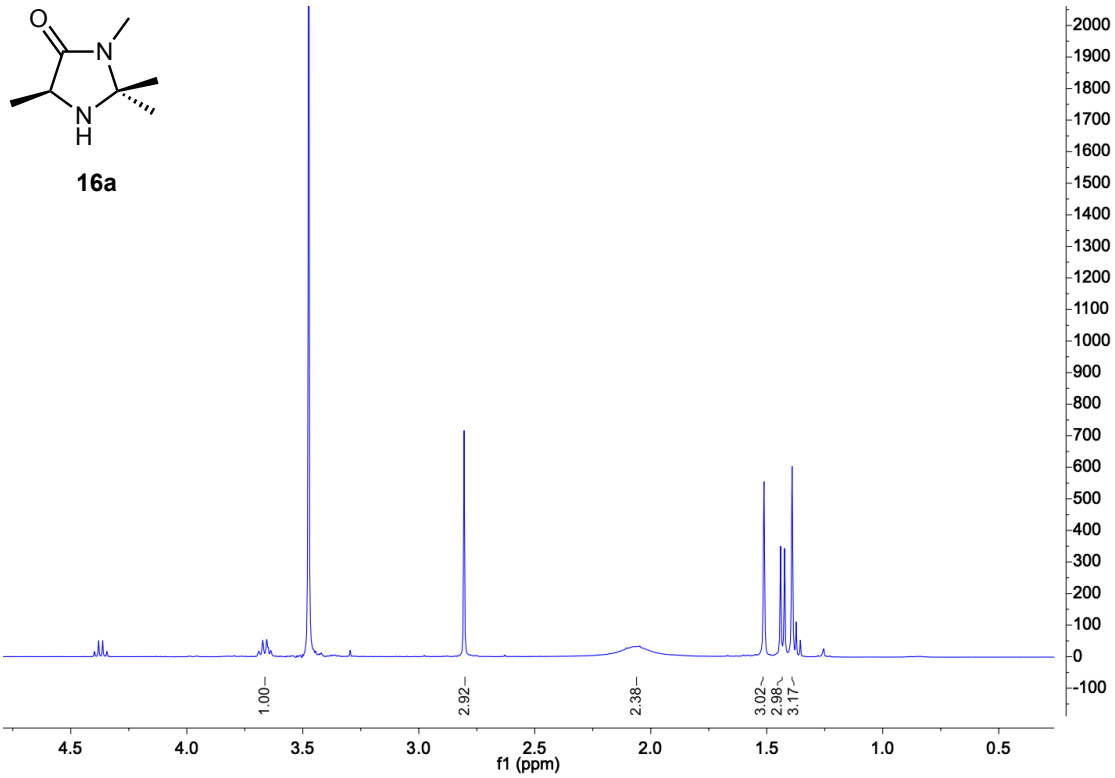


Figure 89. $^{1}$H-NMR spectrum ($CDCl_3$, 400 MHz) of compound **16a**

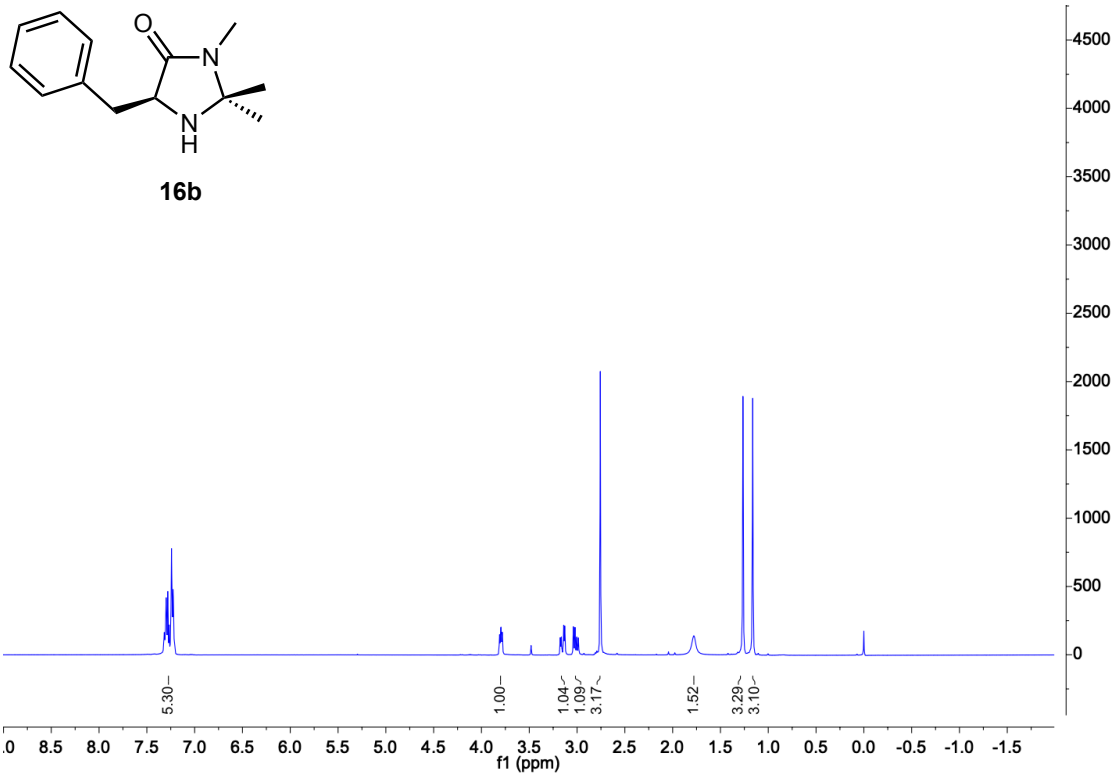


Figure 90. $^{1}$H-NMR spectrum ($CDCl_3$, 400 MHz) of compound **16b**

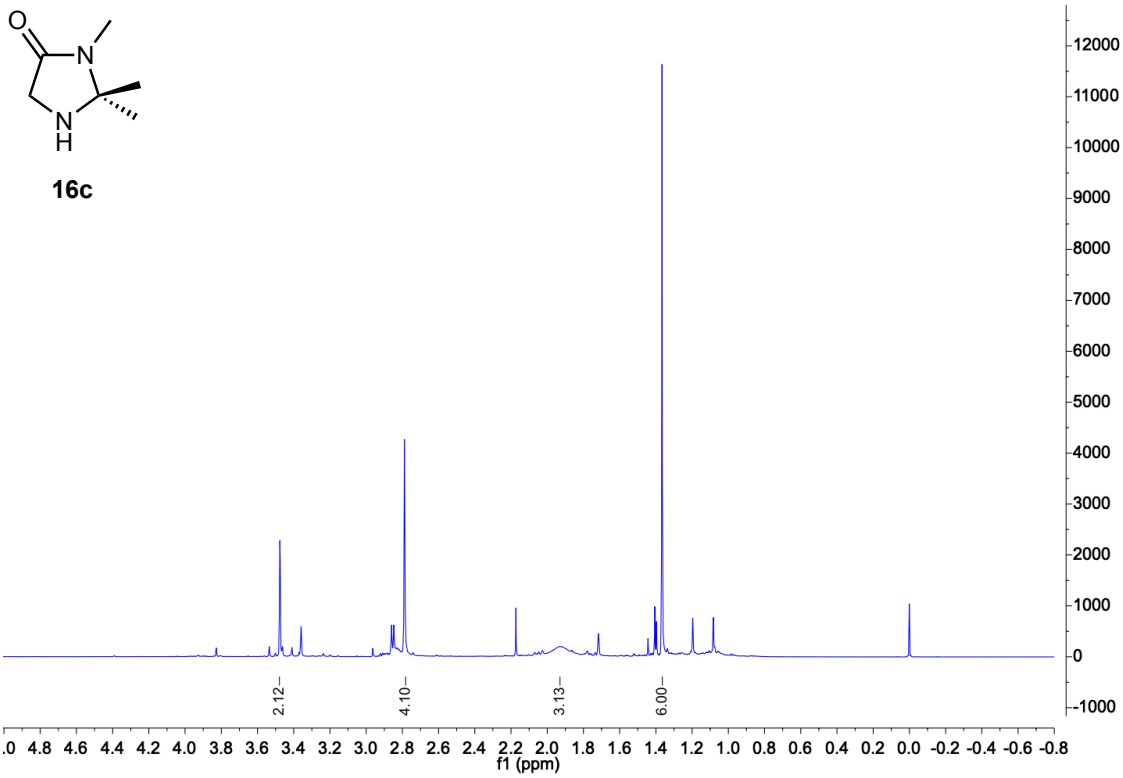


Figure 91. $^{1}$H-NMR spectrum ($CDCl_3$, 400 MHz) of compound **16c**

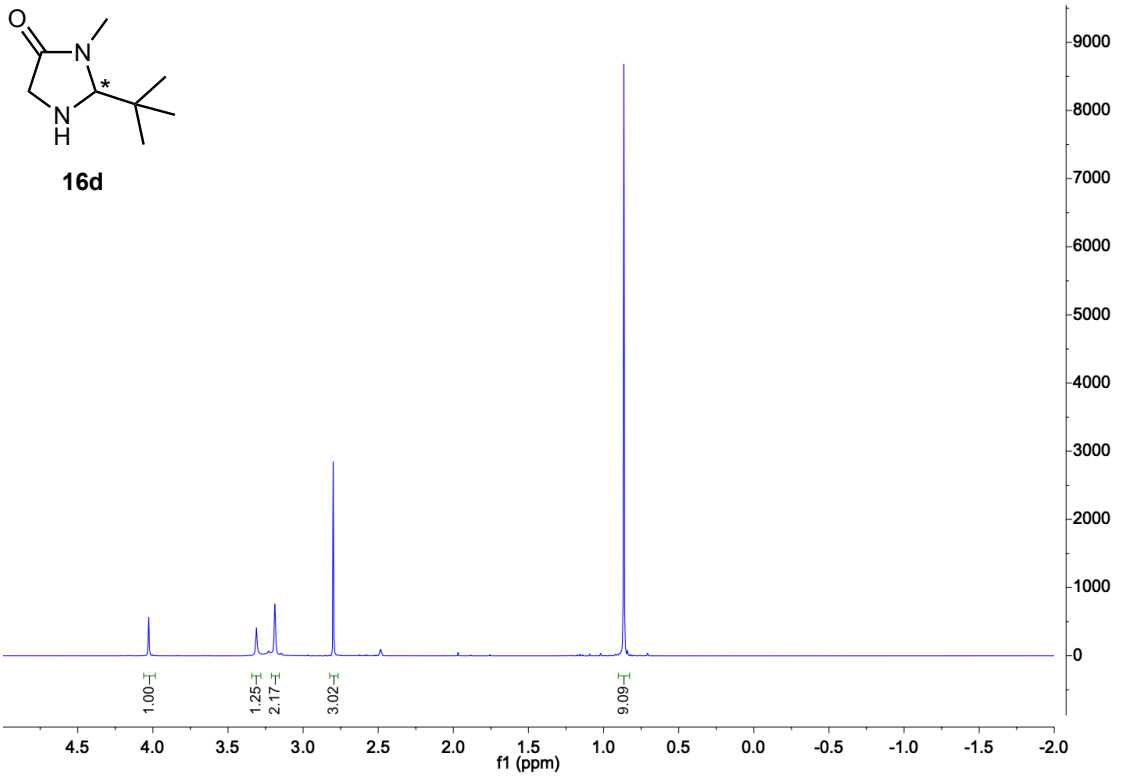


Figure 92. $^{1}$H-NMR spectrum ($CDCl_3$, 400 MHz) of compound **16d**

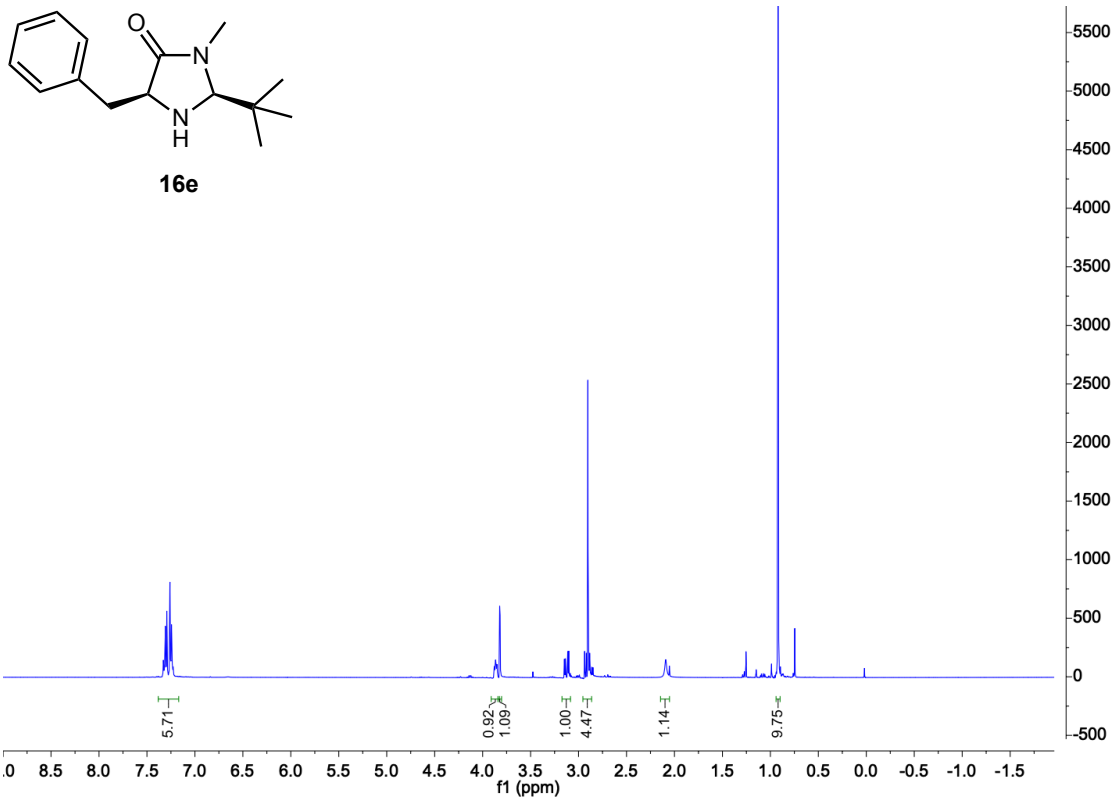


Figure 93. $^{1}$H-NMR spectrum ($CDCl_3$, 400 MHz) of compound **16e**

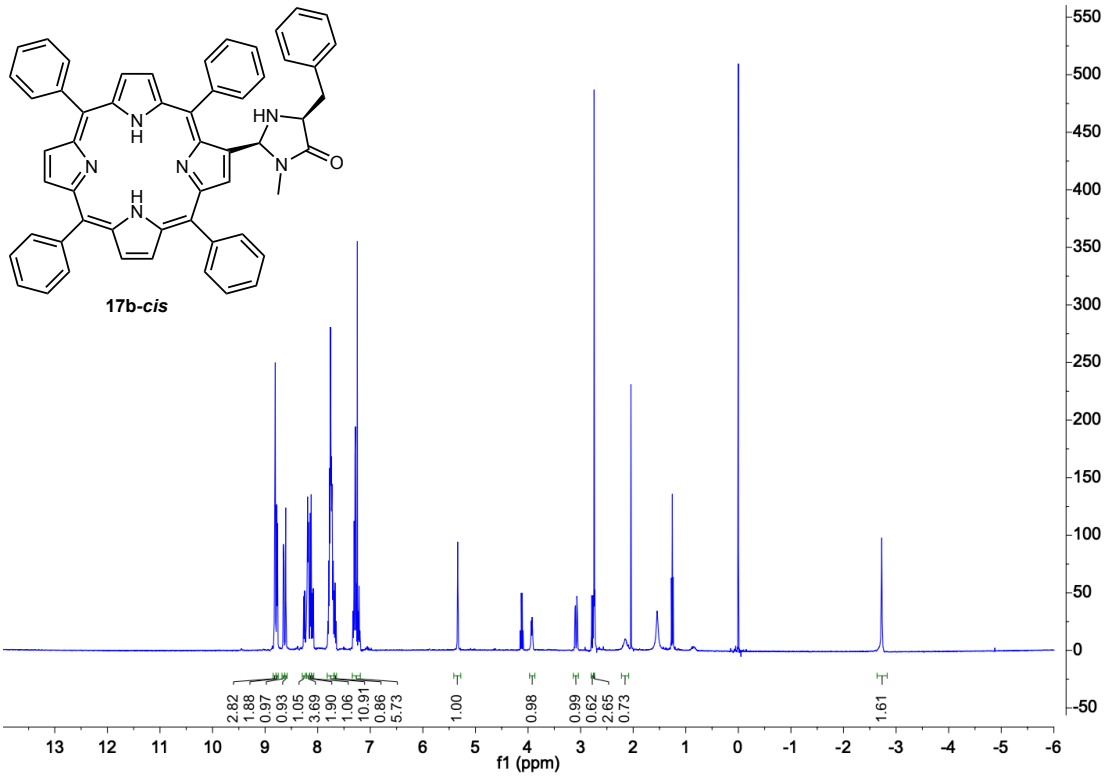


Figure 94. $^{1}$H-NMR spectrum ($CDCl_3$, 400 MHz) of compound **17b-*cis***

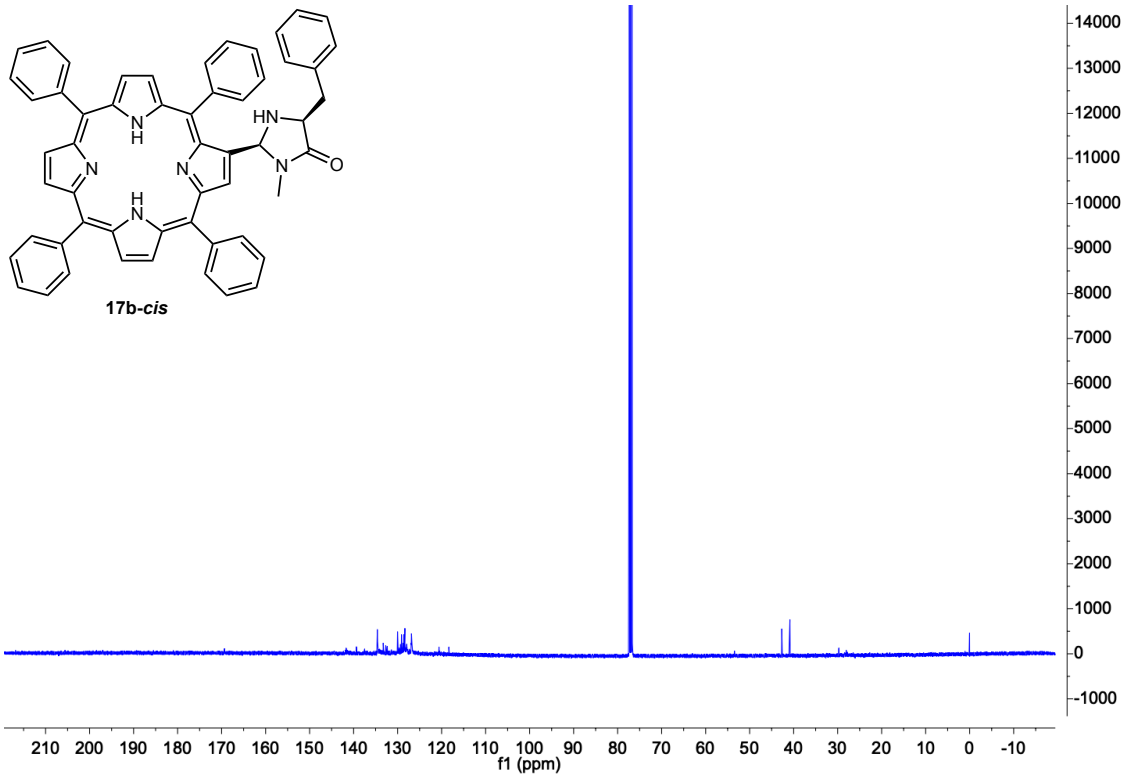


Figure 95. $^{13}$C-NMR spectrum ($CDCl_3$, 400 MHz) of compound **17b-*cis***

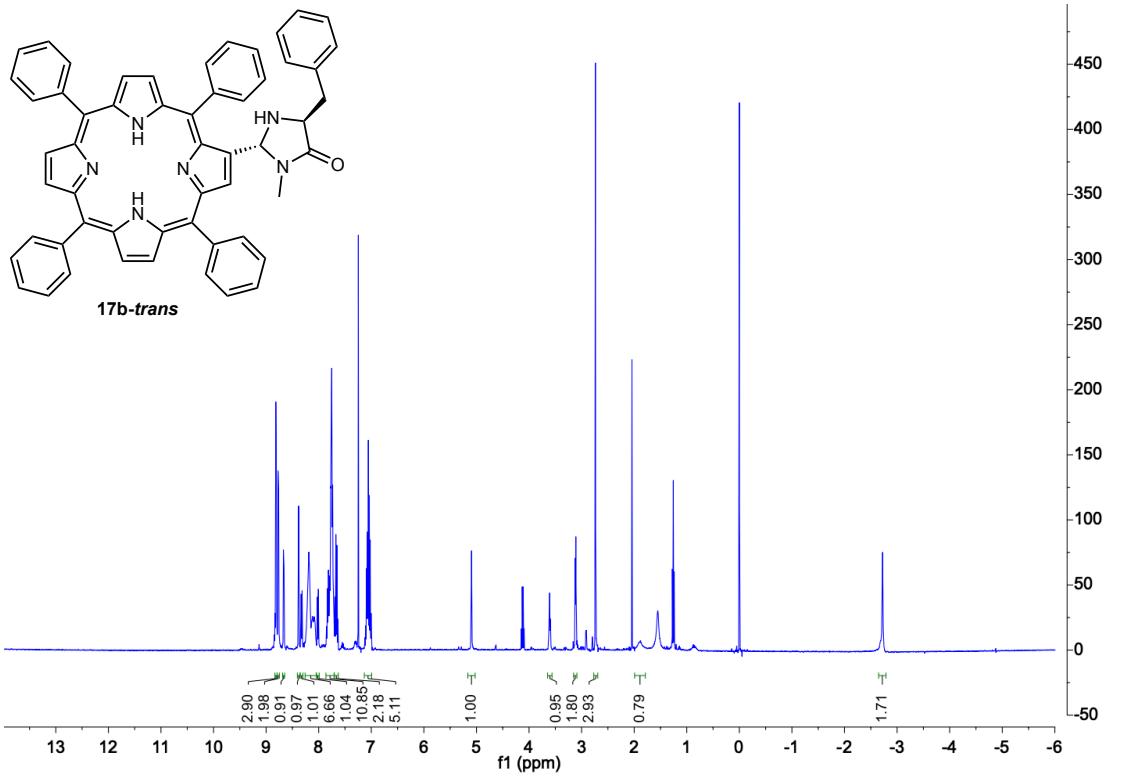


Figure 96. $^{1}$H-NMR spectrum ($CDCl_3$, 400 MHz) of compound **17b-*trans***

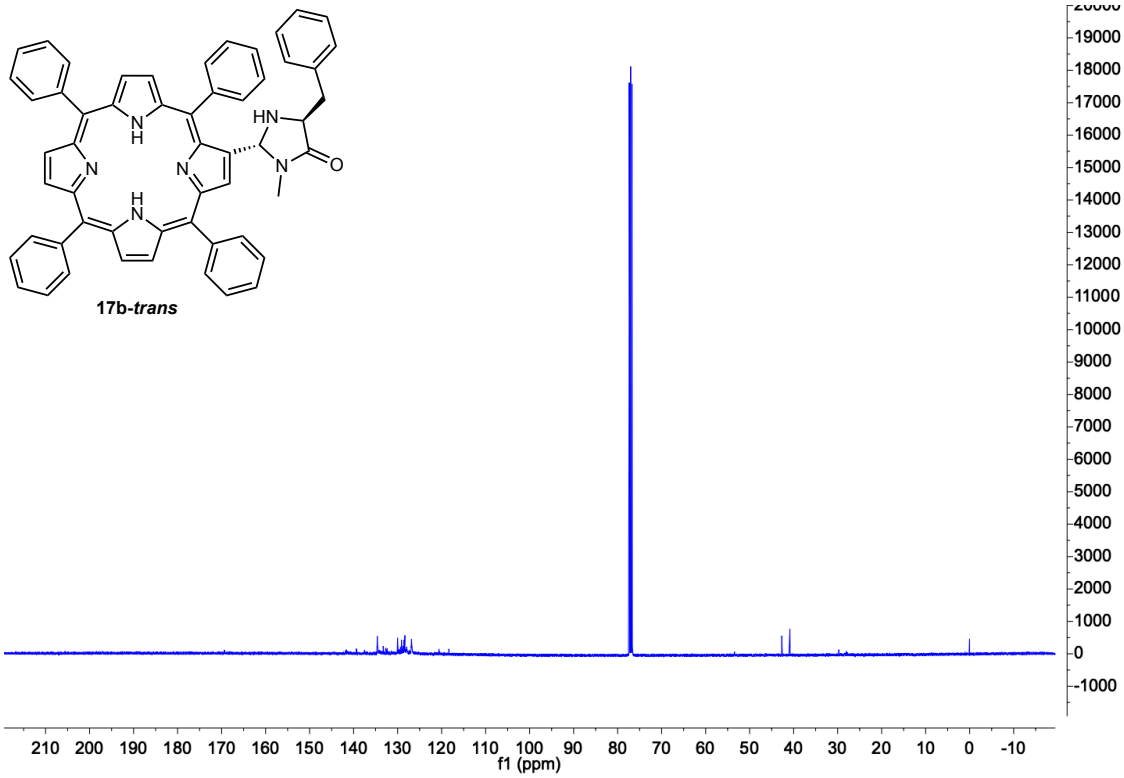


Figure 97. $^{13}$C-NMR spectrum ($CDCl_3$, 400 MHz) of compound **17b-*trans***

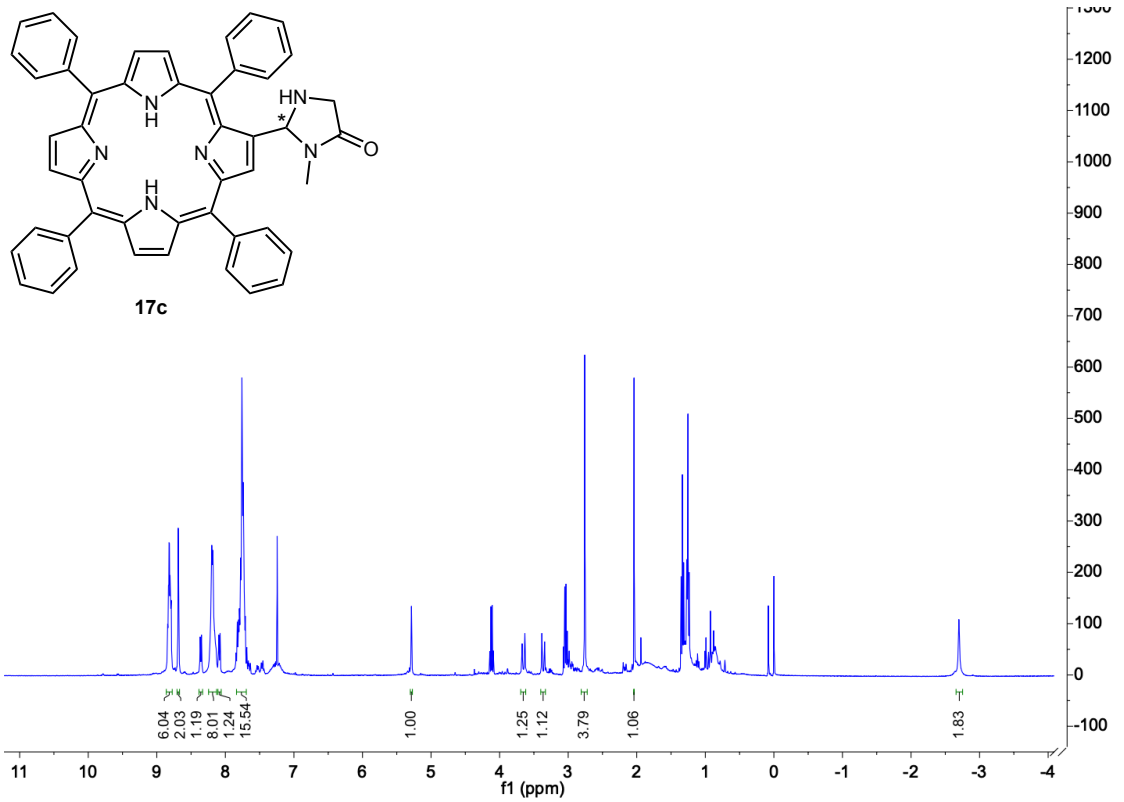


Figure 98. $^{1}$H-NMR spectrum ($CDCl_3$, 400 MHz) of compound **17c**

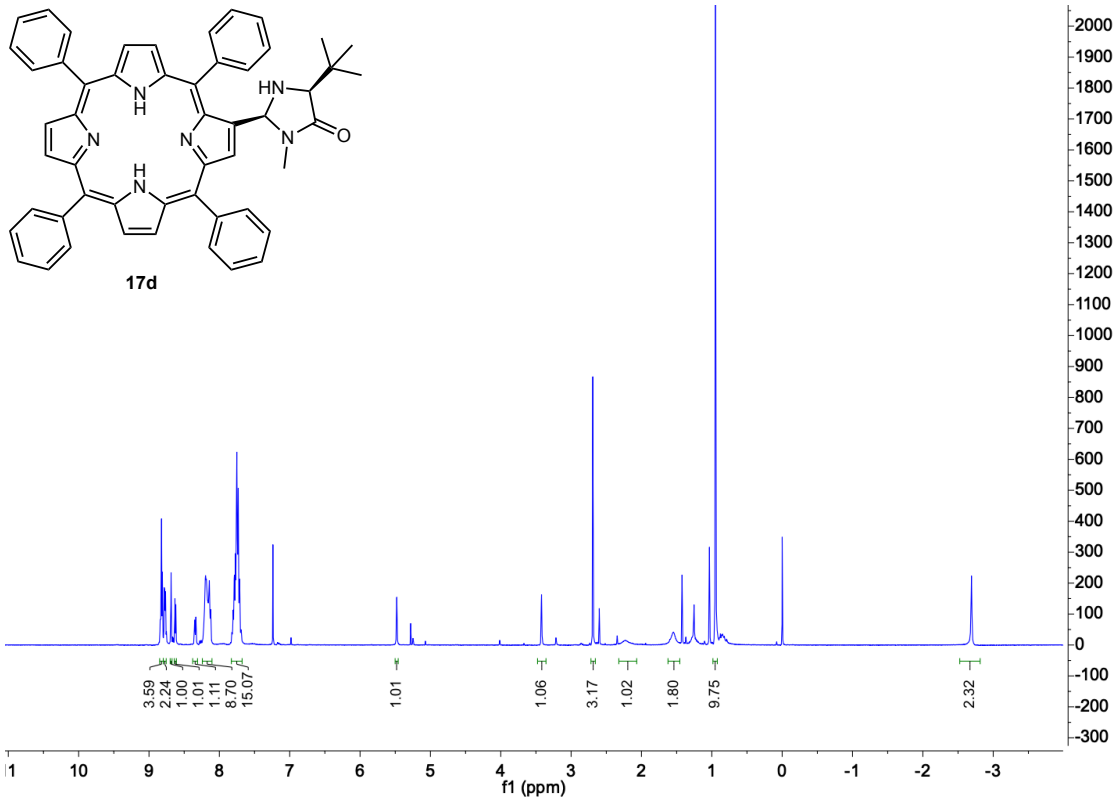


Figure 99. $^{1}$H-NMR spectrum ($CDCl_3$, 400 MHz) of compound **17d**

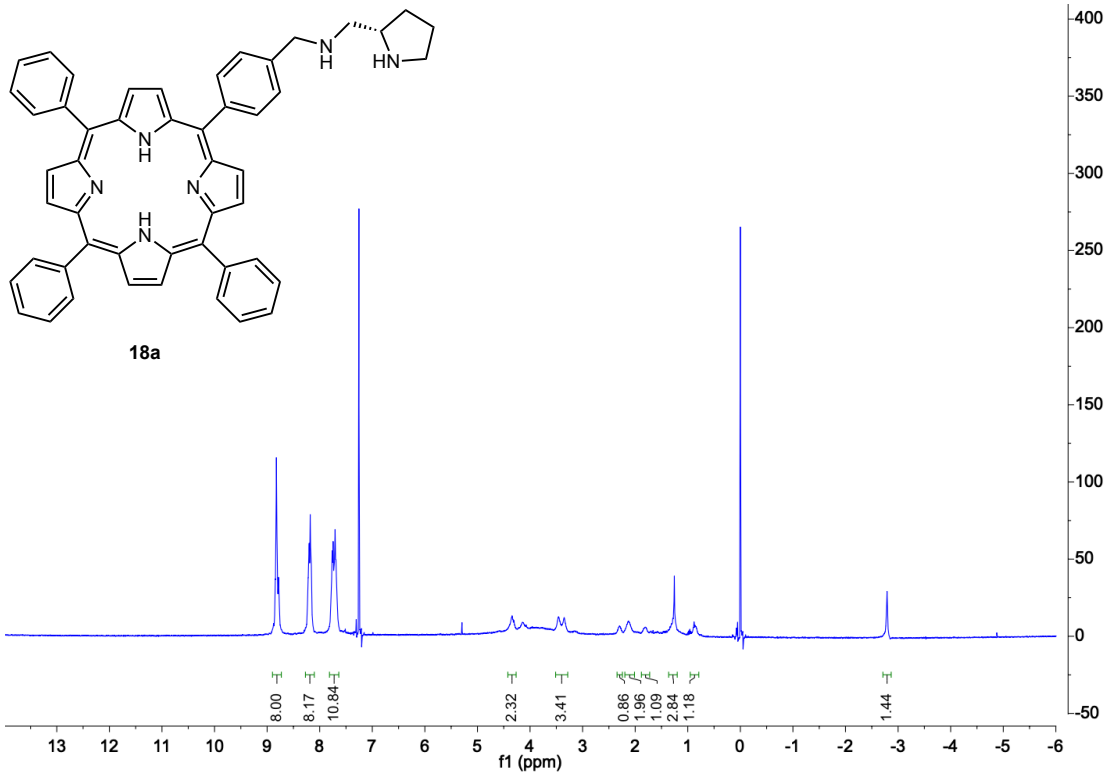


Figure 100. $^{1}$H-NMR spectrum ($CDCl_3$, 400 MHz) of compound **18a**

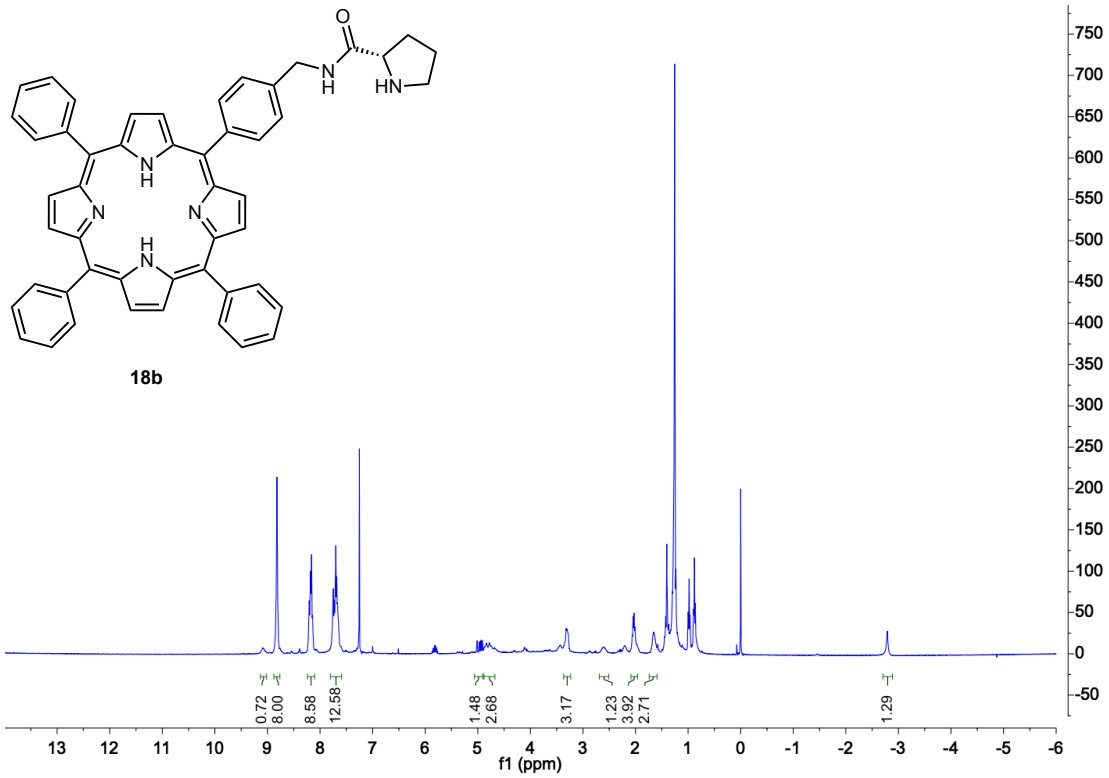


Figure 101. $^{1}$H-NMR spectrum ($CDCl_3$, 400 MHz) of compound **18b**

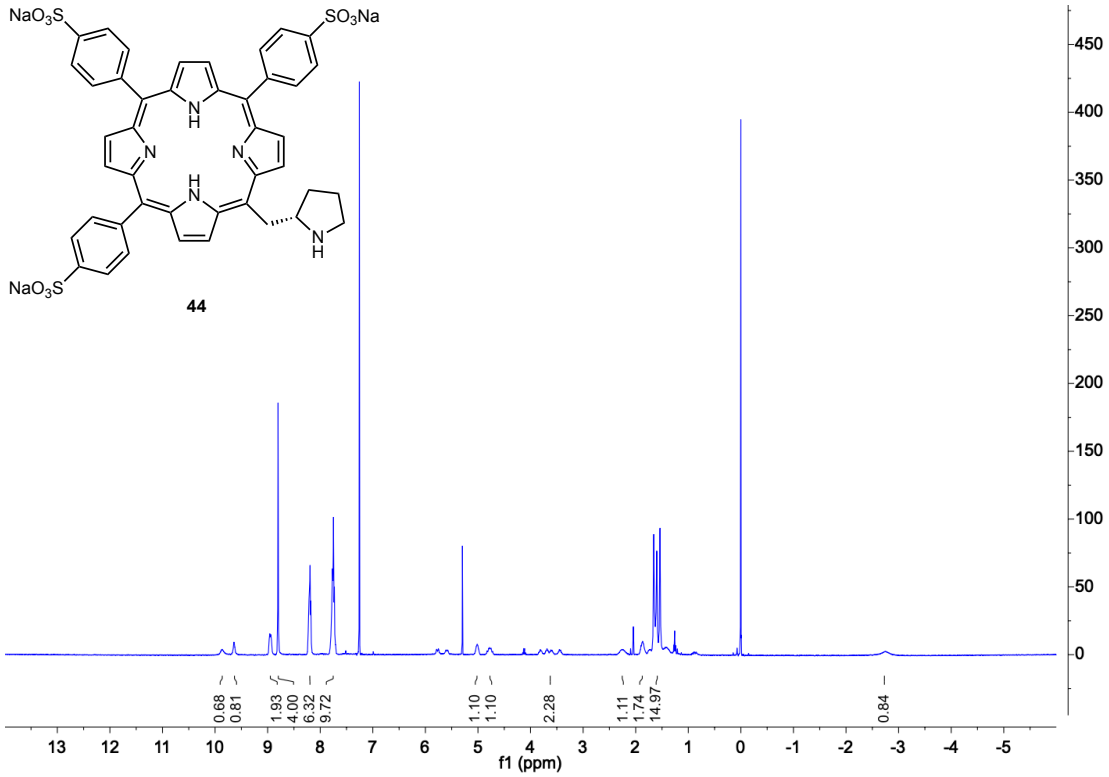


Figure 102. $^{1}$H-NMR spectrum (DMSO-$d_6$, 400 MHz) of compound **44**

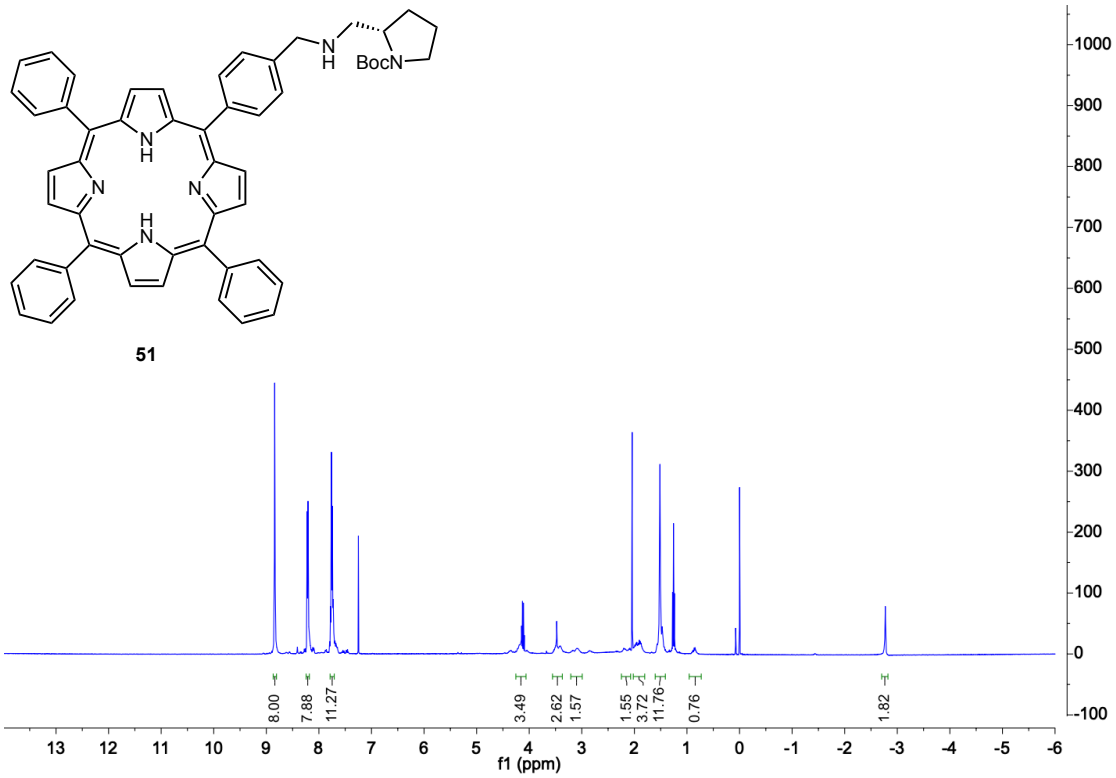


Figure 103. $^{1}$H-NMR spectrum ($CDCl_3$, 400 MHz) of compound **51**

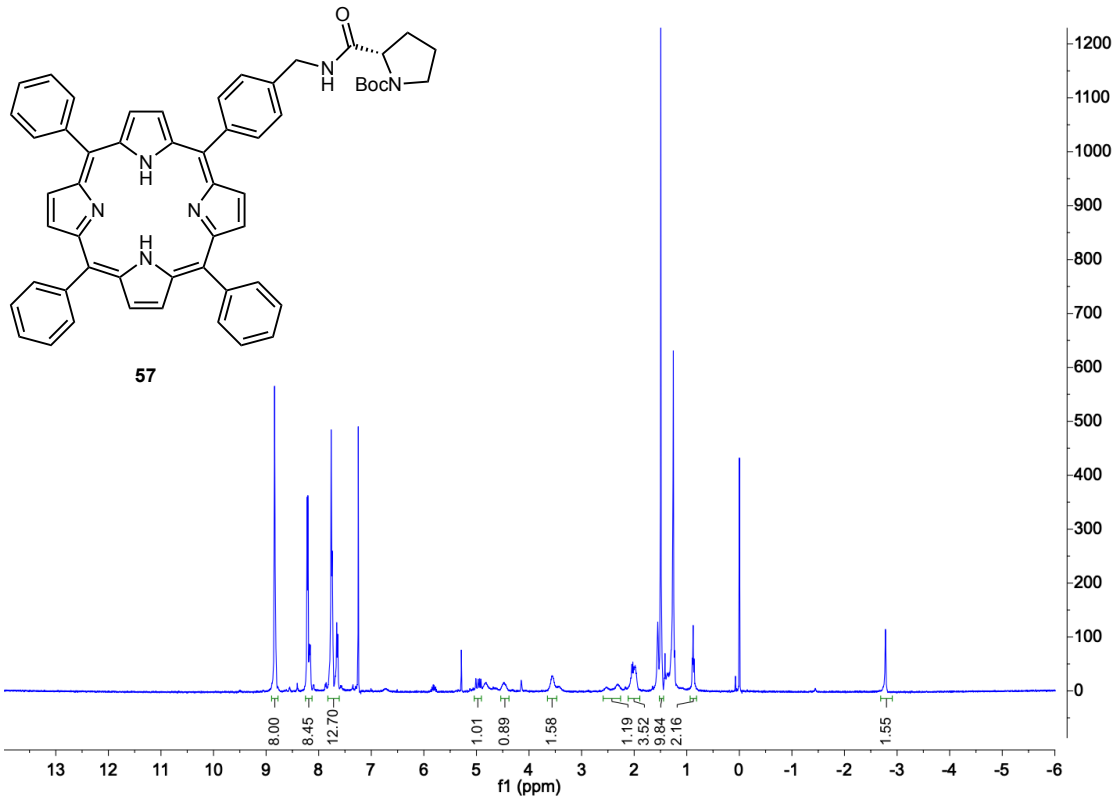


Figure 104. $^{1}$H-NMR spectrum ($CDCl_3$, 400 MHz) of compound **57**

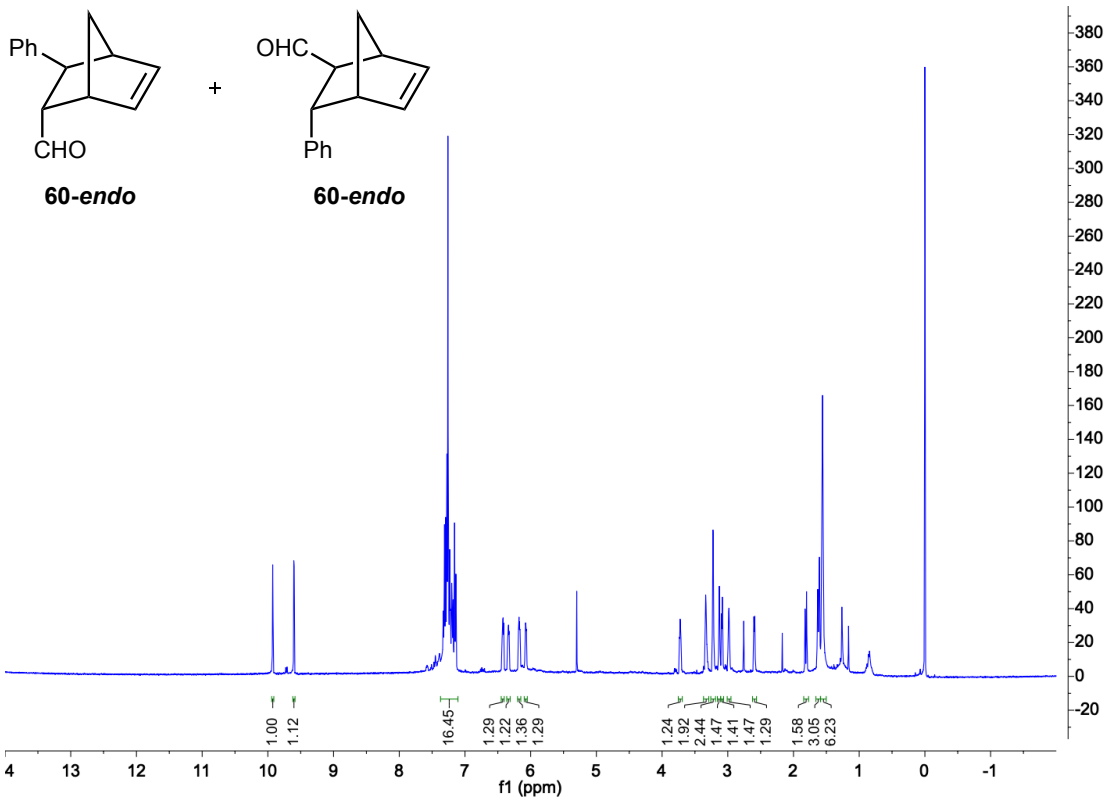


Figure 105. $^{1}$H-NMR spectrum ($CDCl_3$, 400 MHz) of compounds **60-*endo*** and **60-*exo***

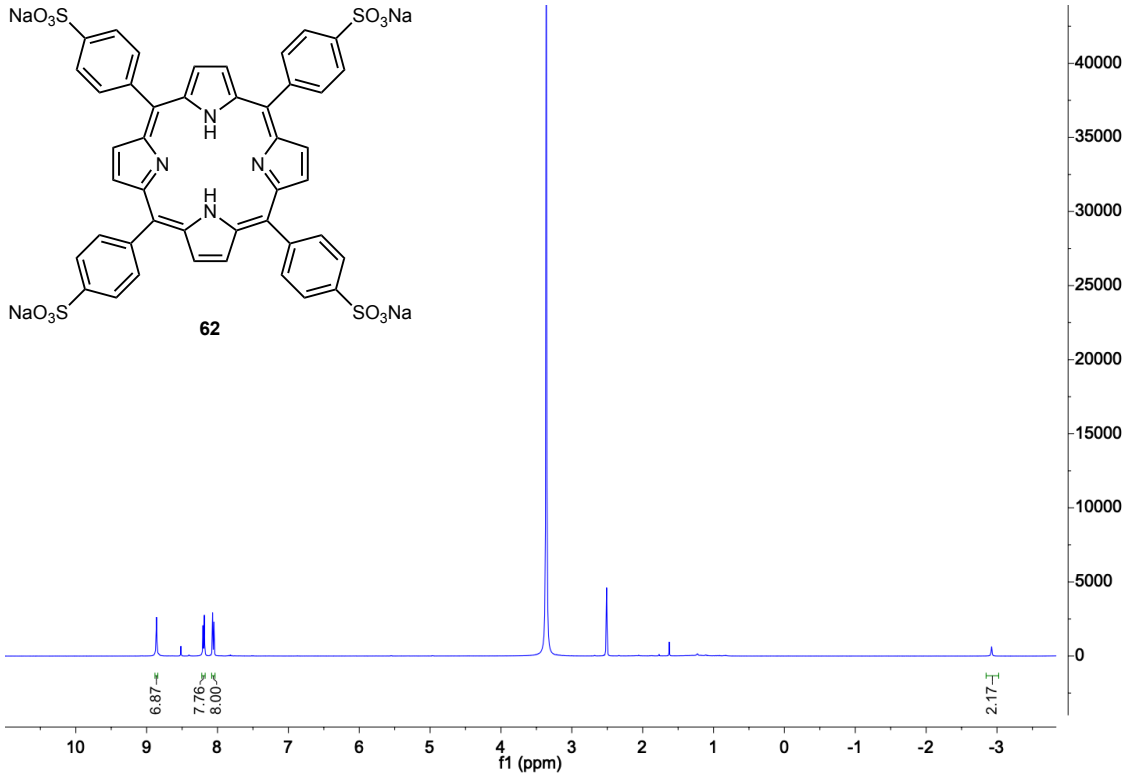


Figure 106. $^{1}$H-NMR spectrum (DMSO-$d_6$, 400 MHz) of compound **62**

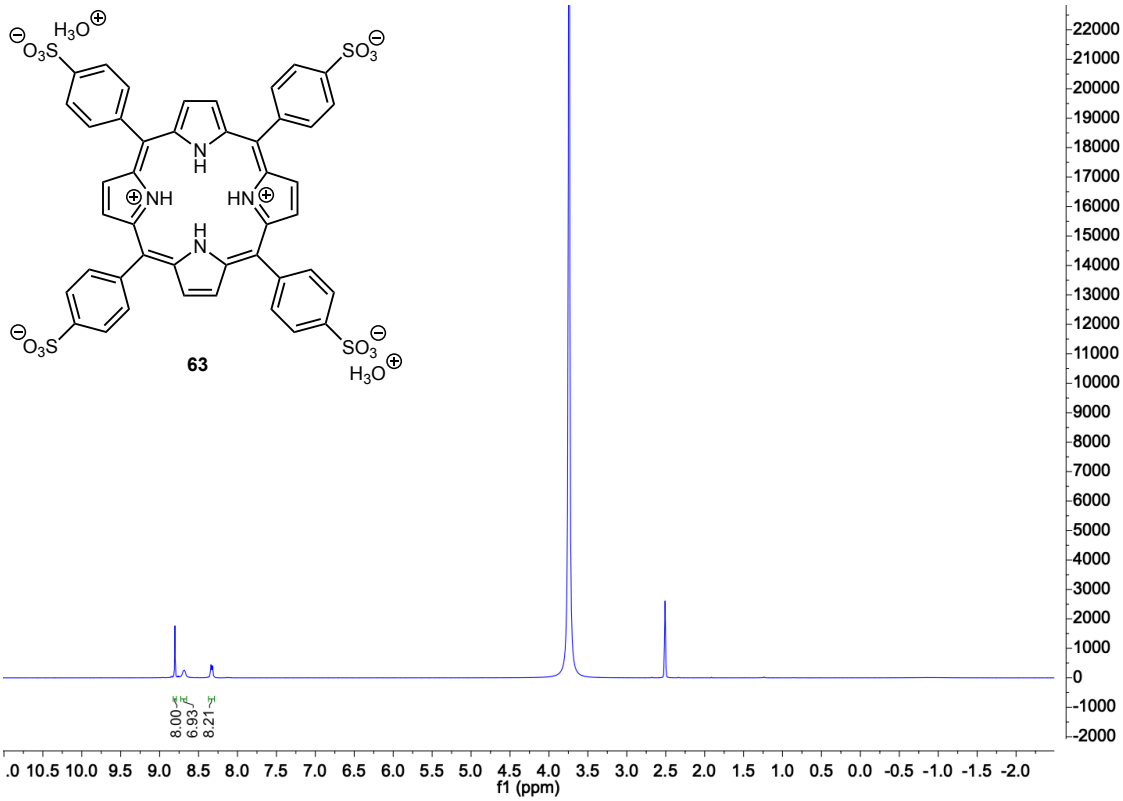


Figure 107. $^{1}$H-NMR spectrum (DMSO-$d_6$, 400 MHz) of compound **63**

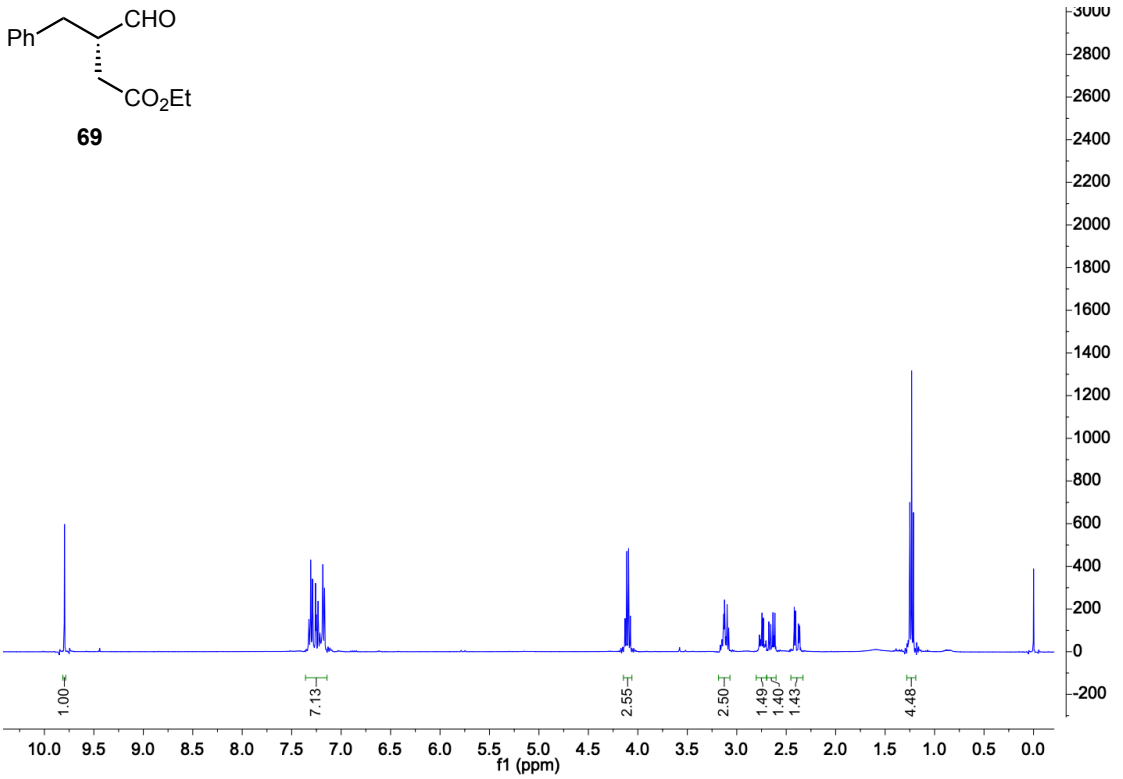


Figure 108. $^{1}$H-NMR spectrum ($CDCl_3$, 400 MHz) of enantiopure compound **69**

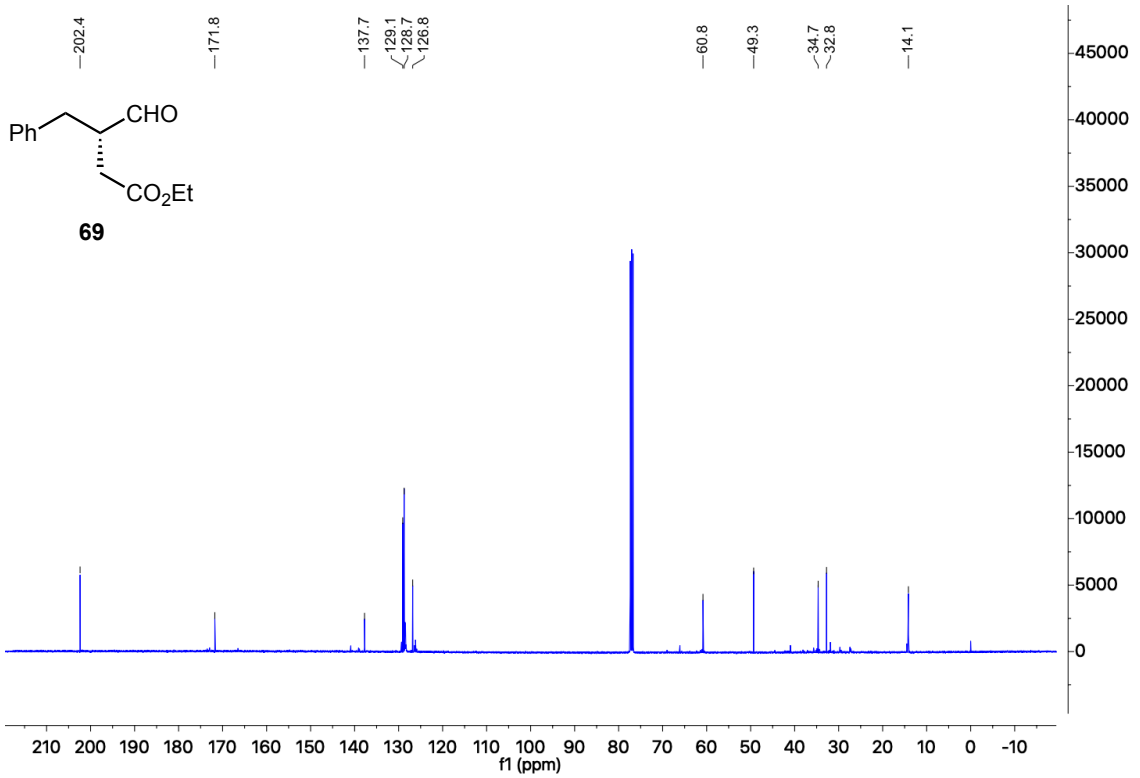


Figure 109. $^{13}$C-NMR spectrum ($CDCl_3$, 400 MHz) of enantiopure compound **69**

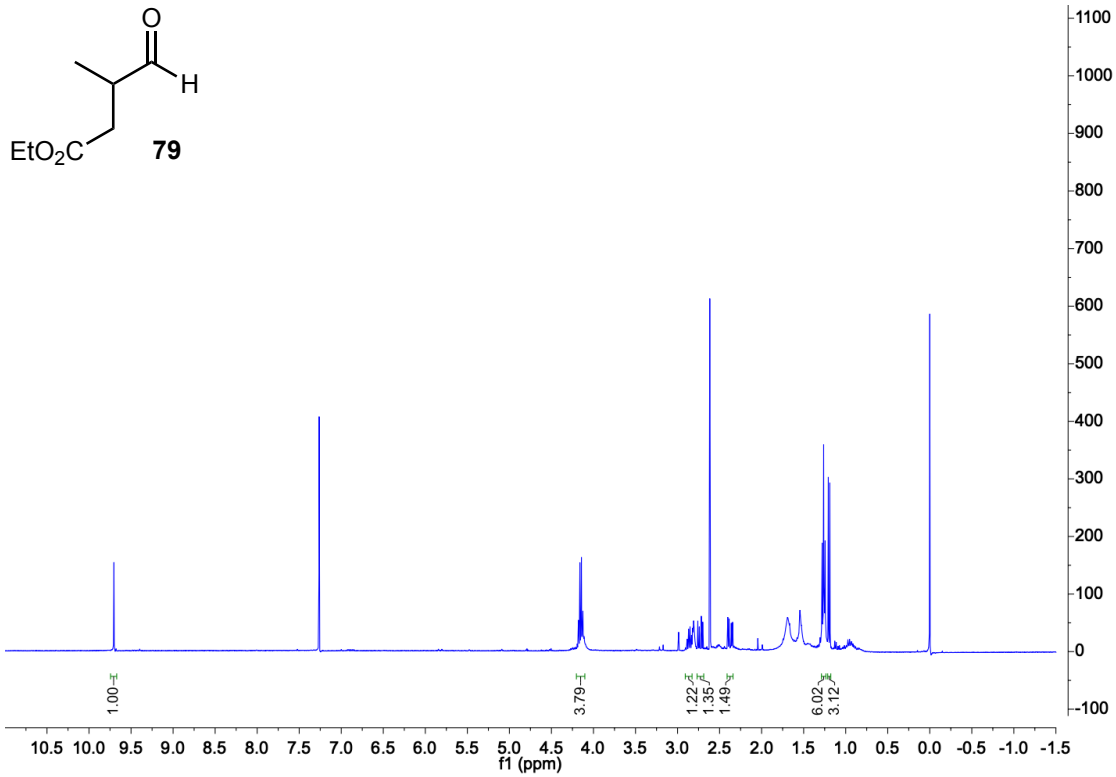


Figure 110. $^{1}$H-NMR spectrum ($CDCl_3$, 400 MHz) of compound **79**

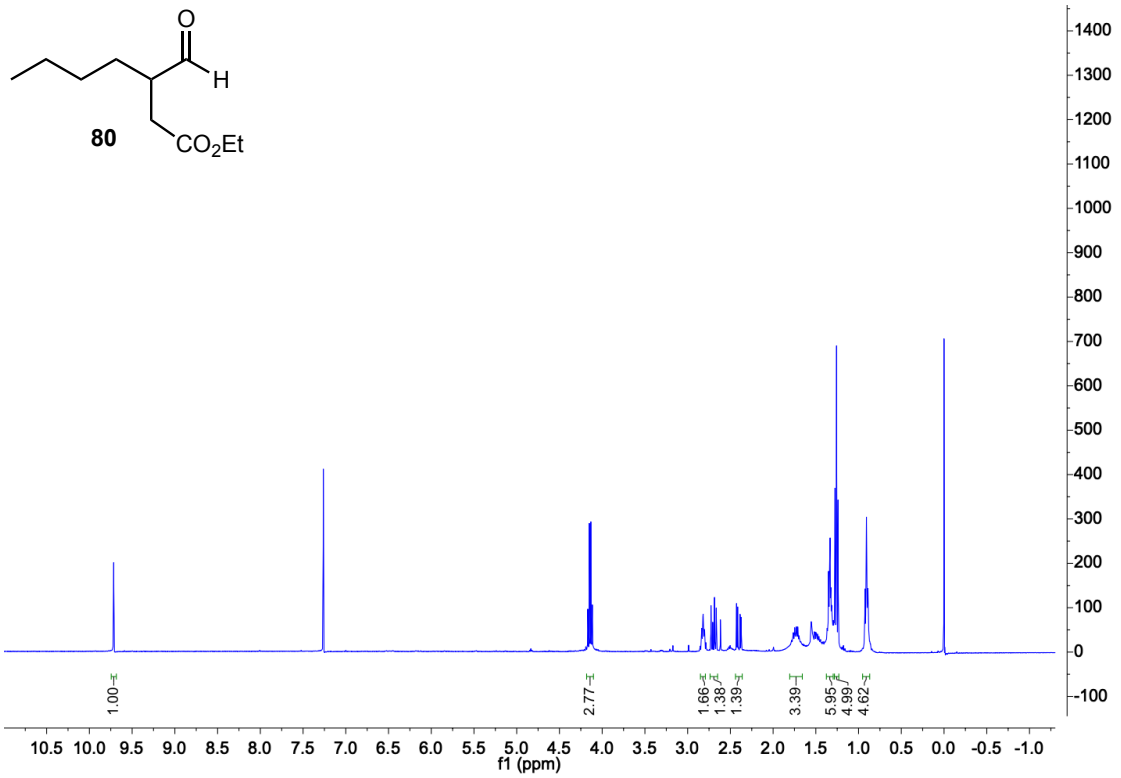


Figure 111. $^{1}$H-NMR spectrum ($CDCl_3$, 400 MHz) of compound **80**

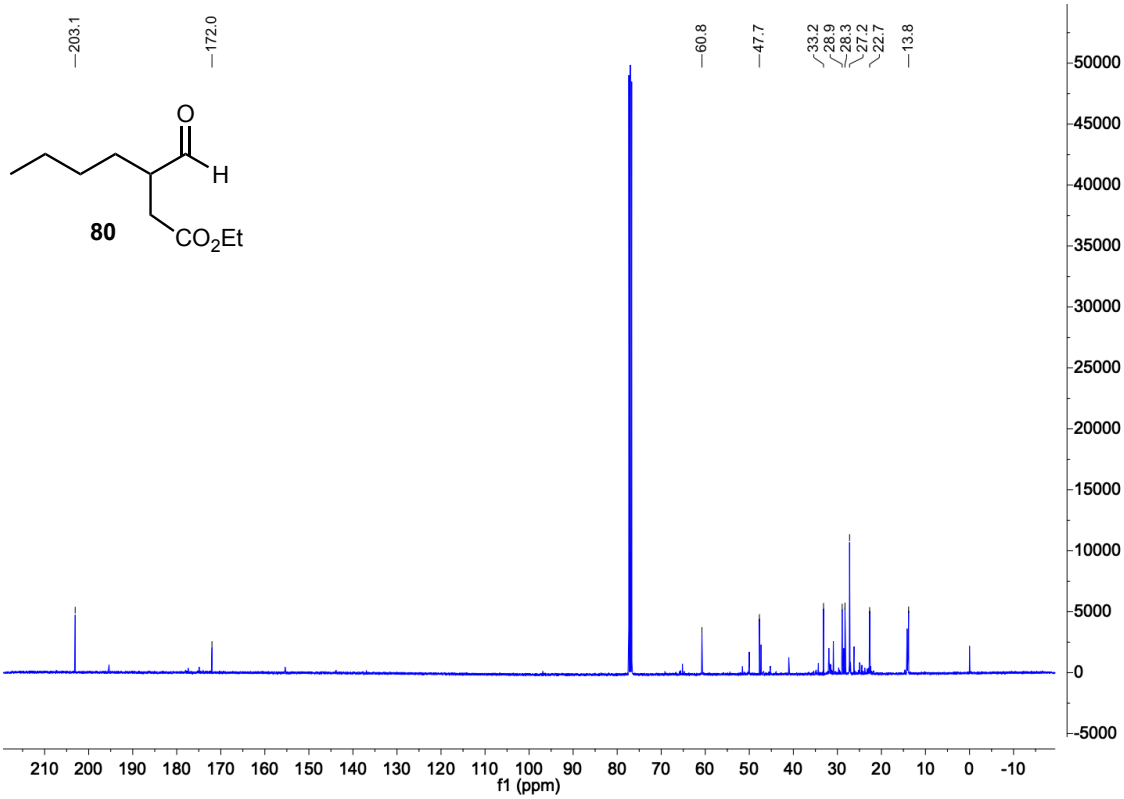


Figure 112. $^{13}$C-NMR spectrum ($CDCl_3$, 400 MHz) of compound **80**

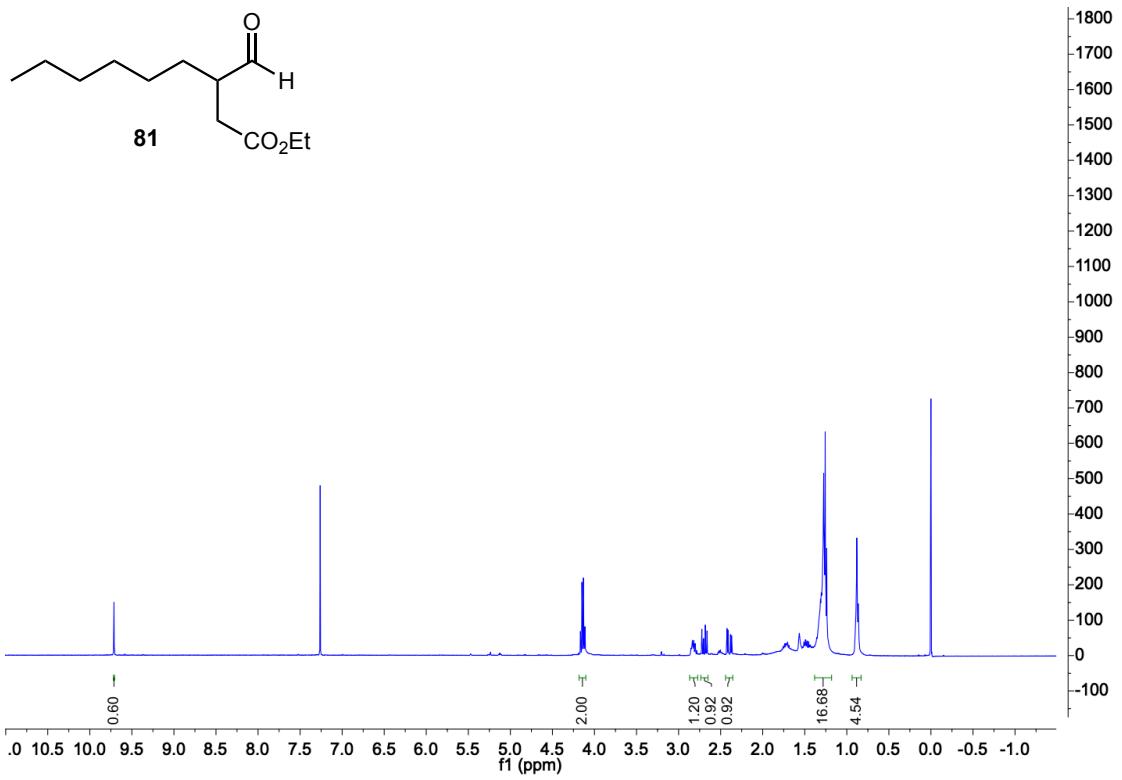


Figure 113. $^{1}$H-NMR spectrum ($CDCl_3$, 400 MHz) of compound **81**

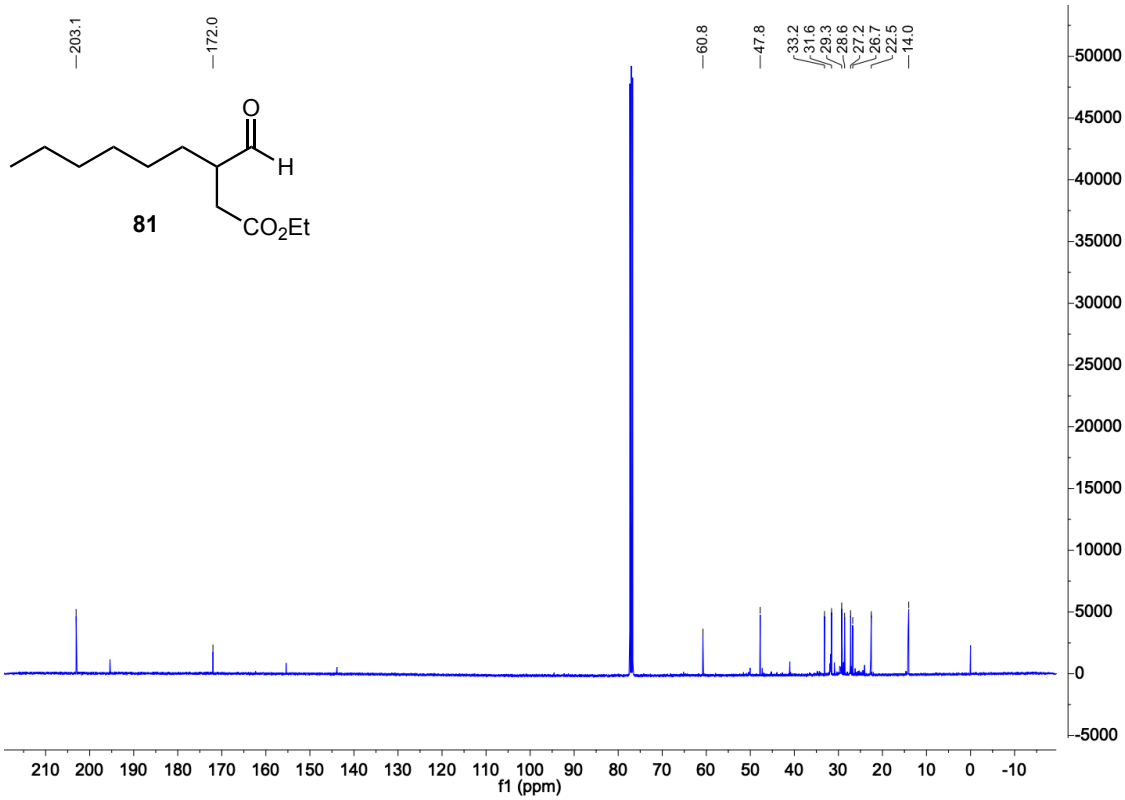


Figure 114. $^{13}$C-NMR spectrum ($CDCl_3$, 400 MHz) of compound **81**

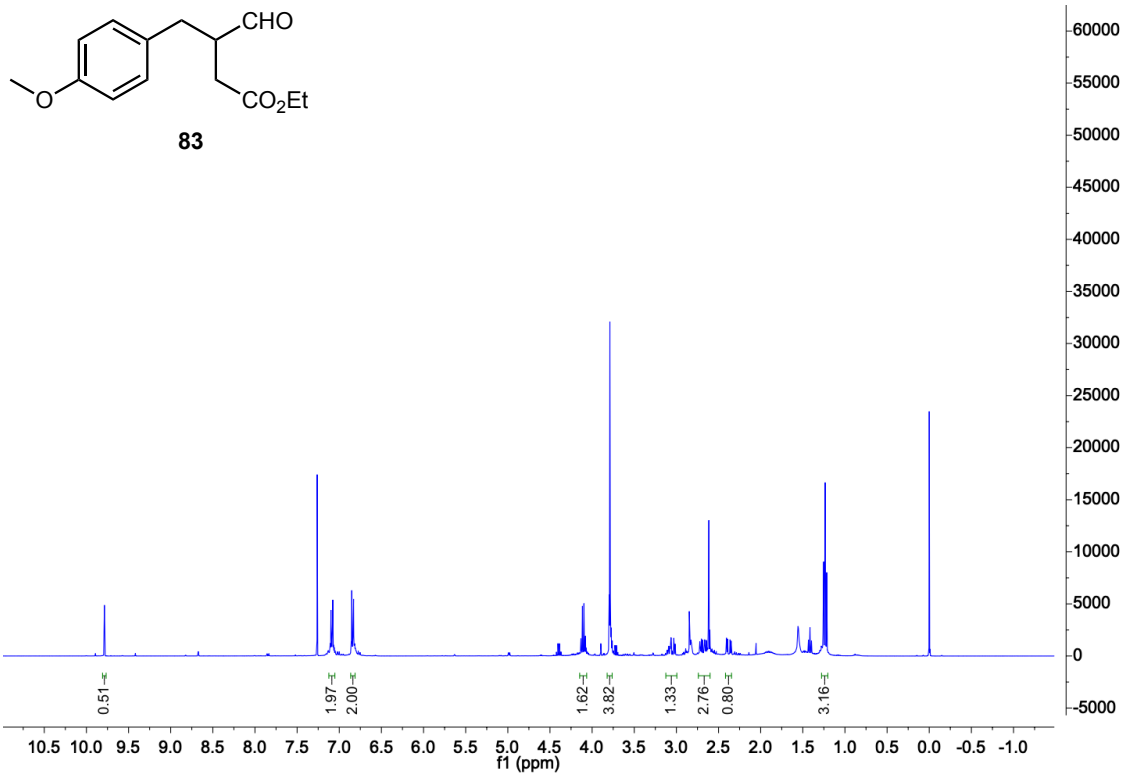


Figure 115. $^{1}$H-NMR spectrum ($CDCl_3$, 400 MHz) of compound **83**

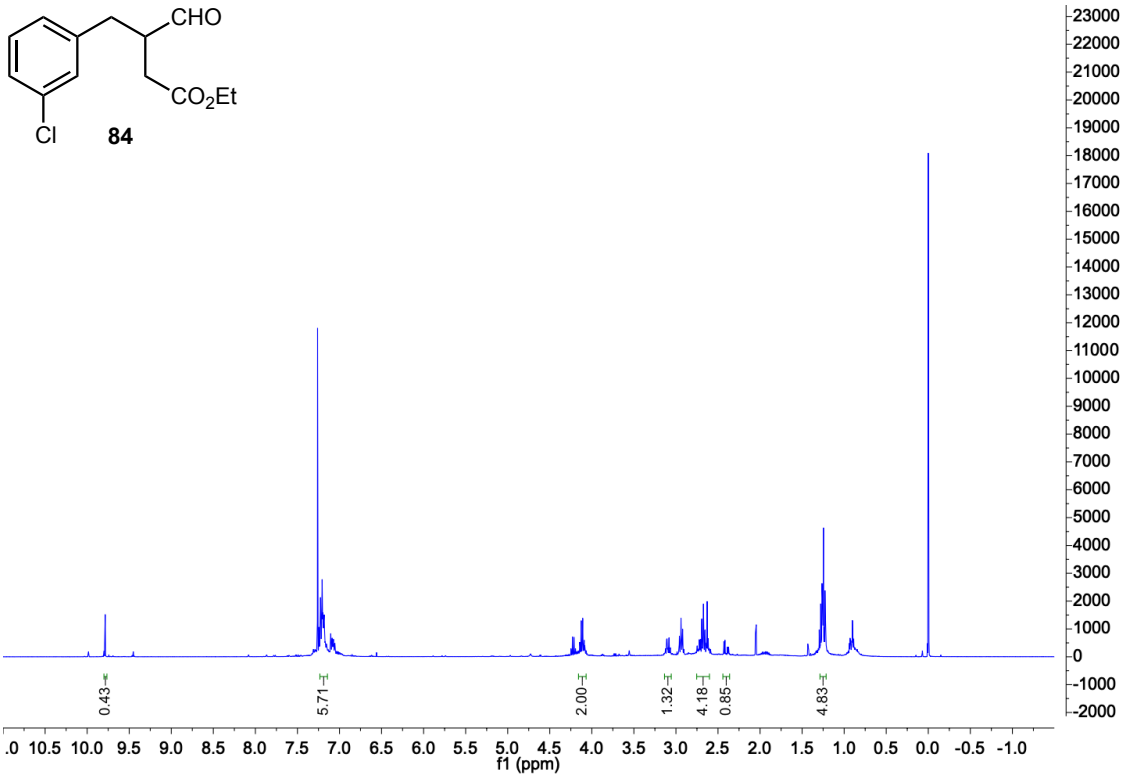


Figure 116. $^{1}$H-NMR spectrum ($CDCl_3$, 400 MHz) of compound **84**

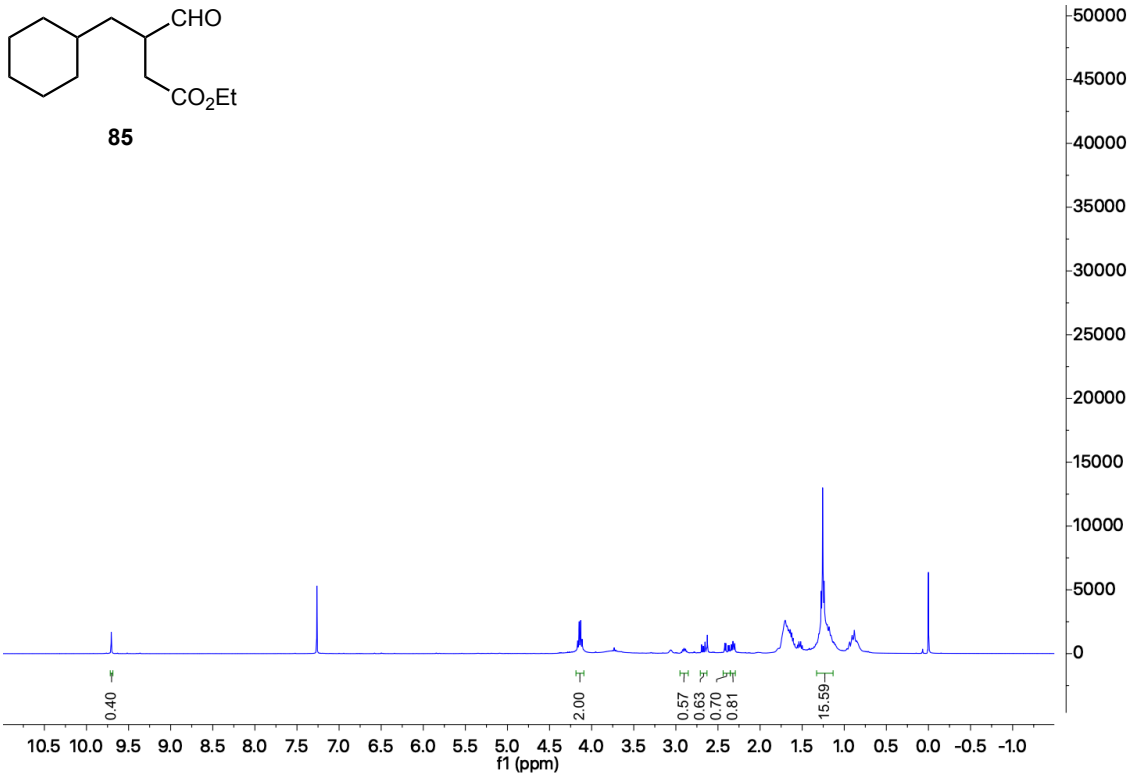


Figure 117. $^{1}$H-NMR spectrum ($CDCl_3$, 400 MHz) of compound **85**

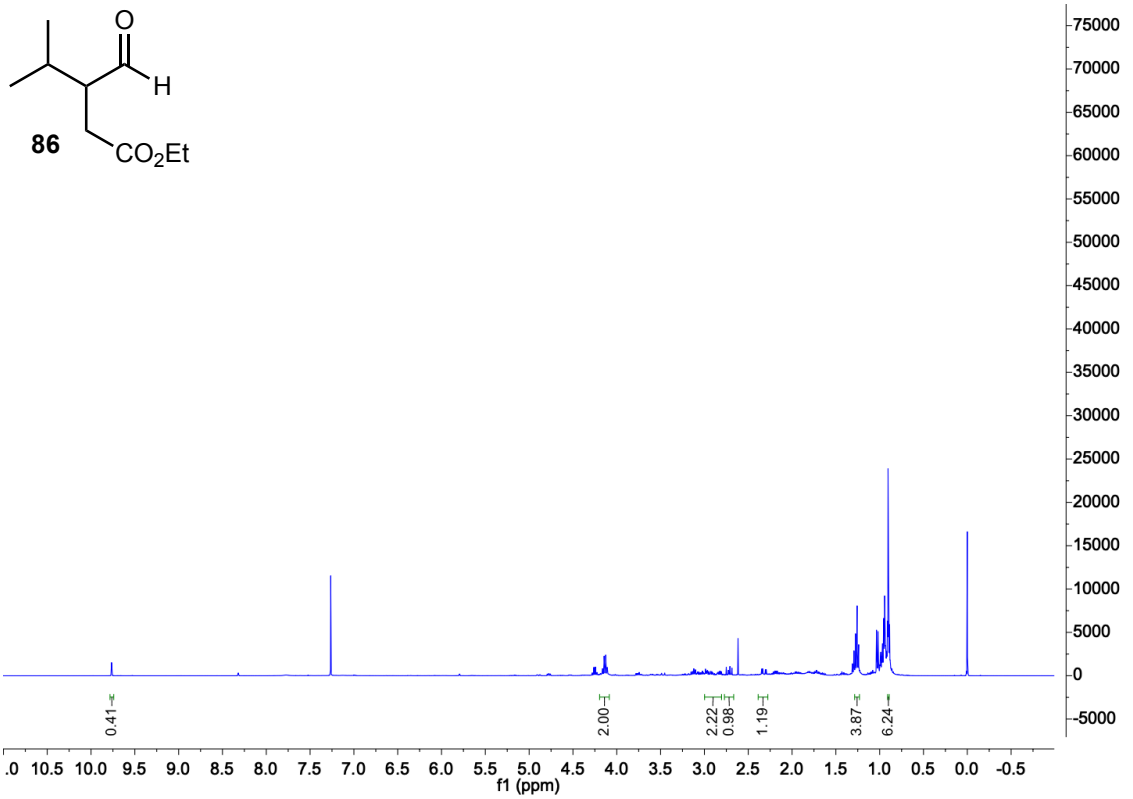


Figure 118. $^{1}$H-NMR spectrum ($CDCl_3$, 400 MHz) of compound **86**

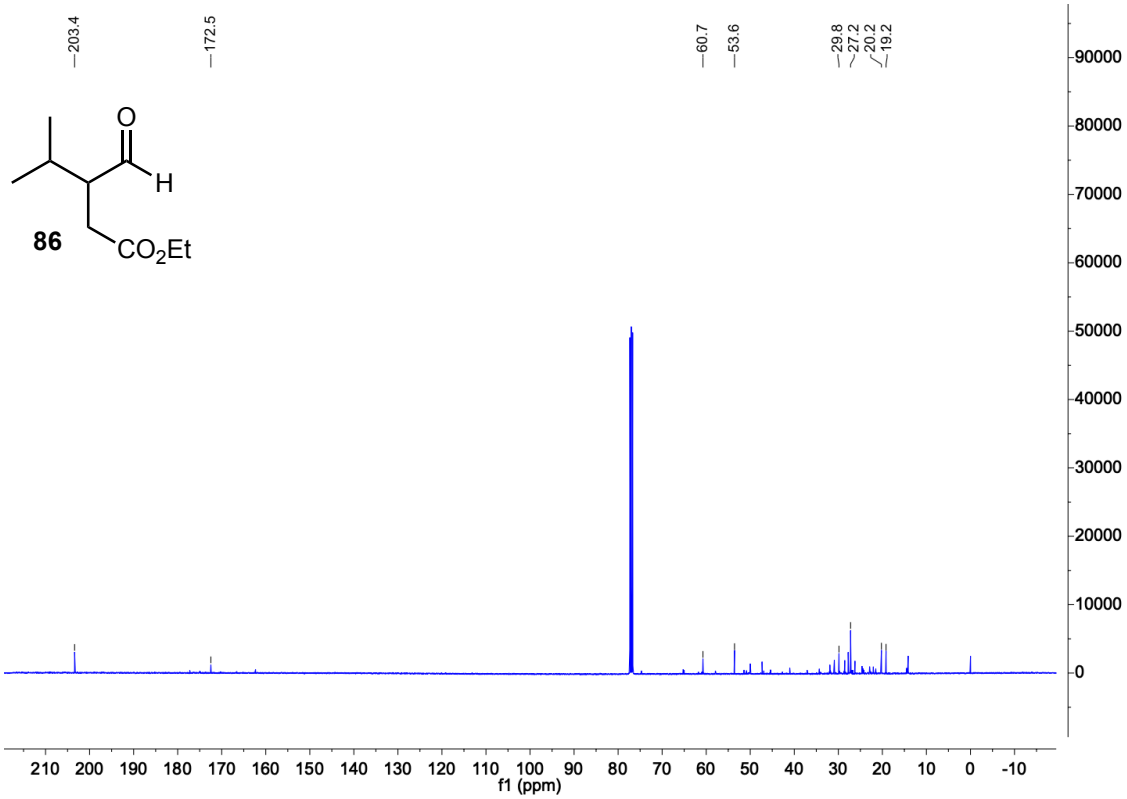


Figure 119. $^{13}$C-NMR spectrum ($CDCl_3$, 400 MHz) of compound **86**

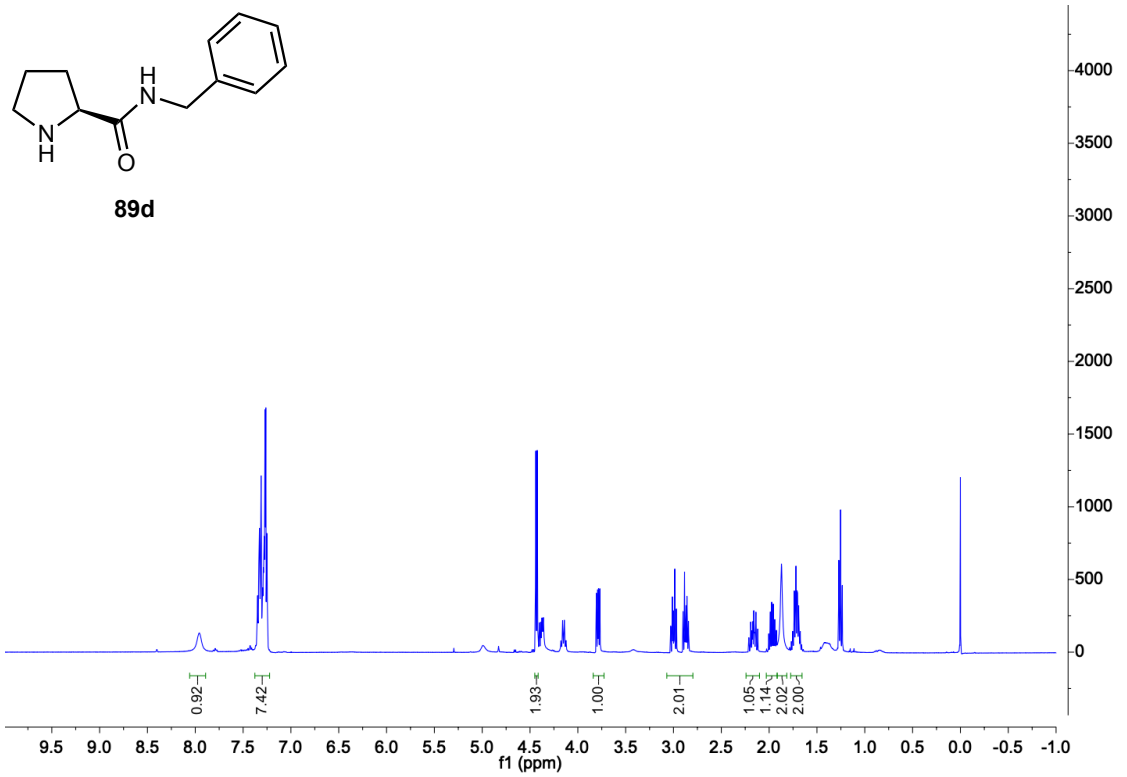


Figure 120. $^{1}$H-NMR spectrum ($CDCl_3$, 400 MHz) of compound **89d**

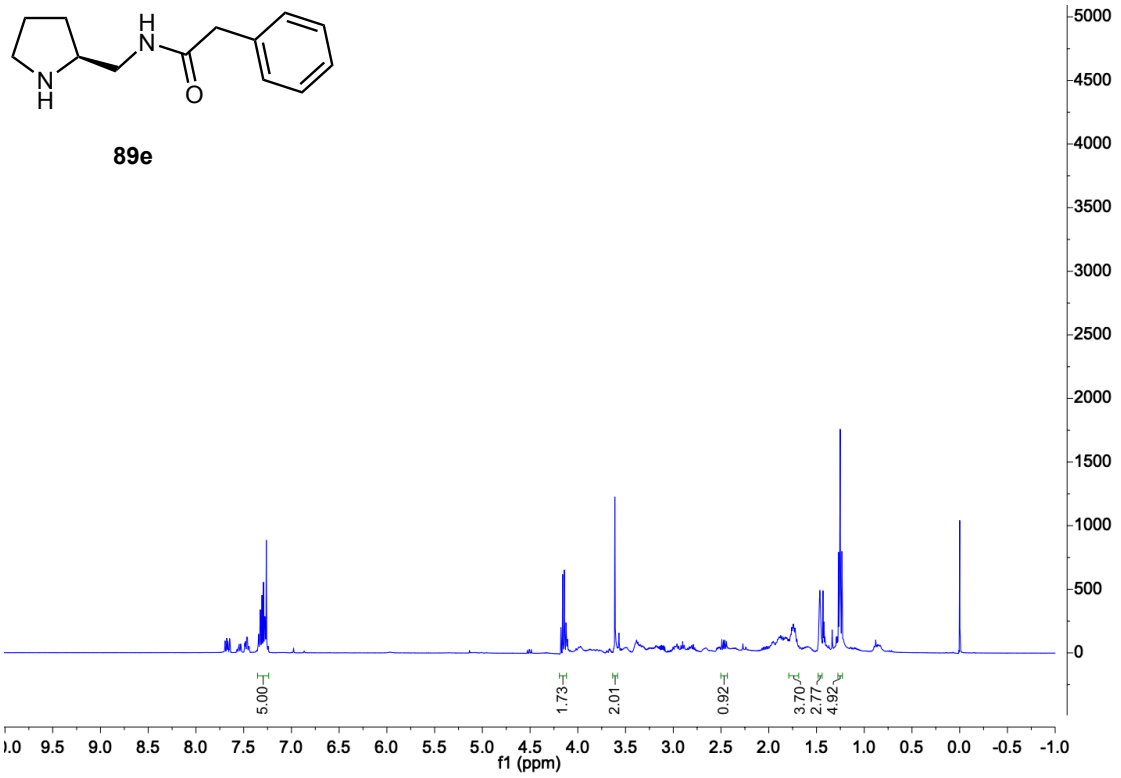


Figure 121. $^{1}$H-NMR spectrum ($CDCl_3$, 400 MHz) of compound **89e**

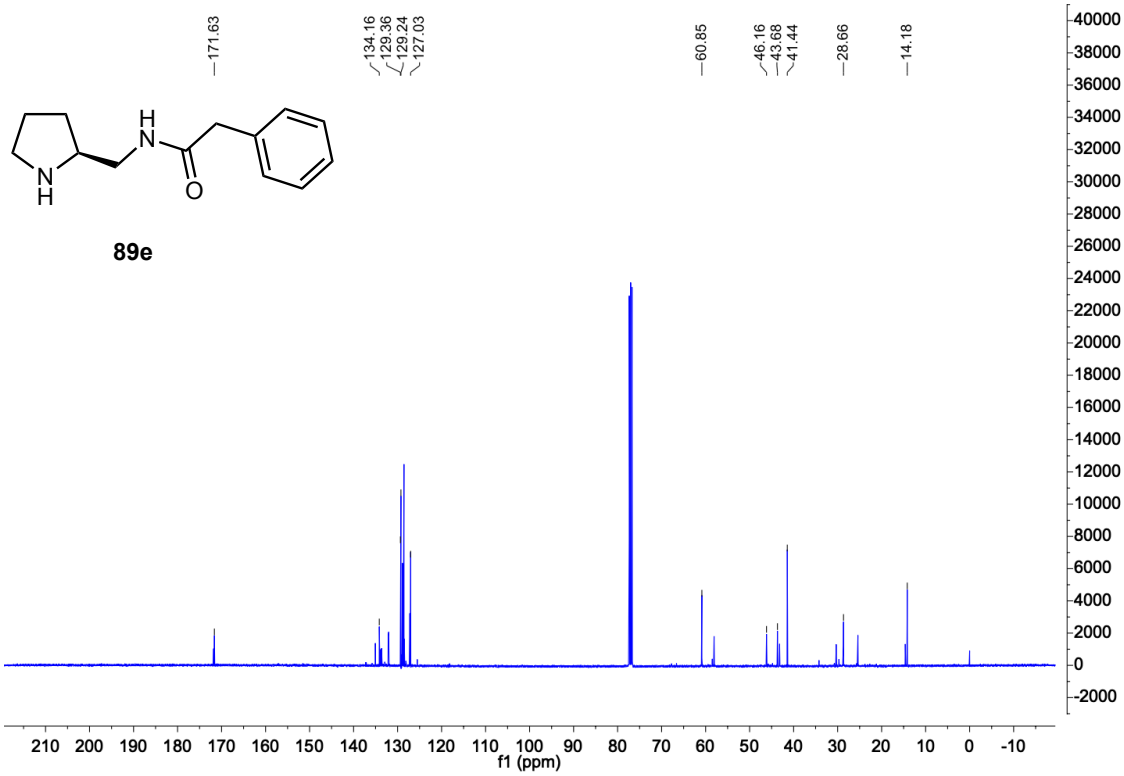


Figure 122. $^{13}$C-NMR spectrum ($CDCl_3$, 400 MHz) of compound **89e**

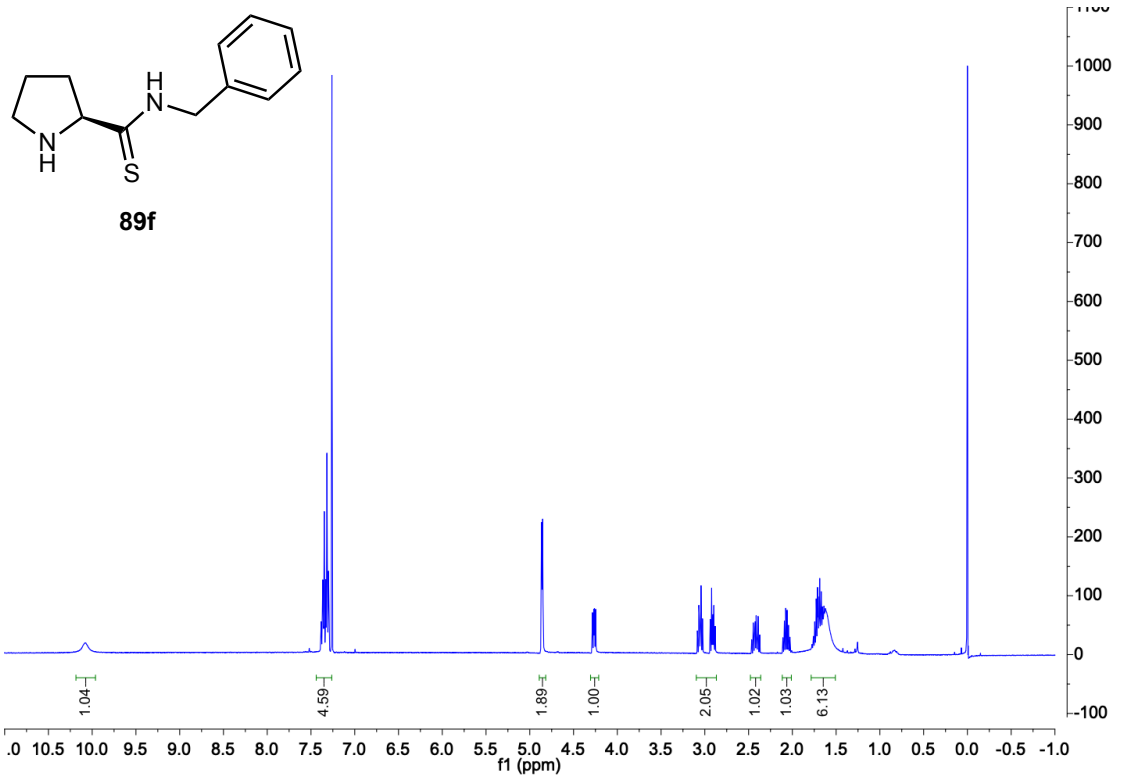


Figure 123. $^{1}$H-NMR spectrum ($CDCl_3$, 400 MHz) of compound **89f**

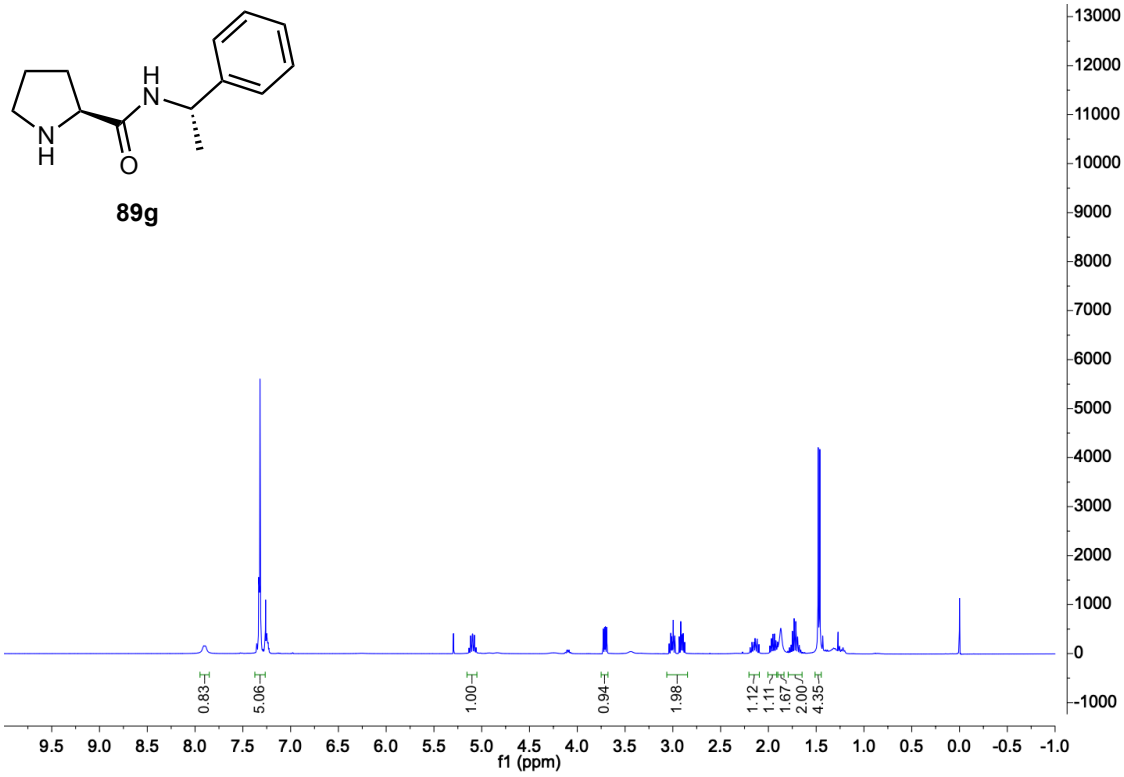


Figure 124. $^{1}$H-NMR spectrum ($CDCl_3$, 400 MHz) of compound **89g**

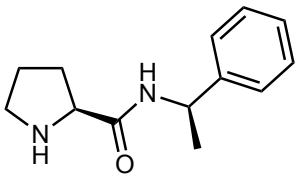

**89h**




Figure 125. $^{1}$H-NMR spectrum ($CDCl_3$, 400 MHz) of compound **89h**

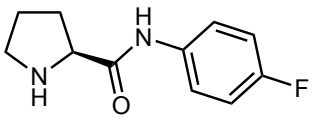

**89i**




Figure 126. $^{1}$H-NMR spectrum ($CDCl_3$, 400 MHz) of compound **89i**

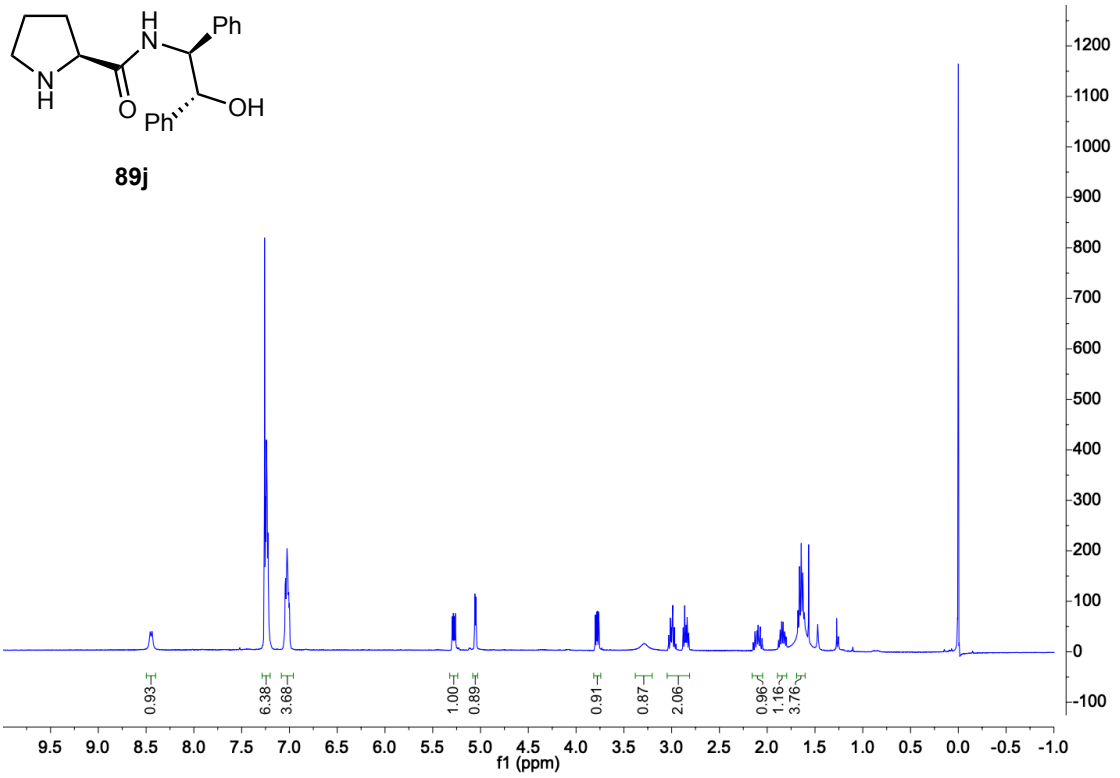


Figure 127. $^{1}$H-NMR spectrum ($CDCl_3$, 400 MHz) of compound **89j**

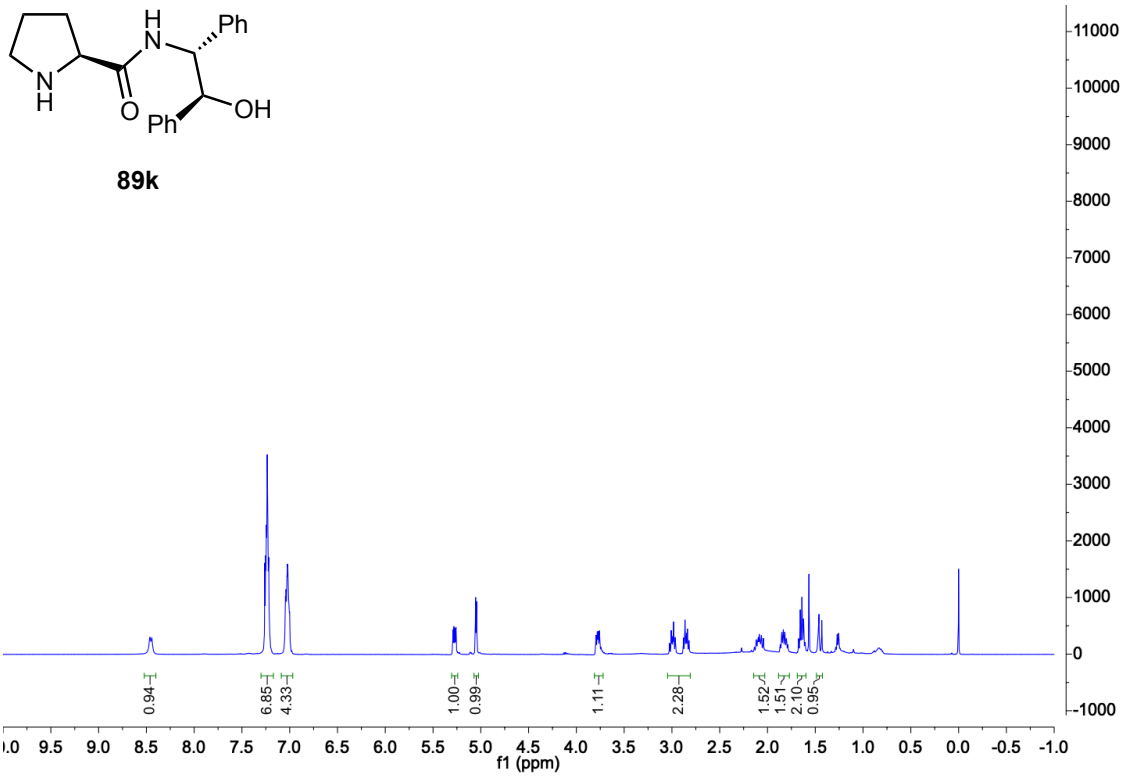


Figure 128. $^{1}$H-NMR spectrum ($CDCl_3$, 400 MHz) of compound **89k**

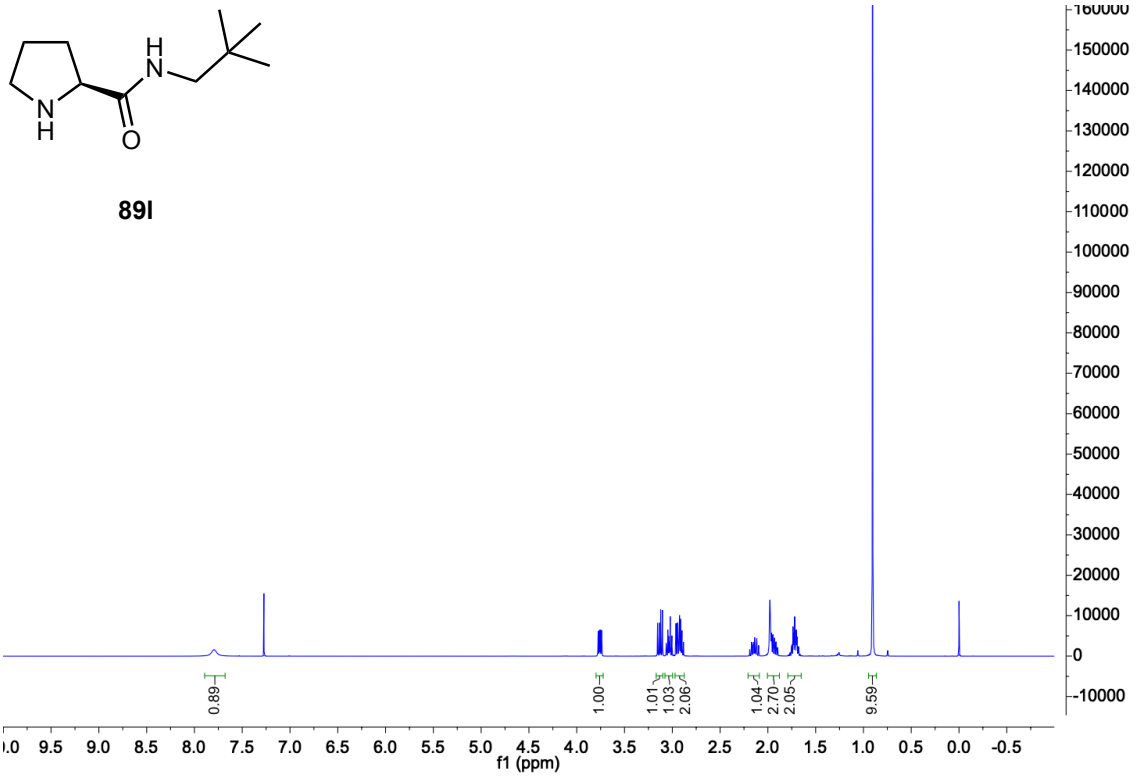


Figure 129. $^{1}$H-NMR spectrum ($CDCl_3$, 400 MHz) of compound **89l**

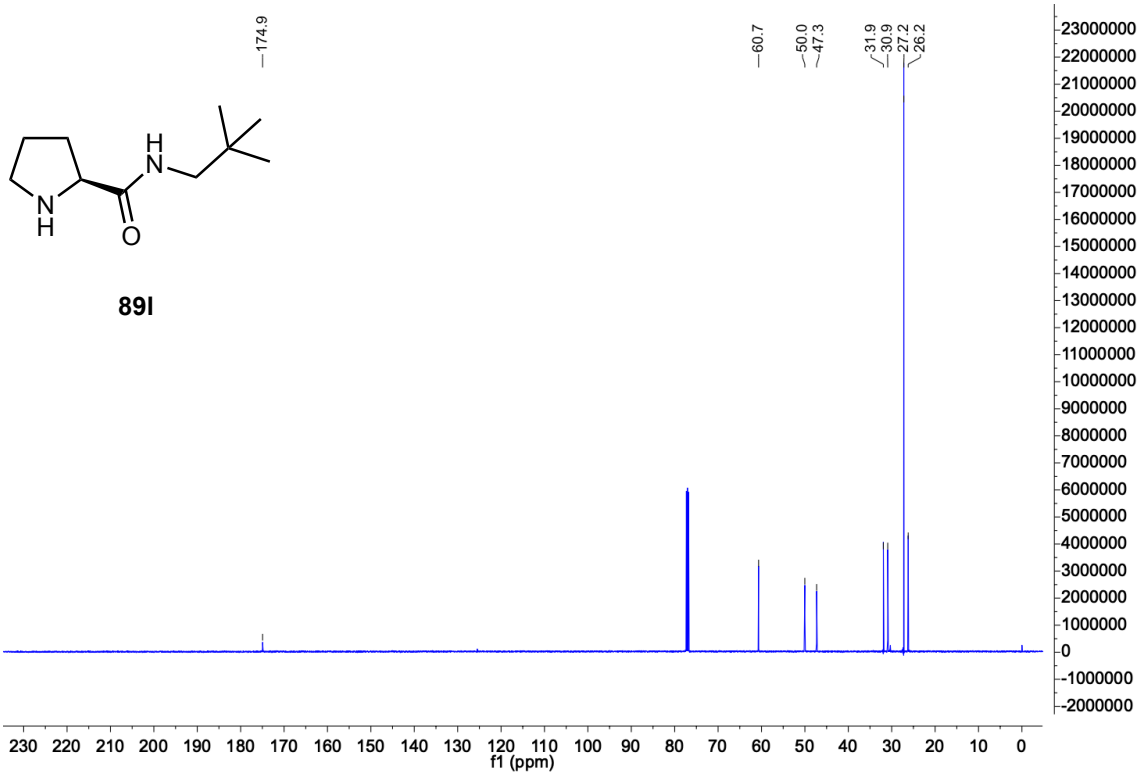


Figure 130. $^{13}$C-NMR spectrum ($CDCl_3$, 400 MHz) of compound **89l**

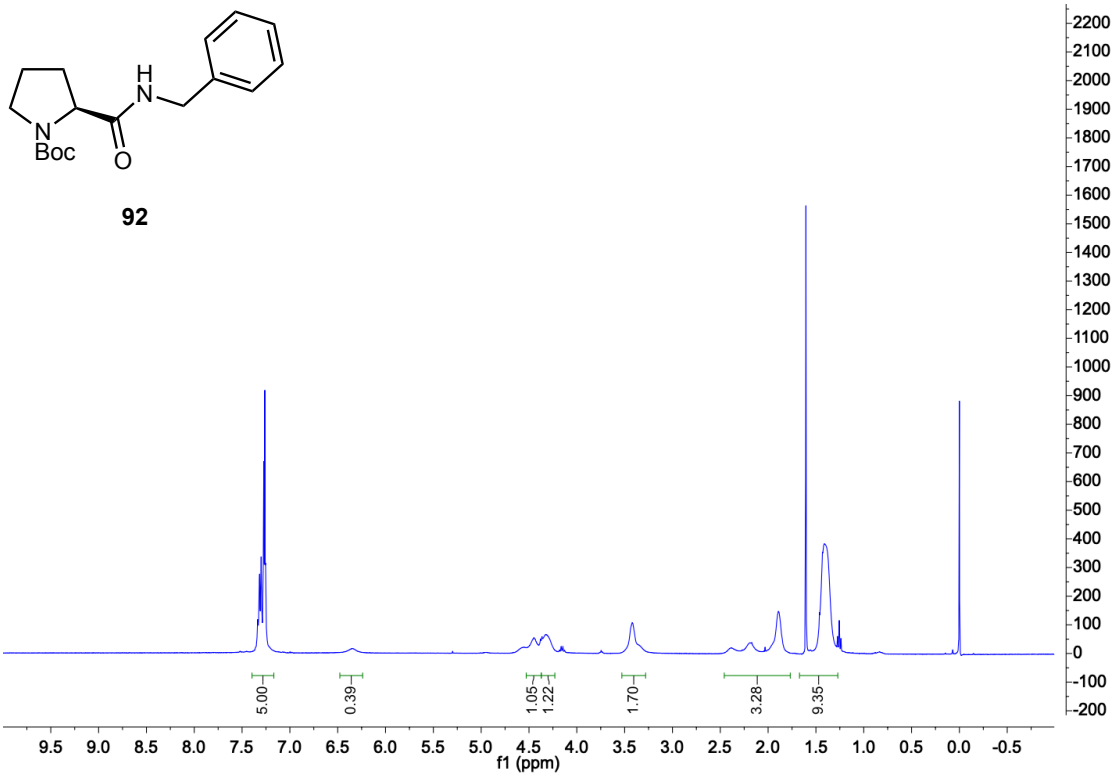


Figure 131. $^{1}$H-NMR spectrum ($CDCl_3$, 400 MHz) of compound **92**

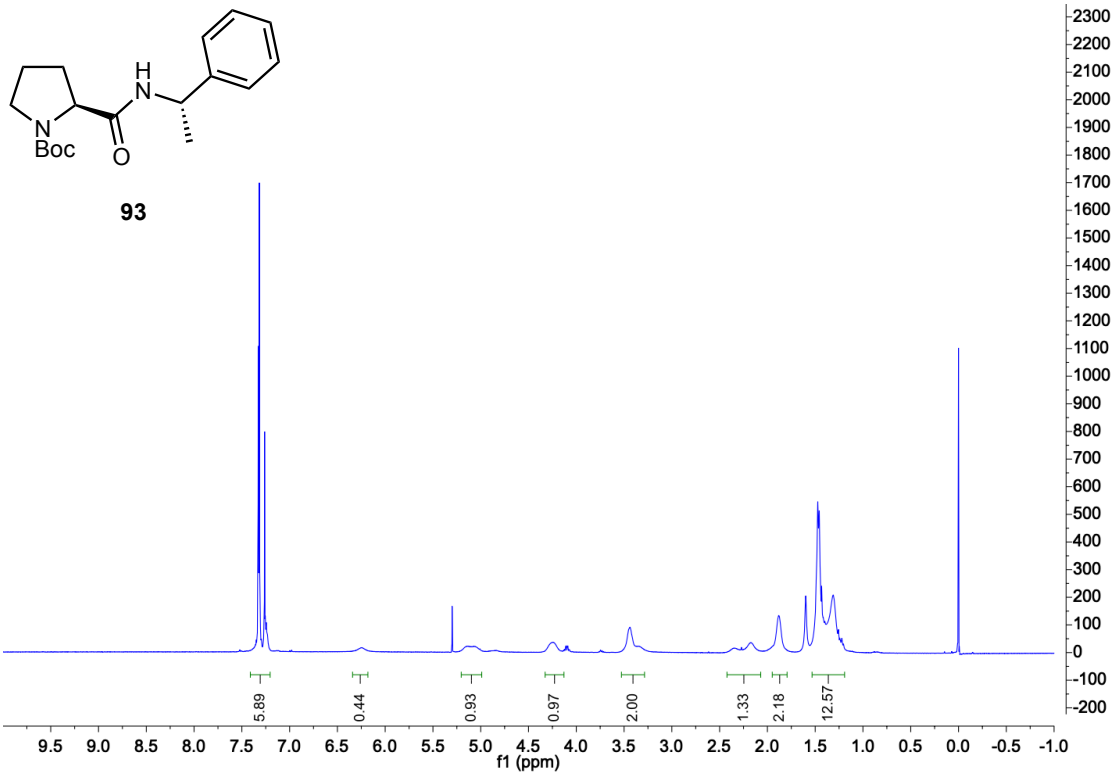


Figure 132. $^{1}$H-NMR spectrum ($CDCl_3$, 400 MHz) of compound **93**

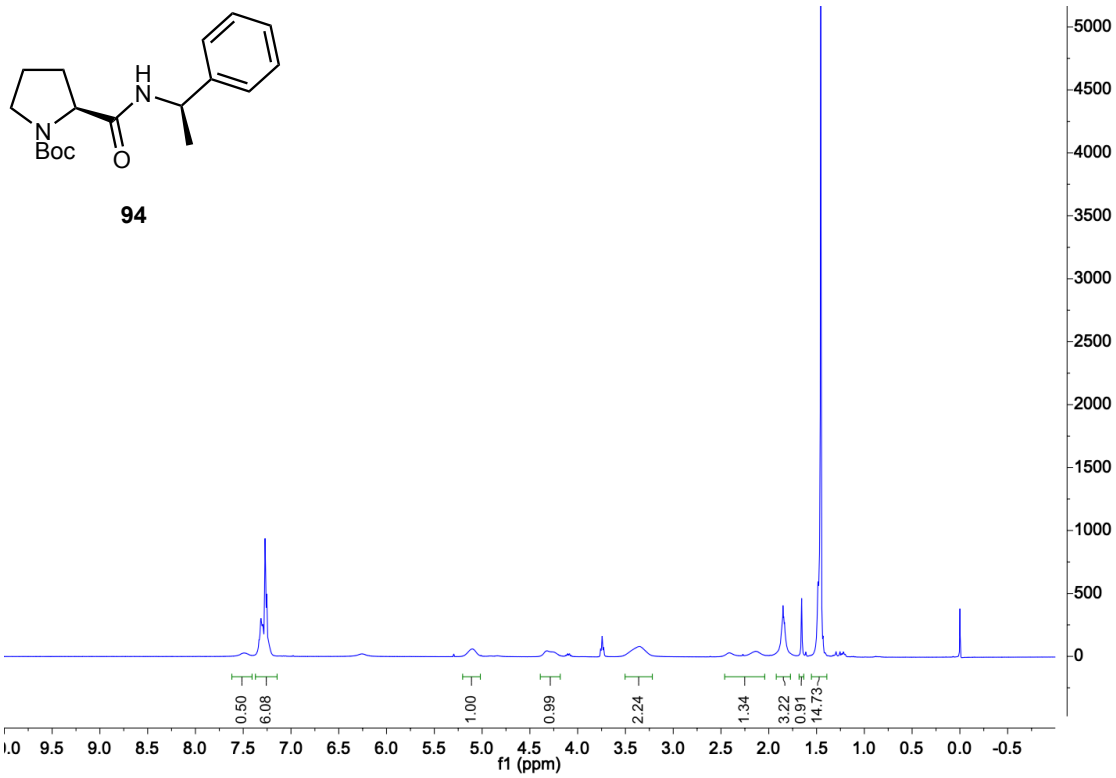


Figure 133. $^{1}$H-NMR spectrum ($CDCl_3$, 400 MHz) of compound **94**

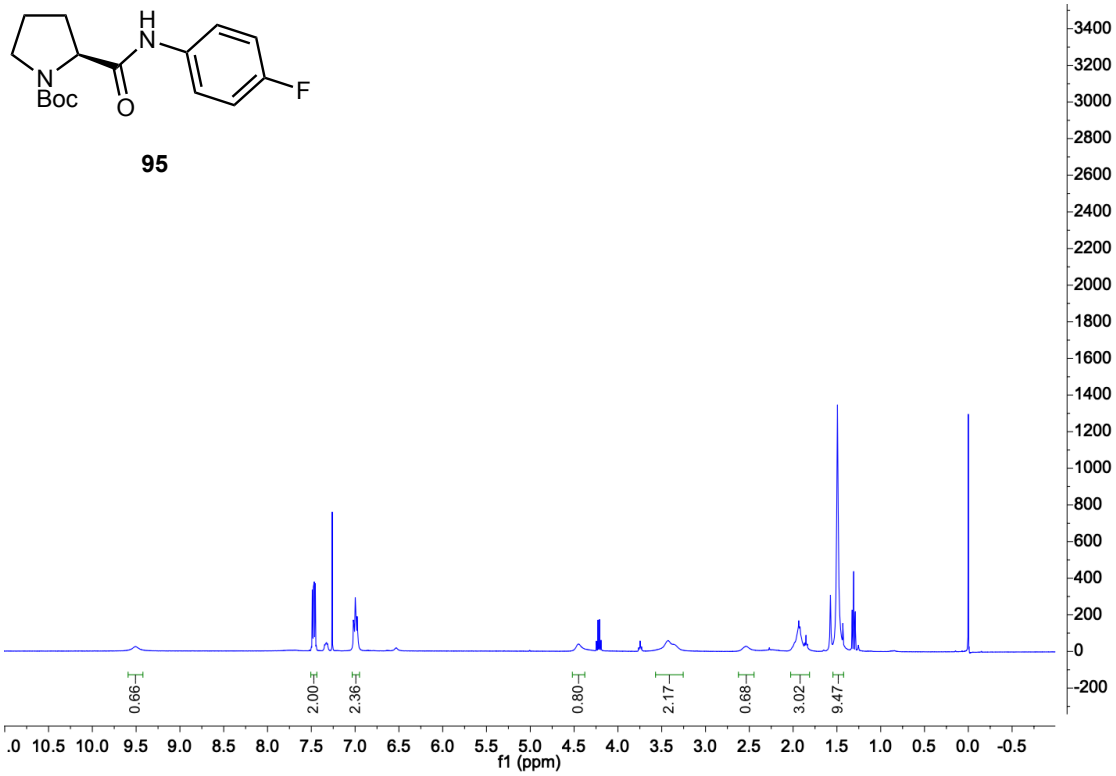


Figure 134. $^{1}$H-NMR spectrum ($CDCl_3$, 400 MHz) of compound **95**

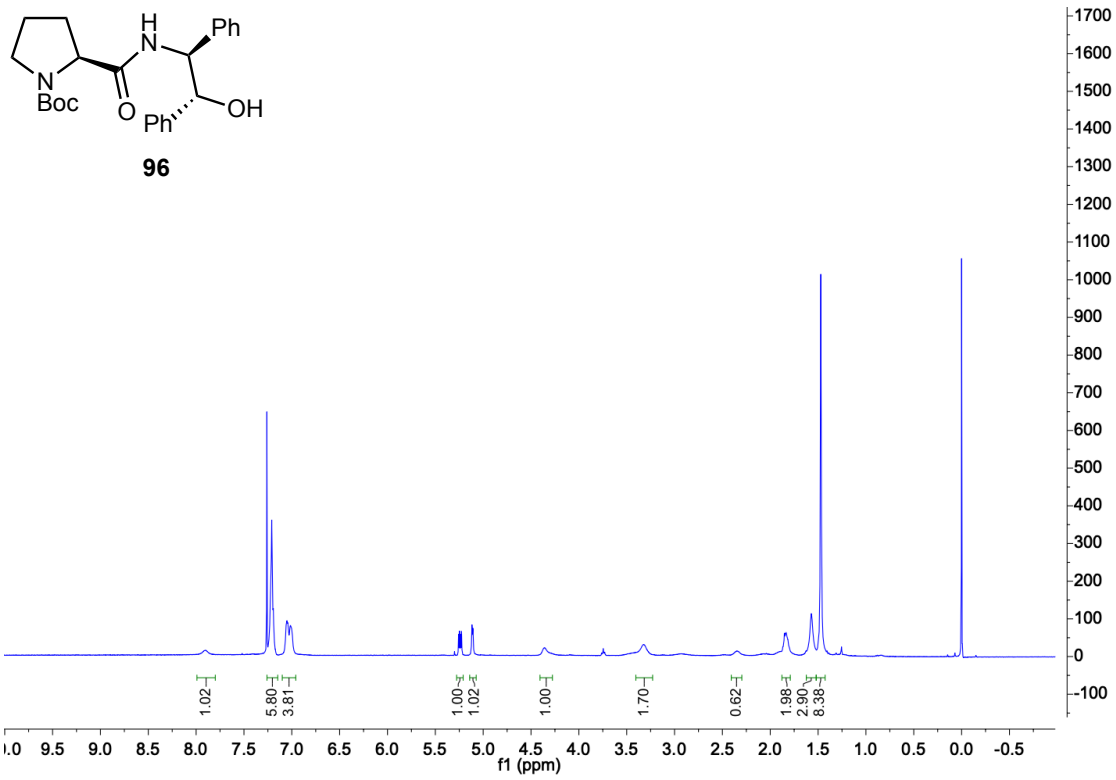


Figure 135. $^{1}$H-NMR spectrum ($CDCl_3$, 400 MHz) of compound **96**

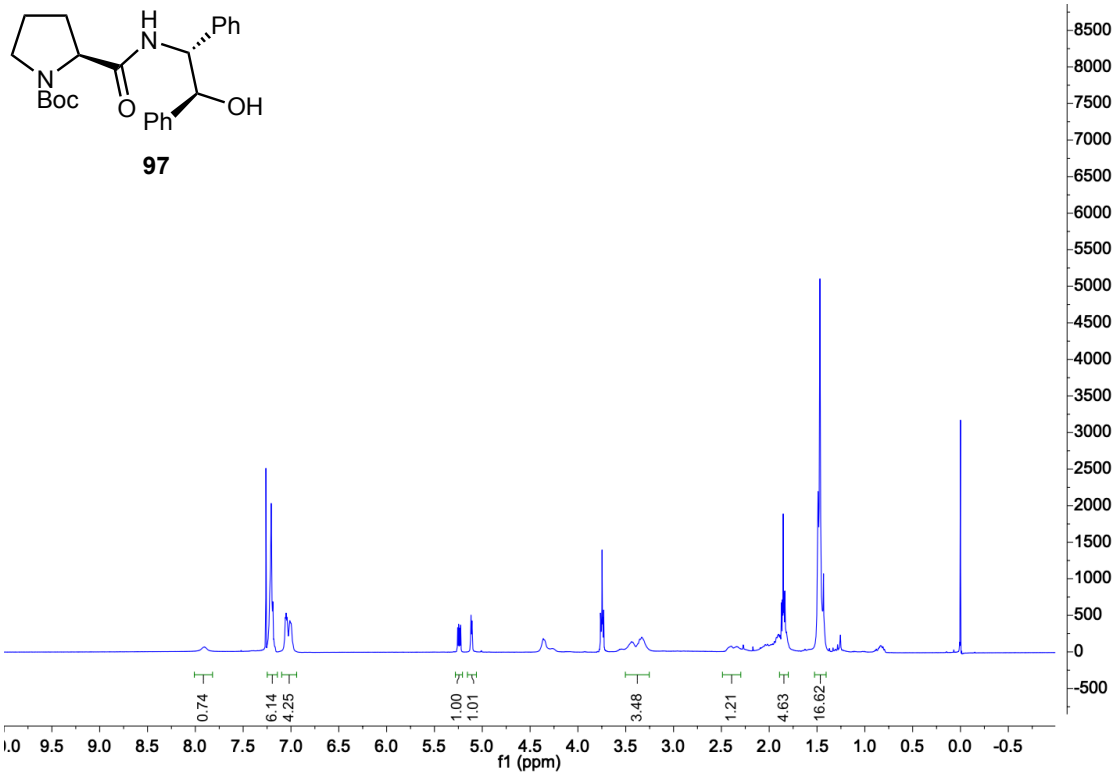


Figure 136. $^{1}$H-NMR spectrum ($CDCl_3$, 400 MHz) of compound **97**

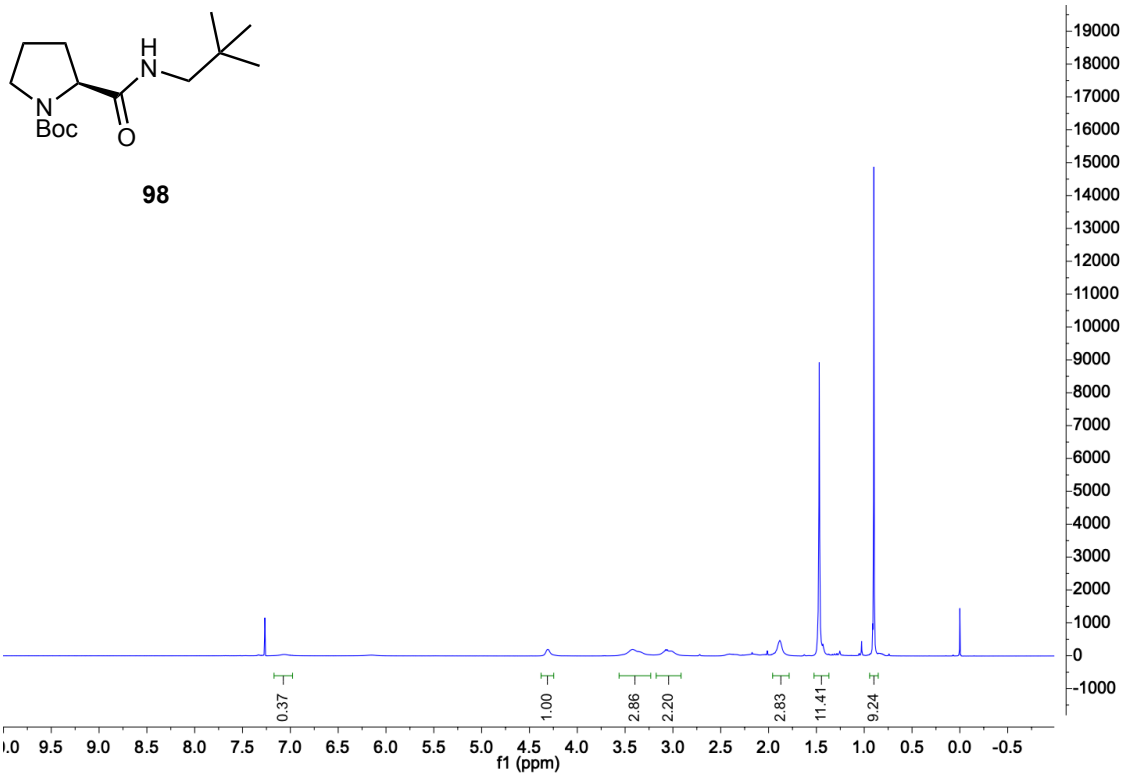


Figure 137. $^{1}$H-NMR spectrum ($CDCl_3$, 400 MHz) of compound **98**

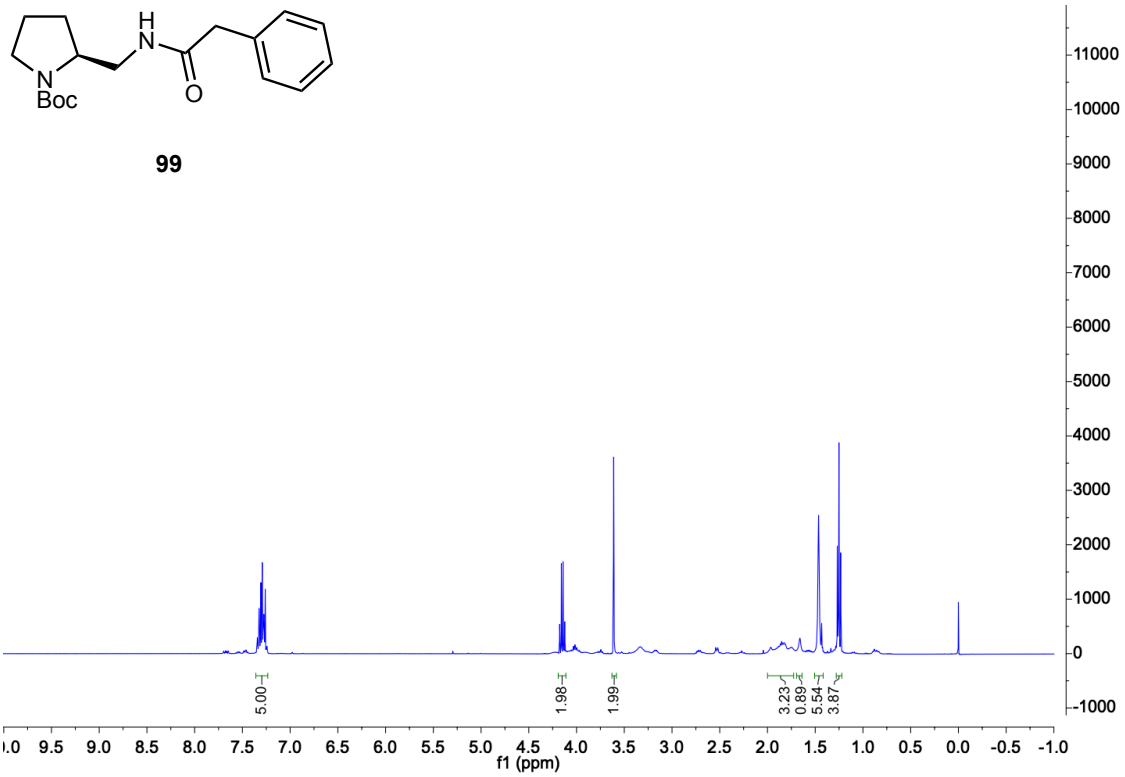


Figure 138. $^{1}$H-NMR spectrum ($CDCl_3$, 400 MHz) of compound **99**

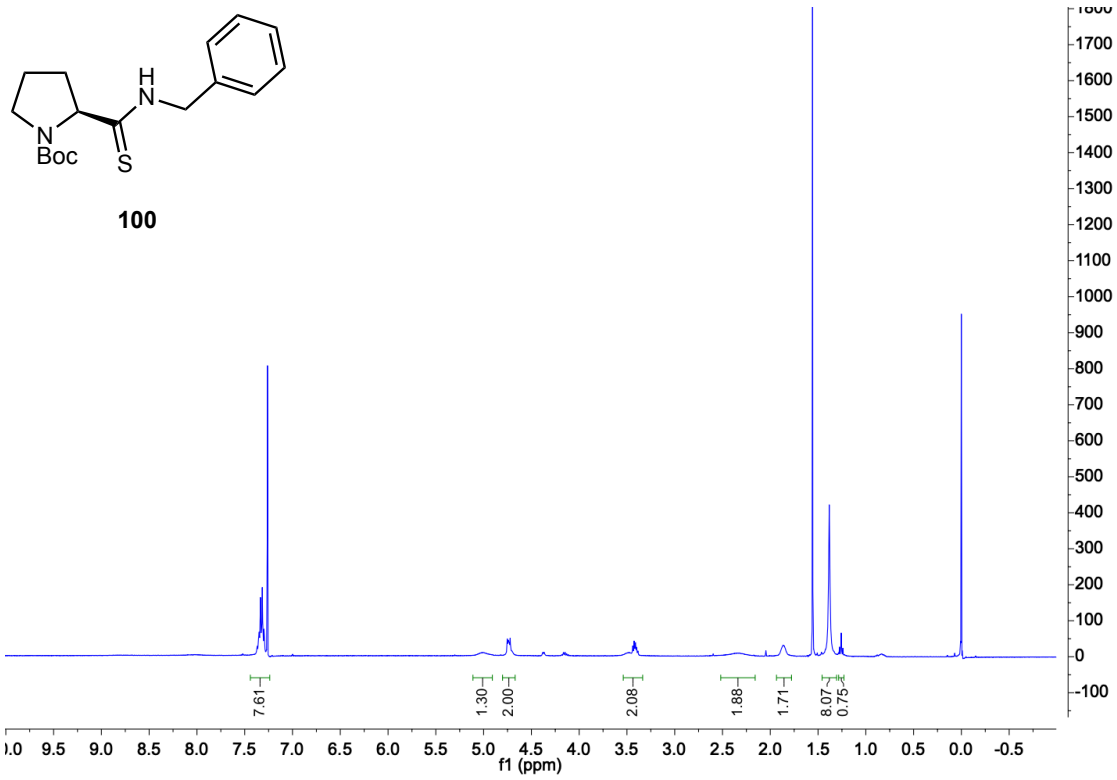


Figure 139. $^{1}$H-NMR spectrum ($CDCl_3$, 400 MHz) of compound **100**

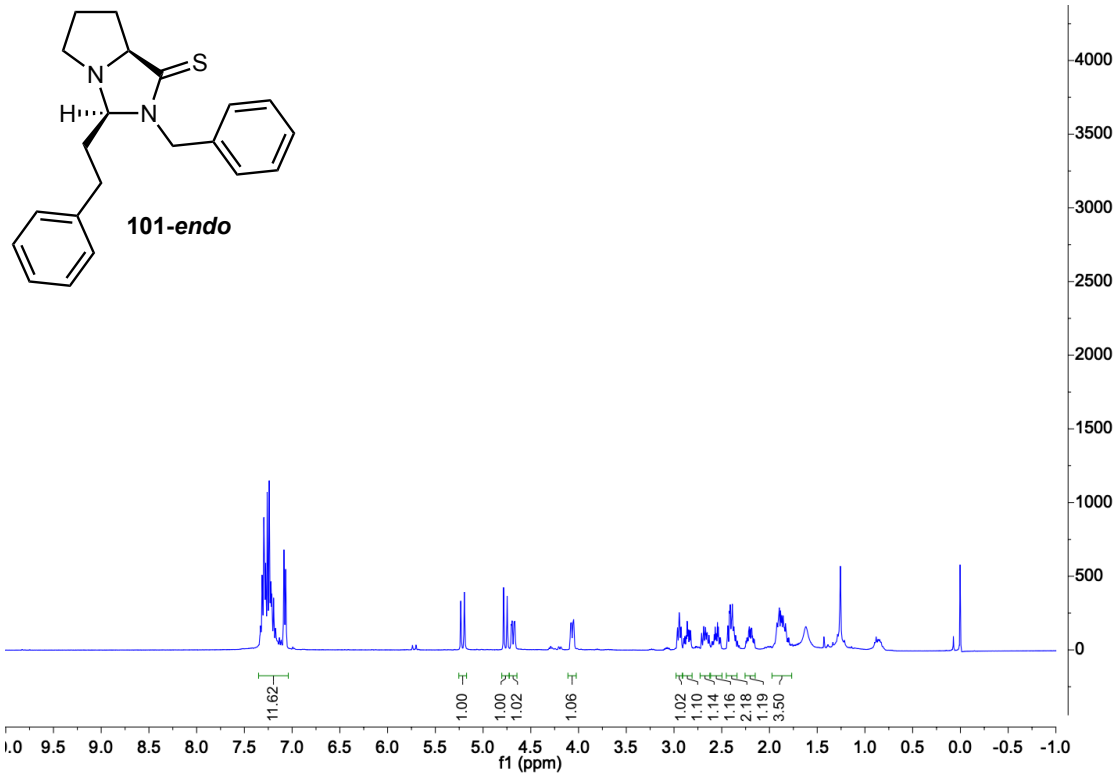


Figure 140. $^{1}$H-NMR spectrum ($CDCl_3$, 400 MHz) of compound **101-*endo***

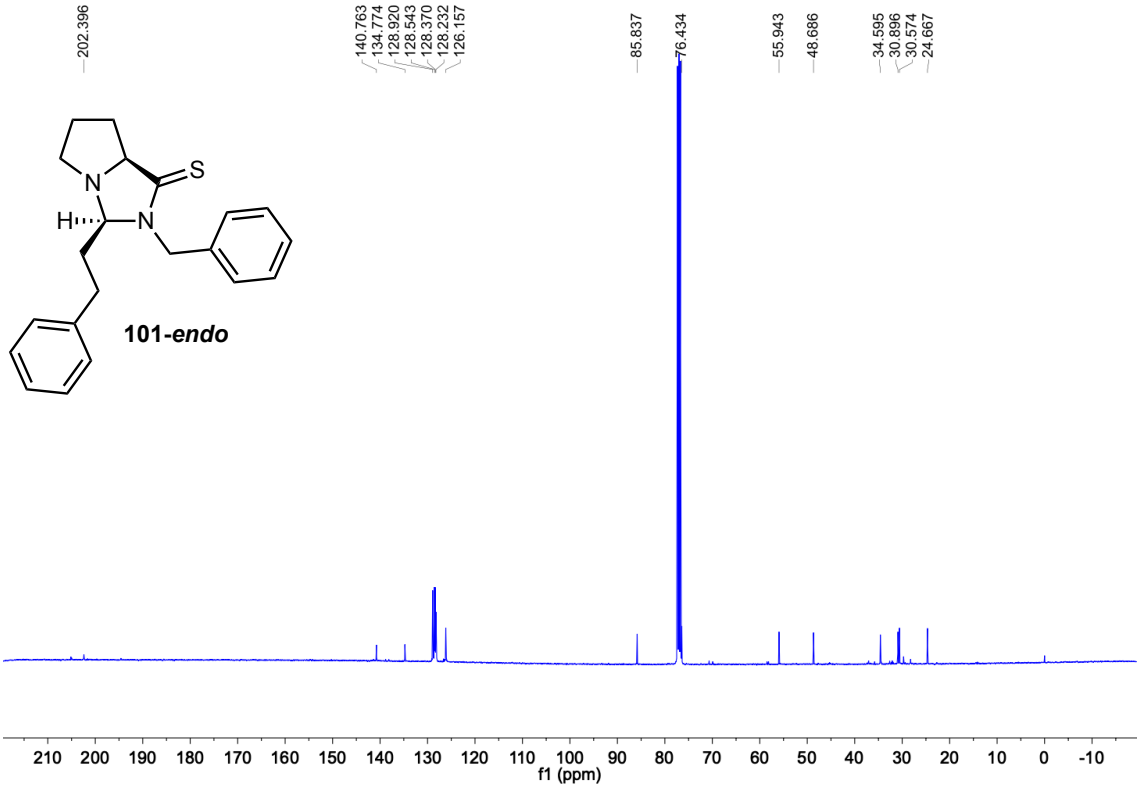


Figure 141. $^{13}$C-NMR spectrum ($CDCl_3$, 400 MHz) of compound **101-*endo***

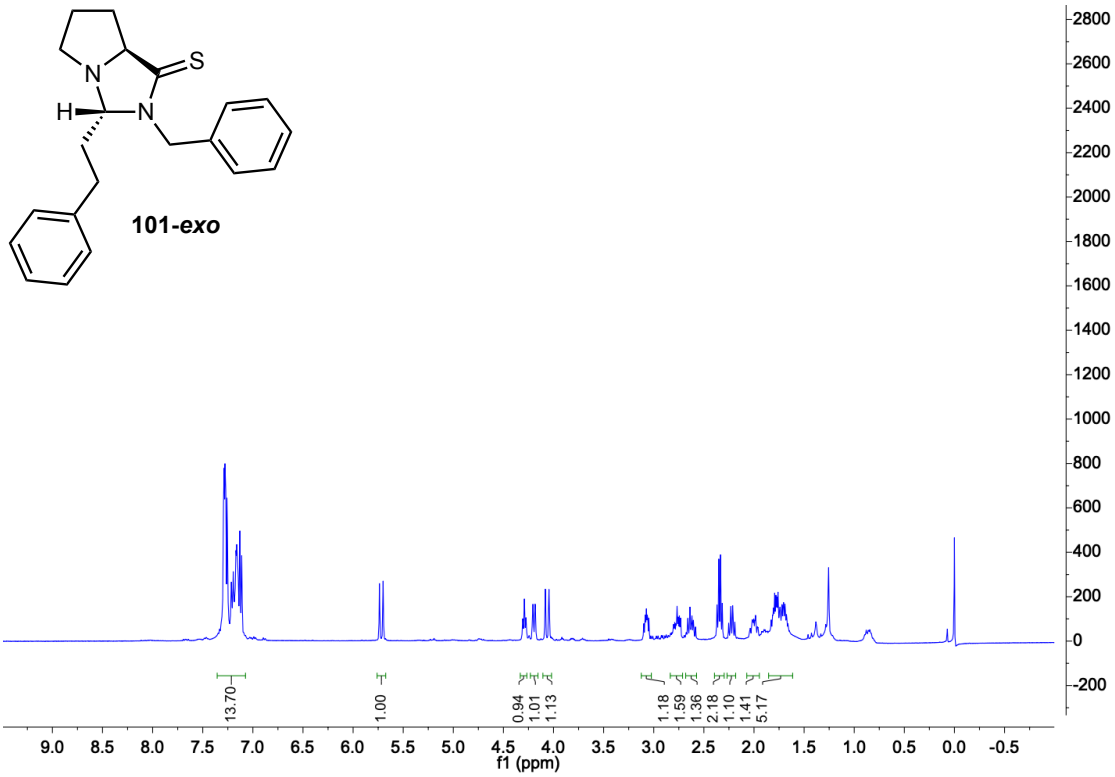


Figure 142. $^{1}$H-NMR spectrum ($CDCl_3$, 400 MHz) of compound **101-*exo***

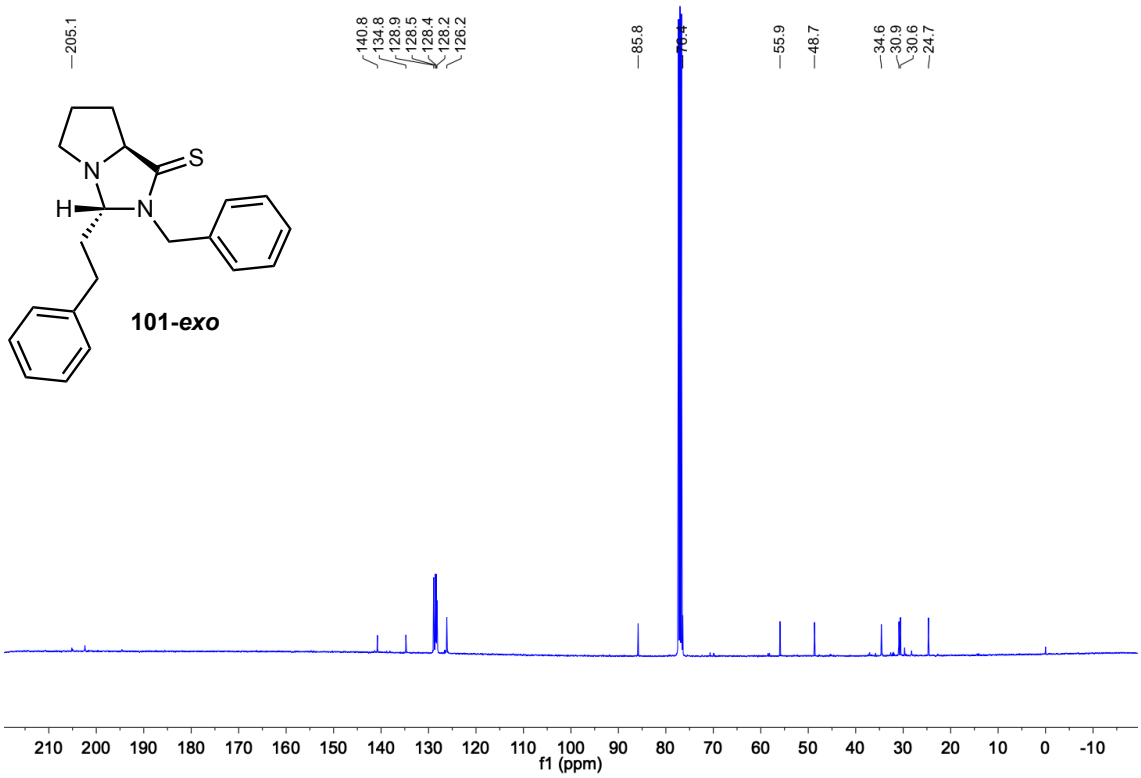


Figure 143. $^{13}$C-NMR spectrum ($CDCl_3$, 400 MHz) of compound **101-*exo***

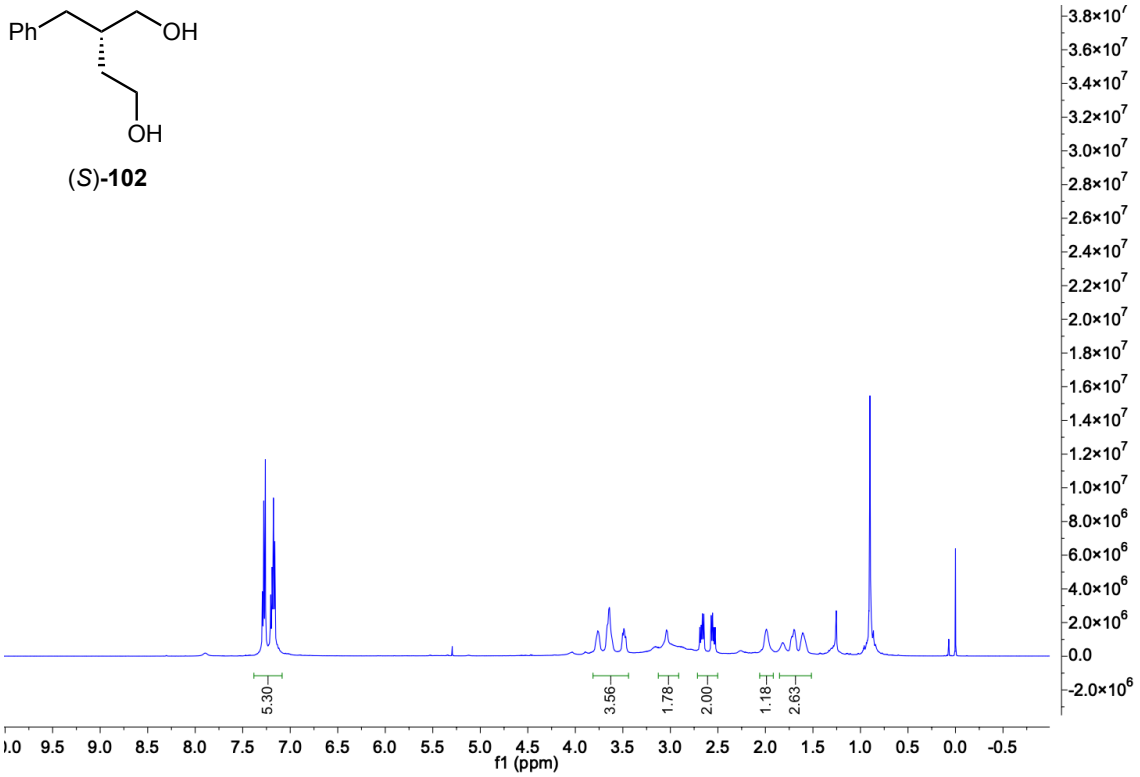


Figure 144. $^{1}$H-NMR spectrum ($CDCl_3$, 400 MHz) of enantiopure compound **102**

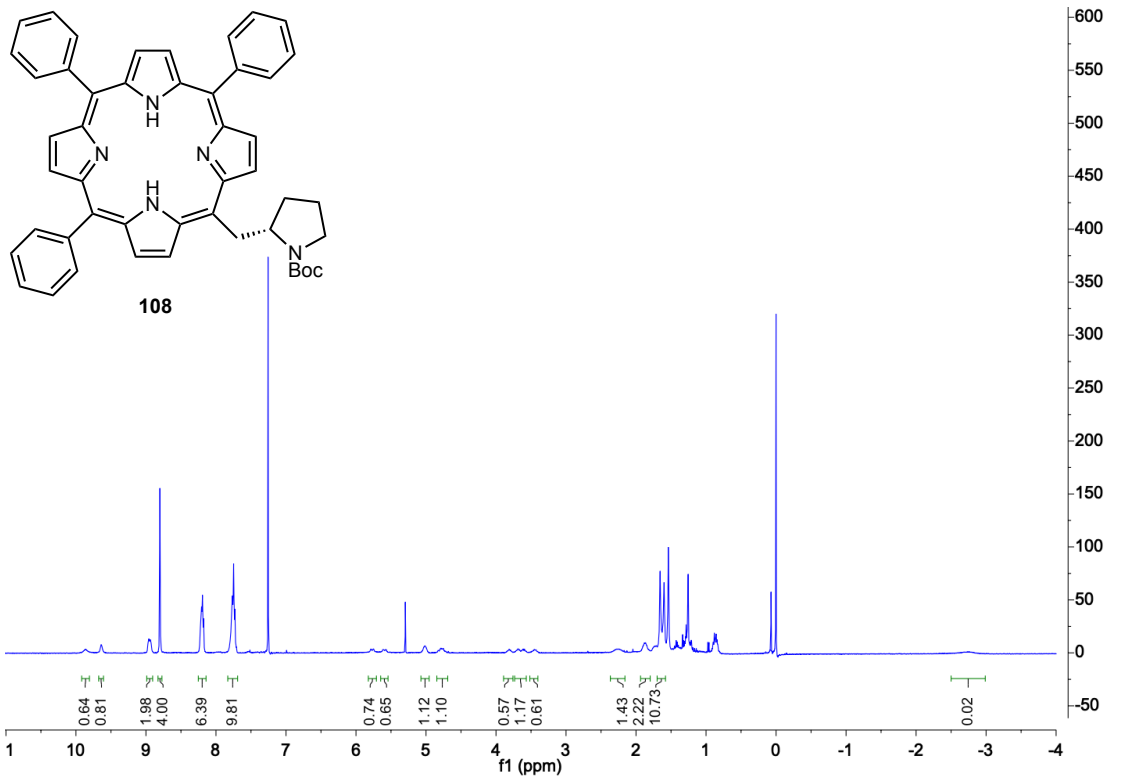


Figure 145. $^{1}$H-NMR spectrum ($CDCl_3$, 400 MHz) of compound **108**

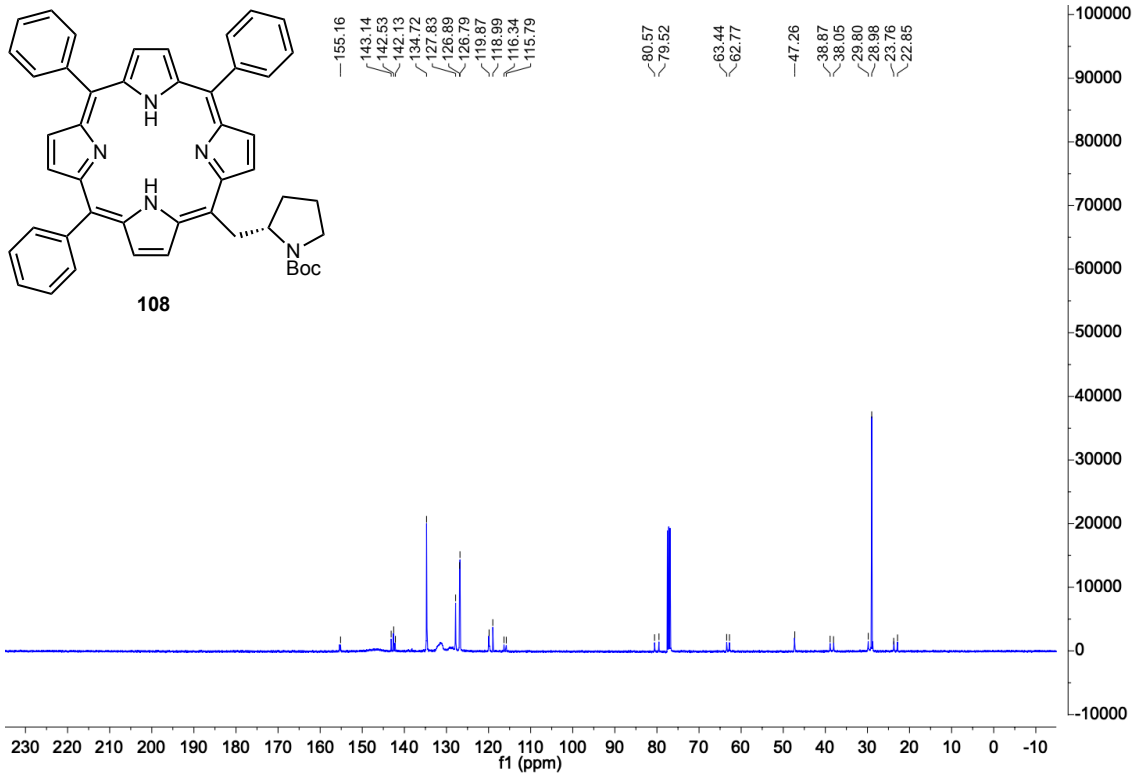


Figure 146. $^{13}$C-NMR spectrum ($CDCl_3$, 400 MHz) of compound **108**

# APPENDIX 4: HPLC CHROMATOGRAMS

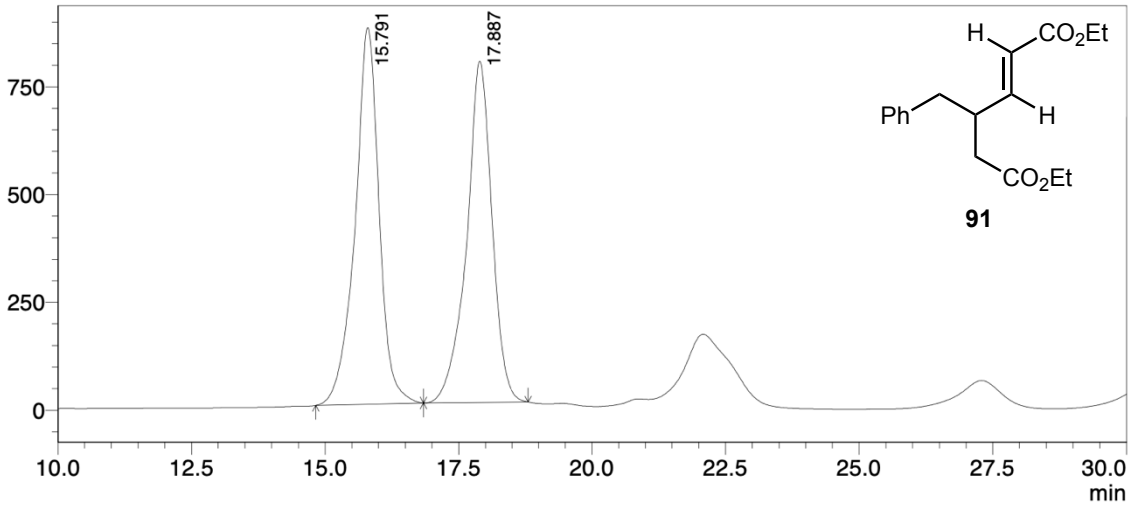


Figure 147. HPLC chromatogram of compound **91**. HPLC conditions: Phenomenex i-cellulose 5 column; hexane/IPA 1%; flow rate 1 mL/min; λ = 218 nm.

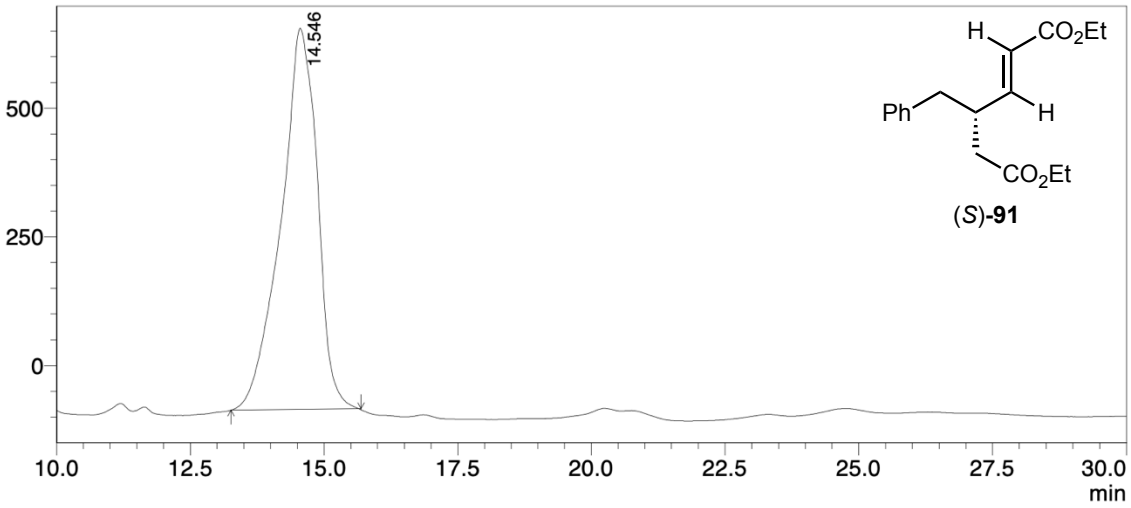


Figure 148. HPLC chromatogram of enantiopure compound **91**. HPLC conditions: Phenomenex i-cellulose 5 column; hexane/IPA 1%; flow rate 1 mL/min; λ = 218 nm.

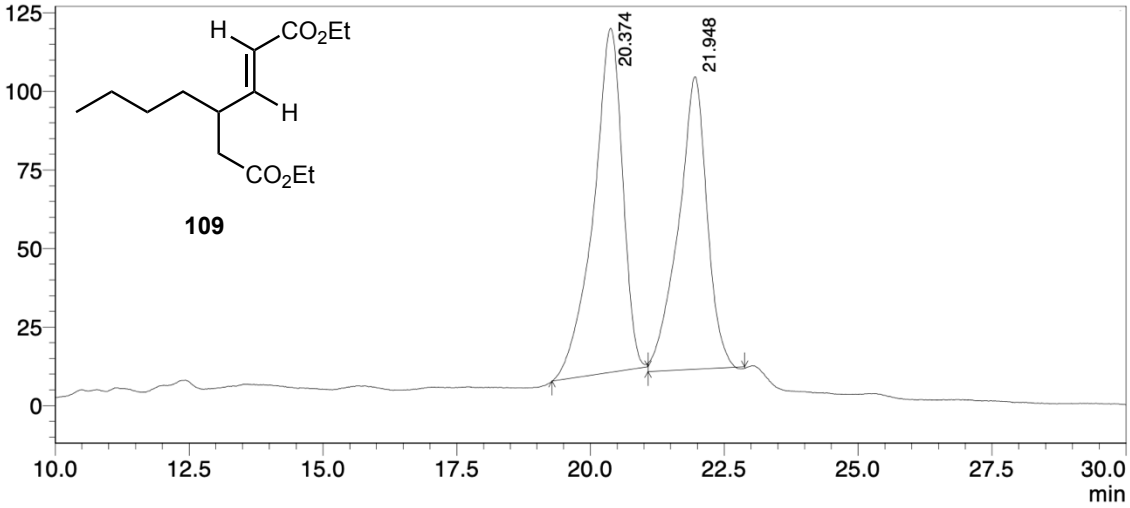


Figure 149. HPLC chromatogram of compound **109**. HPLC conditions: Phenomenex i-cellulose 5 column; hexane/IPA 1%; flow rate 1 mL/min; λ = 218 nm.

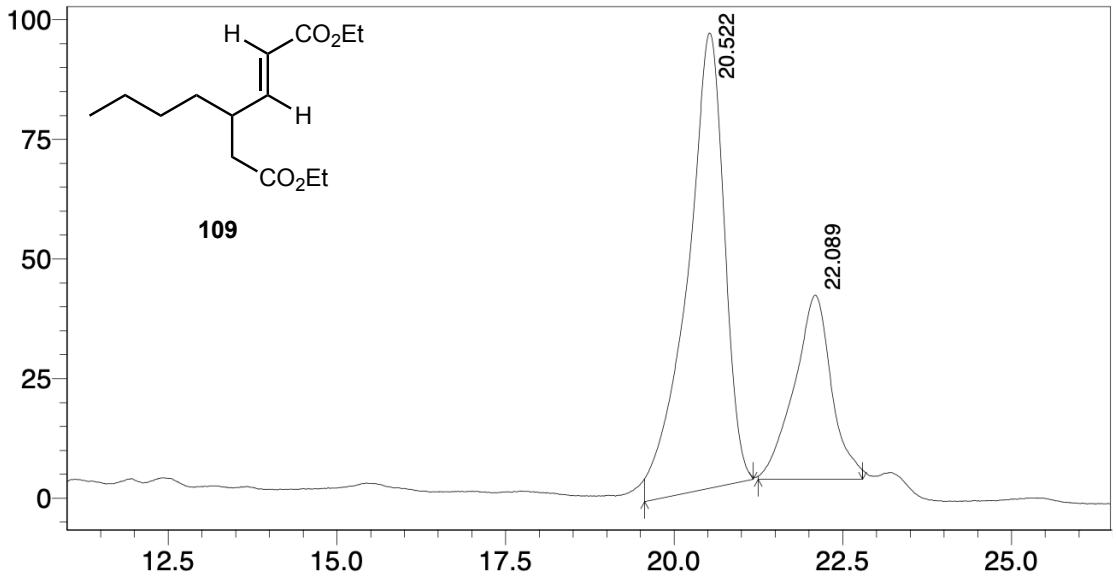


Figure 150. HPLC chromatogram of enantioenriched compound **109**. HPLC conditions: Phenomenex i-cellulose 5 column; hexane/IPA 1%; flow rate 1 mL/min; λ = 218 nm.

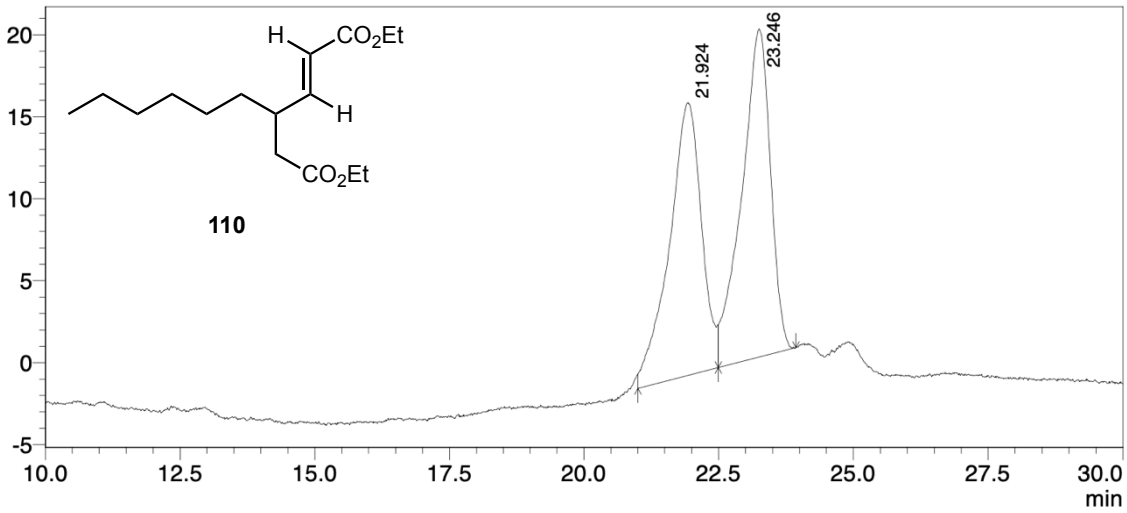


Figure 151. HPLC chromatogram of compound **110**. HPLC conditions: Phenomenex i-cellulose 5 column; hexane/IPA 1%; flow rate 1 mL/min; λ = 218 nm.

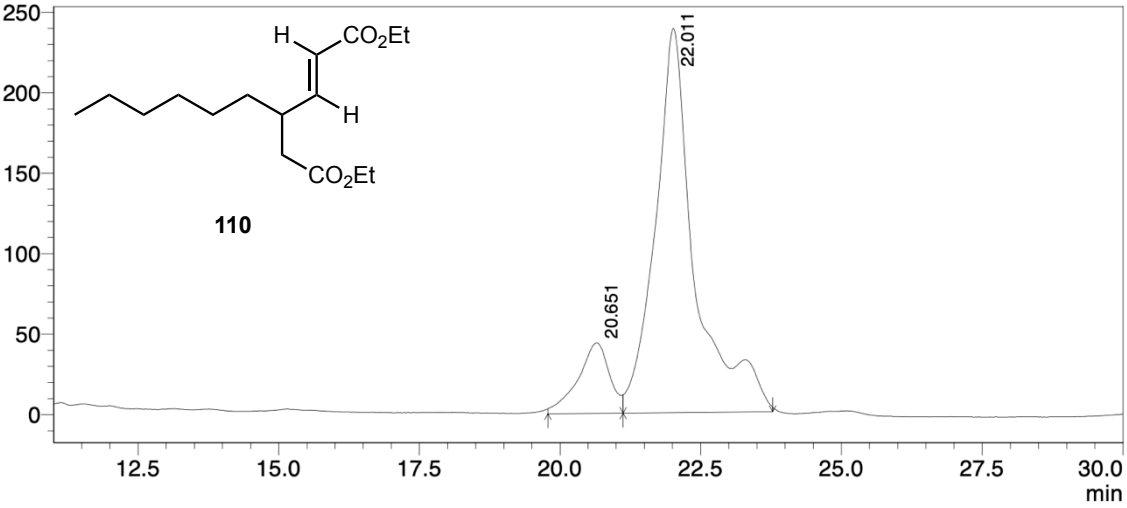


Figure 152. HPLC chromatogram of enantioenriched compound **110**. HPLC conditions: Phenomenex i-cellulose 5 column; hexane/IPA 1%; flow rate 1 mL/min; λ = 218 nm.

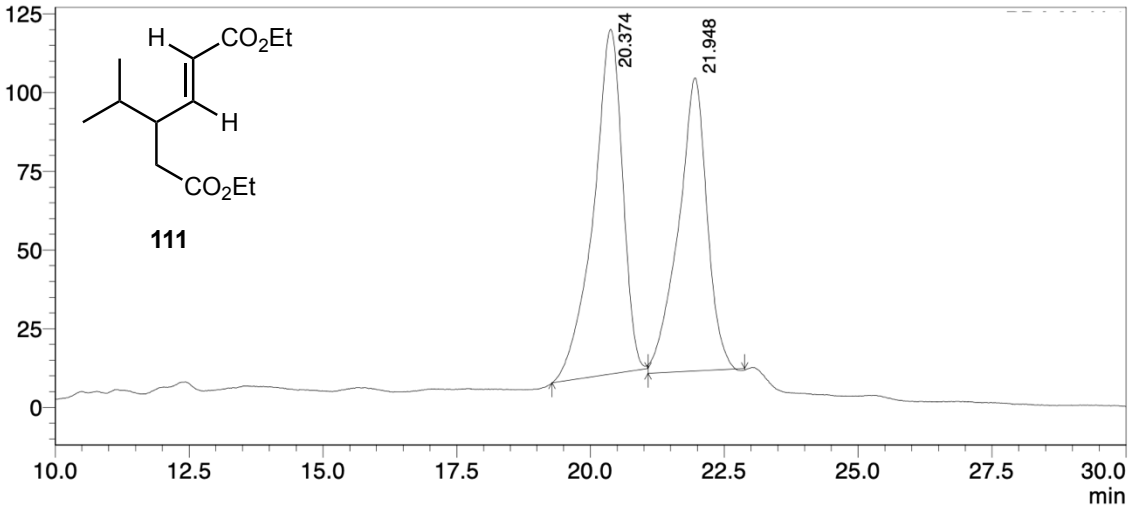


Figure 153. HPLC chromatogram of compound **111**. HPLC conditions: Phenomenex i-cellulose 5 column; hexane/IPA 1%; flow rate 1 mL/min; λ = 218 nm.

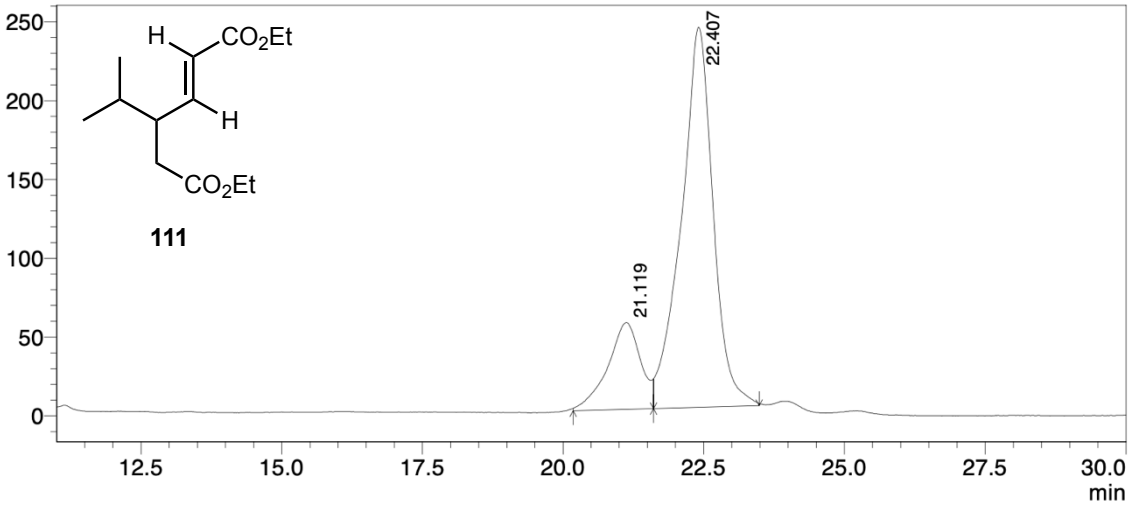


Figure 154. HPLC chromatogram of enantioenriched compound **111**. HPLC conditions: Phenomenex i-cellulose 5 column; hexane/IPA 1%; flow rate 1 mL/min; λ = 218 nm.

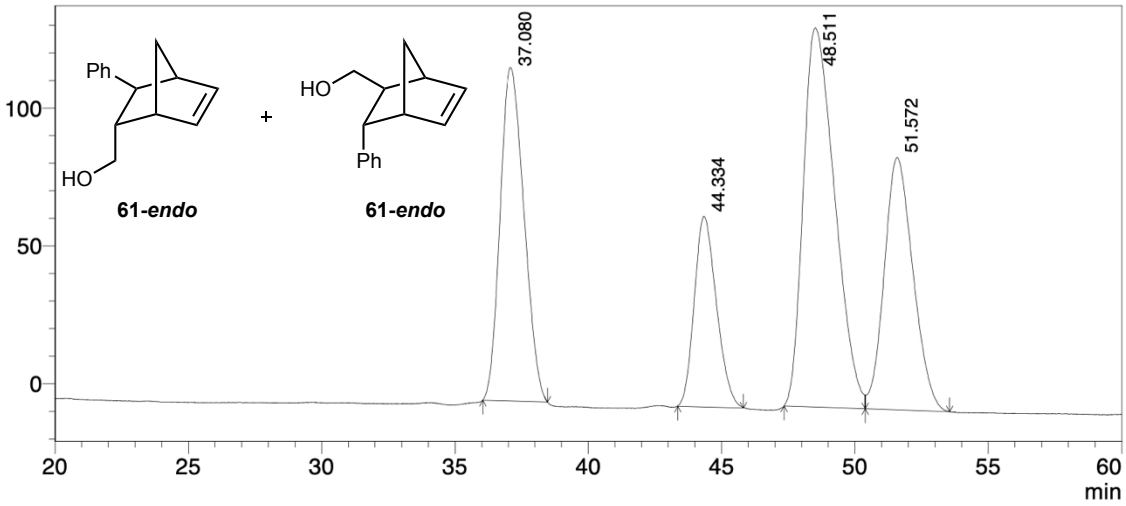


Figure 155. HPLC chromatogram of compounds **61-*endo*** and **61-*exo***. HPLC conditions: Phenomenex i-cellulose 5 column; hexane/IPA 0.8%; flow rate 1 mL/min; $\lambda$ = 210 nm.

# REFERENCES

[1]. Ahrendt, K. A., Borths, C. J., MacMillan, D. W. C., New Strategies for Organic Catalysis: The First Highly Enantioselective Organocatalysis Diels-Alder Reaction, *J. Am. Chem. Soc.*, **2000**, 122, 4243

[2]. List, B., Lerner, R. A., Barbas, C. F. III, Proline-Catalyzed Direct Asymmetric Aldol Reactions, *J. Am. Chem. Soc.*, **2000**, 122, 2395

[3]. a) Alemán, J., Cabrera, S., Applications of Asymmetric Organocatalysis in Medicinal Chemistry, *Chem. Soc. Rev.*, **2013**, 42, 774, b) Han, B., He, X. -H., Liu, Y. -Q., He, G., Peng, C., Li, J. -L., Asymmetric Organocatalysis: An Enabling Technology for Medicinal Chemistry, *Chem. Soc. Rev.*, **2021**, 50, 1522

[4]. Marcia de Figueiredo, R., Christmann, M., Organocatalytic Synhtesis of Drugs and Bioactive Natural Products, *Eur. J. Org. Chem.*, **2007**, 2575

[5]. Bromwmick, S., Mondal, A., Gosh, A., Bhowmick, K. C., Water: The Most Versatile and Nature's Friendly Media in Asymmetric Organocatalyzed Direct Aldol Reactions, *Tetrahedron: Asymmetry*, **2015**, 26, 1215

[6]. Mlynarski, J., Bas, S., Catalytic asymmetric aldol reactions in aqueous media – a 5 year update, *Chem. Soc. Rev.*, **2014**, 43, 577

[7]. a) Seayad, J., List, B., Asymmetric Organocatalysis, *Org. Biomol. Chem.*, **2005**, 3, 719, b) Moyano, A., in *Stereoselective Organocatalysis*, ed. R. Rios, 1st edition, **2013**, Chapter 2, 11-81

[8]. Hajos, Z. G., Parrish, D. R., Synthesis and Conversion of 2-methyl-2-(3-oxobutyl)-1,3-cyclopentanedione to the Isomeric Racemic Ketols of the [3.2.1]bicyclooctane and of the Perhydroindane Series, *J. Org. Chem.*, **1974**, 39, 1612

[9]. Eder, B. U., Sauer, G., Wiechert, R., New Type of Asymmetric Cyclization to Optically Active Stereoid CD Partial Structures, *Angew. Chem. Int. Ed*., **1971**, 10, 496

[10]. Pihko, P. M., Laurikainen, K. M., Usano, A., Nyeberg, A. I., Kaavi, J. A., Effect of Additives on the Proline-Catalyzed Ketone-Aldehyde Aldol Reactions, *Tetrahedron*, **2006**, 62, 317

[11]. Nyeberg, A. I., Usano, A., Pihko, P. M., Proline-Catalyzed Ketone-Aldehyde Aldol Reactions are Accelerated by Water, *Synlett.*, **2004**, 1891

[12]. Cobb, A. J. A., Shaw, D. M., Ley, S. V., 5-Pyrrolidin-2-yltetrazole: A New, Catalytic, More Soluble Alternative to Proline in an Organocatalytic Asymmetric Mannich-type Reaction, *Synlett.*, **2004**, 3, 558

[13]. Torii, H., Nakadai, M., Ishihara, K., Saito, S., Yamamoto, H., Asymmetric Direct Aldol Reaction Assisted by Water and A Proline-Derived Tetrazole Catalyst, *Angew. Chem. Int. Ed.*, **2004**, 43, 1983

[14]. Robak, M. T., Herbage, M. A., Ellman, J. A., Development of an *N*-sulfinyl Prolinamide for the Asymmetric Aldol Reaction, *Tetrahedron*, **2011**, 67, 4412

[15]. Chimni, S. S., Singh, S., Kumar, A., The pH of the Reaction Controls the Stereoselectivity Of Organocatalyzed Direct Aldol Reactions in Water, *Tetrahedron: Asymmetry*, **2009**, 20, 1722

[16]. Tang, Z., Jiang, F., Yu, L. -T., Cui, X., Gong, L. -Z., Mi, A. -Q., Jiang, Y. -Z., Wu, Y. -D., Novel Small Organic Molecules for a Highly Enantioselective Direct Aldol Reaction, *J. Am. Chem. Soc.*, **2003**, 125, 5262

[17]. Gryko, D., Lipiński, R., Asymmetric Direct Aldol Reaction Catalyzed by L-Prolinethioamides *Eur. J. Org. Chem.*, **2006**, 17, 3864

[18]. Melchiorre, P., Marigo, M., Carlone, A., Bartoli, G., Asymmetric Aminocatalysis – Gold Rush in Organic Chemistry, *Angew. Chem. Int. Ed.*, **2008**, 47, 6138

[19]. Bahmanyar, S., Houk, K. N., Harry, J. M., List, B., Quantum Mechanical Predictions of the Stereoselectivities of Proline-Catalyzed Asymmetric Intermolecular Aldol Reactions, *J. Am. Chem. Soc.*, **2003**, 125, 2475

[20]. Paras, N. A., MacMillan, D. W. C., New Strategies in Organic Catalysis: The First Enantioselective Organocatalytic Friedel-Crafts Alkylation, *J. Am. Chem. Soc.*, **2001**, 123, 4370

[21]. Bertelsen, S., Dinér, D., Johansen, R. L., Jørgensen, K. A., Asymmetric Organocatalytic β-Hydroxylation of α,β-Unsaturated Aldehydes, *J. Am. Chem. Soc.*, **2007**, 129, 1536

[22]. Moss, G. P., *Biochemical Nomenclature and Related Documents*, 2nd edition, Portland Press, **1992**, 278-329

[23]. Kadish, K. M., Smith, K. M., Guilard, R., *Porphyrin Handbook*, 1st edition, Academic Press, **2000**

[24]. Mansuy, D., Battioni, P., in *Porphyrin Handbook V4: Biochemistry and Binding: Activation of Small Molecules*, ed. Kadish, K. M., Smith, K. M., Guilard, R., 1st edition, Academic Press, **2000**, Chapter 26, 1-17

[25]. Collman, J. P., Boulatov, R., Sunderland, C. J., in *Porphyrin Handbook V11: Bioinorganic and Bioorganic Chemistry*, ed. Kadish, K. M., Smith, K. M., Guilard, R., 1st edition, Academic Press, **2000**, Chapter 62, 1-49

[26]. Bottomley, S.S., in *Porphyrin Handbook V14: Medical Aspects of Porphyrins*, ed. Kadish, K. M., Smith, K. M., Guilard, R., 1st edition, Academic Press, **2000**, Chapter 85, 1-21

[27]. Cuesta, V., TFM, Universitat de Barcelona, **2017**

[28]. Würthner, F., Kaiser, T.E., Saha-Möller, C. R., J-Aggregates: From Serendipitous Discovery to Supramolecular Engineering of Functional Dye Materials, *Angew. Chem. Int. Ed.*, **2011**, 50, 3376

[29]. Gouterman, M., Wagnière, G. M., Snyder, L. C., Spectra of Porphyrins: Part II. Four Orbital Model, *J. Mol. Spectrosc.*, **1963**, 11, 108

[30]. Guillén, M., TFM, Universitat de Barcelona, **2020**

[31]. Buchler, J. W. in *The Porphyrins V1: Structure and Synthesis. Part A*, ed. D. Dolphin, **1978**, Chapter 10, 390-474

[32]. Sanders, J. K. M., Bampos, N., Clyde-Watson, Z., Darling, S. L., Hawley, J. C., Kim, H. -J., Mak, C. C., Webb, S. J., in *Porphyrin Handbook V3: Inorganic, Organometallic and Coordination Chemistry*, ed. Kadish, K. M., Smith, K. M., Guilard, R., 1st edition, Academic Press, **2000**, Chapter 15, 1-49

[33]. Alder, A. D., *In the Chemical and Physical Behavior of Porphyrin Compounds and Related Structures. Annales New York Academy Science*, 206, **1973**, Vol. 206, 7-17

[34]. Wedel, M., Walter, A., Montforts, F. -P., Synthesis of Metalloporphyrins and Metallochlorins for Immobilization on Electrodes Surfaces, *Eur. J. Org. Chem.*, **2001**, 1681

[35]. Kumar, A., Maji, S., Dubey, P., Abhilash, G. J., Pandey, S., Sarkar, S., One-Pot General Synthesis of Metalloporphyrins, *Tetrahedron Letters*, **2007**, 48, 7287

[36]. Beletskaya, I., Tyurin, V. S., Tsivadze, A. Y., Guilard, R., Stern, C., Supramolecular Chemistry of Metalloporphyrins, *Chem. Rev.*, **2009**, 109, 1659

[37]. Chou, J. -H., Nalwa, H. S., Kosal, M. E., Rakow, N: A., Suslik, K. S., in *Porphyrin Handbook V6: Application of Porphyrins and Metalloporphyrins to Material Chemistry*, ed. Kadish, K. M., Smith, K. M., Guilard, R., 1st edition, Academic Press, **2000**, Chapter 41, 43-103

[38]. Drain, C. M., Lehn, J. M., Self-Assembly of Square Multiporphyrin Arrays by Metal Ion Coordinate, *J. Chem. Soc. Chem. Comm.*, **1994**, 2313

[39]. Dini, D., Hanack, M., in *Porphyrin Handbook V17: Phthalocyanines: Properties and Materials*, ed. Kadish, K. M., Smith, K. M., Guilard, R., 1st edition, Academic Press, **2000**, Chapter 107, 1-36

[40]. Hartley, j. A., Forrow, S. M., Souhami, R. L., Photosensitization of Human Leukemic Cells by Anthracenedione Antitumor Agents, *Cancer Res.*, **1990**, 50, 1936

[41]. Richeter, S., Jeandon, C., Gisselbrecht, J-P., Ruppert, R., Callot, H., Syntheses and Optical and Electrochemical Properties of Porphyrin Dimers Linked by Metal Ions, *J. Am. Chem. Soc.*, **2002**, 124, 6168

[42]. Da Graça H. Vicente, M., in *Porphyrin Handbook V1: Synthesis and Organic Chemistry*, ed. Kadish, K. M., Smith, K. M., Guilard, R., 1st edition, Academic Press, **2000**, Chapter 4, 149-201

[43]. Baldwin, J. E., Crossley, M. J., DeBernardis, J., Efficient Peripheral Functionalization of Porphyrins, *Tetrahedron*, **1982**, 38, 685

[44]. Catalano, M. M., Crossley, M. J., Harding, M. M., Lionel, G. K., Control of Reactivity at the Porphyrin Periphery by Metal Ion Coordination: A General Method for Specific Nitration at the β-Pyrrolic Position of 5,10,15,20-tetra-arylporphyrins, *J. Chem. Soc. Chem. Commun.*, **1984**, 22, 1535

[45]. Ogawa, T., Nishimoto, Y., Yoshida, N., Ono, N., Osuka, A., Completely Regioselective Synthesis of Directly Linked *meso,meso* and meso,β Porphyrin Dimers by One-Pot Electrochemical Oxidation of Metalloporphyrins, *Angew. Chem. Int. Ed.*, **1999**, 38, 176

[46]. Rothermund, P., Formation of Porphyrins from Pyrrole and Aldehydes, *J. Am. Chem. Soc.*, **1935**, 57, 2010

[47]. Rothermund, P., A New Porphyrin Synthesis. The Synhtesis of Porphin, *J. Am. Chem. Soc.*, **1936**, 58, 625

[48]. Rothermund, P., Mennoti, A. R., Porphyrin Studies. IV. The Synthesis of α,β,γ,δ-Tetraphenylporphine, *J. Am. Chem. Soc.*, **1941**, 63, 267

[49]. Adler, A. D., Longo, F. R., Finarelli, J. D., Goldmacher, J., Assour, J., Korsakoff, L., A Simplified Synthesis for *meso*-Tetraphenylporphine, *J. Org. Chem.*, **1967**, 32, 476

[50]. Lindsey, J. S., Mixed Aldehyde Condensation*., Porphyr. Handb*., **2000**, 1, Chapter 2, 53-55

[51]. Kong, J. L., Loach, P. A., Syntheses of Covalently-Linked Porphyn-Quinone Complexes, *J. Heterocyclic Chem.*, **1980**, 17, 737

[52]. García, H., PhD Thesis, Universitat de Barcelona, **2003**

[53]. Arlegui, A., El-Hachemi, Z., Crusats, J., Moyano, A., 5-Phenyl-10,15,20-Tris(4-sulfonatophenyl)porphyn: Synthesis, Catalysis, and Structural Studies, *Molecules*, **2018**, 23, 3363

[54]. Arlegui, A., PhD Thesis, Universitat de Barcelona, **2019**

[55]. Möltgen, M., Kleihermanns, K., Holzwarth, A. R., Self-Assembly of [Et,Et]-Bacteriochlorophyll $C_F$ on Highly Oriented Pyrolytic Graphite Revealed by Scanning Tunneling Microscopy, *Photochem. Photobiol.*, **2002**, 75, 619

[56]. Hunter, C. A., Meldola Lecture. The Role of Aromatic Interactions in Molecular Recognition, *Chem. Soc. Rev.*, **1994**, 23, 101

[57]. Arlegui, A., Torres, P., Cuesta, V., Crusats, J., Moyano, A., Chiral Amphiphilic Secondary Amine-Porphyrin Hybrids for Aqueous Organocatalysis, *Molecules*, **2020**, 25, 3420

[58]. Arlegui, A., Torres, P., Cuesta, V., Crusats, J., Moyano, A., A pH-Switchable Aqueous Organocatalysis with Amphiphilic Secondary Amine-Porphyrin Hybrids, *Eur. J. Org. Chem.*, **2020**, 4399

[59]. Oelgemöller, M., Solar Photochemical Synthesis: From the Beginnings of Organic Photochemistry to the Solar Manufacturing of Commodity Chemicals, *Chem. Rev.*, **2016**, 116, 9664

[60]. Ciamician, G., Silber, P., Chemische Lichtwirkungen, Ber. Dtsch. *Chem. Ges.*, **1908**, 41, 1928

[61]. Ciamician, G., The Photochemistry of the Future, *Science*, **1912**, 36, 385

[62]. Rigotti, T., Alemán, J., Visible Light Photocatalysis – From Racemic to Asymmetric Activation Strategies, *Chem. Commun.*, **2020**, 56, 11169

[63]. Stephenson, C. R. J., Yoon, T. P., MacMillan, D. W. C., *Wiley-VCH*, **2018**

[64]. Brimioulle, R., Lenhart, D., Maturi, M., M., Bach, T., Enantioselective Catalysis of Photochemical Reactions, *Angew. Chem. Int. Ed.*, **2015**, 54, 3872

[65]. Meggers, E., Asymmetric Catalysis Activated by Visible Light, *Chem. Commun.*, **2015**, 51, 3290

[66]. Gamido-Castro, A. F., Maestro, M. C., Alemán, J., Asymmetric Induction in Photocatalysis – Discovering a New Side to Light-Driven Chemistry, *Tetrahedron Lett.*, **2018**, 59, 1286

[67]. Jiang, C., Chen, W., Zheng, W. H., Lu, H., Advances in Asymmetric Visible-Light Photocatalysis, 2015-2019, *Org. Biomol. Chem.*, **2019**, 17, 8673

[68]. Silvi, M., Melchiorre, P., Enhancing the Potential of Enantioselective Organocatalysis with Light, *Nature*, **2018**, 554, 41

[69]. Zang, H. H., Chen, H., Zhu, C., Yu, S., A Review of Enantioselective Dual Transition Metal/Photoredox Catalysis, *Sci. China Chem.*, **2020**, 63, 637

[70]. Albini, A., *Photochemistry: Past, Present and Future*, **2016**

[71]. Nick, C., Jirat, J., Kosata, B., *IUPAC Gold Book: Photosensitization*

[72]. Michelin, C., Hoffmann, N., Photosensitization and Photocatalysis – Perspectives in Organic Synthesis, *ACS Catal.*, **2018**, 8, 12046

[73]. Daniell, M. D., Hill, J. S., A History of Photodynamic Therapy, *Aust. N. Z. J. Surg*, **1991**, 61, 340

[74]. O'Regan, B., Grätzel, M., A Low-Cost, High-Efficiency Solar Cell Based on Dye-Sensitized Colloidal $TiO_2$ Films, *Nature*, **1991**, 353, 6346

[75]. Gómez-Álvarez, E., Wortham, H., Strekowski, R., Zetzsch, C., Gligorovski, S., Atmospheric Photosensitized Heterogeneous and Multiphase Reactions: From Outdoors to Indoors, *Environmental Science and Technology*, **2012**, 46, 1955

[76]. Zhang, Y., Lee, T. S., Petersen, J. L., Milsmann, C., A Zirconium Photosensitizer with a Long-Lived Excited State: Mechanistic Insight into Photoinduced Single-Electron Transfer, *J. Am. Chem. Soc.*, **2018**, 140, 5934

[77]. Prier, C. K., Rankic, D. A., MacMillan, D. W. C., Visible Light Photoredox Catalysis with Transition Metal Complexes: Applications in Organic Synthesis, *Chem. Rev.*, **2013**, 113, 5322

[78]. Romero, N. A., Nicewicz, D. A., Organic Photoredox Catalysis, *Chem. Rev.*, **2016**, 116, 10075

[79]. Cauwenberg, R., Shoubhik, D., Photocatalysis: A Green Tool for Redox Reactions, *Synlett.*, **2022**, 33, 129

[80]. Takeda, H., Ohashi, M., Tani, T., Ishitani, O., Inagaki, S., Enhanced Photocatalysis of Rhenium(I) Complex by Light-Harvesting Periodic Mesoporous Organosilica, *Inorg. Chem.*, **2010**, 49, 4554

[81]. Ho, X-H., Mho, S., Kang, H., Jang, H-Y., Electro-Organocatalysis: Enantioselective α-Alkylation of Aldehydes, *Eur. J. Org. Chem.*, **2010**, 4436

[82]. Skubi, K. L., Blum, T. R., Yoon, T. P., Dual Catalysis Strategies in Photochemical Synthesis, *Chem. Rev.*, **2016**, 116, 10035

[83]. Accessed on 26/07/2022: https://chemistry-europe.onlinelibrary.wiley.com/doi/toc/10.1002/(ISSN)1099-0690.PhotoredoxCatalysis

[84]. Pac, C., Ihawa, M., Yasuda, M., Miyauchi, Y., Sakurai, H., Tris(2,2'-bipyridine)ruthenium(2+)-Mediated Photoreduction of Olefins with 1-Benzyl-1,4-Dihydronicotinamide: A Mechanistic Probe for Electron-Transfer Reactions of NAD(P)H-Model Compounds, *J. Am. Chem. Soc.*, **1981**, 103, 6495

[85]. Fukuzimi, S., Mochizuki, S., Tanaka, T., Photocatalytic Reduction of Phenacyl Halides by 9-10,dihydro-10-methylacridine: Control Between the Reductive and Oxidative Quenching Pathways of Tris(bipyridine)ruthenium Complex Utilizing an Acid Catalysis, *J. Phys. Chem.*, **1990**, 94, 722

[86]. Cano-Yelo, H., Deronzier, A., Photooxidation of Some Carbinols by the Ru (II) Polypyridyl Complex-Aryl Diazonium Salt System, *Tetrahedron Lett.*, **1984**, 25, 5517

[87]. Ischay, M. A., Anzovino, M. E., Du, J., Yoon, T. P., Efficient Visible Light Photocatalysis of [2+2] Enone Cycloadditions, *J. Am. Chem. Soc.*, **2008**, 130, 12886

[88]. Nicewicz, D. A., MacMillan, D. W. C., Merging Photoredox Catalysis with Organocatalysis: The Direct Asymmetric Alkylation of Aldehydes, *Science*, **2008**, 322, 77

[89]. Narayanam, J. M. R., Tucker, J. W., Stephenson, C. R. J., Electron-Transfer Photoredox Catalysis: Development of a Tin-Free Reductive Dehalogenation Reaction, *J. Am. Chem. Soc.*, **2009**, 131, 8756

[90]. Gentry, E. C., Knowles, R. R., Synthetic Applications of Protons-Coupled Electron Transfer, *Acc. Chem. Ress.*, **2016**, 49, 1546

[91]. Ashby, E. C., Single-Electron Transfer, A Major Reaction Pathway in Organic Chemistry. An Answer to Recent Criticisms, *Acc. Chem. Ress.*, **1988**, 21, 414

[92]. Chuantragol, P., Kurandina, D., Gevorgyan, V., Catalysis with Palladium Complexes Photoexcited by Visible Light, *Angew. Chem. Int. Ed.*, **2019**, 58, 11586

[93]. Reckenthäler, M., Griesbeck, A. G., Photoredox Catalysis for Organic Syntheses, *Adv. Synth. Catal.*, **2013**, 355, 2727

[94]. Shaw, M. M., Twilton, J., MacMillan, D. W. C., Photoredox Catalysis in Organic Chemistry, *J. Org. Chem.*, **2016**, 81, 6898

[95]. Guindon, Y., Jung, G., Guérin, B., Oglivie, W. W., Hydrogen and Allylation Transfer Reactions in Acyclic Free Radicals, *Synlett.*, **1998**, 3, 213

[96]. Tucker, J. W., Narayanam, J. M. R., Krabbe, S. W., Stephenson, C. R. J., Electron Transfer Photoredox Catalysis: Intramolecular Radical Addition to Indoles and Pyrroles, *Org. Lett.*, **2010**, 12, 368

[97]. Furst, L., Narayanam, J. M. R., Stephenson, C. R. J., Total Synthesis of (+)-Gliocladin C Enabled by Visible-Light Photoredox Catalysis, *Angew. Chem. Int. Ed.*, **2012**, 41, 9655

[98]. Cheng, Y., Yang, J., Qu, Y., Li, P., Aerobic Visible-Light Photoredox Radical C-H Functionalization: Catalytic Synthesis of 2-Substituted Benzothiazoles, *Org. Lett.*, **2012**, 14, 98

[99]. Maity, S., Zheng, N., A Visible-Light-Mediated Oxidative C-N Bond Formation/Aromatization Cascade: Photocatalytic Preparation of *N*-Arylindoles, *Angew. Chem. Int. Ed.*, **2012**, 51, 9562

[100]. Cai, S., Zhao, X., Wang, X., Liu, Q., Li, Z., Wang, D. Z., Visible-Light-Promoted C-C Bond Cleavage: Photocatalytic Generation of Iminium Ions and Amino Radicals, *Angew. Chem. Int. Ed.*, **2012**, 51, 8050

[101]. Condie, A. G., González-Gómez, J. C., Stephenson, C. R. J., Visible-Light Photoredox Catalysis: Aza-Henry Reactions via C-H Functionalization, *J. Am. Chem. Soc.*, **2010**, 132, 1464

[102]. Xi, Y, Yi, H., Lei, A., Synthetic Applications of Photoredox Catalysis with Visible Light, *Org. Biomol. Chem.*, **2013**, 11, 2387

[103]. Tyson, E. L., Farney, E. P., Yoon, P. T., Photocatalytic [2+2] Cycloadditions of Enones with Cleavable Redox Auxiliaries, *Org. Lett.*, **2012**, 14, 1110

[104]. Du, J., Skubi, K. L., Schultz, D. M., Yoon, T. P., A Dual-Catalysis Approach to Enantioselective [2+2] Photocycloadditions Using Visible Light *Science*, **2014**, 344, 392

[105]. Lin, S., Ischay, M. A., Fry, C. G., Yoon, T. P., Radical Cation Diels-Alder Cycloadditions by Visible-Light Photocatalysis, *J. Am. Chem. Soc.*, **2011**, 133, 19350

[106]. NcNally, A., Prier, C. K., MacMillan, D. W. C., Discovery of an $\alpha$-Amino C-H Arylation Reaction Using the Strategy of Accelerated Serendipity, *Science*, **2011**, 334, 1114

[107]. Zuo, Z., MacMillan, D. W. C., Decarboxylative Arylation of $\alpha$-Amino Acids via Photoredox Catalysis: A One-Step Conversion of Biomass to Drug Pharmacophore, *J. Am. Chem. Soc.*, **2014**, 136, 5257

[108]. Ventre, S., Petronijevic, F. R., MacMillan, D. W. C., Decarboxylative Fluorination of Aliphatic Carboxylic Acids via Photoredox Catalysis, *J. Am. Chem. Soc.*, **2015**, 137, 5654

[109]. Rueda-Becerril, H., Mahé, O., Drouin, M., Majewski, M. B., West, J. G., Wolf, M. O., Sammis, G. H., Paquin, J-F., Direct C-F Bond Formation Using Photoredox Catalysis, *J. Am. Chem. Soc.*, **2014**, 136, 2637

[110]. Cole, R. S., Hammond, G. S., Asymmetric Induction during Energy Transfer, *J. Am. Chem. Soc.*, **1965**, 87, 3257

[111]. Kim, J-I., Schuster, G. B., Enantioselective Catalysis of the Triplex Diels-Alder Reaction: Addition of trans-.beta.-methylstyrene to 1,3-Cyclohexadiene Photosensitized with (-)-1,1'-bis(2,4-dicyanonaphthalene), *J. Am. Chem. Soc.*, **1990**, 112, 9635

[112]. Hoffmann, R., Inoue, Y., Trapped Optically Active (*E*)-Cycloheptene Generated by Enantiodifferentiating *Z-E* Photoisomerization of Cycloheptene Sensitized by Chiral Aromatic Esters, *J. Am. Chem. Soc.*, **1999**, 121, 10702

[113]. Zou, Y.-Q., Hörmann, F. M., Bach, T., Iminium and Enamine Catalysis in Enantioselective Photochemical Reactions, *Chem. Soc. Rev.*, **2018**, 47, 278

[114]. Beeson, T. D., Mastracchio, A., Hong, J. -B., Ashton, K., MacMillan, D. W. C., Enantioselective Organocatalysis Using SOMO Activation, *Science*, **2007**, 316, 582

[115]. Nagib, D. A., Scott, M. E., MacMillan, D. W. C., Enantioselective $\alpha$-Trifluoromethylation of Aldehydes via Photoredox Organocatalysis, *J. Am. Chem. Soc.*, **2009**, 131, 10875

[116]. Welin, E. R., Warkentin, A. A., Conrad, J. C., MacMillan, D. W. C., Enantioselective α-Alkylation of Aldehydes by Photoredox Organocatalysis: Rapid Access to Pharmacophore Fragments form β-Cyanoaldehydes, *Angew. Chem. Int. Ed.*, **2015**, 54, 9668

[117]. Capacci, A. G., Malinowski, J. T., McAlpine, N. J., Kuhne, J., MacMillan, D. W. C., Direct, Enantioselective α-Alkylation of Aldehydes Using Simple Olefins, *Nat. Chem.*, **2017**, 6, 1073

[118]. Neumann, M., Füldner, S., König, B., Zeitler, K., Metal-Free, Cooperative Asymmetric Organophotoredox Catalysis with Visible Light, *Angew. Chem. In. Ed.*, **2011**, 50, 951

[119]. Fidaly, K., Ceballos, C., Falguières, A., Veitia, M. S. I., Guy, A., Ferroud, C., Visible Light Photoredox Organocatalysis: A Fully Transition Metal-Free Direct Asymmetric α-Alkylation of Aldehydes, *Green Chem.*, **2012**, 14, 1293

[120]. (a) Arceo, A., Jurberg, I. D., Álvarez-Fernández, A., Melchiorre, P., Photochemical Activity of a Key Donor-Acceptor Complex Can Drive Stereoselective Catalytic α-Alkylation of Aldehydes, *Nat. Chem.*, **2013**, 5, 750, (b) Silvi, M., Arceo, A., Jurberg, I. D., Cassani, C., Melchiorre, P., Enantioselective Organocatalytic Alkylation of Aldehydes and Enals Driven by the Direct Photoexcitation of Enamines, *J. Am. Chem. Soc.*, **2015**, 137, 6120, (c) Bahamonde, A., Melchiorre, P., Mechanism of the Stereoselective α-Alkylation of Aldehydes Driven by the Photochemical Activity of Enamines, *J. Am. Chem. Soc.*, **2016**, 138, 8019, (d) Filippini, G., Silvi, M., Melchiorre, P., Enantioselective Formal α-Methylation and α-Benzylation of Aldehydes by Means of Photo-Organocatalysis, *Angew. Chem. Int. Ed.*, **2017**, 56, 4447

[121]. Rigotti, T., Casado-Sánchez, A., Cabrera, S., Pérez-Ruiz, R., Liras, M., de la Peña O'Shea, V. A., Alemán, J., A Bifunctional Photoaminocatalyst for the Alkylation of Aldehydes: Design, Analysis, and Mechanistic Studies, *ACS Catal.*, **2018**, 8, 5928

[122]. Casas, J., Ibrahem, I., Engqvist, M., Sundén, H., Córdova, A., The Direct Amino Acid-Catalyzed Asymmetric Incorporation of Molecular Oxygen to Organic Compounds, *J. Am. Chem. Soc.*, **2004**, 126, 8914

[123]. Walaszek, D. J., Rybicka-Jasińska, K., Smoleń, S., Karczewski, M., Gryko, D., Mechanistic Insights into Enantioselective C-H Photooxygenation of Aldehydes via Enamine Catalysis, *Adv. Synth. Catal.*, **2015**, 357, 2061

[124]. Walaszek, D. J., Jawiczuk, M., Durka, J., Drapala, O., Gryko, D., α-Photooxygenation of Chiral Aldehydes with Singlet Oxygen, *Beilstein J. Org. Chem.*, **2019**, 15, 2076

[125]. Cai, X., Chang, V., Chen, C., Kim, H. -J., Mariano, P. S., A Potentially General Method to Control Relative Stereochemistry in Enone-Olefin [2+2] Photocycloaddition Reactions by Using Eniminium Salt Surrogates, *Tetrahedron Lett.*, **2000**, 41, 9445

[126]. Chen, C., Chang, V., Cai, X., Duesler, E., Mariano, P. S., A General Strategy for Absolute Stereochemical Control in Enone-Olefin [2+2] Photocycloaddition Reactions, *J. Am. Chem. Soc.*, **2001**, 123, 6433

[127]. Rigotti, T., Mas-Ballesté, R., Alemán, J., Enantioselective Aminocatalytic [2+2] Cycloaddition through Visible Light Excitation, *ACS Catal.*, **2020**, 10, 5335

[128]. Murphy, J. J., Bastida, D., Paria, S., Fagnoni, M., Melchiorre, P., Direct, Enantioselective $\alpha$-Alkylation of Aldehydes Using Simple Olefins, *Nat. Chem.*, **2017**, 6, 1073

[129]. (a) Silvi, M., Verrier, C., Rey, Y. P., Buzzetti, L., Melchiorre, P., Visible-Light Excitation of Iminium Ions Enables the Enantioselective Catalytic $\beta$-Alkylation of Enals, *Nat. Chem.*, **2017**, 9, 868, (b) Verrier, C., Alandini, N., Pezzetta, C., Moliterno, M., Buzzetti, L., Hepburn, H. B., Vega-Peñaloza, A., Silvi, M., Melchiorre, P., Direct Stereoselective Installation of Alkyl Fragments at the $\beta$-Carbon of Enals via Excited Iminium Ion Catalysis, *ACS Catal.*, **2018**, 8, 1062, (c) Mazzarella, D., Crisenza, G. E. H., Melchiorre, P., Asymmetric Photocatalytic C-H Functionalization of Toluene and Derivatives, *J. Am. Chem. Soc.*, **2018**, 140, 8439, (d) Bonilla, P., Rey, Y., Holden, C., Melchiorre, P., Photo-Organocatalytic Enantioselective Radical Cascade Reactions of Unactivated Olefins, *Angew. Chem. Int. Ed.*, **2018**, 57, 12819, (e) Perego, L. A., Bonilla, P., Melchiorre, P., Photo-Organocatalytic Enantioselective Radical Cascade Enabled by Single-Electron Transfer Activation of Allenes, *Adv. Synth. Catal.*, **2020**, 362, 302

[130]. Costa, R., Oliveira da Silva, L., Bartolomeu, A., Brocksom, T. J., de Oliveira, K. T., Recent Applications of Porphyrins as Photocatalysts in Organic Synthesis: Batch and Continuous Flow Approaches, *Beilstein J. Org. Chem.*, **2020**, 16, 917

[131]. de Souza, A. A. N., Silva, N. S., Müller, A. V., Polo, A. S., Brocksom, T. J., de Oliveira, K. T., Porphyrins as Photoredox Catalysts in $Csp^2$-H Arylations: Batch and Continuous Flow Approaches, *J. Org. Chem.*, **2018**, 83, 15077

[132]. Tucker, J. W., Stephenson, C. R. J., Shining Light on Photoredox Catalysis: Theory and Synthetic Applications, *J. Org. Chem.*, **2012**, 77, 1617

[133]. Di Mascio, P., Martínez, G. R., Miyamoto, S., Ronsein, G. E., Medeiros, M. H. G., Cadet, J., Singlet Molecular Oxygen Reactions with nucleic Acids, Lipids, and Proteins, *Chem. Rev.*, **2019**, 119, 2043

[134]. Clennan, E. L., Pace, A., Advances in Singlet Oxygen Chemistry, *Tetrahedron*, **2005**, 61, 6665

[135]. Schenck, G. O., Ziegler, K., Die Synthese des Ascaridols, *Naturwissenschaften*, **1944**, 32, 157

[136]. Dechy-Cabaret, O., Benoit-Vical, F., Loup, C., Robert, A., Gornitzka, H., Bonhoure, A., Vial, H., Magnaval, J. -F., Séguéla, J. -P., Meunier, B., Synthesis and Antimalarial Activity of Trioxaquine Derivatives, *Chem. Eur. J.*, **2004**, 10, 1625

[137]. Lévesque, F., Seeberg, P. H., Continuous-Flow Synthesis of the Anti-Malaria Drug Artemisinin, *Angew. Chem. Int. Ed.*, **2012**, 51, 1706

[138]. Turconi, J., Griolet, F., Guevel, R., Oddon, G., Villa, R., Geatti, A., Hvala, M., Rossen, K., Göller, R., Burgard, A., Semisynthetic Artemisinin, the Chemical Path to Industrial Production, *Org. Process Res. Dev.*, **2014**, 18, 417

[139]. Amara, Z., Bellamy, J. F. B., Horvath, R., Miller, S. J., Beeby, A., Burgard, A., Rossen, K., Poliakoff, M., George, M., Applying Green Chemistry to the Photochemical Route to Artemisinin, *Nat. Chem.*, **2015**, 7, 489

[140]. Roscales, S., Plumet, J., Biosynthesis and Biological Activity of Carbasugars *Int. J. Carbohydr. Chem.*, **2016**, 1

[141]. Salamci, E., Seçen, H., Sütbeyaz, Y., Balci, M., A Concise and Convenient Synthesis of DL-*Proto*-Quercitol and DL-*gala*-Quercitol via Ene Reaction of Singlet Oxygen Combined with Cycloaddition to Cyclohexadiene, *J. Org. Chem.*, **1997**, 62, 2453

[142]. Lipp, A., Selt, M., Ferenc, D., Schollmeyer, D., Waldvogel, S. R., Opatz, T., Total Synthesis of (-)-Oxycodone via Anodic Aryl-Aryl Coupling, *Org. Lett.*, **2019**, 21, 1828

[143]. Burchill, L., George, J. H., Total Synthesis of Rhodonoids A, B, E, and F, Enabled by Singlet Oxygen Ene Reactions, *J. Org. Chem.*, **2020**, 85, 2260

[144]. de Souza, J. M., Brocksom, T. J., McQuade, D. T., de Oliveira, K. T., Continuous Endoperoxidation of Conjugated Dienes and Subsequent Rearrangements Leading to C-H Oxidized Synthons, *J. Org. Chem.*, **2018**, 83, 7574

[145]. Lian, M., Li, Z., Cai, Y., Meng, Q., Cao, Z., Enantioselective Photooxygenation of β-Keto Esters by Chiral Phase-Transfer Catalysis using Molecular Oxygen, *Chem. -Asian J.*, **2012**, 7, 2019

[146]. Wang, Y., Zheng, Z., Lian, M., Yin, H., Zhao, J., Meng, Q., Gao, Z., Photo-Organocatalytic Enantioselective α-Hydroxylation of β-Keto Esters and β-Keto Amides with Oxygen under Phase-Transfer Catalysis, *Green Chem.*, **2016**, 18, 5493

[147]. Tang, X., Feng, S., Wang, Y., Yang, F., Zheng, Z., Zhao, J., Wu, Y., Yin, H., Liu, G., Meng, Q., Bifunctional Metal-Free Photo-Organocatalysts for Enantioselective Aerobic Oxidation of β-Dicarbonyl Compounds, *Tetrahedron*, **2018**, 74, 3624

[148]. Mojarrad, A. G., Zakavi, S., Simple Low Cost Porphyrinic Photosensitizers for Large Scale Chemoselective Oxidation of Sulfides to Sulfoxides under Green Conditions: Targeted Protonation of Porphyrins, *Catal. Sci. Technol.*, **2018**, 8, 768

[149]. Jiang, J., Luo, R., Zhou, X., Chen, Y., Ji, H., Photocatalytic Properties and Mechanistic Insights into Visible Light-Promoted Aerobic Oxidation of Sulfides to Sulfoxides via Tin Porphyrin-Based Porous Aromatic Frameworks, *Adv. Synth. Catal.*, **2018**, 360, 4402

[150]. Meng, Y., Luo, Y., Shi, j., Ding, H., Lang, X., Chen, W., Zheng, A., Sun, J., Wang, C., 2D and 3D Porphyrinic Covalent Organic Frameworks: the Influence of Dimensionality on Functionality, *Angew. Chem. Int. Ed.*, **2020**, 59, 3624

[151]. Ushakov, D. B., Gilmore, K., Kopetzki, D., McQuade, D. T., Seeberg, P. H., Continuous-Flow Oxidative Cyanation of Primary and Secondary Amines using Singlet Oxygen, *Angew, Chem. Int. Ed.*, **2014**, 53, 557

[152]. Jiang, G., Chen, J., Huang, J. -S., Che, C. -M., Highly Efficient Oxidation of Amines to Imines by Singlet Oxygen and its Application in Ugi-type Reactions, *Org. Lett.*, **2009**, 11, 4568

[153]. Johnson, J. A., Luo, J., Zhang, X., Chen, Y. -S., Morton, M. D., Echeverría, E., Torres, F. E., Zhang, J., Porphyrin-Metallation-Mediated Tuning of Photoredox Catalytic Properties in Metal-Organic Frameworks, *ACS Catal.*, **2015**, 5, 5283

[154]. Chen, R., Shi, J. -L., Ma, Y., Lin, G., Lang, X., Wang, C., Designed Synthesis of a 2D Porphyrin-Based $sp^2$ Carbon-Conjugated Covalent Organic Framework for Heterogeneous Photocatalysis, *Angew. Chem. Int. Ed.*, **2019**, 58, 6430

[155]. Marzo, L., Pagire, S. K., Reiser, O., König, B., Visible-Light Photocatalysis: Does it Make a Difference in Organic Synthesis?, *Angew. Chem. Int. Ed.*, **2018**, 57, 10034

[156]. Rybicka-Jasińska, K., König, B., Gryko, D., Porphyrin-Catalyzed Photochemical C-H Arylation of Heteroarenes, *Eur. J. Org. Chem.*, **2017**, 15, 2104

[157]. Moritz, M. N. O., Gonçalves, J. L. S., Linares, I. A. P., Perusi, J. R., de Oliveira, K. T., Semi-Synthesis and PDT Activities of a New Amphiphilic Chlorin Derivative, *Photodiagn. Photodyn. Ther.*, **2017**, 17, 39

[158]. Diogo, P., Fernandes, C., Caramelo, F., Mota, M., Miranda, I. M., Faustino, M. A. F., Neves, M. G. P. M. S., Uliana, M. P., de Oliveira, K. T., Santos, J. M., Gonçalves, T., Antimicrobial Photodynamic Therapy Against Endodontic *Enterococcus Faecalis* and *Candida Albicans*

Mono and Mixed Biofilms in the Presence of Photosensitizers: A Comparative Study with Classical Endodontic Irrigants, *Front. Microbiol.*, **2017**, 8, 498

[159]. Barona-Castaño, J., Carmona-Vargas, C., Brocksom, T., de Oliveira, K. T., Porphyrins as Catalysts in Scalable Organic Reactions, *Molecules*, **2016**, 21, 310

[160]. Mandal, T., Das, S., De Sarkar, S., Nickel (II) Tetraphenylporphyrin as an Efficient Photocatalyst Featuring Visible Light Promoted Dual Redox Activities, *Adv. Synth. Catal.*, **2019**, 361, 3200

[161]. Meng, Q. -Y., Zhong, J. -J., Liu, Q., Gao, X. -W., Zhang, H. -H., Lei, T., Li, Z. -J., Feng, K., Chen, B., Tung, C. -H., Wu, L. -Z., A Cascade Cross-Coupling Hydrogen Evolution Reaction by Visible Light Catalysis, *J. Am. Chem. Soc.*, **2013**, 135, 19052

[162]. Rueping, M., Zhu, S., Koenigs, R. M., Photoredox Catalyzed C-P Bond Forming Reactions-Visible Light Mediated Oxidative Phosphonylations of Amines, *Chem. Commun.*, **2011**, 47, 8679

[163]. Zuo, Z., Ahneman, D. T., Chu, L., Terrett, J. A., Doyle, A. G., MacMillan, D. W. C., Merging Photoredox with Nickel Catalysis: Coupling of $\alpha$-Carboxyl $sp^3$-Carbons with Aryl Halides, *Science*, **2014**, 345, 437

[164]. (a) Liu, X., Liu, L., Wang, Z., Fu, X., Visible Light Promoted Hydration of Alkynes Catalyzed by Rhodium (III) Porphyrins, *Chem. Commun.*, **2015**, 51, 11896. (b) Liu, X., Wang, Z., Zhao, X., Fu, X., Light Induced Catalytic Hydrodefluorination of Perfluoroarenes by Porphyrin Rhodium, *Inorg. Chem. Front.*, **2016**, 3, 861. (c) Liu, X., Wang, Z., Fu, X., Light Induced Catalytic Intramolecular Hydrofunctionalization of Allylphenols Mediated by Porphyrin Rhodium (III) Complexes, *Dalton Trans.*, **2016**, 45, 13308. (d) Chambers, D. R., Junean, A., Ludwig, C. T., Frenette, M., Martin, D. B. C., C-O Bond Cleavage of Alcohols via Visible Light Activation of Cobalt Alkoxycarbonyls, *Organometallics*, **2019**, 38, 4570

[165]. Toyao, T., Ueno, N., Niyahara, K., Matsui, Y., Kin, T. -H., Horiuchi, Y., Ikeda, H., Matsuoka, M., Visible-Light, Photoredox Catalyzed, Oxidative Hydroxylation of Arylboronic Acids using a Metal-Organic Framework Containing Tetrakis(carboxyphenyl)porphyrin Groups, *Chem. Commun.*, **2015**, 51, 16103

[166]. Wen, J., Yang, X., Sun, Z., Yang, J., Han, P., Liu, Q., Dong, H., Gu, M., Huang, L., Wang, H., Biomimetic Photocatalytic Sulfonation of Alkenes to Access $\beta$-Ketosulfones with Single-Atom Iron Site, *Green Chem.*, **2020**, 22, 230

[167]. Ghaleno, M. R., Ghaffari-Moghaddam, M., Khajeb, M., Reza Oveisi, A., Bohlooli, M., Iron Species Supported on a Mesoporous Zirconium Metal-Organic Framework for Visible Light

Driven Synthesis of Quinazolin-4(3*H*)-ones Through One-Pot Three-Step Tandem Reaction, *J. Colloid Interface Sci.*, **2019**, 535, 214

[168]. Lee, J., Papatzimas, J. W., Bromby, A. D., Gorobets, E., Derksen, D. J., Thiaporphyrin-Mediated Photocatalysis using Red Light, *RSC Adv.*, **2016**, 6, 59269

[169]. Rybicka-Jasińska, K., Shao, W., Zawada, K., Kadish, K. M., Gryko, D., Porphyrins as Photoredox Catalysts: Experimental and Theoretical Studies, *J. Am. Chem. Soc.*, **2016**, 138, 15451

[170]. Samulis, L., Tomkinson, N. C.O., Preparation of the MacMillan Imidazolidinones, *Tetrahedron*, **2011**, 67, 4263

[171]. Li, R., Cui, J., Zhu, Y., Yao, S., Ge, Z., Cheng, T., US Patent 2012/135921 A1, **2012**

[172]. Liu, G., Khlobystov, A. N., Charalambidis, G., Coutsolelos, A. G., Briggs, G. A. D., Porfyrakis, K., N@$C_{60}$-Porphyrin: A Dyad of Two Radical Centers, *J. Am. Chem. Soc.*, **2012**, 134, 1938

[173]. Tome, J. P. C., Nieves, M. G. P. M. S., Tome, A. C., Cavaleiro, J. A. S., Mendonca, A. F., Pegado, I. N., Duearte, R., Valdeire, M. L., Synthesis of Glycoporphyrin Derivatives and their Antiviral Activity Against Herpes Simplex Virus Types 1 and 2, *Bioorg. Med. Chem.*, **2005**, 13, 3878

[174]. Harwood, L. M., Moody, C. J., *Experimental Organic Chemistry: Principles and Practice*, **1989**, Blackwell

[175]. Liu, J., Li, P., Zhang, Y., Ren, K., Wang, L., Wang, G., Recyclable Merrified Resin-Supported Organocatalysts Containing Pyrrolidine Unit through $A^3$-Coupling Reaction Linkage for Asymmetric Michael Addition, *Chirality*, **2010**, 22, 432

[176]. Grenga, P. N., Sumbler, B. L., Beland, F., Priefer, R., Reductive Amination Agents: Comparison of Na(CN)$BH_3$ and Si-CBH, *Tetrahedron: Lett.*, **2009**, 50, 6658

[177]. Bonfantini, E. E., Burrell, A. K., Campbell, W.M., Crossley, M. J., Gosper, J. J., Harding, M. M., Officer, D. L., Reid, D. C. W., Efficient Synthesis of Free-Base-2-formyl-5,10,15,20-tetraarylporphyrins, their Reduction and Conversion to [(porphyrin-2-yl)methyl]phosphonium Salts, *J. Porphyrins Phthalocyanines*, **2002**, 6, 708

[178]. Li, B., Berliner, H., Buzon, R., Chin, C. K. -F., Colgan, S. T., Kaneko, T., Keene, N., Kissel, W., Le, T., Leeman, K. R., Marquez, B., Morris, R., Newell, L., Wunderwald, S., Witt, M., Weaver, J., Zhang, Z., Zhang, Z., Aqueous Phosphoric Acid as a Mild Reagent for Deprotection of *tert*-Butyl Carbamates, Esters and Ethers, *J. Org. Chem.*, **2006**, 71, 9045

[179]. Li, J., Liu, Y., Song, X., Wu, T., Meng, J., Zheng, Y., Qin, Q., zhao, D., Cheng, M., An Acid Catalyzed Epoxide Ring-Opening/Transesterification Cascade Cyclization to

Diastereoselective Syntheses of (±)-β-Noscapine and (±)-β-Hydrastine, *J. Org. Chem.*, **2019**, 21, 7149

[180]. Jacobsen, J. L., Berget, P. E., Varela, M. C., Vu, T., Schore, N. E., Martin, K. E., Shelnutt, J. A., Santos, L. M., Medfort, C. J., Synthesis and Nanostructures of 5,10,15,20-tetrakis-(4-piperidyl)porphyrin, *Tetrahedron*, **2013**, 69, 10507

[181]. Huy, P., Neudoerfl, J-M., Schmalz, H-G., A Practical Synthesis of *Trans*-3-Substituted Proline Derivatives through 1,4-Addition, *Org. Lett.*, **2011**, 13, 216

[182]. Bryden, F., Boyle, R. W., A Mild, Facile, One-Pot Synthesis of Zinc Azido Porphyrins as Substrates for Use in Click Chemistry, *Synlett.*, **2013**, 24, 1978

[183]. Kagan, H. B., Riant, O., Catalytic Asymmetric Diels-Alder reactions, *Chem. Rev.*, **1992**, 92, 1007

[184]. Corey, E. J., Catalytic Enantioselective Diels-Alder Reactions: Methods, Mechanistic Fundamentals, Pathways, and Applications, *Angew. Chem. Int. Ed.*, **2002**, 41, 1650

[185]. Hayashi, Y., Samana, S., Gotoh, H., Ishikawa, H., Asymmetric Diels-Alder Reactions of α,β-Unsaturated Aldehydes Catalyzed by a Diarylprolinol Silyl Ether Salt in the Presence of Water, *Angew. Chem. Int. Ed.*, **2008**, 47, 6634

[186]. Cai, X. -H., Tan, Q. -G., Liu, Y. -P., Feng, T., Du, Z. -Z., Li, W. -Q., Luo, X. -D., A Cage-Monoterpene Indole Alkaloid from *Alstonia Scholaris*, Org. Lett., 2008, 10, 577

[187]. Saktura, M., Grzelak, P., Dybowska, J., Albrecht, U., Asymmetric Synthesis of [2.2.2]-Bicyclic Lactones via All-Carbon Inverse-Electron-Demand Diel-Alder Reaction, *Org. Lett.*, **2020**, 22, 1813

[188]. Liu, Q., Zu, L., Organocatalytic Enantioselective Cross-Vinylogous Rauhut-Currier Reaction of Methyl Coumalate with Enals, *Angew. Chem. Int. Ed.*, **2018**, 57, 9505

[189]. Alonso, R., Bach, T., A Chiral Thioxanthone as an Organocatalyst for Enantioselective [2+2] Photocycloaddition Reactions Induced by Visible Light, *Angew. Chem. Int. Ed.*, **2014**, 53, 4368

[190]. Mayr, F., Brimioulle, R., Bach, T., A Chiral Thiourea as a Template for Enantioselective Intramolecular [2+2] Photocycloaddition Reactions, *J. Org. Chem.*, **2016**, 81, 6965

[191]. Tröster, A., Alonso, R., Bauer, A, Bach, T., Enantioselective Intramolecular [2+2] Photocycloaddition Reactions of 2(1*H*)-Quinolines Induced by Visible Light Irradiation, *J. Am. Chem. Soc.*, **2016**, 138, 7808

[192]. Rybicka-Jasińska, K., Ciszewski, L. W., Gryko, D., Photocatalytic Reaction of Diazo Compounds with Aldehydes, *Adv. Synth. Catal.*, **2016**, 358, 1671

[193]. Jarho, E. M., Venaelainen, J. I., Poutiainen, S., Leskinen, H., Vepsaelainen, J., Christiaans, J. A. M., Fosberg, M. M., Maennistoe, P. T., Wallen, E. A. A., 2(*S*)-(Cycloalk-1-enecarbonyl)-1-(4-phenylbutanoyl)pyrrolidines and 2(*S*)-(aroyl)-1-(4-phenylbutanoyl) pyrrolidines as Prolyl Oligopeptidase Inhibitors, *Bioorg. Med. Chem.*, **2007**, 15, 2024

[194]. Valero, G., PhD Thesis, Universitat de Barcelona, **2014**

[195]. Reid, G. P., Brear, K. W., Robins, D. J., Diastereoselective Conjugate Addition of Grignard Reagents to a Homochiral Fumaramide Derived from Oppolzer's Sultam, *Tetrahedron: Asymmetry*, **2004**, 15, 793

[196]. Jiménez, M., TFM, Universitat de Barcelona, **2022**

[197]. Müller, S. T. R., Smith, D., Hellier, P., Wirth, T., Safe Generation and Direct Use of Diazoesters in Flow Chemistry, *Synlett.*, **2014**, 25, 871.

[198]. González-Granda, S., Costin, T. A., Sá, M. M., Gotor-Fernández, V., Stereoselective Bioreduction of $\alpha$-diazo-$\beta$-keto Esters, *Molecules*, **2020**, 25, 931

[199]. El-Hachemi, Z., PhD Thesis, Universitat de Barcelona, **2002**

[200]. Chee, J., Johanson, J.N., Hayser, F., Parsons, W. H., Rupprecht, K. M., US 2002/13348 A1, **2002**

[201]. Molander, G. A., Romero, J. A. C., Investigations Concerning the Organolanthanide and Group 3 Metallocene-Catalyzed Cyclization-Functionalization of Nitrogen-Containing Dienes, *Tetrahedron*, **2005**, 61, 2631

[202]. WO Pat., WO 03064411 A1, **2003**

[203]. Singh, R., Panda, G., L-Proline Derived Nitrogenous Steroidal Systems: An Asymmetric Approach to 14-Azasteroids, *RSC Advances*, **2013**, 3, 19533

[204]. Holland, M. C., Metternich, B., Daniliuc, C., Schweizer, W. B., Gilmour, R., Aromatic Interactions in Organocatalyst Design: Augmenting Selectivity Reversal in Iminium Ion Activation, *Chemistry – A European Journal*, **2015**, 6, 10031

[205]. López, M. C., Royal, G., Philouze, C., Chavant, P. Y., Blandin, V., *Eur. J. Org. Chem.*, **2014**, 2014, 4884

[206]. Chimni, S. S., Mahajan, D., Small Organic Molecule Catalyzed Enantioselective Direct Aldol Reaction in Water, *Tetrahedron: Asymmetry*, **2006**, 17, 2108

[207]. Rhyoo, H. Y., Yoon, Y. -A., Park, H. -J., Chung, Y. K., Use of Amino Amides Derived from Proline as Chiral Ligands in the Ruthenium (II)-Catalyzed Transfer Hydrogenation Reaction of Ketones, *Tetrahedron Lett.*, **2001**, 42, 5045

[208]. Dzambaski, Z., Tzaras, D. -I., Lee, S., Kokotos, C. G., Bondzic, B. P., Enantioselective Organocatalytic Enamine C-H Oxidation/Diels-Alder Reaction, *Adv. Synth. Catal.*, **2019**, 361, 1792